U.PORTO
FACULDADE DE CIÊNCIAS
UNIVERSIDADE DO PORTO

Ciências ULisboa
Faculdade de Ciências da Universidade de Lisboa

PhD

3rd CYCLE

FCUP
2025

U.PORTO

From microclimates and thermal ecotypes to macroecological consequences.

Luís Filipe Ferreira Pereira

FC

U.PORTO
FACULDADE DE CIÊNCIAS
UNIVERSIDADE DO PORTO

Ciências ULisboa
Faculdade de Ciências da Universidade de Lisboa

From microclimates and thermal ecotypes to macroecological consequences

Luís Filipe Ferreira Pereira
Doctoral Program in Biodiversity, Genetics and Evolution
Department of Biology
Faculty of Sciences of the University of Porto and Faculty of Sciences of the University of Lisbon
2025



From microclimates and thermal ecotypes to macroecological consequences

Luís Filipe Ferreira Pereira

Thesis carried out as part of the Doctoral Program in Biodiversity, Genetics and Evolution

2025

Supervisor

Dr. Fernando Pádua Silva e Lima, Investigador Auxiliar, Centro de Investigação em Biodiversidade e Recursos Genéticos (CIBIO-InBIO)

Co-supervisors

Dr. Rui Seabra Alves Martinho, Post-Doc Researcher, Centro de Investigação em Biodiversidade e Recursos Genéticos (CIBIO-InBIO)

Dr. Francisco Arenas Parra, Principal investigator, Centro Interdisciplinar de Investigação Marinha e Ambiental (CIIMAR)

Acknowledgements

Looking back on the journey that brought me to the completion of this PhD, I see an adventure far beyond anything I could have imagined or prepared for. It was a path filled with challenges, moments of doubt, but also with discovery, growth, and the unwavering support from many people.

To my main supervisor, Fernando P. Lima, thank you for all your support and dedication. Your enthusiasm for new methods and gadgets was the spark that ignited the beginning of this PhD. I am grateful for your encouragement and trust in my ideas, which not only gave me the freedom to explore new paths but also made this journey both more challenging and enriching. I am deeply thankful for your friendship and trust.

To Rui Seabra, my co-supervisor, thank you for your support, especially for your invaluable help in collecting temperature data, a task so critical to our work yet often unnoticed. Thank you for all the R scripts and for showing me just how implicit R coding can be.

Thank you, Francisco arenas, the most supportive and hands-on co-supervisor any student could ask for. Your willingness to be there, whether for fieldwork, statistics, laboratory sampling, or all sorts of *pichelaria,* has been truly invaluable. With you, no experiment is ever too crazy, and no student ever works alone.

I also want to thank Prof. Jorge Teixeira for his warm welcome and willingness to help me, for your guidance in understanding oxidative stress protocols and for your support in the laboratory.

A big thank you to Prof. João Serôdio and Silja Frankenbach for their availability and support with the PAM analysis. I am also grateful for your trust in me as an engineer and for allowing me to contribute to your innovative ideas.

To the amazing Benthic ecology team, without whom I would still be picking up thousands of fronds on the beach or running P-I curves in the catacombs of BOGA. Vittoria, João, Oscar, Hugo, Axel, Harold, Rui, Julia, Noemi, thank you for all your help and friendship.

I also want to thank Cândida Vale and Pedro Ribeiro for their help with modelling and data collection. Your contributions were invaluable to the completion of some critical chapters.

Thank you to all my friends from CIBIO and the now long gone Barracoins, Mafalda, Luke, Walter, Marisa, João, Iolanda, Bárbara, Duarte, Cátia, Joana, Rita, Rocio. For the laughter, the complaints, and the midday sunbathing outside CIBIO.

Aos veteranos do CIIMAR, Francisca, Filipa, Thais, Augusto, Renato e Fernando, obrigado pela amizade, pelos momentos passados na varanda do CIIMAR e os almoços no Padrão. A vossa companhia a reclamar e rir do trabalho tornou tudo muito mais fácil.

Um grande obrigado ao Bruno Loureiro, pela amizade e inúmeras lições de engenharia. Por me encorajares a tornar-me um engenheiro mais confiante e organizado. Pelas corridas, pelos novos amigos e por seres a prova viva de que nunca se tem ferramentas a mais.

Aos meus amigos de sempre, Gaspar, Sara, Telos, Bruna, Soneqa, Fernando, obrigado por todos os bons momentos em que ninguém me perguntava sobre o meu doutoramento, pelas longas conversas sobre jogos e filmes, pelas jantaradas e pelos dias passados à volta de um carro.

Por fim, à minha familia, obrigado mãe por por cuidares de mim e me incentivares a seguir o que me faz feliz. Obrigado ao meu irmao, por não me teres deixado desistir da licenciatura em Biologia, por me teres ido buscar todos os dias à porta do ISEP, por estares sempre disponivel para me tentar ajudar, por seres o meu melhor amigo.

Por fim, à Carolina, obrigado pelo infindável apoio e motivação, por nunca me deixares duvidar de mim, por voares ao meu lado, por acreditares no nosso futuro.

Resumo

As alterações climáticas estão a transformar os ecossistemas em todo o mundo, sendo a temperatura um fator chave que influencia a fisiologia e ecologia dos organismos. Na zona intertidal, estes impactos são particularmente pronunciados, uma vez que as espécies podem enfrentar extremos térmicos tanto no ambiente marinho como no terrestre. Este habitat dinâmico é moldado pelos ciclos das marés e pela complexidade topográfica de pequena escala, criando um mosaico de microclimas. Como resultado, este habitat é um modelo exemplar para estudar como o ambiente físico influencia a fisiologia das espécies, as suas interações bióticas e padrões ecológicos. No entanto, capturar e replicar com precisão esta complexidade continua a ser um desafio substancial, frequentemente conduzindo a simplificações que comprometem a nossa capacidade de avaliar os limites térmicos das espécies intertidais e prever as suas respostas às alterações climáticas. Para enfrentar estes desafios e melhorar a nossa compreensão da suscetibilidade das espécies às alterações climáticas, esta tese centra-se em dois elementos complementares: o desenvolvimento de ferramentas inovadoras e a sua aplicação.

No primeiro capítulo, desenvolvo o enquadramento científico desta tese, apresentando os principais conceitos teóricos, descrevendo o contexto ecológico, as espécies estudadas, e identificando as lacunas de conhecimento existentes.

No segundo capítulo, abordo o principal desafio de capturar a variabilidade térmica à escala das espécies na zona intertidal. Embora esta variabilidade ser crucial para compreender os fatores ambientais que moldam este sistema, as condições rigorosas e dinâmicas da zona intertidal colocam desafios significativos à implantação a longo prazo de sensores de temperatura capazes de fornecer uma caracterização térmica fiável. Neste capítulo eu avalio o desempenho de sensores de temperatura tradicionais, colocados à superfície da rocha, em comparação com uma abordagem inovadora que utiliza sensores embutidos na rocha na zona intertidal. Esta comparação demonstrou que os sensores embutidos na rocha fornecem medições de temperatura mais fiáveis, uma vez que não são afetados pela sua cor, sendo ainda mais resistentes a danos ou perdas. Além disso, este capítulo examina o impacto da frequência de amostragem na captura precisa dos perfis térmicos ao longo das zonas intertidais, revelando que uma frequência de amostragem insuficiente pode resultar em erros significativos, incluindo subestimações da temperatura máxima diária, que se tornam mais pronunciadas nos níveis superiores da zona intertidal.

No terceiro capítulo, abordo o desafio de replicar a complexidade térmica da zona intertidais em condições laboratoriais. Embora os avanços na monitorização térmica de longa duração tenham tornado a captura da variabilidade térmica intertidal mais viável, a reprodução dessas condições em experiências laboratoriais controladas continua a ser tecnicamente desafiante. Para superar esta limitação, desenvolvi e avaliei a *Intertidal Environmental Chamber* — um sistema modular de acesso publico, especificamente concebido para simular de forma realista as complexas condições térmicas dos habitats intertidais. Este sistema inovador permite o controlo independente das marés, temperaturas de imersão e emersão, intensidade luminosa e de trocas de água, possibilitando uma replicação mais precisa e fiável dos ambientes térmicos intertidais em contextos experimentais.

Com base nos desenvolvimentos metodológicos anteriores, no quarto capítulo investigo as respostas fisiológicas à variação térmica de macroalgas de diferentes níveis intertidais (*Fucus serratus*, *Fucus spiralis*, *Ascophyllum nodosum* e *Pelvetia canaliculata*), no Noroeste da Península Ibérica, o limite sul da sua distribuição. Este capítulo incorpora dados de temperatura recolhidos no campo no desenho de uma experiência realista e na interpretação das respostas fisiológicas observadas. Os resultados deste capítulo enfatizam o papel crítico da exposição durante a emersão na resistência térmica das espécies, sublinhando a particular vulnerabilidade da *Fucus serratus*.

O quinto capítulo foca-se exclusivamente em *Ascophyllum nodosum* e expande a análise da tolerância térmica a múltiplas populações ao longo da sua distribuição europeia. Esta abordagem permitiu identificar potenciais ecótipos térmicos e explorar como fatores locais, como a influência de águas de afloramento e temperaturas extremas na maré baixa, podem influenciar a fisiologia da espécie. Os resultados revelam que o stress térmico na *Ascophyllum nodosum* é impulsionado, sobretudo, pelo contraste de temperatura entre a maré alta e baixa, em vez das temperaturas máximas absolutas. Curiosamente, indivíduos em tratamentos experimentais com águas quentes apresentaram melhor desempenho do que os expostos a águas frias, sugerindo que a presença de águas frias de afloramento no extremo sul da distribuição da espécie pode não ser o principal fator limitante à sua distribuição. Ao integrar estas respostas fisiológicas com projeções microclimáticas dos locais estudados, este capítulo sugere que, mesmo ecótipos termicamente resilientes podem estar em risco de serem ultrapassados pelo rápido aquecimento, com consequências macroecológicas para a distribuição da espécie.

Por fim, o sexto capítulo apresenta uma discussão geral que integra e sintetiza os resultados desta tese. Analisando as amplas implicações das abordagens utilizadas para a compreensão da dinâmica térmica intertidal e explora os fatores biológicos que podem influenciar a vulnerabilidade de *Ascophyllum nodosum* às alterações climáticas.

Palavras-chave: Sensores de temperatura, Microclima, Macroalgas, Stress térmico intertidal, Ascophyllum nodosum, Ecótipo térmico, Macroecologia.

Abstract

Climate change is transforming ecosystems worldwide, with temperature emerging as a key factor influencing the physiology and ecology of organisms. In the intertidal zone, these impacts are particularly pronounced, as species can experience thermal extremes on both marine and terrestrial environment. This dynamic habitat is shaped by tidal cycles and fine-scale topographical complexity, creating a mosaic of microclimates. As a result, this habitat is an exemplary model for studying how the physical environment influences species' physiology, biotic interactions, and ecological patterns. However, accurately capturing and replicating this complexity remains a substantial challenge, often leading to oversimplifications that compromise our ability to evaluate intertidal species' thermal thresholds and predict their responses to climate change. To tackle these challenges and enhance our understanding of species' susceptibility to climate change, this thesis focuses on two complementary elements: the development of innovative tools and their application.

In the first chapter, I will establish the foundation of this thesis by presenting the key theoretical concepts, describing the ecological context, the studied species, and identifying the existing knowledge gaps.

In the second chapter, I address the main challenge of capturing thermal variability at the species scale in the intertidal zone. This variability is crucial for understanding the environmental drivers shaping this system, yet the harsh and dynamic conditions of the intertidal zone pose significant challenges to the long-term deployment of temperature sensors capable of providing reliable thermal characterization. In this chapter I evaluate the performance of traditional surface-deployed temperature sensors compared to an innovative approach using rock-embedded sensors in the intertidal environment. This analysis demonstrates that rock-embedded sensors provide more reliable temperature measurements, remaining unaffected by the colour bias observed in surface sensors, while also being more resilient to damage or loss. Furthermore, this chapter examines the impact of sampling frequency on accurately capturing thermal profiles across different intertidal levels, revealing that insufficient sampling frequency can result in significant errors, including underestimations of the daily maximum temperature that become more pronounced at higher shore levels.

In the third chapter, I address the challenge of replicating intertidal thermal complexity in laboratory settings. While advancements in long-term temperature monitoring have made capturing intertidal thermal variability increasingly feasible, reproducing these

conditions in controlled experiments remains technically challenging. To overcome this, I developed and evaluated the *Intertidal Environmental Chamber* — a modular, open-source system specifically designed to realistically simulate the intricate thermal conditions of intertidal habitats. This innovative system enables independent control of tides, immersion and emersion temperatures, light intensity, and water exchange, allowing for more precise and reliable replication of intertidal thermal environments in experimental settings.

The fourth chapter builds on the previous methodological developments to investigate the physiological responses of macroalgae from different intertidal levels (*Fucus serratus, Fucus spiralis, Ascophyllum nodosum,* and *Pelvetia canaliculata*), at their southern distribution limit in the Northwest Iberian Peninsula. This experiment incorporated in-situ temperature data to design a realistic experiment and align the physiological results with the temperatures observed in the field. The findings highlight the critical role of emersion exposure in shaping species' thermal resilience, underscoring the particular vulnerability of *Fucus serratus*.

The fifth chapter focus solely on *Ascophyllum nodosum* and extends the thermal tolerance analysis to multiple populations, spanning its European distribution. This approach enabled the identification of potential thermal ecotypes and explore how localized factors, such as upwelling waters and extreme temperatures at low tide can influence the species' physiology. The findings reveal that thermal stress in *Ascophyllum nodosum* is more strongly driven by temperature contrast between high and low tides rather than absolute maximum temperatures. Interestingly, individuals in warmer water outperformed those in colder conditions, suggesting that cold upwelled waters at the species' southern range may not be the main limiting factor to its distribution. By integrating empirical physiological data with site-specific microclimate projections, this chapter suggests that even thermally resilient ecotypes can be at risk of being outpaced by rapid warming, with significant macroecological consequences for the species' distribution

Finally, the sixth chapter presents a general discussion that integrates and synthesizes the findings of this thesis. It examines the broad implications of the approaches employed for understanding intertidal thermal dynamics and explores the biological factors that could influence *Ascophyllum nodosum's* vulnerability to climate change.

Keywords: Temperature loggers, Microclimate, Macroalgae, Intertidal thermal stress, *Ascophyllum nodosum*, Thermal ecotype, Macroecology.

Table of Contents

List of Tables XIII

List of Figures XVI

List of Abbreviations XXVIII

Chapter 1 - General introduction 1

1.1. Climate Change 1

1.2. Temperature in the rocky intertidal zone 2

1.3. Recreating heat stress 8

1.4. Seaweed and climate change 9

1.5. Seaweeds along the North Atlantic intertidal shores 10

1.6. The canopy-forming seaweed *Ascophyllum nodosum* 12

1.7. Analysing heat stress responses in seaweeds 14

1.7.1. Photosynthetic performance 14

1.7.2. Oxygen production 15

1.8. Forecasting species responses to climate change 17

1.9. Work outline 19

1.10. References 21

Chapter 2 - Autonomous, high-frequency and long-term monitoring of substrate temperature in rocky intertidal zones 36

2.1. Abstract 37

2.2. Introduction 38

2.3. Materials and Methods 41

2.3.1. Performance of temperature loggers 41

2.3.2. Long-term logger loss rate in challenging environments 44

2.3.3. Sampling frequency 44

2.4. Results 45

2.4.1. Performance of temperature loggers 45

2.4.2. Long-term logger loss rate in challenging environments 48

2.4.3. Sampling frequency 49

2.5. Discussion 51

2.6. Acknowledgements 54

2.7. References 55

2.8. Supplementary Figures 59

2.9. Supplementary Tables 64

2.10. Supplementary References 65

Chapter 3 - Intertidal Environmental Chamber: an automatic system to accurately simulate the thermal complexity of intertidal environments 66

3.1. Abstract 67

3.2. Introduction 68

3.3. Design and features 69

3.3.1. Architecture 69

3.3.2. Water control 70

3.3.3. Temperature and visible light control 71

3.3.4. Control panel, display, and online mirroring 71

3.3.5. How to run an experiment 73

3.3.6. Protection and safety 73

3.4. Benchmarking and validation 74

3.4.1. Light performance 74

3.4.2. Temperature limits and performance benchmarks 75

3.4.3. Validation 77

3.5. Discussion and conclusions 79

3.6. Acknowledgements 81

3.7. References 82

3.8. Supplementary Text 84

3.9. Supplementary Figures 87

3.10. Supplementary Tables 88

Chapter 4 - Intertidal Fucales response to low tide heat stress at their southern distribution edge 90

4.1. Abstract 91

4.2. Introduction 92

4.3. Materials and methods 94

4.3.1. Sample collection 94

4.3.2. Experimental design 96

4.3.3. Field intertidal zonation 97

4.3.4. Growth, chlorophyll fluorescence and mortality 98

4.3.5. Lipid peroxidation 99

4.3.6. Statistical analysis 99

4.4. Results 100

4.5. Discussion 104

4.6. Acknowledgements 109

4.7. References 110

4.8. Supplementary Tables 120

Chapter 5 - Heat stress on the brown seaweed *Ascophyllum nodosum*: differential population sensitivity to future climate 126

5.1. Abstract 127

5.2. Introduction 128

5.3. Materials and methods 131

5.3.1. Sample collection 131

5.3.2. Experimental design 132

5.3.3. Experimental common-garden system 133

5.3.4. Relative growth rates 133

5.3.5. Survival 134

5.3.6. Primary productivity 134

5.3.7. Statistical analysis 135

5.3.8. Modelling strategy 136

5.3.9. Forecasting *in-situ* data 136

5.3.10. Model projection 137

5.3.11. Yearly cumulative-product survival 137

5.3.12. Population size projection 138

5.4. Results 139

5.4.1. Experimental heat stress simulations 139

5.4.2. Population forecasts 143

5.5. Discussion 146

5.5.1. The importance of cold, upwelled waters 146

5.5.2. Thermal stress response from high to low tides 147

5.5.3. Thermal sensitivity across the species distribution 149

5.5.4. Population hindcasts, forecasts, and extinction risk 150

5.6. Acknowledgements 153

5.7. References 154

5.8. Supplementary Figures 163

5.9. Supplementary Tables 166

Chapter 6 - General discussion 170

6.1. Developments in assessing and replicating intertidal heat stress 171

6.2. Impact of heat stress on intertidal species 173

6.3. Heat stress on *Ascophyllum nodosum* 176

6.4. The future of *Ascophyllum nodosum* 179

6.5. Conclusions and future prospects 182

6.6. References 184

Appendix A - A fully automated heart frequency recording device and associated data processing R package 194

A.1. Abstract 194

A.2. Introduction 195

A.3. Materials and Methods 196

A.3.1. Hardware 196

A.3.2. System deployment 198

A.3.3. R package *heartbeatr* 199

A.3.4. System validation and statistical analysis 201

A.4. Results 202

A.5. Discussion 206

A.6. Acknowledgements 208

A.7. References 208

Appendix B - A wireless temperature control system for field and laboratory experiments in aquatic mesocosms 210

B.1. Abstract 210

B.2. Introduction 211

B.3. Design and features 211

B.4. Operation 214

B.5. Performance and future improvements 216

B.6. Acknowledgements 220

B.7. References 220

Appendix C - Multispectral: an open-source platform for continuous and adjustable photobiology experiments 221

C.1. Abstract 221

C.2. Introduction 222

C.3. Design and features 222

C.4. Operation 224

C.5. Current application 227

C.6. Acknowledgements 229

C.6. References 229

List of Tables

Chapter 2

Table 2.1: Main technical specifications of the temperature loggers evaluated in this study..…….. 42

Table 2.2: Overall performance of the temperature loggers, combined across replicates (n = 3) and rocks (n = 3). Metrics include Pearson's correlation coefficient (R), normalised standard deviation (NSD), centred root mean square error (cRMSE), root mean square error (RMSE) and mean bias (MB)..…… 45

Table 2.3: Loss rates of temperature loggers equivalent to those evaluated in this study, deployed in similar habitats. Note that while the loss rates of iButtons are expressed in % per month, the loss rates of all other loggers are expressed in % per year. …… 48

Table S2.1: Combined performance of the replicate temperature loggers (n = 3), separately for each type of rock. Metrics include mean bias (MB), centred root mean square error (cRMSE), root mean square error (RMSE), Pearson's correlation coefficient (PCC), and normalised standard deviation (NSD). Rock albedo was roughly estimated by quantifying brightness in ImageJ (Schneider et al., 2012) from standardised, replicated areas (n= 3) in digital photographs of the rocks, using a reference A4 sheet of office paper (with a known albedo of ~0.65) included in each image..…….. 64

Chapter 3

Table S3.1: Distribution of visible light intensity in PAR (µmol m-2 s-1 photons) and LUX (lx) at low tide inside the Experimental Chamber. Illuminance was measured using an ILM-01 light meter (ISO-TECH, UK), and Photosynthetically Active Radiation (PAR) was measured with an MQ-510 sensor (Apogee Instruments, USA). LED intensities ranged from 0% to 100%, increasing in 10% increments, and light was measured at 15 evenly spaced points (3 x 5 grid) inside the Experimental Chamber. Colour gradients represent PAR or LUX (10 to 100%) values separately..…… 88

Chapter 4

Table 4.1: Summarised results of GLMs used to test the effects of low tide temperatures and species. Significant effects are in bold (*P*-value < 0.05). Models presented are for growth, F_v/F_m and LPO at the 10th and 20th day separately (T1 and T2, respectively)…103

Table S4.1: Pairwise contrasts summary of GLM model for growth described in Table 4.1. Analysis was performed for T1 and T2 separate models with a focus on species contrast within each temperature treatment (Degrees of freedom: T1= 728 and T2= 341). Significant effects are indicated in bold (P-value < 0.05), and * indicates marginal significance. The t-ratio test is represented as t.…… 120

Table S4.2: Pairwise contrasts summary of GLM model for growth described in Table 4.1. Analysis performed for T1 and T2 separate models with a focus on each species response at various temperatures (Degrees of freedom: T1 = 728 and T2=341). Contrasts towards control temperature (28 ºC) are as indicated in Fig. 4.1. Significant effects are indicated in bold (P-value < 0.05), and * indicates marginal significance. The t-ratio test is represented as t.…… 122

Chapter 5

Table S5.1: Coordinates for the sampled populations…… 166

Table S5.2: Summary of the results from generalized linear mixed models (GLMMs) testing the effects of low-tide temperatures (Air), hight-tide temperatures (Water), Region, Population as a nested random effect within Region (Population (Region)), Tank as cross-random effect, and their interactions for best model in each parameter. Significant effects (p < 0.05) are indicated in bold, while * denotes marginal significance. The models presented cover growth, net oxygen production and respiration, after the heat stress and the recovery periods…….. 166

Table S5.3: Survival rate equation constants, per population. Equations followed the form “Survival rate = β0 + β1 LPT + β2 SST + β3 TankR” where LPT represents low tide peak temperature, SST represents water temperature (SST), and TankR represents cross random effect of experimental tank. Models selected by their AIC..…….. 168

Table 5.4: Coordinates sampled on the ERA5 dataset. Data was accessed in January 2024…..……..……..…….. 168

Table 5.5: Coordinates sample on the CMIP6 dataset. Data was accessed in January 2024 ..…….……..…….. 169

Table 5.6: Survival ratio for the five size classes relative to size class 1, and fertility inflation ratios for all populations. Survival ratio values are organized by size class (1 to 5) and represent the natural survivability of each size class compared to size class 1. The equation used to determine a size class's survival is: Survival rate = 1 - ((1 - Size class 1 survival rate / respective size class ratio). Survival ratios are derived from demographic matrixes obtained from Åberg (1992a) and Araujo et al. (2014). Fertility inflation was calculated based on the population's requirement to maintain the same size in 2014 it had in 1850, using a stochastic approach with historical CMIP6 data (1850 to 2014)..……..…….. 169

Appendix A

Table A.1: Main functions and descriptions of the *heartbeat* R package.…….…. 200

List of Figures

Chapter 1

Figure 1.1: Changes in atmospheric CO2 concentration and global surface temperature estimates over the past 800,000 years; data retrieved from Lüthi et al. (2008) and Figure adapted from NOAA - http://www. climate.gov, published April 9, 2024. The inset shows the rapid rise in CO2 to 419.3 ppm and temperature anomaly, reference to the pre-industrial period only (1850-1900); data retrieved from www.climate.copernicus.eu (ERA5 reanalysis) and figure adapted from www.temperaturerecord.org.……3

Figure 1.2: a) Mean air surface temperature anomalies (relative to 1991-2023, global mean 0.60 °C); b) Mean Sea surface temperature anomaly (relative to 1993-2023); Adapted from www.climate.copernicus.eu..……..……..……4

Figure 1.3: a) DS1925L iButton (Thermochron, Maxim Integrated Products, USA); b) HOBO TidbiT MX Temp 5000 (Onset Corporation, USA); c) EnvLogger T7.3 (ElectricBlue CRL, PT); d) Biskit (Alpha Mach, CA).……..……6

Figure 1.4: Distribution of Fucaceae species in the North Atlantic; a) *Fucus serratus*; b) *Fucus spiralis*; c) *Ascophyllum nodosum*; d) *Pelvetia canaliculata*. Figure adapted from Neiva et al. (2016).……...……10

Figure 1.5: a) Measurement of *Ascophyllum nodosum* with 186 cm at Soulougan (France; Latitude: 48.672389; Longitude: -4.313694) b) *Ascophyllum nodosum* dense canopy during low tide in Île-Tudy (France; Latitude: 47.839222; Longitude: -4.169472).……..…12

Figure 1.6: Light activation energy in the reaction centres of photosystem (PS) I and PS II is used for photochemical work and emitted as heat and chlorophyll-a fluorescence. Photochemical work reduces NADP+ to NADPH, which is required for carbon fixation in the Calvin Cycle. Figure based on Baker (2008) and (Schreiber et al., 1995).……..…14

Figure 1.7: Oxygen productivity (P) in response to Irradiance (I). Net primary production (NPP) results from the deduction of basal oxygen consumption (Respiration) upon the gross primary production (GPP). The compensation point (IC) refers to the light intensity at which neutral NPP is achieved. In contrast, the saturation point refers to the light

intensity that promotes the highest GPP, beyond which light intensity becomes excessive and causes photoinhibition. Figure based on Eilers and Peeters (1988) and Lalli and Parsons (1997).……..……..…15

Figure 1.8: a) Global surface air temperature change between 1950-2100 as a difference to the 1850-1900 period; b) Sea surface temperature (SST) change since 1950-2100 as a difference to the 1950-1980 period. Both refer to model projections built upon the historical data until the end of 2014. These are an adaptation of figures Figure SPM.8 (Chapter 8) and Figure SPM.9.3 (Chapter 9) from the IPCC 6th Assessment Report WGI Summary for Policy Makers (IPCC, 2022).……..…18

Chapter 2

Figure 2.1: An array of temperature loggers and thermocouples deployed on a fine-grain granite rock (foreground) and another array in a coarse-grain granite rock (background) in the intertidal zone at Praia de Sampaio (41.2797° N, -8.7305° W; June 20, 2020), photographed at low tide. Each type of logger was deployed in triplicate. Green smudges on the rock surface indicate locations where EnvLoggers were embedded within the substrate. The large plastic boxes housed the electronics required to read and log thermocouple data. ……..……..……..……..…41

Figure 2.2: Overall performance of temperature loggers compared to reference thermocouple; a) Distribution of biases; b) Taylor diagram where each coloured circle represents a logger type, while the white circle at the bottom shows the reference thermocouple data. The azimuth angle of each coloured circle corresponds to its correlation coefficient with the reference (R). The radial distance from the graph's origin indicates Normalized Standard Deviation (NSD), and the concentric lines centred on the reference represent Centered Root Mean Square Error (cRMSE). The best-performing loggers are located at the same radial distance as the reference (indicating better NSD), lower on the graph (indicating higher R), and closer to the reference circle (indicating lower cRMSE).……..……..……..…… 46

Figure 2.3: Overall temperature distribution between each type of temperature logger and its nearest thermocouple (reference). The 1:1 red line indicates perfect correspondence. Black ellipses enclose 95% of data points (grey crosses). Points above the red line represent loggers recording higher temperatures than their reference thermocouple ("running hot"), while points below indicate lower temperatures ("running cold") at specific values. ……..…… 47

Figure 2.4: Cross-correlation analysis between each type of temperature logger and its nearest thermocouple (reference). A peak away from zero and in the negative half of the graph would indicate a lag of the logger behind the reference. ……..…47

Figure 2.5: Average differences in daily maximum and minimum temperature estimations across various sampling rates relative to 1-minute sampling (reference) in distinct intertidal zones and microhabitats (supratidal, high, mid, and low intertidal zones across various compass orientations and tide pools). Since the study site is located in the northern hemisphere, south-facing loggers correspond to the warmest microhabitats, and north-facing loggers to the coolest. Negative values indicate underestimation, while positive values indicate overestimation relative to the 1-minute reference. For more details, see Supplementary Figs. S2.4 and S2.5. ……..…….. 50

Figure 2.6: Percentage distribution of timing errors when using rarefied data to estimate the hottest or coldest day of the week. The x-axis represents the sampling intervals tested, from the 1-minute reference to every 360 minutes. The y-axis shows the absolute timing error in days. Each box's colour intensity indicates the percentage of occurrences for a given timing error at each sampling interval (also shown as white text inside each box), with warmer (reddish) colours representing higher percentages. The closer to 100% on the lower row, the fewer errors are being introduced in the identification of the days when the extremes occurred. For a breakdown of timing errors across intertidal zones and orientations, see Supplementary Fig. S2.6. ……..…… 51

Figure S2.1: Typical temperature profiles recorded by different types of loggers, illustrated by the set of loggers nearest to thermocouple on the fine-grain granite rock during low tide on July 21, 2020. Temperatures in the period up to around 6:20, on the left side of the graph, were recorded underwater, while the rest was recorded during low tide. ……..…… 59

Figure S2.2: Determination of the greyscale tone for white, grey, and black EnvLoggers. The color gradient was obtained by varying the proportions of black and white opaque acrylic paint during logger manufacturing; a) Sample image of the loggers with a calibration greyscale from https://sachverstaendigen-zubehoer.de; b) Linear regression (with 95% confidence intervals) between pixel values from the calibration scale images and their actual greyscale values (cross symbols), using three replicate images taken under slightly different lighting conditions. Pixel measurements were obtained using Affinity Photo software; c) Proportions of acrylic paint used in each logger type and their corresponding absolute greyscale values. ……..…… 59

Figure S2.3: Process of embedding EnvLoggers into the rock; a) Using a battery-powered DCH133M1 DeWALT driller with a 30 mm DeWALT DT9618-QZ drill bit to make a hole in the rock; b) A 30 mm wide and 15 mm deep hole in the rock; c) Pressing an EnvLogger against the rock with A-788 Z-Spar Splash Zone Compound (Carboline, USA. The antenna side of the logger must be kept facing up. d) On the left, covering a EnvLogger with a ~1 mm layer of the same compound; on the right, a logger still to be covered..... 60

Figure S2.4: Box plots (with outliers) showing differences in daily maximum and daily minimum temperature estimates at various sampling intervals compared to the 1-minute sampling reference across intertidal zones and orientations. Sampling intervals range from 1 to 360 minutes, with results shown for supratidal, high, mid, and low intertidal zones in south, east, west, and north orientations, as well as for a tide pool microhabitat. Since the study site is located in the northern hemisphere, south-facing loggers correspond to the warmest microhabitats, and north-facing loggers are representative of the coolest. Negative values indicate underestimations, and positive values indicate overestimations relative to the 1-minute reference, highlighting how sampling frequency impacts temperature accuracy in each zone and orientation..... 61

Figure S2.5: Impact of reduced sampling rates on temperature estimates, with 1-minute sampling at one of the high-intertidal, south-facing loggers as the reference (where temperature fluctuates the most). To enhance clarity, only selected sampling rates are shown, separated into two plots. Sampling intervals include 15, 30, 60, 90, 120, and 240 minutes. It can be clearly seen that reduced frequency reduces the details that can be extracted from the data. In particular, estimations of the daily extremes can include large biases at the lowest sampling frequencies..... 62

Figure S2.6: Percentage distribution of timing errors when using rarefied data to estimate the hottest or coldest day of the week, across intertidal zones and orientations. The x-axis represents the sampling intervals tested, from the 1-minute reference to every 360 minutes. The y-axis shows the absolute timing error in days. Each box's colour intensity indicates the percentage of occurrences for a given timing error at each sampling interval, with warmer (reddish) colours representing higher percentages. The closer to 100% on the lower row, the fewer errors are being introduced in the identification of the days when the extremes occurred..... 63

Chapter 3

Figure 3.1: a) The Intertidal Environmental Chamber: 1 - ECU with manual override switches and LCD display, 2 – Experimental Tank's Lid, 3 – Experimental Tank, 4 – Water Storage Tank; b) Detail of the Experimental Tank at high tide, showing the LED strips, black IR lamps and air-circulating fans at the top, various mollusc specimens and seaweed underwater, and temperature sensors...……...69

Figure 3.2: Schematic illustration of an Intertidal Environmental Chamber..……..….70

Figure 3.3: Example of the display on the Electronic Control Unit…….……72

Figure 3.4: a) Hourly temperature data from a temperature logger deployed in a rocky intertidal environment; b) Simplified experiment profile replicating the field conditions. Key experimental steps and their respective temperatures are marked, with submerged steps shown in blue and immersed steps in yellow; c) Actual experiment results from an Intertidal Environmental Chamber. In all plots, submersion periods are highlighted in light blue…..……72

Figure 3.5: Visible light intensity in PAR (µmol m-2 s-1 photons) and LUX (klx) measured at low tide, showing similar average response curves (black line) ±SD (grey shade).……75

Figure 3.6: a a) Water temperature and warming rate in the Experiment Tank during 12 h of constant heating; b) Water temperature and cooling rate during 12 h of constant cooling. Red lines represent the average temperature, and blue lines represent the average rate of change. The shaded grey area indicates the standard deviation (SD) between the three sensors..……...……..……76

Figure 3.7: a) Low-tide temperature and warming rate in the Experiment Tank during 1h30m warming up to 50 ºC. b) Low-tide temperature and cooling rate during 4h of constant cooling. Red lines represent the average temperature, and blue lines represent the average rate of temperature change. The shaded grey area indicates the standard deviation (SD) between the three sensors.……76

Figure 3.8: a) Light intensity; b) Measured experimental temperatures; c) Standard deviation among the temperature sensors within the Experimental tanks (n=3 per chamber). d) Instantaneous difference between experimental and target temperatures (Error). e) Mean bias between experimental and target temperatures during low-tide

(yellow) and high-tide (blue) periods. Vertical blue bars on plots b, c, and d indicate high tide periods.……..……78

Figure S3.1: Visual representation of the experiment profile instructions provided above; a) Profile.txt lines (1 to 9); b) Temperature targets and in-between interpolation; c) Light intensities (%); d) Tide states (1=High, 0=Low); e) Water change states (instantaneous, 1=On, 0=Off)…….…87

Chapter 4

Figure 4.1: Photos showing the typical morphology of the four target seaweeds species at the collection site (Viana do Castelo; Portugal)..…… 95

Figure 4.2: Diurnal heat stress treatment profiles. Coloured lines depict temperature profiles during daily low tides (10h-14h). Control treatment (28 ºC) is shown as a green line and experimental treatments (35 ºC to 41 ºC) are represented by lines ranging from yellow to red, respectively. High tide periods (14h-22h and 02h-10h) were identical in all treatments (15 ºC). Temperature during nocturnal low tides (22h-02h) was kept around 15 °C, remaining close to water temperature. Tidal cycle (8:4; high:low) and heat stress profiles were repeated daily for the whole 20 days of the experiment..…… 96

Figure 4.3: a) Daily temperature maximum observed at the sampling site at low, mid and high tide levels (n= 2 or 3; green, orange and red lines, respectively). Sensors were placed at a height of -0.81 ± 0.25, -0.18 ± 0.04 and 0.84 ± 0.05 meters relative to mean sea level (MSL) for low, mid and high tide, respectively; b) Intertidal heights for target species and loggers relative to MSL, and temperature occurrences at each intertidal level in hours/year above experimental temperatures. Target species height at Viana do Castelo (Portugal) was measured as: *P. canaliculata* (0.71 ± 0.09 to 1.19 ± 0.13 m), *A. nodosum* (-0.33 ± 0.16 to 0.58 ± 0.06 m), *F. spiralis* (-0.37± 0.04 to 0.04 ± 0.18 m) and *F. serratus* (-1.51 ± 0.10 to -0.48 ± 0.15 m)..…… 101

Figure 4.4: a, b) Growth at instants T1 and T2 expressed as percentage relative to initial weight (mean ± SD); c, d) F_v/F_m at instants T1 and T2 (mean ± SD); e, f) Mortality as percentage of total individuals at instants T1 and T2; g) Lipid Peroxidation at instant T1 (mean ± SD); Bottom axes indicate low tide (emersion) temperatures for all eight treatments (28 [control], 35, 36, 37, 38, 39, 40 and 41 ºC). Significance asterisks refer to pair-wise comparisons within the same species and sampling instant (T1 or T2) against

respective control treatments (28 ºC). Significance levels: * $P < 0.05$, ** $P < 0.01$, *** $P < 0.001$..…… 102

Chapter 5

Figure 5.1: a) Map of the study area. Numbers 1–10 indicate the locations of the ten populations sampled (1– Viana do Castelo, PT; 2- Ría de Muros, ES; 3- Ría de Foz, ES; 4- Ría de Villaviciosa, ES; 5- Île-Tudy, FR; 6- Penmarch, FR; 7- Landunvez, FR; 8- Soulougan, FR; 9- Blomsterdalen, NO; 10- Straumøyna, NO); b) Average diurnal low tide temperatures within each experimental tank for the 8 treatments (black line) ± SD (light green and dark green for cold- and warm-water treatments, 15 ºC and 20.5 ºC, respectively). Nocturnal low tide temperatures remained close to their respective water temperatures. The tide cycle of 7:5 (high: low) was repeated twice daily for the whole 20 days of the experiment. Map created in R (R Development Core Team, 2023) using the Rnaturalearth library v1.0.0..…… 131

Figure 5.2: Average relative growth rate per day (% RGR day-1) (mean ± SD; n = 20 per population) after ten days of thermal stress. Experimental treatments are arranged from left to right based on the absolute temperature difference between lower temperatures at high tide and peak heating temperatures at low tide. Therefore, absolute differences ranged from 8 ºC to 25.5 ºC. Experimental temperatures are represented in shades of green (high-tide temperatures) and pink (low-tide peak temperatures). Points show individual growth rates, while bars show the overall interquartile distribution for each region, color-coded as blue (north populations), yellow (center populations), and red (south populations). Statistical analysis focused only on pairwise comparisons between regions within the same treatment. Significance levels: * p < .05, ** p < .01, *** p < .001..……..…139

Figure 5.3: Linear model of survival rate of A. nodosum fronds at the end of the experiment (day 20). Treatments are arranged from left to right based on the absolute temperature difference between lower temperatures at high tide and peak heating temperatures at low tide. Treatment temperatures are represented in shades of green (high-tide temperatures) and pink (low-tide temperatures). Shaded areas show the model's regional predictions with 95 % confidence intervals, and lines represent the survival of each population. Populations from the north are shown in blue, the centre in yellow, and the south in red..…… 140

Figure 5.4: Maximum net primary production (Nppmax; μmol O_2 g^{-1} h^{-1}) and maximum respiration rate (Rmax; μmol O_2 g^{-1} h^{-1}) (mean + SD; n = 24 per region for south and centre; n= 12 for north) after the heatwave stress (on the day 10). Regions are colour-coded as blue (north populations), yellow (centre populations), and red (south populations). Nppmax is shown as positive values, while Rmax is shown as negative values (and indicates consumption). The treatments are arranged from left to right based on the absolute temperature difference between lower temperatures at high tide and peak heating temperatures at low tide. Therefore, absolute differences ranged from 8 ºC to 25.5 ºC. Treatment temperatures are represented in shades of green (high-tide temperatures) and pink (low-tide temperatures). Statistical analysis focused only on pairwise comparisons between regions within the same treatment. Significance levels: * p < .05, ** p < .01, *** p < .001….…… 142

Figure 5.5: Yearly cumulative-product survival results for all ten populations from 1850 to 2100 under different SSP scenarios (SSP26, SSP45, and SSP85). The x axis represents time in yearly increments, while the vertical axis shows the regions and their respective populations. Final survival rates for each year are depicted as heatmap bars in grayscale (black represents 0% survival, and white represents 100% survival). Survival rates are reset to 100% at the beginning of each year. Plots in the left column, labelled "common climate," show survival rates based on population-specific survivability equations applied to a single common climate (in this case, the climate experienced by the southernmost population, at Viana do Castelo, population 1, Portugal). Plots in the right column, labelled "respective climates," indicate survival rates based on population-specific survivability equations applied to their own local climates..…… 144

Figure 5.6: Projected population sizes for all ten populations by the end of 2100 under different SSP scenarios (SSP26, SSP45, and SSP85). Black circumferences represent the population size in 2014, while coloured filled circles indicate the expected population size in 2100, with the size of each circle proportional to the population size. Filled circles smaller than the black circumference indicate population contraction, while empty circumferences represent population extinction. Each projection considers respective climate conditions (based on CMIP6 climatic data), yearly survival rates, and regional demographic matrices. The map was created in R (R Development Core Team, 2023) using the Rnaturalearth library v1.0.0..…… 145

Figure S5.1: Average relative growth rate in percentage per day (%RGR day^{-1}) (mean ± SD; n = 20 per population) after recovery period (twentieth day). Bottom axis refers to

heating intensity during low tide emersion period (8 to 25.5 ºC), e.g., difference between water temperature at high tide and peak temperature at low tide. Experiment treatments high and low tide temperatures are identified in coloured rectangles on bottom axis with green and pink background palette, respectively Statistical analysis considered only pair-wise comparisons between regions within the same treatment. Significance levels: * p < 0.05, ** p < 0.01, *** p < 0.001..... 163

Figure S5.2: Linear model of survival rate of *A. nodosum* fronds after heatwave stress event (10th day). Bottom axis refers to heating intensity during low tide emersion period (8 to 25.5 ºC), e.g., difference between water temperature at high tide and peak temperature at low tide. Experiment treatments high and low tide temperatures are identified in coloured rectangles on bottom axis with green and pink background palette, respectively. Lines and shaded areas are model predictions and 95% confidence intervals. Dashed lines correspond to population modelled survival, while solid line refer to regional averaged values..... 164

Figure S5.3: Maximum net primary production (Npp_{max}; µmol O_2 L^{-1} g^{-1} h^{-1}) and maximum respiration rate (R_{max}; µmol O_2 L^{-1} g^{-1} h^{-1}) (mean + SD; n = 24 per region for South and Centre; n=12 for North) after recovery (twentieth day). Npp_{max} and R_{max} are shown with opposite signals, positive and negative respectively. Hence, negative production values represent consumption. Horizontal dashed line indicates null oxygen production or consumption. Bottom axis refers to heating intensity during low tide emersion period (8 to 25.5 ºC), e.g., difference between water temperature at high tide and peak temperature at low tide. Experiment treatments high and low tide temperatures are identified in coloured rectangles on bottom axis with green and pink background palette, respectively Statistical analysis considered only pair-wise comparisons between regions within the same treatment. Significance levels: * p < 0.05, ** p < 0.01, *** p < 0.001..... 165

Chapter 6

Figure 6.1: Current temperature logger deployment in global scale networks; Dark and light blue dots represent deployed and expected CCTBON temperature loggers respectively (225 deployed out of 412 total)..... 172

Figure 6.2: a) Set of ten A. nodosum fronds from 25.5 ºC in **Chapter 5** temperature difference treatment after 20 days, distributed and marked according to each population (cable tags numbered 0 to 9, from left to right); b) Fv/Fm ratio picture of the same set of

fronds, displaying variation within South and Centre populations but no detection of any chlorophyll-a fluorescence in the northern populations (two fronds at the right)..... 178

Figure 6.3: Predicted in-situ temperature difference data according to SSP45 at four populations; Lines are coloured according to three temperature differences tested in **Chapter 5** (grey for < 16 ºC, green for >16 ºC, yellow for >20 ºC and red > 25.5 ºC); a) Population 1, Viana do Castelo (Portugal); b) Population 2, Ría de Villaviciosa (Spain); c) Population 8, Soulougan (France) and d) Population 10, Straumøyna (Norway).... 179

Appendix A

Figure A.1: Functional schematic diagram of the IR cardiac sensing amplification and signal conditioning circuit. See complete bill of materials at the GitHub repository..... 197

Figure A.2: a) Full system showing the ten amplification knobs at the front, two cabled CNY70 sensors connected on top and a power adaptor; b) glueing a CNY70 sensor to a blue mussel (Mytilus sp.); c) several limpet s(Patella sp.) with CNY70 attached to their shell, over their heart; d) the heartbeat of a blue mussel (Mytilus sp.) as shown on the LCD screen..... 198

Figure A.3: Impact of signal smoothing intensity (the bandwidth parameter) on the proportion of data points correctly classified as “keep” or “reject” by the *heartbeatr* package. Panels a) and d) correspond to correct classifications (human and *heartbeatr* agree in retaining or rejecting data points), while panels b) and c) correspond, respectively, to false positives (type-1 error, retaining data points that should have been rejected) and false negatives (type-2 error, rejecting data points that should have been retained). In the context of the *heartbeatr* workflow, minimizing the number of data points that fall on panel b) is the priority. Red and blue lines depict the performance curves relative to two distinct workflow strategies. In the simplest and quicker option (red lines), quality was assessed using data smoothed using only the respective bandwidth value. In the other case (blue lines), quality was assessed using not only the same smoothed data but also the raw, unsmoothed data and choosing the best estimate for each data point. Finally, the blue dot depicts a third, more computing-intensive strategy in which the best estimate was chosen from among unsmoothed data and data smoothed at all bandwidth levels tested..... 203

Figure A.4: Impact of cutoff SD level (the lim_sd parameter) on the proportion of data points correctly classified as “keep” or “reject” by the *heartbeatr* package. Similarly to Fig. A.3, panels a) and d) correspond to correct classifications, while panels b) and c) correspond to false positives (type-1 error) and false negatives (type-2 error), respectively. The red dashed line indicates a cutoff SD level of 0.7…….. 204

Figure A.5: 2D kernel density plot showing the distribution of automatically-assessed heartbeat frequency estimates against human-assessed values. Data is aggregated in 0.1 x 0.1 bins. The colour scale depicts cumulative probabilities (grey bins are indicative of bin combinations with marginal representation in the overall dataset). The black diagonal line marks a 1:1 relationship between values determined manually and values automatically, while the dashed lines indicate 2:1 (automatically-assessed values are twice the real value) and 1:2 (automatically-assessed values are half the real value) relationships. The red contour encompasses 90% of the data in each panel. Labels in the top-right corner show the number of data points included in each panel and the proportion of data points relative to the entire dataset. ……..…… 205

Appendix B

Figure B.1: Functional schematic diagram of Mesocosm system circuit. See complete bill of materials at the GitHub repository.……..…….. 212

Figure B.2: a) Electronic board layout; b) Electronic 3D board layout (128.6 x 98.6 mm); c) Mesocosm unit composed by a Polycarbonate IP67 box (160x120x91 mm)…….. 213

Figure B.3: a) Mesocosm system network architecture; b) Close-up view of a Mesocosm unit fixed to its pond; c) Overall Mesocosm system perspective encompassing 36 ponds, distributed along a 100 x 100 meter area in Vairão (Longitude: 41.325890, Latitude: -8.677546; Portugal)……..…….. 214

Figure B.4: Online dashboard appearance on Blynk IoT platform (Blynk, Inc., USA)..216

Figure B.5: Data transfer success between Mesocosm units at 10 m, 75 m and 150 m from the Master in Trial 1. Percentual values refer to minimum delivery success found within the three communicating devices (Master and two Heaters). Success rates refer to data found on the Master Logs (stored in the microSD card) after periods of 24 h periods, communicating every two minutes……..….. 217

Figure B.6: a) Temperature data from all five units (a Master, two Heaters and two Viewers), together with the Viewers average and Heater's target; b) Heaters' error between the observed and target temperature for the two units…… 218

Appendix C

Figure C.1: a) Multispectral 3D explosion view; b) Main and push-buttons PCBs 3D view; c) Perspective of two Multispectral units, left unit is open to show lens and LED light and the right unit is placed on top of the microplate, ready to be used…….. 223

Figure C.2: a) Wells numbering for profile experiment design; b) LCD display during initial Profile choosing; c) LCD display during ongoing Profile……..…….. 225

Figure C.3: a) Wells numbering for profile experiment design; b) Example profile rows; c) Light intensities of LED 1; d) Light intensities of LED 2; e) Light intensities of LED 3; f) Light intensities of all other LEDs (4th to 24th)……..…… 226

Figure C.4: a) Nominal intensity readings along the wavelengths emitted by Multispectral units aimed at evaluating effects of visible light; b) Nominal intensity readings along the wavelengths emitted from one Multispectral unit aimed at evaluating effects of near infrared light; Readings obtained via SpectraPen min (Photoystems Instruments, Poland) at 1 nm resolution (n = 4 LEDs). Note: Missing readings from 591 nm peak emission LED were not obtained at the time of this document.……...…… 227

List of Abbreviations

AIC	Akaike information criterion
AOI	Area of interest
ANOVA	Analysis of variance
ATP	Adenosine triphosphate
BIC	Bayesian information criterion
BLE	Bluetooth Low Energy
CMIP6	Coupled Model Intercomparison Project Phase 6
cRMSE	Centred root mean square error
ECU	Electronic control unit
ECMWF	European Centre for Medium-Range Weather Forecasts
ENM	Ecological niche model
ERA5	Fifth generation ECMWF atmospheric reanalysis
ETC	Electron transport chain
Fm	Maximum fluorescence
FW	Fresh weight
Fv	Variable fluorescence
Fv/Fm	Variable to maximum fluorescence ratio
GLM	Generalized linear model
GLMMs	Generalized linear mixed-model
GNSS	Global navigation satellite systems
GPP	Gross primary production
Ic	Compensation radiation point
IR	Infrared
Is	Saturation radiation point

Kya	Thousands of years ago
LCD	Liquid crystal display
LPO	Lipid peroxidation
MB	Mean bias
MSL	Mean sea level
NADP+	Oxidized form of nicotinamide adenine dinucleotide phosphate
NADPH	Reduced form of nicotinamide adenine dinucleotide phosphate
NE	Northeast
NFC	Near Field Communication
NOAA	National Oceanic and Atmospheric Administration
NPP	Net primary production
NTRIP	Networked Transport of RTCM via Internet Protocol
NSD	Normalized standard deviation
NW	Northwest
PAM	Pulse amplitude modulation
PAR	Photosynthetically active radiation
PE	Photosynthesis-irradiance
PP	Polypropylene
PSII	Photosystem 1
PSII	Photosystem 2
PVC	Polyvinyl chloride
R	Pearson's correlation coefficient
RCP	Representative concentration pathway
ReNEP	National GNSS Permanent Stations Network
RF	Radio frequency identification
RMSE	Root mean square error

ROS	Reactive oxygen species
RT	Room temperature
RTK	Real-Time Kinematic
SDM	Species distribution model
SSP	Shared socioeconomic pathway
SST	Sea surface temperature
Wi-Fi	Wireless fidelity

Chapter 1

General introduction

The escalating impacts of climate change are driving rapid environmental transformations, exerting unprecedented pressure on species to adapt to shifting thermal landscapes and habitat conditions. Predicting the biological consequences of these changes requires a detailed understanding of small-scale temperature variability and its effects on individual physiology and population dynamics. However, accurately determining a population's current and future vulnerability remains remarkably complex. This challenge can be particularly pronounced in the intertidal zone, where organisms experience extreme and highly variable environmental conditions. Despite substantial research, our ability to characterize the environmental drivers shaping intertidal ecosystems is still limited, constraining our understanding of species distributions. The inherent complexity of these environments further complicates simulations, making it difficult to effectively assess species vulnerability. Additionally, species with broad geographic ranges and low mobility may exhibit significant geographical variability in their physiological responses, potentially altering the overall species-level response.

In this thesis, I develop and implement different methodologies to better capture and replicate the thermal complexity of intertidal systems, enabling a more precise understanding of how thermal stress impacts organisms at the microclimate scale. The findings demonstrate that the interaction between population-specific sensitivities and localized climate scenarios determines species' responses to future climate conditions.

1.1. Climate change

Climate refers to the long-term patterns observed in weather conditions, mainly characterized by temperature, wind, precipitation, and other atmospheric elements. The classification of Earth's diverse climate regimes is inherently tied to specific time spans and geographic areas (Werndl, 2016). Consequently, the interpretation of climate change largely depends on the scales considered within a given spatiotemporal analysis. Throughout Earth's history, climate-driven environmental changes have exerted intense pressure on ecosystems, serving as a powerful driver of evolution (Precht, 2013). These transformations, while profound, follow cyclic patterns of glacial and interglacial phases, driving species evolution and range shifts by pushing species toward the equator during glacial periods and enabling recolonization in warmer phases (Byun et al., 1999; Gavin et al., 2014; Hewitt, 2003).

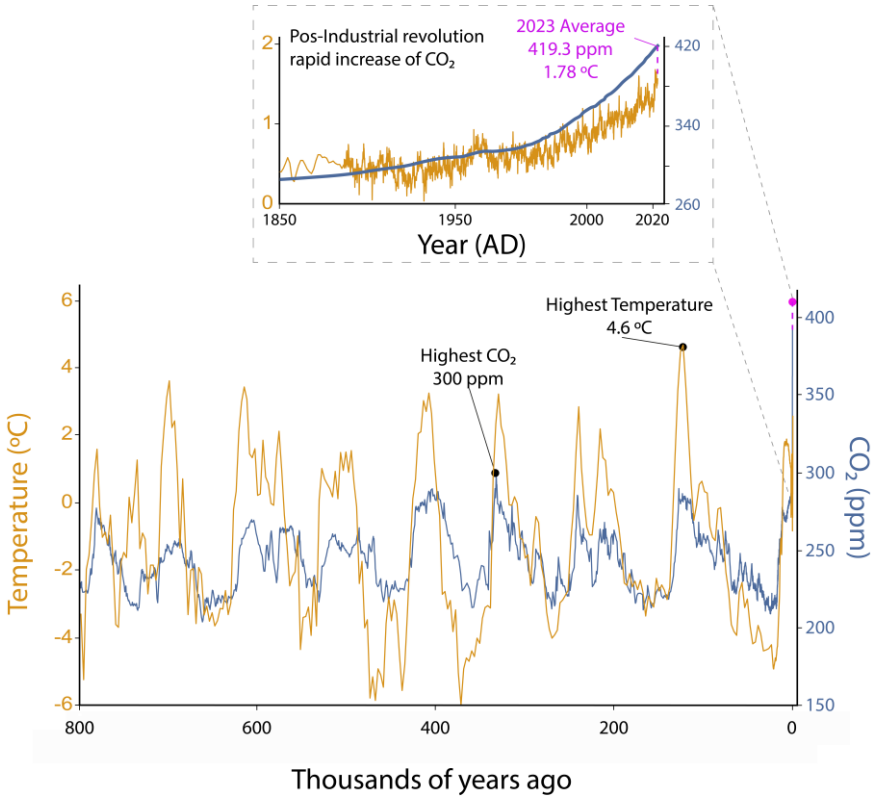


Figure 1.1: Changes in atmospheric CO2 concentration and global surface temperature estimates over the past 800,000 years; data retrieved from Lüthi et al. (2008) and Figure adapted from NOAA - http://www. climate.gov, published April 9, 2024. The inset shows the rapid rise in CO2 to 419.3 ppm and temperature anomaly, reference to the pre-industrial period only (1850-1900); data retrieved from www.climate.copernicus.eu (ERA5 reanalysis) and figure adapted from www.temperaturerecord.org.

Temperature fluctuations have been closely linked to atmospheric carbon dioxide (CO_2) levels (**Fig.1.1**; Augustin et al. (2004)). Alarmingly, with the expansion of the human population and particularly since the Industrial Revolution in the 19th century, fossil fuel combustion has driven a drastic rise in CO_2 — from 280 ppm to 420 ppm — exceeding the natural variability by over 100 ppm (Bezić et al., 2022). This rapid increase has had profound global effects, accelerating atmospheric and ocean warming, intensifying ocean acidification (Hofmann & Schellnhuber, 2010), and altering precipitation patterns (Fowler et al., 2021).

Focusing on temperature, the current global warming rate of 0.26 °C per decade (2014–2023; Forster et al. (2024)) far exceeds the natural interglacial rate (~0.01 °C per decade; Bader et al. (2020)). In 2023 alone, annual surface air temperatures averaged 1.5 °C above the last three decades (**Fig. 1.2a**; Cattiaux et al. (2024)). Likewise, global average

sea surface temperature (SST) has increased by over 0.4 °C since 1993 with shallower and semi-enclosed seas experiencing even greater warming (**Fig. 1.2b**; Samset et al. (2024)).

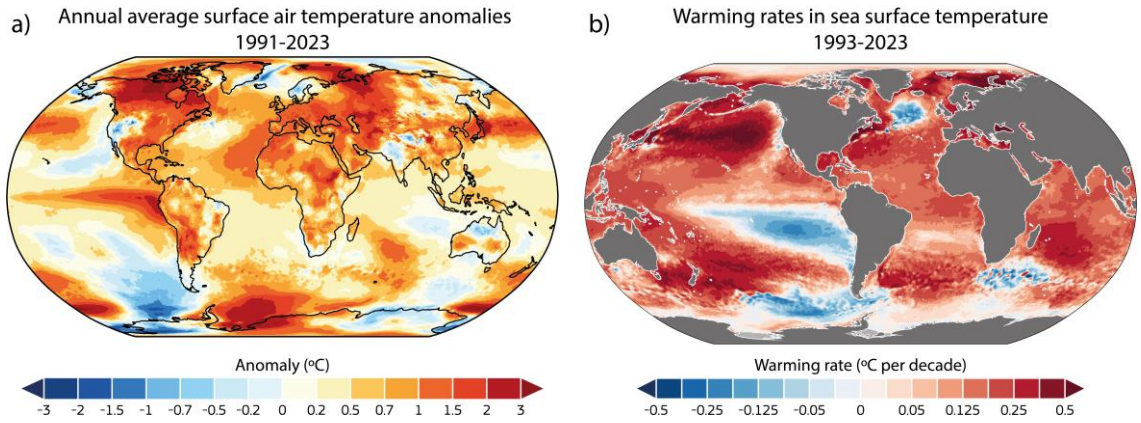


Figure 1.2: a) Mean air surface temperature anomalies (relative to 1991-2023, global mean 0.60 °C); b) Mean Sea surface temperature anomaly (relative to 1993-2023); Adapted from www.climate.copernicus.eu.

Notably, the Arctic Ocean stands out as one of the fastest-warming regions, with increases reaching up to 0.75 °C per decade (Rantanen et al., 2022). Additionally, extreme heat events – including both marine and atmospheric heatwaves - are becoming more frequent and intense (Hennessy et al., 2022; Seneviratne et al., 2021). These increasing temperatures and extreme heat events pose significant challenges for organisms, influencing their survival and adaptability (Garrabou et al., 2022; Raymond et al., 2022; Smith et al., 2024; Zhang et al., 2024). As temperature changes, so do biochemical reactions, which can, to a certain extent, prompt molecular plasticity that enable organisms to tolerate and even thrive in different environments (Carter et al., 2023). However, beyond the species' thermal tolerance, temperature stress can disrupt the organism internal balance, limiting survival and ultimately shaping geographic distribution (Amarasekare, 2024; Clarke, 2003).

1.2. Temperature in the rocky intertidal zone

Although the impacts of temperature changes are being felt across various ecosystems, the intertidal environment may be at greater risk due to its unique exposure to both marine and atmospheric stressors (Mieszkowska et al., 2021). Here, temperature is one of the most critical abiotic factors. Locally, temperature can determine the vertical distribution of organisms based on their thermal resilience, while at broader scales, it

defines distribution boundaries for most intertidal species (Helmuth, Mieszkowska, et al., 2006; Seabra et al., 2011; Somero, 2002). While thermal tolerances to SST often explain species distribution limits (Fischer-Piette, 1955; Lima et al., 2007; Lüning, 1990), increasing evidence highlights the crucial role of temperatures experienced during low tides (Martinez et al., 2012; Pearson et al., 2009; Román et al., 2020).

Monitoring temperature at the intertidal environment can be particularly challenging. Tidal cycles create fast alternating conditions between thermally stable submersion periods and highly variable aerial exposures, creating a harsh and unforgiving environment for in-situ monitoring devices. Traditionally, this has been bypassed through remotely sensed climatic datasets. However, it is becoming increasingly clear that their coarse resolution renders them unsuitable for most studies on the intertidal fringe (Meneghesso et al., 2020; Seabra et al., 2011). During high tide, SST recorded by offshore buoys or satellites can differ considerably from water temperature measured at the nearshore, mostly due to the spatially complex patterns of upwelling waters and variations in cloud cover (Meneghesso et al., 2020; Pfister et al., 2007). Such discrepancies can be more pronounced at low tide when the intertidal zone's complex topography and the variability of aerial factors, such as air temperature, humidity, solar radiation, and wind, combine to generate an intricate thermal mosaic that remote sensing struggles to detect (Helmuth, Broitman, et al., 2006). Crucially, the inaccurate assessment of the thermal characteristics of intertidal habitats can result in misleading conclusions about the heat stress experienced by intertidal organisms. This is particularly concerning, as studies have shown that many of these species are already living close to their thermal tolerance limits (Lima et al., 2016; Somero, 2010).

Alternatively, the widespread use of in-situ temperature loggers has the potential to address some of these limitations by allowing the quantification of thermal landscape characteristics with far more detail. Networks of such loggers can capture small and localised thermal variations, such as cooling upwelling waters or the differences between shaded and sun-exposed areas — all valuable and important details to organisms that remote sensing would likely miss.

While advancements in electronics have increased the availability and capabilities of temperature loggers, the relative importance of each feature depends on the specific ecological question. For example, logger size is often considered a key characteristic, as only smaller devices may be embedded inside gastropod shells and similar structures to create biomimetic devices that can more closely match the thermal properties of their

target organism. Robomussels (Helmuth & Hofmann, 2001) and robolimpets (Lima & Wethey, 2009), which incorporate iButtons (Thermochron, Maxim Integrated Products, USA) and Tidbit temperature loggers (Onset Corporation, USA; Lima and Helmuth (2011)) are examples of such biomimetic devices. These logger models have also been widely used for collecting climatic data (Harley & Lopez, 2005; Helmuth et al., 2002). However, for broad, long-term climatic monitoring networks that do not aim to target specific species (biomimetic), sensor size may be less critical. Here, reliability and servicing costs can take precedence, as the costs of maintaining such network is largely dependent on the logger's memory capacity and battery life, whichever depletes first.

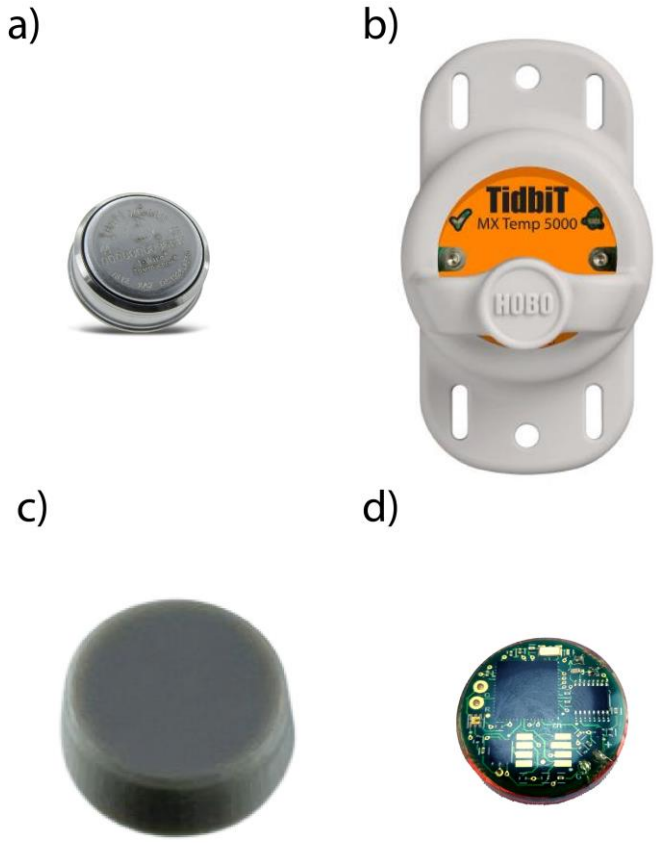


Figure 1.3: a) DS1925L iButton (Thermochron, Maxim Integrated Products, USA); b) HOBO TidbiT MX Temp 5000 (Onset Corporation, USA); c) EnvLogger T7.3 (ElectricBlue CRL, PT); d) Biskit (Alpha Mach, CA).

Recent advancements in temperature logging technology are reshaping how intertidal thermal landscapes can be recorded. For example, the DS1925L iButton (**Fig. 1.3a**) and TidbiT MX (**Fig. 1.3b**) can now record temperature data for up to five years (battery-limited). This is a notable achievement, especially when compared to the DS1922L iButton from 2015, which could not even record for an entire year (at hourly intervals with

0.0625 ºC resolution). Still, in 2022, ElectricBlue, CRL introduced the EnvLogger T7.3 (**Fig. 1.3c**), capable of recording temperature data in a memory module that is large enough to store 15 years of readings (at hourly intervals with 0.1 °C resolution). Additionally, the memory of the EnvLogger T7.3 is non-volatile, meaning that recorded data can be retrieved even after the battery runs out.

While longer-lasting memory modules and batteries are prerequisites for longer deployment periods, the conventional deployment of loggers on the substrate surface exposes them to external threats. This is especially problematic in the intertidal zone, where storms can result in substantial impacts from waves and hurled rocks and debris (Denny, 1985), regularly dislodging and damaging organisms and loggers (Paine & Levin, 1981). The EnvLogger T7.3 is fully encased in resin and relies on Near Field Communication (NFC) for mission programming and data download. This means that EnvLoggers T7.3 are extremely rugged and do not require direct access for data transfer. Unlike the HOBO TidbiT V2, which communicates through light pulses, or the Biskit loggers (**Fig. 1.3d**) that need a special antenna to surround the loggers during data transfer via radio frequency identification (RFID), the Envlogger T7.3 only needs its top side to be tapped with a smartphone for all operations to take place. This, in turn, means that these devices can be deployed inside the rock (up to 18 mm deep), away from external factors that could jeopardise their structure, and still communicate unhindered. Despite the potential benefits to the durability of the loggers brought about by this simple methodological modification, it remains unclear if embedding a logger into the rock could affect the logger's accuracy, as this changes the rate at which heat is transferred to and from the rock (Roznik & Alford, 2012). Additionally, the removal of exposure of the entire logger to incoming solar radiation may further differentiate its readings from loggers deployed at the surface (Huwald et al., 2009), risking a discontinuity with previous datasets built upon surface deployments. Nevertheless, due to its novel features, EnvLoggers are being steadily adopted by the scientific community across various fields, including monitoring thermal conditions in the intertidal environment (Cheng et al., 2024; Parry-Wilson et al., 2024), recording water temperature experienced by sharks (Spurgeon et al., 2024) and assessing temperature variation inside bird nests (Richards et al., 2024).

Lastly, another crucial aspect of field deployment is the choice of sampling frequency. While frequent sampling allows for better characterization of short-term extreme events (e.g., heat waves: Hobday et al. (2016); upwelling surge: Meneghesso et al. (2020)) it can significantly limit the duration of the monitoring mission and lead to cascading

logistical implications that may ultimately restrict the spatiotemporal extent of any given network. Conversely, while less frequent sampling may unburden the logistics of large logger networks, there is a risk that readings may become too scarce to adequately capture the thermal profile of the landscape (Fischer et al., 2021). Selecting an appropriate sampling frequency for temperature loggers in intertidal zones should be guided by specific research goals and the temporal variability of the environment. However, there is still limited understanding of how sampling frequency affects the detection of key thermal events, such as daily extremes and their timings.

1.3. Recreating heat stress

Evaluating the effects of temperature on a species' performance is critical when assessing their vulnerability to current and future climate conditions (Bennett et al., 2021). Typically, researchers evaluate species' thermal limits by transplanting the organisms to other regions or conducting common-garden laboratory experiments (King et al., 2018). The latter method has significant advantages, as it minimizes logistical complexity and allows exposure to environmental conditions beyond those of the experimental location. However, assembling and operating common-garden systems to realistically simulate environmental conditions can involve considerable technical complexity. Naturally, this challenge depends upon the details considered in the experiment. For example, conducting a thermal stress experiment on intertidal organisms often raises the critical question of whether the tidal cycle might influence the results. Although many studies have produced clear results from experiments where intertidal organisms are kept permanently submerged (Freitas et al., 2023; Lourenço et al., 2016; Wilson et al., 2015), the impact of overlooking their unavoidable intertidal cycle can only be fully understood through more comprehensive experiments. In fact, evidence suggests that one should not be considered without the other, as experiments with marine gastropods suggested that elevated air and water temperatures have a compounding effect on thermal stress (Seabra et al., 2016) and that cooling waters during high tides can provide thermal relief, especially during spring tides (Mortensen & Dunphy, 2016). Similarly, studies on macroalgae reveal that heat stress during emersion is important (Finke et al., 2007; Martinez et al., 2012; Román et al., 2020), especially when it occurs at mid-afternoon, when daily air temperatures tend to be higher (Mislan et al., 2009). Furthermore, this effect may be exacerbated by the organism's life history traits, as most intertidal species are slow-moving or sessile, and have short adult life spans (Menge & Branch, 2001).

While various laboratory experiments have examined thermal stress in the context of the intertidal cycle, most have focused on animals, particularly gastropods and bivalves (Barker et al., 2021; Pincebourde et al., 2013; Schneider, 2008; Seabra et al., 2016), with relatively few studies on seaweed species. Importantly, these experimental setups are often custom-built for a single experiment, and it is rare, if not entirely absent, to find similar systems replicated across different research groups. This reveals a lack of standardization, raising concerns about the comparability of these studies. Additionally, analysing heat stress in the intertidal zone by isolating immersion and emersion cycles may limit the ecological relevance of the findings in either situation. Therefore, the development of a standardized laboratory method with automated, long-term control over the critical aspects limiting the intertidal organisms, like tidal cycles, temperature fluctuations during both submersion and emersion, and light, would significantly enhance the assessment of species' thermal thresholds and improve synergy between different research groups.

1.4. Seaweed and climate change

Seaweeds are vital primary producers and ecosystem engineers, playing an essential role in coastal ecosystems that range from deep subtidal kelp forests to intertidal canopies on rocky shores (Lüning, 1990). Canopy-forming seaweeds are particularly important because they are habitat providers, food sources, nursery grounds, and protection from climatic extremes (Cotas et al., 2023; Pfister et al., 2019; Seitz et al., 2013). Furthermore, they hold substantial economic value by supplying food, medicine, and chemicals (Ali et al., 2024). Beyond these tangible benefits, kelp forests alone have been estimated to provide global ecological services valued at approximately $500 billion annually (Eger et al., 2023). Seaweeds also play a critical role in carbon sequestration and are increasingly recognized for their potential in climate change mitigation strategies (Pessarrodona et al., 2024; Ross et al., 2023).

The distribution of seaweeds is primarily determined by their temperature tolerance (Breeman, 1988; Eggert, 2012b) and thus closely follows oceanic isotherms (Lüning, 1990). Recent research has highlighted significant shifts in cold-adapted seaweed distributions during the 21st century, strongly linked to climate change, with contractions predominantly occurring at the warm edge of species' ranges rather than uniformly across their distribution. For instance, along the western coast of Australia, marine heatwaves over the past two decades (>2001) have caused a 43% decline in kelp forests (*Ecklonia radiata*), resulting in a 100 km contraction at their northern warm edge

(Wernberg, 2021). Similarly, in northern California, rising SST has driven a 90% reduction in bull kelp (*Nereocystis luetkeana*) across a 350 km stretch of coastline (Rogers-Bennett & Catton, 2019). However, warm edge contractions may not always be uniform, particularly in regions where local phenomena, such as upwelling, create thermal refugia that disrupt latitudinal trends (Lima et al., 2007). A notable example of heterogenous contraction is the decade-long contraction of seaweeds along the Iberian Peninsula, where populations have retreated towards the northwest, especially east of the Cantabrian Sea, with reductions ranging from 6% to 45% (Casado-Amezúa et al., 2019). Still, these range shifts do not necessarily imply a contraction, as evidence suggests some species may gain suitable habitat at their colder edges, with climate change facilitating a poleward shift in distribution (Jueterbock et al., 2016; Wernberg et al., 2011).

1.5. Seaweeds along the North Atlantic intertidal shores

North Atlantic shores offer a favourable habitat for canopy-forming seaweeds belonging to the Fucaceae family, predominantly in the cold-temperate region (Van den Hoek, 1975). These species are constrained at their northern limit by the summer temperatures (>15 ºC) and at their southern limit by the winter isotherm (<20 ºC) (Van den Hoek, 1975). Low emersion temperatures and ice scour in the northernmost regions restrict canopy-forming species mainly to subtidal zones (Van den Hoek, 1975; Wiencke & Amsler, 2012). Conversely, at the southern boundary, intensified herbivory and warmer, unfavourable climate limits the growth and survival of these species (Lüning, 1990).

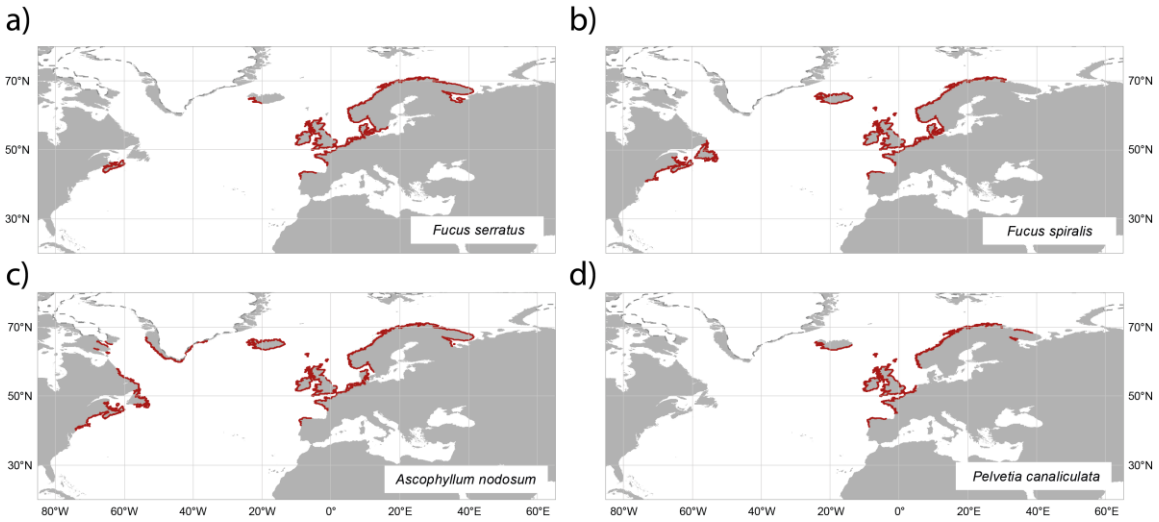


Figure 1.4: Distribution of Fucaceae species in the North Atlantic; a) *Fucus serratus*; b) *Fucus spiralis*; c) *Ascophyllum nodosum*; d) *Pelvetia canaliculata*. Figure adapted from Neiva et al. (2016).

The western Iberian coastline is a biogeographical transition zone where many warm- and cold-adapted species reach their northernmost or southernmost distribution limits (Lima et al., 2007; Rubal et al., 2013). This region acts as a secondary southern boundary for numerous cold-water species following a distribution gap in the Bay of Biscay (Lüning, 1990). This extension is facilitated by the Canary Current upwelling system, which keeps summer SST cool, enabling cold-adapted species to exist further south than they would otherwise (Alvarez et al., 2011). In this region, four fucoids often form dense canopies, dominating the intertidal rocky shores: *Fucus serratus*, *Fucus spiralis*, *Ascophyllum nodosum,* and *Pelvetia canaliculata*. These species have their southern limit near Viana do Castelo (**Fig. 1.4**; northern Portugal 41 ºN), a well-known biogeographic stronghold for cold-adapted species due to the referred upwelling but also its wave-sheltered shore (Fischer-Piette, 1963; Lalegerie & Stengel, 2022; Neiva et al., 2016; Pereira et al., 2022; Pereira et al., 2020). Of these species, *F. serratus* has received the most attention. Studies show that rising SST correlates with the species' range retraction in northern Spain (Álvarez-Losada et al., 2020; Casado-Amezúa et al., 2019). In northern Portugal, however, where summer upwelling supplies colder water, emersion-related heat stress is believed to limit its upper intertidal boundary (Pearson et al., 2009). Combined, these high- and low-tide impacts suggest that Iberian populations may struggle to cope with a warming climate.

Research on the climate vulnerability of *F. spiralis* and *P. canaliculata* is relatively rare. However, long-term surveys (1977–2007) in northern Iberia have reported decreased biomass for *P. canaliculata* and reduced growth for *F. spiralis*, both correlated with rising air and SST (Lamela-Silvarrey et al., 2012). Similarly, a fine-scale assessment of the distributional limits of several macroalgae in NW Iberia reported the absence of both species from historical sites (Monteiro et al., 2022). Furthermore, edge populations of these fucoids appear to have lost genetic diversity through cycles of extinction and recolonization driven by thermal stress (Coyer et al., 2003; Olsen et al., 2010); such genetic erosion could further compromise their resilience to environmental challenges (Jueterbock et al., 2018; Orr & Unckless, 2008). As ecosystem engineers, these seaweeds are crucial in moderating environmental conditions and reducing stress for their associated organisms. Their persistence will be increasingly vital for maintaining ecosystem functions under the warmer and more stressful conditions projected for the future (Halpern et al., 2007).

1.6. The canopy-forming seaweed *Ascophyllum nodosum*

Ascophyllum nodosum is a perennial brown seaweed belonging to the order Fucales, and the only species in its genus. It is characterized by an olive-green branching system that can reach up to 200 cm in length (**Fig. 1.5a**, Pereira et al. (2020)). This system includes a primary thallus with apical growth and several secondary branches of limited growth. These secondary branches emerge either as lateral shoots from the primary thallus or directly from the holdfast — a discoid structure that anchors the seaweed to rocky surfaces. While smaller and slower-growing, holdfast-derived branches can take over full growth if the primary axis is lost. After the first two years, air bladders develop annually on the branches emerging from the base, providing buoyancy and increasing the ability to capture light during high tide (Baardseth, 1955; Garbary et al., 2019). The species is dioecious and long-living (50–60 years; (Åberg, 1992)). The reproduction season occurs in late spring and is characterized by a brief receptacle maturation (lasting just a few days) followed by gamete release over about two 'spring' tidal cycles (Bacon & Vadas, 1991).

a) **b)**



Figure 1.5: a) Measurement of *Ascophyllum nodosum* with 186 cm at Soulougan (France; Latitude: 48.672389; Longitude: -4.313694) b) *Ascophyllum nodosum* dense canopy during low tide in Île-Tudy (France; Latitude: 47.839222; Longitude: -4.169472).

On rocky shores dominated by *Ascophyllum nodosum*, it creates an intricate rope-like covering, which has led to its common name, "knotted wrack" (**Fig. 1.5b**). On the East Atlantic, it ranges from northern Norway (69.7 ºN) to the northwest (NW) coast of the Iberian peninsula (41.3 ºN; Åberg (1996)).

Studies suggest that factors such as the absence of sheltered rocky shores and elevated summer water temperatures are responsible for the distribution gaps in the southern part of the North Sea and the Bay of Biscay (**Fig. 1.4c**; Lüning (1990)). Despite these distribution gaps, *A. nodosum* is one of the most widespread cold-adapted seaweeds of the North Atlantic (Garbary & Deckert, 2001). However, previous analyses have also shown that this has not always been the case, with significant expansions and retractions following major climatic changes. During the last glacial maximum (LGM), around 20 kya, low temperatures pushed *A. nodosum* southwards into the periglacial refugia (Olsen et al., 2010). In these refugia, *A. nodosum* survived during the cold period. Once the LGM ended, the surviving populations expanded northwards and re-established again along the northern coastlines, an expansion that continued during the Holocene (Assis et al., 2016).

Thermal tolerances can vary significantly among populations due to local adaptation and/or phenotypic plasticity, resulting in different thermal ecotypes across a species' geographic range (Sanford & Kelly, 2011). Recognizing these population-specific variations is critical for accurately assessing vulnerability to climate change, particularly for species with broad distributions spanning diverse thermal environments (Bennett et al., 2015; King et al., 2018). Previous studies evaluating the vulnerability of *A. nodosum* to climate change, employing both mechanistic and modelling approaches, have consistently indicated that climate change could prompt a poleward shift in its range (Hernández et al., 2023; Jueterbock et al., 2013; Westmeijer et al., 2019). However, these studies often disregard regional variations in thermal tolerance or focus too narrowly on responses to elevated sea temperatures, neglecting the role of emersion stress and thermal ecotypes. For instance, evidence from laboratory experiments focused solely on SST tolerance suggested that the thermal niche of southern populations could extend south of the Iberian Peninsula (Hernández et al., 2023). However, field surveys of southern Iberian Peninsula populations show that they not only experience higher mortality rates than northern populations but also persist in this region due to increased reproductive investment at the expense of growth (Araujo et al., 2014). These contradicting evidence between thermally adapted and struggling warm-edge populations, indicates that the factors defining the distribution limits of *A. nodosum* may be mischaracterised.

1.7. Analysing heat stress responses in seaweeds

To quantify the impact of climate change on a species, it is critical to evaluate its responses to rising temperatures (e.g., Williams et al., 2008; Sorte et al., 2010a; Sorte et al., 2011). As species are exposed to temperatures beyond their optimal range, their fitness typically declines due to physiological stress, reducing growth, reproduction, and survival (Eggert, 2012a; Schulte et al., 2011).

1.7.1. Photosynthetic performance

Rising temperatures can impair the efficiency of photosynthetic reaction centres (Berry & Bjorkman, 1980) in photosynthetic organisms, and therefore, assessing photosynthetic efficiency provides an immediate indication of heat stress. When a photosynthetic organism absorbs light, its energy drives an electron transport chain (ETC) from Photosystem II (PSII) to Photosystem I (PSI). The mobilized electrons enable the photochemical processes within each photosystem and ultimately lead to the formation of NADPH and ATP, which are required for carbon fixation in the Calvin cycle (**Fig. 1.6**; Baker (2008), Schreiber et al. (1995)).

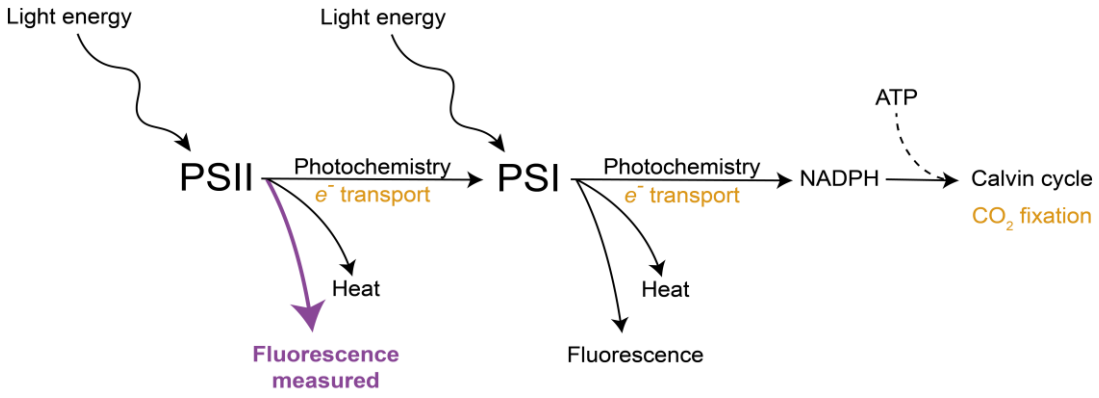


Figure 1.6: Light activation energy in the reaction centres of photosystem (PS) I and PS II is used for photochemical work and emitted as heat and chlorophyll-a fluorescence. Photochemical work reduces NADP+ to NADPH, which is required for carbon fixation in the Calvin Cycle. Figure based on Baker (2008) and (Schreiber et al., 1995).

However, part of the absorbed energy is lost as heat and chlorophyll-*a* fluorescence at both PSII and PSI. Under temperature stress, the efficiency of the photosynthetic reaction centres in transferring energy to the ETC declines. As the less absorbed light energy is used on the ETC, more energy is emitted as heat and chlorophyll fluorescence from both reaction centres. Due to the particular sensitivity of the PSII and greater

fluorescence compared to PSI, its fluorescence provides a marker for assessing photosynthetic performance and stress. The rise in chlorophyll-*a* fluorescence and the corresponding decrease in photosynthetic performance can be measured with a fluorometer by tracking the increase in fluorescence upon light exposure. Since fluorescence depends on recent light exposure, photosynthetic efficiency is often quantified by measuring the variable fluorescence (F_v), which is the difference between minimum (F_0) and maximum (F_m) fluorescence. However, because both F_0 and F_m can be influenced by heat stress, as well as other factors like plant development stage or chlorophyll content, studies typically use the ratio of F_v to F_m, also known as Maximum PSII Efficiency (F_v/F_m), to provide a normalised measurement of photosynthetic performance (Maxwell & Johnson, 2000).

1.7.2. Oxygen production

While PSII efficiency provides immediate insights into potential structural damage affecting the early stages of light absorption, it does not fully account for downstream processes such as PSI inefficiency, carbon fixation, ATP utilization, nutrient limitations,

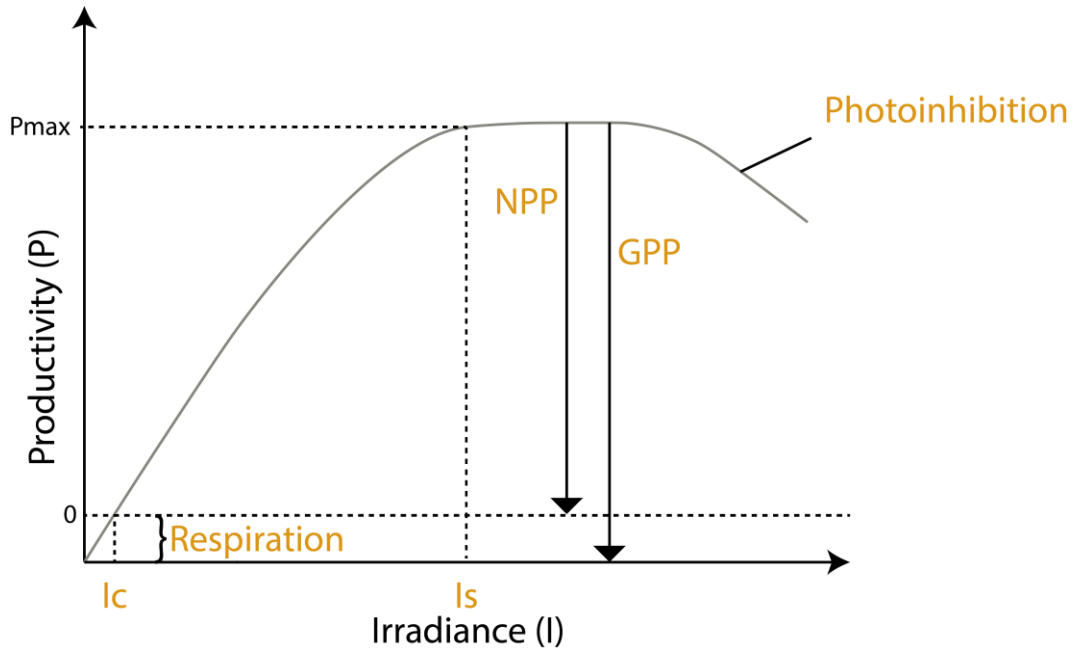


Figure 1.7: Oxygen productivity (P) in response to Irradiance (I). Net primary production (NPP) results from the deduction of basal oxygen consumption (Respiration) upon the gross primary production (GPP). The compensation point (IC) refers to the light intensity at which neutral NPP is achieved. In contrast, the saturation point refers to the light intensity that promotes the highest GPP, beyond which light intensity becomes excessive and causes photoinhibition. Figure based on Eilers and Peeters (1988) and Lalli and Parsons (1997).

or increased respiration. Oxygen production, on the other hand, directly measures the end product of photosynthesis and is, therefore, directly correlated to growth and survival in photosynthetic organisms (Holloway-Phillips, 2018; Martins et al., 2023).

Evidence suggests that seaweeds may produce more oxygen at elevated temperatures (Hanelt et al., 2003). However, the increased metabolic demands can lead to higher respiration rates, potentially decreasing overall productivity and growth (Tait & Schiel, 2013; Vona et al., 2004). Therefore, some studies suggest that the susceptibility of seaweeds to warming environments might be inferred from the temperature dependence of photosynthesis and respiration (Eggert & Wiencke, 2000; Piñeiro-Corbeira et al., 2018; Staehr & Wernberg, 2009). In contrast, the predicted rise in ocean CO_2 concentration is likely to positively affect growth and photosynthesis because most marine photosynthesis is carbon-limited (Koch et al., 2013). However, in coastal environments, such as seagrass beds and kelp forests, such correlation is unlikely to hold, as the predicted rise in CO_2 remains lower than the currently observed natural variability (Duarte et al., 2018; Saderne et al., 2013).

In seaweed, the thermal response of productivity has traditionally been measured in the laboratory, using chambers that control abiotic factors and electrodes capable of detecting oxygen levels (Hatcher et al., 1977). Because photosynthesis varies with light intensity, oxygen production must be quantified across a range of light levels. This is done through Photosynthesis-Irradiance (P-I) curves, assessing oxygen production rates under different light intensities. To obtain a P-I curve, photosynthetic organisms must be exposed to light levels from darkness to saturation — and even potential photoinhibition (**Fig. 1.7**). In the presence of light, organisms will consume and produce oxygen. Under favourable conditions, oxygen production will exceed consumption, and a net positive oxygen balance will be observed, corresponding to net primary production (NPP). To determine the baseline oxygen consumption (respiration rate), organisms are placed in complete darkness, where only oxygen consumption occurs. Adding respiration to NPP informs on the gross primary production (GPP). This P-I curve also provides other key photosynthetic parameters, such as the compensation point (where oxygen production balances respiration; I_c) and the saturation point (where photosynthesis plateaus I_s), offering a more comprehensive view of the organism's productivity and light adaptation (Eilers & Peeters, 1988; Lalli & Parsons, 1997).

It is also important to consider that while elevated temperatures can increase oxygen production in seaweeds and initially benefit photosynthetic efficiency, high temperatures

also raise levels of reactive oxygen species (ROS), leading to oxidative stress and potential cellular damage (Collen, 1999; Dring, 2005). Research suggests that rising temperatures can disrupt the balance between ROS production and the seaweed's antioxidant defences (Bischof & Rautenberger, 2012). Although still poorly studied, especially under the scope of climate change, heat stress during emersion cycles may serve as a significant trigger for ROS production in seaweeds (Contreras-Porcia et al., 2010; Maharana et al., 2015; Martins et al., 2021).

1.8. Forecasting species responses to climate change

To predict species' responses to future climatic-driven environmental changes, it is first necessary to infer its climatic niche. This can be achieved using one of two fundamentally different approaches: either correlative or mechanistic (Kearney, 2006; Kearney & Porter, 2009). The first, often referred to as "Ecological Niche Modelling" (ENM) or "Species Distribution Modelling" (SDM), estimates a species' realized niche space (the set of conditions required for a suitable habitat) by analysing the relationship between the species geographic distribution and the environmental conditions where it occurs. The main advantage of this method compared to a mechanistic approach is that it allows researchers to build distribution-wide models without requiring empirical fitness data from every site. However, these correlative approaches have a notable limitation: they often overlook available knowledge about the species physiology, life history, and population-specific thermal tolerances (e.g., thermal ecotypes; (Straub et al., 2019). In contrast, the mechanistic approach is based on a species' physiological response to external drivers, often determined through laboratory common-garden experiments (Westmeijer et al., 2019). This enables the evaluation of distinct physiological responses and the incorporation of population-specific heat tolerance information, which can offer a better understanding of species' climatic tolerance and their potential responses to future climatic changes.

Once species' climatic limits have been established, these can be projected onto predicted future environmental conditions to assess species responses. This process helps identify potential habitat loss or expansion and, consequently, shifts in species' geographic distributions. Predictive models of future environmental conditions commonly explore hypothetical trajectories of radiative climate forcing and underlying greenhouse gas emissions (**Fig. 1.8**; O'Neill et al. (2014), Van Vuuren et al. (2011)) widely used framework is the Shared Socioeconomic Pathways (SSPs), which outline five distinct socioeconomic storylines.

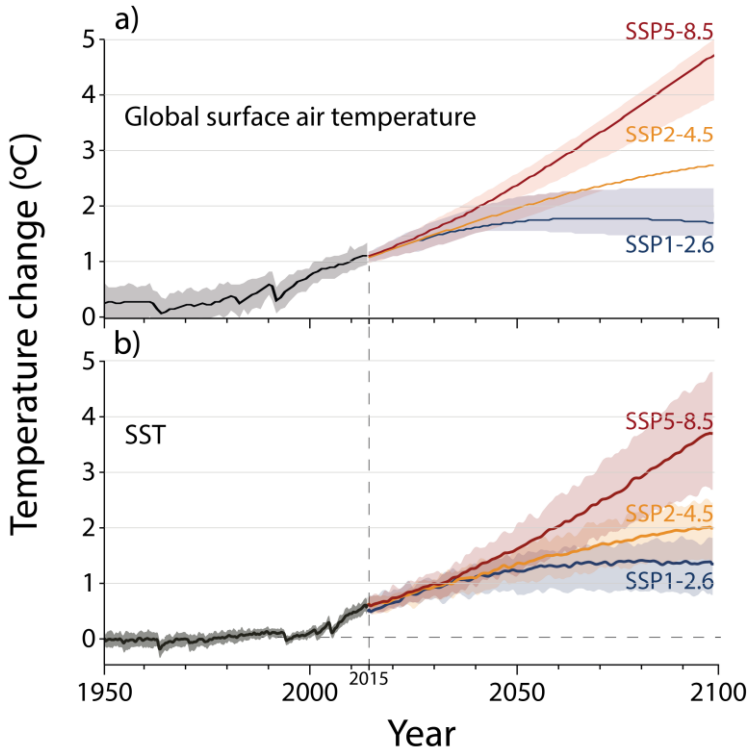


Figure 1.8: a) Global surface air temperature change between 1950-2100 as a difference to the 1850-1900 period; b) Sea surface temperature (SST) change since 1950-2100 as a difference to the 1950-1980 period. Both refer to model projections built upon the historical data until the end of 2014. These are an adaptation of figures Figure SPM.8 (Chapter 8) and Figure SPM.9.3 (Chapter 9) from the IPCC 6th Assessment Report WGI Summary for Policy Makers (IPCC, 2022).

These represent different global development trajectories, each with varying levels of challenges and adaptations to climate change experienced by societies (Riahi et al., 2017). These scenarios are directly correlated with analogous Representative Concentration Pathways (RCP Van Vuuren et al. (2011)). While both frameworks provide a guideline for climatic prediction, SSPs may prove more intuitive as they refer to the path societies must follow to achieve each scenario rather than focusing solely on the physical outcomes of greenhouse gas concentrations, as represented by RCPs.

The projected responses of species to climate change can vary significantly depending on the methods used to estimate climatic tolerance and the scenarios selected for prediction. Based on a correlative approach, a recent study that modelled the suitable habitat for 207 macrophytes, showed the loss in area of occupancy to be dependent of the climatic trajectory, ranging from 5% at SSP2 to 11% at SSP5 by 2100 (Manca et al., 2024). Although, these do not consider mechanistic information. Several studies based

on mechanistic approaches have found that macrophytes populations from lower latitudes show high tolerance to increasing temperatures (Bennett et al., 2022; Chiaramonte et al., 2024; King et al., 2019; Sandoval-Castillo et al., 2020). In fact, a study focusing on kelp (*Ecklonia radiata*) found thermal plasticity among populations, predicting that at higher temperatures, cooler-edge populations will have higher densities but consist of smaller individuals due to trade-offs between survival and growth (Veenhof et al., 2024). These findings highlight the importance of accounting thermal ecotypes and varying population demographic structures when predicting species response to climatic change. Nevertheless, even when mechanistic information is considered, its predictive power can be hindered by experimental designs that do not accurately reflect natural conditions. As discussed for *A. nodosum*, a mismatch between these findings and field observations limits our ability to accurately infer the species' current thermal niche and, consequently, predict its response to future climatic changes.

1.9. Work outline

This thesis is structured as a compilation of six Chapters. **Chapter 1** provides a general introduction, while **Chapters 2** through **5** present four submitted manuscripts focused on advancing the assessment of thermal stress patterns in the intertidal environment. Finally, **Chapter 6** provides a general discussion that integrates and synthesizes the findings of this thesis.

In **Chapter 2,** we address the challenges of measuring temperature at the scale of individual organisms, particularly in intertidal environments. In these ecosystems, in-situ sensors have been shown to more accurately reflect the thermal stress experienced by organisms. However, the harsh conditions of the intertidal zone often compromise the durability of traditional surface-deployed sensors. To tackle this issue, we evaluate the performance of a robust, rock-embedded temperature sensors and compare it to conventional surface-deployed ones.

Pereira, F. L., Seabra R., Silva, R., Loureiro, B., Lima F. P. (Submitted). Autonomous, high-frequency and long-term monitoring of substrate temperature in rocky intertidal zones.

In **Chapter 3**, we address the significant technical challenges of replicating the complex conditions of intertidal environments by developing and testing the Intertidal Environmental Chamber, an open-source system designed to precisely simulate intertidal conditions by controlling tides, light, temperatures during high and low tides, and water exchange.

Pereira, F. L., Seabra R., Loureiro, B., Arenas, F., Lima F. P. (Submitted). Intertidal Environmental Chamber: an automatic system to accurately simulate the thermal complexity of intertidal environments.

Chapter 4 builds on the previous technical developments to investigate the physiological responses of four key macroalgae species (*Fucus serratus*, *Fucus spiralis*, *Ascophyllum nodosum*, and *Pelvetia canaliculata*) at their southern distribution limit, in the northwest of the Iberian Peninsula.

Pereira, F. L., Monteiro, C., Serôdio, J., Silva J., Teixeira, J., Seabra, R., Lima F. P., Arenas, F. (Submitted). Intertidal Fucales response to realistic temperature stress.

In **Chapter 5**, we examine geographical variability in heat tolerance among multiple intertidal fucoid *Ascophyllum nodosum* populations across its European range. Using detailed physiological data, we modelled population-specific thermal stress tolerance and incorporated this variability into localized climate projections to evaluate resilience.

Pereira, F. L., Arenas, F., Seabra, R., Silva, R., Monteiro, C., Pereira, J., Vale, C. G., Serôdio, J., Frankenback, S., Ghiglione, V., Ribeiro, P., Lima F. P. (Submitted) Heat stress on the brown seaweed *Ascophyllum nodosum*: differential population sensitivity to future climate.

Additionally, this thesis appendix includes three other devices I have developed. Although these methodologies were not directly employed in the thesis, they were designed to improve ecological experiments and are shared in an open-source framework to enhance researchers' access to innovative tools.

1.10. References

Åberg, P. (1992). Size_based demography of the seaweed ascophyllum nodosum in stochastic environments. *Ecology*, *73(4)*, 1488-1501. https://doi.org/10.2307/1940692

Åberg, P. (1996). Patterns of reproductive effort in the brown alga Ascophyllum nodosum. https://doi.org/10.3354/meps138199

Ali, M. Q., Azhar, M. A., Munaim, M. S. A., Ruslan, N. F., Alsubhi, L. M., Ahmad, N., & Noman, A. E. (2024). Seaweed organic compounds source of hydrocolloids and sustainable food packaging: properties, application, and future direction. *Discover Food*, *4*(1), 101. https://doi.org/10.1007/s44187-024-00173-w

Álvarez-Losada, Ó., Arrontes, J., Martínez, B., Fernández, C., & Viejo, R. M. (2020). A regime shift in intertidal assemblages triggered by loss of algal canopies: A multidecadal survey. *Marine environmental research*, *160*, 104981. https://doi.org/10.1016/j.marenvres.2020.104981

Alvarez, I., Gomez-Gesteira, M., deCastro, M., Lorenzo, M. N., Crespo, A. J. C., & Dias, J. M. (2011). Comparative analysis of upwelling influence between the western and northern coast of the Iberian Peninsula. *Continental Shelf Research*, *31*(5), 388-399. https://doi.org/10.1016/j.csr.2010.07.009

Amarasekare, P. (2024). Temperature-dependent dispersal and ectotherm species' distributions in a warming world. *Journal of Animal Ecology*, *93*(4), 428-446. https://doi.org/10.1111/1365-2656.14054

Araujo, R. M., Serrao, E. A., Sousa-Pinto, I., & Åberg, P. (2014). Spatial and temporal dynamics of fucoid populations (*Ascophyllum nodosum* and *Fucus serratus*): a comparison between central and range edge populations. *PLoS One*, *9*(3), e92177. https://doi.org/10.1371/journal.pone.0092177

Assis, J., Lucas, A. V., Barbara, I., & Serrao, E. A. (2016). Future climate change is predicted to shift long-term persistence zones in the cold-temperate kelp Laminaria hyperborea. *Marine environmental research*, *113*, 174-182. https://doi.org/10.1016/j.marenvres.2015.11.005

Augustin, L., Barbante, C., Barnes, P., Barnola, J., Bigler, M., Castellano, E., & a/., e. (2004). Eight glacial cycles from an Antarctic ice core. *Nature*, *429*(6992), 623-628. https://doi.org/10.1038/nature02599

Baardseth, E. M. (1955). *Regrowth of Ascophyllum nodosum after harvesting*. Institute for Industrial Research and Standards.

Bacon, & Vadas. (1991). A model for gamete release in Ascophyllum nodosum. *Journal of Phycology*, *27*, 166-173. https://doi.org/10.1111/j.0022-3646.1991.00166.x

Bader, J., Jungclaus, J., Krivova, N., Lorenz, S., Maycock, A., Raddatz, T., Schmidt, H., Toohey, M., Wu, C.-J., & Claussen, M. (2020). Global temperature modes shed light on the Holocene temperature conundrum. *Nature Communications*, *11*(1), 4726. https://doi.org/10.1038/s41467-020-18478-6

Baker, N. R. (2008). Chlorophyll fluorescence: a probe of photosynthesis in vivo. *Annual review of plant biology*, *59*(1), 89-113. https://doi.org/10.1146/annurev.arplant.59.032607.092759

Barker, C., Monaco, C. J., & McQuaid, C. D. (2021). Exposure to fluctuating temperature increases thermal sensitivity in two lineages of the intertidal mussel Perna perna. *Marine Ecology Progress Series*, *668*, 85-95. https://doi.org/10.3354/meps13713

Bennett, J. M., Sunday, J., Calosi, P., Villalobos, F., Martinez, B., Molina-Venegas, R., Araujo, M. B., Algar, A. C., Clusella-Trullas, S., Hawkins, B. A., Keith, S. A., Kuhn, I., Rahbek, C., Rodriguez, L., Singer, A., Morales-Castilla, I., & Olalla-Tarraga, M. A. (2021). The evolution of critical thermal limits of life on Earth. *Nature Communications*, *12*(1), 1198. https://doi.org/10.1038/s41467-021-21263-8

Bennett, S., Vaquer-Sunyer, R., Jordá, G., Forteza, M., Roca, G., & Marbà, N. (2022). Thermal Performance of Seaweeds and Seagrasses Across a Regional Climate Gradient. *Frontiers in Marine Science*, *9*. https://doi.org/10.3389/fmars.2022.733315

Bennett, S., Wernberg, T., Arackal Joy, B., de Bettignies, T., & Campbell, A. H. (2015). Central and rear-edge populations can be equally vulnerable to warming. *Nature Communications*, *6*, 10280. https://doi.org/10.1038/ncomms10280

Berry, J., & Bjorkman, O. (1980). Photosynthetic response and adaptation to temperature in higher plants. *Annual Review of plant physiology*, *31*(1), 491-543. https://doi.org/10.1146/annurev.pp.31.060180.002423

Bezić, H., Mance, D., & Balaž, D. (2022). Panel evidence from EU countries on CO2 emission indicators during the Fourth Industrial Revolution. *Sustainability*, *14*(19), 12554. https://doi.org/10.3390/su141912554

Bischof, K., & Rautenberger, R. (2012). Seaweed Responses to Environmental Stress: Reactive Oxygen and Antioxidative Strategies. In *Seaweed Biology* (pp. 109-132). https://doi.org/10.1007/978-3-642-28451-9_6

Breeman, A. (1988). Relative importance of temperature and other factors in determining geographic boundaries of seaweeds: experimental and phenological evidence. *Helgoländer Meeresuntersuchungen*, *42*, 199-241. https://doi.org/10.1007/BF02366043

Byun, A., Koop, B., & Reimchen, T. (1999). Coastal refugia and postglacial recolonization routes: a reply to Demboski, Stone, and Cook. *Evolution*, 2013-2015. https://doi.org/10.2307/2640463

Carter, M. J., Cortes, P. A., & Rezende, E. L. (2023). Temperature variability and metabolic adaptation in terrestrial and aquatic ectotherms. *Journal of Thermal Biology*, *115*, 103565. https://doi.org/10.1016/j.jtherbio.2023.103565

Casado-Amezúa, P., Araújo, R., Bárbara, I., Bermejo, R., Borja, Á., Díez, I., Fernández, C., Gorostiaga, J., Guinda, X., & Hernández, I. (2019). Distributional shifts of canopy-forming seaweeds from the Atlantic coast of Southern Europe. *Biodiversity and Conservation*, *28*(5), 1151-1172. https://doi.org/10.1007/s10531-019-01716-9

Cattiaux, J., Ribes, A., & Cariou, E. (2024). How Extreme Were Daily Global Temperatures in 2023 and Early 2024? *Geophysical Research Letters*, *51*(19), e2024GL110531. https://doi.org/10.1029/2024GL110531

Cheng, M., Zamora, L., Ragg, N., Hickey, A., & Dunphy, B. (2024). Responses of the New Zealand green-lipped mussel, Perna canaliculus, to acute environmental changes designed to depress metabolism. *Aquaculture*, *580*, 740332. https://doi.org/10.1016/j.aquaculture.2023.740332

Chiaramonte, A. R., Faria, A. V., & Plastino, E. M. (2024). Thermal tolerance of the red alga Gracilaria caudata reveals ecotypes for the Brazilian coast. *Journal of Applied Phycology*, *36*(2), 1009-1022. https://doi.org/10.1007/s10811-023-03048-2

Clarke, A. (2003). Costs and consequences of evolutionary temperature adaptation. *Trends in Ecology & Evolution*, *18*(11), 573-581. https://doi.org/10.1016/j.tree.2003.08.007

Collen, J. D., R. (1999). Reactive oxygen production and damage in intertidal Fucus spp. (Phaeophyceae). *Journal of Phycology*, *35*, 54-61. https://doi.org/10.1046/j.1529-8817.1999.3510054.x

Contreras-Porcia, L., Thomas, D., Flores, V., & Correa, J. (2010). Tolerance to oxidative stress induced by desiccation in Porphyra columbina (Bangiales, Rhodophyta). *Journal of experimental botany*, *62*, 1815-1829. https://doi.org/10.1093/jxb/erq364

Cotas, J., Gomes, L., Pacheco, D., & Pereira, L. (2023). Ecosystem Services Provided by Seaweeds. *Hydrobiology*, *2*(1), 75-96. https://doi.org/10.3390/hydrobiology2010006

Coyer, J., Peters, A., Stam, W., & Olsen, J. (2003). Post-ice age recolonization and differentiation of Fucus serratus L.(Phaeophyceae; Fucaceae) populations in Northern Europe. *Molecular Ecology*, *12*(7), 1817-1829. https://doi.org/10.1046/j.1365-294x.2003.01850.x

Dring, M. J. (2005). Stress Resistance and Disease Resistance in Seaweeds: The Role of Reactive Oxygen Metabolism. In *Incorporating Advances in Plant Pathology* (pp. 175-207). https://doi.org/10.1016/s0065-2296(05)43004-9

Duarte, B., Martins, I., Rosa, R., Matos, A. R., Roleda, M. Y., Reusch, T. B. H., Engelen, A. H., Serrão, E. A., Pearson, G. A., Marques, J. C., Caçador, I., Duarte, C. M., & Jueterbock, A. (2018). Climate Change Impacts on Seagrass Meadows and Macroalgal Forests: An Integrative Perspective on Acclimation and Adaptation Potential [Review]. *Frontiers in Marine Science*, *5*(190). https://doi.org/10.3389/fmars.2018.00190

Eger, A. M., Marzinelli, E. M., Beas-Luna, R., Blain, C. O., Blamey, L. K., Byrnes, J. E. K., Carnell, P. E., Choi, C. G., Hessing-Lewis, M., Kim, K. Y., Kumagai, N. H., Lorda, J., Moore, P., Nakamura, Y., Perez-Matus, A., Pontier, O., Smale, D., Steinberg, P. D., & Verges, A. (2023). The value of ecosystem services in global marine kelp forests. *Nat Commun*, *14*(1), 1894. https://doi.org/10.1038/s41467-023-37385-0

Eggert, A. (2012a). Seaweed Responses to Temperature. In C. Wiencke & K. Bischof (Eds.), *Seaweed Biology: Novel Insights into Ecophysiology, Ecology and Utilization* (pp. 47-66). Springer Berlin Heidelberg. https://doi.org/10.1007/978-3-642-28451-9_3

Eggert, A. (2012b). Seaweed Responses to Temperature. In *Seaweed Biology* (pp. 47-66). https://doi.org/10.1007/978-3-642-28451-9_3

Eggert, A., & Wiencke, C. (2000). Adaptation and acclimation of growth and photosynthesis of five Antarctic red algae to low temperatures. *Polar Biology*, *23*, 609-618. https://doi.org/10.1007/s003000000130

Eilers, P. H. C., & Peeters, J. C. H. (1988). A model for the relationship between light intensity and the rate of photosynthesis in phytoplankton. *Ecological Modelling*. https://doi.org/10.1016/0304-3800(88)90057-9

Finke, G. R., Navarrete, S. A., & Bozinovic, F. (2007). Tidal regimes of temperate coasts and their influences on aerial exposure for intertidal organisms. *Marine Ecology Progress Series*, *343*, 57-62. https://doi.org/10.3354/meps06918

Fischer-Piette, E. (1955). *Répartition, le long des côtes septentrionales de l'Espagne, des principales espèces peuplant les rochers intercotidaux.* (Vol. 31). Masson et Cie.

Fischer-Piette, E. (1963). La distribution des principaux organisms nord-ibériques en 1954-55. *Annales de l'Institut Océanographique Paris 40*(3), 165-311.

Fischer, P., Dietrich, P., Achterberg, E. P., Anselm, N., Brix, H., Bussmann, I., Eickelmann, L., Flöser, G., Friedrich, M., Rust, H., Schütze, C., & Koedel, U. (2021). Effects of Measuring Devices and Sampling Strategies on the Interpretation of Monitoring

Data for Long-Term Trend Analysis [Original Research]. *Frontiers in Marine Science*, *8*. https://doi.org/10.3389/fmars.2021.770977

Forster, P. M., Smith, C., Walsh, T., Lamb, W. F., Lamboll, R., Hall, B., Hauser, M., Ribes, A., Rosen, D., & Gillett, N. P. (2024). Indicators of Global Climate Change 2023: annual update of key indicators of the state of the climate system and human influence. *Earth System Science Data*, *16*(6), 2625-2658. https://doi.org/10.5194/essd-16-2625-2024

Fowler, H. J., Lenderink, G., Prein, A. F., Westra, S., Allan, R. P., Ban, N., Barbero, R., Berg, P., Blenkinsop, S., & Do, H. X. (2021). Anthropogenic intensification of short-duration rainfall extremes. *Nature Reviews Earth & Environment*, *2*(2), 107-122. https://doi.org/10.1038/s43017-020-00128-6

Freitas, D., Arenas, F., Vale, C. G., Pinto, I. S., & Borges, D. (2023). Warning of warming limpets: sea temperature effects upon intertidal rocky assemblages. *Journal of the Marine Biological Association of the United Kingdom*, *103*. https://doi.org/10.1017/s0025315422001096

Garbary, D., & Deckert, R. (2001). Three part harmony—Ascophyllum and its symbionts. In *Symbiosis: mechanisms and model systems* (pp. 309-321). Springer. https://doi.org/10.1007/0-306-48173-1_19

Garbary, D. J., Brackenbury, A., McLean, A. M., & Morrison, D. (2019). Structure and development of air bladders inFucusandAscophyllum(Fucales, Phaeophyceae). *Phycologia*, *45*(5), 557-566. https://doi.org/10.2216/05-62.1

Garrabou, J., Gomez-Gras, D., Medrano, A., Cerrano, C., Ponti, M., Schlegel, R., Bensoussan, N., Turicchia, E., Sini, M., Gerovasileiou, V., Teixido, N., Mirasole, A., Tamburello, L., Cebrian, E., Rilov, G., Ledoux, J. B., Souissi, J. B., Khamassi, F., Ghanem, R., . . . Harmelin, J. G. (2022). Marine heatwaves drive recurrent mass mortalities in the Mediterranean Sea. *Global Change Biology*, *28*(19), 5708-5725. https://doi.org/10.1111/gcb.16301

Gavin, D. G., Fitzpatrick, M. C., Gugger, P. F., Heath, K. D., Rodríguez-Sánchez, F., Dobrowski, S. Z., Hampe, A., Hu, F. S., Ashcroft, M. B., Bartlein, P. J., Blois, J. L., Carstens, B. C., Davis, E. B., de Lafontaine, G., Edwards, M. E., Fernandez, M., Henne, P. D., Herring, E. M., Holden, Z. A., . . . Williams, J. W. (2014). Climate refugia: joint inference from fossil records, species distribution models and phylogeography. *New Phytologist*, *204*(1), 37-54. https://doi.org/https://doi.org/10.1111/nph.12929

Halpern, B. S., Silliman, B. R., Olden, J. D., Bruno, J. P., & Bertness, M. D. (2007). Incorporating positive interactions in aquatic restoration and conservation. *Frontiers in Ecology and the Environment*, *5*(3), 153-160. https://doi.org/10.1890/1540-9295(2007)5[153:IPIIAR]2.0.CO;2

Hanelt, D., Wiencke, C., & Bischof, K. (2003). Photosynthesis in marine macroalgae. In *Photosynthesis in algae* (pp. 413-435). Springer. https://doi.org/10.1007/978-94-007-1038-2_18

Harley, C. D. G., & Lopez, J. P. (2005). The natural history, thermal physiology, and ecological impacts of intertidal mesopredators, Oedoparena spp. (Diptera: Dryomyzidae). *Invertebrate Biology*, *122*(1), 61-73. https://doi.org/10.1111/j.1744-7410.2003.tb00073.x

Hatcher, B., Chapman, A. O., & Mann, K. (1977). An annual carbon budget for the kelp Laminaria longicruris. *Marine Biology*, *44*, 85-96. https://doi.org/10.1007/BF00386909

Helmuth, B., Broitman, B. R., Blanchette, C. A., Gilman, S., Halpin, P., Harley, C. D. G., O'Donnell, M. J., Hofmann, G. E., Menge, B., & Strickland, D. (2006). Mosaic Patterns of Thermal Stress in the Rocky Intertidal Zone: Implications for Climate Change. *Ecological monographs*, *76*(4), 461-479. https://doi.org/10.1890/0012-9615(2006)076[0461:Mpotsi]2.0.Co;2

Helmuth, B., Harley, C. D., Halpin, P. M., O'Donnell, M., Hofmann, G. E., & Blanchette, C. A. (2002). Climate change and latitudinal patterns of intertidal thermal stress. *Science*, *298*(5595), 1015-1017. https://doi.org/10.1126/science.1076814

Helmuth, B., Mieszkowska, N., Moore, P., & Hawkins, S. J. (2006). Living on the Edge of Two Changing Worlds: Forecasting the Responses of Rocky Intertidal Ecosystems to Climate Change. *Annual Review of Ecology, Evolution, and Systematics*, *37*(1), 373-404. https://doi.org/10.1146/annurev.ecolsys.37.091305.110149

Helmuth, B. S. T., & Hofmann, G. E. (2001). Microhabitats, Thermal Heterogeneity, and Patterns of Physiological Stress in the Rocky Intertidal Zone. *The Biological Bulletin*, *201*(3), 374-384. https://doi.org/10.2307/1543615

Hennessy, K., Lawrence, J., & Mackey, B. (2022). IPCC sixth assessment report (AR6): climate change 2022-impacts, adaptation and vulnerability. https://doi.org/10.1017/9781009325844

Hernández, S., García, A. G., Arenas, F., Escribano, M. P., Jueterbock, A., De Clerck, O., Maggs, C. A., Franco, J. N., & Martínez, B. D. C. (2023). Range-edge populations of seaweeds show niche unfilling and poor adaptation to increased temperatures. *Journal of Biogeography*, *50*(4), 780-791. https://doi.org/10.1111/jbi.14572

Hewitt, G. (2003). Ice ages: Species distributions, and evolution. In *Evolution on planet Earth* (pp. 339-361). Elsevier. https://doi.org/10.1016/B978-012598655-7/50045-8

Hobday, A. J., Alexander, L. V., Perkins, S. E., Smale, D. A., Straub, S. C., Oliver, E. C. J., Benthuysen, J. A., Burrows, M. T., Donat, M. G., Feng, M., Holbrook, N. J.,

Moore, P. J., Scannell, H. A., Sen Gupta, A., & Wernberg, T. (2016). A hierarchical approach to defining marine heatwaves. *Progress in Oceanography*, *141*, 227-238. https://doi.org/10.1016/j.pocean.2015.12.014

Hofmann, M., & Schellnhuber, H. J. (2010). Ocean acidification: a millennial challenge. *Energy & Environmental Science*, *3*(12), 1883-1896. https://doi.org/10.1039/C000820F

Holloway-Phillips, M. (2018). Photosynthetic Oxygen Production: New Method Brings to Light Forgotten Flux. *Plant Physiology*, *177*(1), 7-9. https://doi.org/10.1104/pp.18.00344

Huwald, H., Higgins, C. W., Boldi, M. O., Bou-Zeid, E., Lehning, M., & Parlange, M. B. (2009). Albedo effect on radiative errors in air temperature measurements. *Water Resources Research*, *45*(8). https://doi.org/10.1029/2008WR007600

IPCC. (2022). *Climate Change 2022 – Impacts, Adaptation and Vulnerability: Working Group II Contribution to the Sixth Assessment Report of the Intergovernmental Panel on Climate Change* [Interview]. Cambridge University Press.

Jueterbock, A., Coyer, J. A., Olsen, J. L., & Hoarau, G. (2018). Decadal stability in genetic variation and structure in the intertidal seaweed Fucus serratus (Heterokontophyta: Fucaceae). *BMC Ecology and Evolution*, *18*(1), 94. https://doi.org/10.1186/s12862-018-1213-2

Jueterbock, A., Smolina, I., Coyer, J. A., & Hoarau, G. (2016). The fate of the Arctic seaweed Fucus distichus under climate change: an ecological niche modeling approach. *Ecol Evol*, *6*(6), 1712-1724. https://doi.org/10.1002/ece3.2001

Jueterbock, A., Tyberghein, L., Verbruggen, H., Coyer, J. A., Olsen, J. L., & Hoarau, G. (2013). Climate change impact on seaweed meadow distribution in the North Atlantic rocky intertidal. *Ecol Evol*, *3*(5), 1356-1373. https://doi.org/10.1002/ece3.541

Kearney, M. (2006). Habitat, environment and niche: what are we modelling? *Oikos*, *115*(1), 186-191. https://doi.org/10.1111/j.0030-1299.2008.16273.x

Kearney, M., & Porter, W. (2009). Mechanistic niche modelling: combining physiological and spatial data to predict species' ranges. *Ecology Letters*, *12*(4), 334-350. https://doi.org/10.1111/j.1461-0248.2008.01277.x

King, N. G., McKeown, N. J., Smale, D. A., & Moore, P. J. (2018). The importance of phenotypic plasticity and local adaptation in driving intraspecific variability in thermal niches of marine macrophytes. *Ecography*, *41*(9), 1469-1484. https://doi.org/10.1111/ecog.03186

King, N. G., McKeown, N. J., Smale, D. A., Wilcockson, D. C., Hoelters, L., Groves, E. A., Stamp, T., & Moore, P. J. (2019). Evidence for different thermal ecotypes in

range centre and trailing edge kelp populations. *Journal of Experimental Marine Biology and Ecology*, *514*, 10-17. https://doi.org/10.1016/j.jembe.2019.03.004

Koch, M., Bowes, G., Ross, C., & Zhang, X. H. (2013). Climate change and ocean acidification effects on seagrasses and marine macroalgae. *Global Change Biology*, *19*(1), 103-132. https://doi.org/10.1111/j.1365-2486.2012.02791.x

Lalegerie, F., & Stengel, D. B. (2022). Concise review of the macroalgal species Pelvetia canaliculata (Linnaeus) Decaisne & Thuret. *Journal of Applied Phycology*, *34*(6), 2807-2825. https://doi.org/10.1007/s10811-022-02830-y

Lalli, C., & Parsons, T. R. (1997). *Biological oceanography: an introduction*. Elsevier.

Lamela-Silvarrey, C., Fernández, C., Anadón, R., & Arrontes, J. (2012). Fucoid assemblages on the north coast of Spain: past and present (1977–2007). *Botanica Marina*, *55*(3), 199-207. https://doi.org/10.1515/bot-2011-0081

Lima, F. P., Gomes, F., Seabra, R., Wethey, D. S., Seabra, M. I., Cruz, T., Santos, A. M., & Hilbish, T. J. (2016). Loss of thermal refugia near equatorial range limits. *Global Change Biology*, *22*(1), 254-263. https://doi.org/10.1111/gcb.13115

Lima, F. P., & Helmuth, B. (2011). *Monitoring the Intertidal Environment with Biomimetic Devices* (Vol. 18). https://doi.org/10.5772/14153

Lima, F. P., Ribeiro, P. A., Queiroz, N., Hawkins, S. J., & Santos, A. M. (2007). Do distributional shifts of northern and southern species of algae match the warming pattern? *Global Change Biology*, *13*(12), 2592-2604. https://doi.org/10.1111/j.1365-2486.2007.01451.x

Lima, F. P., & Wethey, D. S. (2009). Robolimpets: measuring intertidal body temperatures using biomimetic loggers. *Limnology and Oceanography: Methods*, *7*(5), 347-353. https://doi.org/10.4319/lom.2009.7.347

Lourenço, C. R., Zardi, G. I., McQuaid, C. D., Serrão, E. A., Pearson, G. A., Jacinto, R., & Nicastro, K. R. (2016). Upwelling areas as climate change refugia for the distribution and genetic diversity of a marine macroalga. *Journal of Biogeography*, *43*(8), 1595-1607. https://doi.org/10.1111/jbi.12744

Lüning, K. (1990). Seaweeds: their environment, biogeography, and ecophysiology. *Journal of the Marine Biological Association of the United Kingdom*, *71*(1), 246-246. https://doi.org/10.1017/S0025315400037632

Lüthi, D., Le Floch, M., Bereiter, B., Blunier, T., Barnola, J.-M., Siegenthaler, U., Raynaud, D., Jouzel, J., Fischer, H., & Kawamura, K. (2008). High-resolution carbon dioxide concentration record 650,000–800,000 years before present. *Nature*, *453*(7193), 379-382. https://doi.org/10.1038/nature06949

Maharana, D., Das, P. B., Verlecar, X. N., Pise, N. M., & Gauns, M. (2015). Oxidative stress tolerance in intertidal red seaweed Hypnea musciformis (Wulfen) in relation to environmental components. *Environmental science and pollution*

research international, *22*(23), 18741-18749. https://doi.org/10.1007/s11356-015-4985-6

Manca, F., Benedetti-Cecchi, L., Bradshaw, C. J. A., Cabeza, M., Gustafsson, C., Norkko, A. M., Roslin, T. V., Thomas, D. N., White, L., & Strona, G. (2024). Projected loss of brown macroalgae and seagrasses with global environmental change. *Nature Communications*, *15*(1), 5344. https://doi.org/10.1038/s41467-024-48273-6

Martinez, B., Arenas, F., Rubal, M., Burgues, S., Esteban, R., Garcia-Plazaola, I., Figueroa, F. L., Pereira, R., Saldana, L., Sousa-Pinto, I., Trilla, A., & Viejo, R. M. (2012). Physical factors driving intertidal macroalgae distribution: physiological stress of a dominant fucoid at its southern limit. *Oecologia*, *170*(2), 341-353. https://doi.org/10.1007/s00442-012-2324-x

Martins, A. P., Colepicolo, P., & Yokoya, N. S. (2023). Concise review on seaweed photosynthesis: From physiological bases to biotechnological applications. *Journal of Photochemistry and Photobiology*, *16*, 100194. https://doi.org/10.1016/j.jpap.2023.100194

Martins, M., Soares, C., Figueiredo, I., Sousa, B., Torres, A. C., Sousa-Pinto, I., Veiga, P., Rubal, M., & Fidalgo, F. (2021). Fucoid Macroalgae Have Distinct Physiological Mechanisms to Face Emersion and Submersion Periods in Their Southern Limit of Distribution. *Plants (Basel)*, *10*(9). https://doi.org/10.3390/plants10091892

Maxwell, K., & Johnson, G. N. (2000). Chlorophyll fluorescence—a practical guide. *Journal of experimental botany*, *51*(345), 659-668. https://doi.org/10.1093/jexbot/51.345.659

Meneghesso, C., Seabra, R., Broitman, B. R., Wethey, D. S., Burrows, M. T., Chan, B. K. K., Guy-Haim, T., Ribeiro, P. A., Rilov, G., Santos, A. M., Sousa, L. L., & Lima, F. P. (2020). Remotely-sensed L4 SST underestimates the thermal fingerprint of coastal upwelling. *Remote Sensing of Environment*, *237*, 111588. https://doi.org/10.1016/j.rse.2019.111588

Menge, B. A., & Branch, G. M. (2001). *Rocky intertidal communities. In 'Marine Community Ecology'.* Sinauer Associates, Inc.: Sunderland, MA, USA.

Mieszkowska, N., Burrows, M. T., Hawkins, S. J., & Sugden, H. (2021). Impacts of Pervasive Climate Change and Extreme Events on Rocky Intertidal Communities: Evidence From Long-Term Data [Original Research]. *Frontiers in Marine Science*, *8*. https://doi.org/10.3389/fmars.2021.642764

Mislan, K., Wethey, D. S., & Helmuth, B. (2009). When to worry about the weather: role of tidal cycle in determining patterns of risk in intertidal ecosystems. *Global Change Biology*, *15*(12), 3056-3065. https://doi.org/10.1111/j.1365-2486.2009.01936.x

Monteiro, C., Pereira, J., Seabra, R., & Lima, F. P. (2022). Fine-scale survey of intertidal macroalgae reveals recent changes in a cold-water biogeographic stronghold. *Frontiers in Marine Science*, *9*. https://doi.org/10.3389/fmars.2022.880074

Mortensen, B. J. D., & Dunphy, B. J. (2016). Effect of tidal regime on the thermal tolerance of the marine gastropod Lunella smaragda (Gmelin 1791). *Journal of Thermal Biology*, *60*, 186-194. https://doi.org/10.1016/j.jtherbio.2016.07.009

Neiva, J., Serrão, E. A., Assis, J., Pearson, G. A., Coyer, J. A., Olsen, J. L., Hoarau, G., & Valero, M. (2016). Climate oscillations, range shifts and phylogeographic patterns of North Atlantic Fucaceae. In *Seaweed phylogeography* (pp. 279-308). Springer. https://doi.org/10.1007/978-94-017-7534-2_11

O'Neill, B. C., Kriegler, E., Riahi, K., Ebi, K. L., Hallegatte, S., Carter, T. R., Mathur, R., & Van Vuuren, D. P. (2014). A new scenario framework for climate change research: the concept of shared socioeconomic pathways. *Climatic Change*, *122*, 387-400. https://doi.org/10.1007/s10584-013-0905-2

Olsen, J. L., Zechman, F. W., Hoarau, G., Coyer, J. A., Stam, W. T., Valero, M., & Åberg, P. (2010). The phylogeographic architecture of the fucoid seaweed Ascophyllum nodosum: an intertidal 'marine tree' and survivor of more than one glacial-interglacial cycle. *Journal of Biogeography*, *37*(5), 842-856. https://doi.org/10.1111/j.1365-2699.2009.02262.x

Orr, H. A., & Unckless, R. L. (2008). Population extinction and the genetics of adaptation. *Am Nat*, *172*(2), 160-169. https://doi.org/10.1086/589460

Paine, R. T., & Levin, S. A. (1981). Intertidal landscapes: disturbance and the dynamics of pattern. *Ecological monographs*, *51*(2), 145-178. https://doi.org/10.2307/2937261

Parry-Wilson, H. M., Fenberg, P. B., Hawkins, S. J., & Mieszkowska, N. (2024). Lethal and sub-lethal responses of rocky shore gastropods to extreme temperatures. *Journal of Experimental Marine Biology and Ecology*, *579*. https://doi.org/10.1016/j.jembe.2024.152044

Pearson, G. A., Lago-Leston, A., & Mota, C. (2009). Frayed at the edges: selective pressure and adaptive response to abiotic stressors are mismatched in low diversity edge populations. *Journal of Ecology*, *97*(3), 450-462. https://doi.org/10.1111/j.1365-2745.2009.01481.x

Pereira, J., Monteiro, C., Seabra, R., & Lima, F. P. (2022). Fine-scale abundance of rocky shore macroalgae species with distribution limits in NW Iberia in 2020/2021. *Biodivers Data J*, *10*, e80798. https://doi.org/10.3897/BDJ.10.e80798

Pereira, L., Morrison, L., Shukla, P. S., & Critchley, A. T. (2020). A concise review of the brown macroalga Ascophyllum nodosum (Linnaeus) Le Jolis. *Journal of Applied Phycology*, *32*(6), 3561-3584. https://doi.org/10.1007/s10811-020-02246-6

Pessarrodona, A., Howard, J., Pidgeon, E., Wernberg, T., & Filbee-Dexter, K. (2024). Carbon removal and climate change mitigation by seaweed farming: A state of knowledge review. *Sci Total Environ*, *918*, 170525. https://doi.org/10.1016/j.scitotenv.2024.170525

Pfister, C. A., Altabet, M. A., & Weigel, B. L. (2019). Kelp beds and their local effects on seawater chemistry, productivity, and microbial communities. *Ecology*, *100*(10), e02798. https://doi.org/10.1002/ecy.2798

Pfister, C. A., Wootton, J. T., & Neufeld, C. J. (2007). Relative roles of coastal and oceanic processes in determining physical and chemical characteristics of an intensively sampled nearshore system. https://doi.org/10.2307/4502333

Pincebourde, S., Sanford, E., & Helmuth, B. (2013). Survival and arm abscission are linked to regional heterothermy in an intertidal sea star. *Journal of Experimental Biology*, *216*(12), 2183-2191. https://doi.org/10.1242/jeb.083881

Piñeiro-Corbeira, C., Barreiro, R., Cremades, J., & Arenas, F. (2018). Seaweed assemblages under a climate change scenario: Functional responses to temperature of eight intertidal seaweeds match recent abundance shifts. *Scientific reports*, *8*(1), 1-9. https://doi.org/10.1038/s41598-018-31357-x

Precht, H. (2013). *Temperature and life*. Springer Science & Business Media.

Rantanen, M., Karpechko, A. Y., Lipponen, A., Nordling, K., Hyvärinen, O., Ruosteenoja, K., Vihma, T., & Laaksonen, A. (2022). The Arctic has warmed nearly four times faster than the globe since 1979. *Communications Earth & Environment*, *3*(1), 168. https://doi.org/10.1038/s43247-022-00498-3

Raymond, W. W., Barber, J. S., Dethier, M. N., Hayford, H. A., Harley, C. D. G., King, T. L., Paul, B., Speck, C. A., Tobin, E. D., Raymond, A. E. T., & McDonald, P. S. (2022). Assessment of the impacts of an unprecedented heatwave on intertidal shellfish of the Salish Sea. *Ecology*, *103*(10), e3798. https://doi.org/10.1002/ecy.3798

Riahi, K., van Vuuren, D. P., Kriegler, E., Edmonds, J., O'Neill, B. C., Fujimori, S., Bauer, N., Calvin, K., Dellink, R., Fricko, O., Lutz, W., Popp, A., Cuaresma, J. C., Kc, S., Leimbach, M., Jiang, L., Kram, T., Rao, S., Emmerling, J., . . . Tavoni, M. (2017). The Shared Socioeconomic Pathways and their energy, land use, and greenhouse gas emissions implications: An overview. *Global Environmental Change*, *42*, 153-168. https://doi.org/10.1016/j.gloenvcha.2016.05.009

Richards, C., Collins, S. M., Fisher, K., Blackmore, R. J., Fifield, D. A., & Bates, A. E. (2024). Burrow nests fall below critical temperatures of threatened seabirds but offer thermal refuge during extreme cold events. *Facets*. https://doi.org/10.1139/facets-2023-0131

Rogers-Bennett, L., & Catton, C. A. (2019). Marine heat wave and multiple stressors tip bull kelp forest to sea urchin barrens. *Scientific reports*, *9*(1), 15050. https://doi.org/10.1038/s41598-019-51114-y

Román, M., Román, S., Vázquez, E., Troncoso, J., & Olabarria, C. (2020). Heatwaves during low tide are critical for the physiological performance of intertidal macroalgae under global warming scenarios. *Scientific reports*, *10*(1), 1-14. https://doi.org/10.1038/s41598-020-78526-5

Ross, F. W. R., Boyd, P. W., Filbee-Dexter, K., Watanabe, K., Ortega, A., Krause-Jensen, D., Lovelock, C., Sondak, C. F. A., Bach, L. T., Duarte, C. M., Serrano, O., Beardall, J., Tarbuck, P., & Macreadie, P. I. (2023). Potential role of seaweeds in climate change mitigation. *Sci Total Environ*, *885*, 163699. https://doi.org/10.1016/j.scitotenv.2023.163699

Roznik, E. A., & Alford, R. A. (2012). Does waterproofing Thermochron iButton dataloggers influence temperature readings? *Journal of Thermal Biology*, *37*(4), 260-264. https://doi.org/10.1016/j.jtherbio.2012.02.004

Rubal, M., Veiga, P., Cacabelos, E., Moreira, J., & Sousa-Pinto, I. (2013). Increasing sea surface temperature and range shifts of intertidal gastropods along the Iberian Peninsula. *Journal of Sea Research*, *77*, 1-10. https://doi.org/10.1016/j.seares.2012.12.003

Saderne, V., Fietzek, P., & Herman, P. M. J. (2013). Extreme variations of pCO2 and pH in a macrophyte meadow of the Baltic Sea in summer: evidence of the effect of photosynthesis and local upwelling. *PLoS One*, *8*(4), e62689. https://doi.org/10.1371/journal.pone.0062689

Samset, B. H., Lund, M. T., Fuglestvedt, J. S., & Wilcox, L. J. (2024). 2023 temperatures reflect steady global warming and internal sea surface temperature variability. *Communications Earth & Environment*, *5*(1), 460. https://doi.org/10.1038/s43247-024-01637-8

Sandoval-Castillo, J., Gates, K., Brauer, C. J., Smith, S., Bernatchez, L., & Beheregaray, L. B. (2020). Adaptation of plasticity to projected maximum temperatures and across climatically defined bioregions. *Proceedings of the National Academy of Sciences*, *117*(29), 17112-17121. https://doi.org/10.1073/pnas.1921124117

Sanford, E., & Kelly, M. W. (2011). Local Adaptation in Marine Invertebrates. *Annual Review of Marine Science*, *3*(Volume 3, 2011), 509-535. https://doi.org/10.1146/annurev-marine-120709-142756

Schneider. (2008). Heat Stress in the Inter tidal_Comparing Survival and Growth of an Invasive and Native Mussel. *The Biological Bulletin*, *3*, 253–264. https://doi.org/10.2307/25470709

Schreiber, U., Bilger, W., & Neubauer, C. (1995). Chlorophyll fluorescence as a nonintrusive indicator for rapid assessment of in vivo photosynthesis. In *Ecophysiology of photosynthesis* (pp. 49-70). Springer. https://doi.org/10.1007/978-3-642-79354-7_3

Schulte, P. M., Healy, T. M., & Fangue, N. A. (2011). Thermal Performance Curves, Phenotypic Plasticity, and the Time Scales of Temperature Exposure. *Integrative and Comparative Biology*, *51*(5), 691-702. https://doi.org/10.1093/icb/icr097

Seabra, R., Wethey, D. S., Santos, A. M., Gomes, F., & Lima, F. P. (2016). Equatorial range limits of an intertidal ectotherm are more linked to water than air temperature. *Global Change Biology*, *22*(10), 3320-3331. https://doi.org/10.1111/gcb.13321

Seabra, R., Wethey, D. S., Santos, A. M., & Lima, F. P. (2011). Side matters: Microhabitat influence on intertidal heat stress over a large geographical scale. *Journal of Experimental Marine Biology and Ecology*, *400*(1-2), 200-208. https://doi.org/10.1016/j.jembe.2011.02.010

Seitz, R. D., Wennhage, H., Bergström, U., Lipcius, R. N., & Ysebaert, T. (2013). Ecological value of coastal habitats for commercially and ecologically important species. *ICES Journal of Marine Science*, *71*(3), 648-665. https://doi.org/10.1093/icesjms/fst152

Seneviratne, S. I., Zhang, X., Adnan, M., Badi, W., Dereczynski, C., Luca, A. D., Ghosh, S., Iskandar, I., Kossin, J., & Lewis, S. (2021). *Weather and climate extreme events in a changing climate in IPCC) Sixth Assessment Report (AR6).* https://doi.org/10.1017/9781009157896.013

Smith, K. E., Aubin, M., Burrows, M. T., Filbee-Dexter, K., Hobday, A. J., Holbrook, N. J., King, N. G., Moore, P. J., Sen Gupta, A., Thomsen, M., Wernberg, T., Wilson, E., & Smale, D. A. (2024). Global impacts of marine heatwaves on coastal foundation species. *Nature Communications*, *15*, 5052. https://doi.org/10.1038/s41467-024-49307-9

Somero, G. N. (2002). Thermal physiology and vertical zonation of intertidal animals: optima, limits, and costs of living. *Integrative and Comparative Biology*, *42*(4), 780-789. https://doi.org/10.1093/icb/42.4.780

Somero, G. N. (2010). The physiology of climate change: how potentials for acclimatization and genetic adaptation will determine 'winners' and 'losers'. *Journal of Experimental Biology*, *213*, 912 - 920. https://doi.org/doi.org/10.1242/jeb.037473

Spurgeon, E., Thompson, M. L., Alexander, M. D., Anderson, J. M., Rex, P. T., Stirling, B., Abbott, K., & Lowe, C. G. (2024). The influence of micro-scale thermal habitat on the movements of juvenile white sharks in their Southern California

aggregation sites. *Frontiers in Marine Science*, *11*, 1290769. https://doi.org/10.3389/fmars.2024.1290769

Staehr, P. A., & Wernberg, T. (2009). Physiological responses of Ecklonia radiata (laminariales) to a latitudinal gradient IN ocean temperature. *Journal of Phycology*, *45*(1), 91-99. https://doi.org/10.1111/j.1529-8817.2008.00635.x

Straub, S. C., Wernberg, T., Thomsen, M. S., Moore, P. J., Burrows, M. T., Harvey, B. P., & Smale, D. A. (2019). Resistance, extinction, and everything in between–The diverse responses of seaweeds to marine heatwaves. *Frontiers in Marine Science*, *6*, 763. https://doi.org/10.3389/fmars.2019.00763

Tait, L. W., & Schiel, D. R. (2013). Impacts of temperature on primary productivity and respiration in naturally structured macroalgal assemblages. *PLoS One*, *8*(9), e74413. https://doi.org/10.1371/journal.pone.0074413

Van den Hoek, C. (1975). Phytogeographic provinces along the coasts of the northern Atlantic Ocean. *Phycologia*, *14*(4), 317-330. https://doi.org/10.2216/i0031-8884-14-4-317.1

Van Vuuren, D. P., Edmonds, J., Kainuma, M., Riahi, K., Thomson, A., Hibbard, K., Hurtt, G. C., Kram, T., Krey, V., & Lamarque, J.-F. (2011). The representative concentration pathways: an overview. *Climatic Change*, *109*, 5-31. https://doi.org/10.1007/s10584-011-0148-z

Veenhof, R. J., Champion, C., Dworjanyn, S. A., Schwoerbel, J., Visch, W., & Coleman, M. A. (2024). Projecting kelp (Ecklonia radiata) gametophyte thermal adaptation and persistence under climate change. *Ann Bot*, *133*(1), 153-168. https://doi.org/10.1093/aob/mcad132

Vona, V., Di Martino Rigano, V., Lobosco, O., Carfagna, S., Esposito, S., & Rigano, C. (2004). Temperature responses of growth, photosynthesis, respiration and NADH: nitrate reductase in cryophilic and mesophilic algae. *New Phytologist*, *163*(2), 325-331. https://doi.org/10.1111/j.1469-8137.2004.01098.x

Wernberg, T. (2021). Marine heatwave drives collapse of kelp forests in Western Australia. In *Ecosystem collapse and climate change* (pp. 325-343). Springer. https://doi.org/10.1007/978-3-030-71330-0_12

Wernberg, T., Russell, B. D., Thomsen, M. S., Gurgel, C. F. D., Bradshaw, C. J., Poloczanska, E. S., & Connell, S. D. (2011). Seaweed communities in retreat from ocean warming. *Current biology*, *21*(21), 1828-1832. https://doi.org/10.1016/j.cub.2011.09.028

Werndl, C. (2016). On defining climate and climate change. *The British Journal for the Philosophy of Science*. https://doi.org/10.1093/bjps/axu048.

Westmeijer, G., Everaert, G., Pirlet, H., De Clerck, O., & Vandegehuchte, M. B. (2019). Mechanistic niche modelling to identify favorable growth sites of temperate macroalgae. *Algal Research*, *41*. https://doi.org/10.1016/j.algal.2019.101529

Wiencke, C., & Amsler, C. D. (2012). Seaweeds and their communities in polar regions. In *Seaweed biology: novel insights into ecophysiology, ecology and utilization* (pp. 265-291). Springer. https://doi.org/10.1007/978-3-642-28451-9_13

Wilson, K., Kay, L., Schmidt, A., & Lotze, H. (2015). Effects of increasing water temperatures on survival and growth of ecologically and economically important seaweeds in Atlantic Canada: implications for climate change. *Marine Biology*, *162*. https://doi.org/10.1007/s00227-015-2769-7

Zhang, T., Liu, H., Lu, Y., Wang, Q., Loh, Y. C., & Li, Z. (2024). Impact of climate change on coastal ecosystem and outdoor activities: a comparative analysis among four largest coastline covering countries. *Environmental Research*, *250*, 118405. https://doi.org/10.1016/j.envres.2024.118405

Chapter 2

Autonomous, high-frequency and long-term monitoring of substrate temperature in rocky intertidal zones

2.1. Abstract

Intertidal zones are characterised by complex and dynamic thermal mosaics, where organisms are subjected to extreme temperature variations influenced by microclimatic factors. Accurate and long-term monitoring of rocky shore temperatures remains challenging due to the limitations of conventional temperature loggers. Surface-deployed logger designs are prone to loss and inaccurate measurements influenced by external factors like solar radiation and wind. We evaluated rock-embedded T7.3 EnvLoggers as an alternative for monitoring intertidal substrate temperatures. The study compared their performance to traditional surface-deployed loggers in accuracy, long-term loss rates, and the impact of sampling frequency on the detection of temperature extremes. Our results show that rock-embedded T7.3 EnvLoggers achieve superior accuracy (mean bias ~0.01 °C), and considerably lower loss rates (~0.1% per year) compared to surface loggers (~7.6–36.8% per year). Sampling intervals of 1 hour effectively captured daily thermal extremes with minimal error (<1 °C), balancing accuracy and feasibility for long-term deployments. Embedding loggers within rocky substrates offers a durable, cost-effective solution for large-scale, long-term temperature monitoring. This approach enables reliable assessment of intertidal thermal environments and provides a scalable framework for studies in other extreme habitats, such as deserts and tropical forests.

Keywords

Data loggers, Microclimate, Sea temperature, Air temperature, Skin temperature, Thermal stress, Heatwaves, Environmental monitoring

2.2. Introduction

Our planet is undergoing a major climatic crisis (Ripple et al., 2023). With temperature records now routinely being broken (Christidis et al., 2015), monitoring temperature variability is essential for quantifying its effects on biodiversity (Lima et al., 2016) and guiding more efficient management actions (Comte & Olden, 2017). Despite significant progress in remote temperature sensing technologies, there is a striking mismatch between the scale at which climate data are typically collected and modelled and the fine-scale climatic conditions that organisms experience across their home ranges (Potter et al., 2013; Pincebourde & Salle, 2020). This has prompted recent developments in in-situ temperature acquisition (Kemppinen et al., 2024) and the creation of microclimate databases (Lembrechts et al., 2020). Still, the thermal environment of certain systems, such as intertidal zones (areas between high and low tide marks along coastlines), remains poorly understood due to inherent complexity and challenging conditions.

In the intertidal, challenges can be broadly grouped into two categories. On the one hand, the thermal landscape can be highly variable, and even nearshore high tide and offshore waters can exhibit significantly different temperatures (Pfister et al., 2007). Direct in-situ measurements are relatively scarce at the coast, and satellite-derived temperature estimates can display biases as high as 6 ºC (Meneghesso et al., 2020). Discrepancies in temperature become even more pronounced at low tide when exposure to terrestrial conditions, such as air temperature, humidity, wind, and solar radiation, dominates the surface energy balance (Helmuth et al., 2006). For example, solar radiation alone can drive body temperature variations of up to 30 ºC within just a few hours, exceeding the effects of seasons, latitude, and shore level (Seabra et al., 2011). Because the amount of solar radiation received depends on substrate slope and compass orientation, organisms located only a few centimetres apart may experience vastly different temperatures and levels of thermal stress (Lima et al., 2016). Therefore, the resulting thermal mosaic is challenging to capture through remote sensing and even difficult to accurately measure in-situ without a comprehensive network of instruments deployed over extended periods. Additionally, the scarcity of data and the complex heat transfer patterns make accurate modelling difficult (Ma et al., 2024).

On the other hand, intertidal systems are difficult to monitor due to their harsh environmental conditions, which are often incompatible with the long-term deployment of instruments. Effective monitoring requires equipment that can withstand cyclic alternations between wet and dry conditions, fluctuating salinity levels, and structural

fatigue from repeated expansion and contraction under extreme temperature changes. Additionally, instruments must endure physical impacts from breaking waves, collisions with driftwood and loose rocks, sandblasting and ice scouring, all while remaining inconspicuous to minimise the risk of human tampering or vandalism.

The challenge of scale has been partially addressed by recent advancements in electronics, leading to miniaturised devices capable of autonomously logging temperature over extended periods. This has been notably explored through the creation of biomimetic loggers — small temperature loggers shaped like or embedded within real shells, such as robomussels (Helmuth & Hofmann, 2001), robolimpets (Lima & Wethey, 2009), and robobarnacles (Chan et al., 2016). Notwithstanding, progress towards a universal logger has been hindered by the fact that each of these loggers is designed to closely capture the temperature trajectory of a particular species, complicating data comparison. In addition, biomimetic logger manufacturing and deployment has been highly specialised and mostly artisanal, resulting in costly loggers with extremely complex interfaces and deployment procedures, severely narrowing their adoption.

The challenge of robustness has been even harder to solve. Most designs rely on iButton (Thermochron, Maxim Integrated Products, USA) or Tidbit temperature loggers (Onset Corporation, USA), both of which require electric or optical contact for communication. Communication ports often compromise waterproofing or limit the range of deployment possibilities. Some recent models, such as the MX2201 HOBO Pendant water temperature logger, use Bluetooth Low Energy (BLE) connectivity, which, despite offering relatively low power consumption, still limits deployment duration. To address this, some logger models feature user-replaceable batteries, an ability that comes at the expense of waterproof integrity, potentially increasing failure rates. Despite these limitations, loggers such as the MX2201 HOBO have been successfully used in studies monitoring marine (Maloney et al., 2024), freshwater (Gilbert et al., 2022), and intertidal (Sun et al., 2023) temperatures.

EnvLoggers (Electricblue CRL, PT), having been specifically designed to withstand harsh environments (e.g., are rated to 20 bar), communicate through Near Field Communication (NFC), which does not require battery power, greatly extending their battery life. Despite being an emerging technology, they have already been adopted in a variety of applications, ranging from the study of coastal sharks (Spurgeon et al., 2024) to monitoring intertidal communities (Parry-Wilson et al., 2024). An added benefit of NFC is that, despite its limited range (~10 mm), it enables EnvLoggers to be embedded within substrates, providing a standardised method for measuring environmental temperatures

without species-specific constraints, while offering enhanced protection against physical disturbance. However, the extent of these potential advantages has yet to be fully quantified.

Another important aspect of long-term monitoring is the selection of sampling frequency. Daily temperature measurements may be too coarse to accurately capture the thermal ecology of small ectotherms (Montalto et al., 2014; Dillon et al., 2019) and can fail to adequately characterise phenomena such as heat waves (Hobday et al., 2016) or upwelling onset events (Meneghesso et al., 2020). However, higher sampling frequencies reduce monitoring duration, increase maintenance requirements and limit the spatial extent of monitoring networks.

This study directly compares rock-embedded T7.3 EnvLoggers with traditional surface-deployed loggers, (i) evaluating their suitability for monitoring surface temperatures in the rocky intertidal, (ii) providing comparative estimates of their loss rates, and (iii) assessing the impact of different sampling rates on their accuracy in capturing daily temperature extremes.

2.3. Materials and Methods

2.3.1. Performance of temperature loggers

Loggers were deployed between July 20 and 31, 2020, roughly at the mid-tide level in Praia de Sampaio (41.2798° N, -8.7306° W), a rocky shore near Matosinhos, Portugal. Temperatures were recorded only at low tide since loggers were submerged in well-mixed water during high tide. In these conditions, loggers quickly reach thermal equilibrium with their surroundings (Seabra et al., 2011), causing high-tide data to artificially reduce differences between the loggers and reference measurements (**Fig. S2.1**, left side).



Figure 2.1: An array of temperature loggers and thermocouples deployed on a fine-grain granite rock (foreground) and another array in a coarse-grain granite rock (background) in the intertidal zone at Praia de Sampaio (41.2797° N, -8.7305° W; June 20, 2020), photographed at low tide. Each type of logger was deployed in triplicate. Green smudges on the rock surface indicate locations where EnvLoggers were embedded within the substrate. The large plastic boxes housed the electronics required to read and log thermocouple data.

Loggers were deployed in triplicates in each one of three different areas, each characterised by a slightly different type of granite (**Supplementary Table S2.1**). The relative arrangement of the loggers was randomly determined, varying across the three

rocks. In each one, three 1.6 mm-diameter type K (chromel/alumel) thermocouples were inserted in 8 mm-diameter, 5 mm-deep holes and secured in place with a small portion of A-788 Z-Spar Splash Zone Compound (Carboline, USA, from now on referred to as marine epoxy). Thermocouples were deployed immediately after the receding tide exposed the deployment rocks and retrieved just as the rising tide reached them, preventing saltwater damage to the thermocouple logging instruments (**Fig. 2.1**). These were assembled following Gandra et al. (2015) but enhanced with a Maxim Integrated MAX31856 Precision Thermocouple to Digital Converter, obtaining a resolution of 0.01 °C and an accuracy of 0.19 ºC.

Table 2.1: Main technical specifications of the temperature loggers evaluated in this study. Memory is in number of readings. Battery life (years) at the sampling rate of one sample per hour. Dimensions is in diameter x height (mm). Clock drift is in seconds per month and values marked with * are dependent on temperature. Comm. stands for communication method.

Datalogger	Memory	Resolution, Precision and Accuracy	Clock drift	Volatile memory	Battery life	Dimensions	Comm.
DS1922L iButtons	8,192	0.0625 ºC; 0.5 ºC; 0.5 ºC	100-200*	Yes	~ 8	17.35 x 5.89	One-wire
T2.4 EnvLoggers (at the surface and as robolimpets)	12,000	0.1 ºC; 0.1 ºC; 0.2 ºC	75 -100*	No	~ 5	27 x 11 or ~ 45 x 15 (robolimpet)	NFC
T7.3 EnvLoggers (embedded in the rock)	131,000	0.1 ºC; 0.1 ºC; 0.2 ºC	8	No	~ 15	29 x 11.5	NFC

The temperature loggers tested included naked DS1922L iButtons (i.e., without any material covering the original metal casing), Robolimpets (as described by Lima and Wethey, 2019, but with a T2.4 EnvLogger inside), naked T2.4 EnvLoggers deployed at the surface, and T7.3 EnvLoggers embedded within the rock. It is worth noting that, for the purposes of this study, the physical differences between T2.4 and T7.3 EnvLoggers are negligible, as they primarily differ in memory size, battery capacity, and clock precision.

Surface-deployed EnvLoggers featured various colours: transparent (no pigment), white, black, or one of three shades of grey, which were achieved by mixing white and black opaque acrylic paint in different proportions during logger manufacturing: 3:1, 1:1 or 1:3 of black:white paint (hereafter named grey 25, grey 50, and grey 75, respectively, with grey 25 being the darkest). A detailed characterisation of their grey scale is provided in **Fig. S2.2**. All surface-deployed loggers were attached using a thin (~2 mm) layer of marine epoxy. The T7.3 EnvLoggers embedded within the rock were glued inside 30 mm wide and 15 mm deep drilled holes using marine epoxy and then covered with a ~1 mm layer of the same epoxy. Holes were drilled with a DCH133M1 driller fitted with a DT9618-QZ drill bit, both from DeWALT, USA (see **Fig. S2.3** for details). All loggers and thermocouples were programmed to record temperatures at their higher resolution and with a sampling period of one minute. The technical characteristics of the loggers are shown in **Table 2.1**.

Taylor diagrams (Taylor, 2001) were used to concisely summarise the degree of similarity between the various temperature logger models and the reference thermocouples in the same rock. These diagrams simultaneously display the centred root mean square error (cRMSE), Pearson's correlation coefficient (R), and normalised standard deviation (NSD) — for an annotated example, see Seabra et al. (2011). Since cRMSE captures only the random scatter of data around their mean, excluding systematic bias, we complemented the Taylor diagrams with bias plots and calculated the root mean square error (RMSE). The RMSE provides a comprehensive measure by combining both the mean bias (MB) relative to the reference and the random scatter around the mean into a single metric.

As even minor changes in surface orientation can result in meaningful differences in temperature (Seabra et al., 2011), each logger was always evaluated against its closest thermocouple. In addition, differences among thermocouples provided an overall estimate of the natural variability within each sampled rock. Furthermore, a cross-correlogram analysis was performed to assess whether temperature fluctuations recorded by the thermocouples preceded those captured by the various loggers, which would indicate the presence of thermal inertia in the loggers. All data manipulation and analyses were done in R 4.4.1 (R Development Core Team, 2024). Taylor plots were produced using the v2.18-2 openair R package (Carslaw & Ropkins, 2014).

2.3.2. Long-term logger loss rate in challenging environments

Long-term loss rates are rarely reported, even in methodological studies (e.g., Rich et al., 2024). Data on the loss rates of naked iButtons deployed in aquatic or damp habitats were sourced from Wolaver and Sharp (2007) and Roznik and Alford (2012), supplemented by our own assessments in the rocky intertidal. Loss rates for robobarnacles (similar to robolimpets) were reported by Chan et al. (2016), while estimates for traditional robolimpets (Lima & Wethey, 2009) were derived from a reanalysis of raw data from Salois et al. (2022). Loss rates for T2.4 EnvLogger robolimpets and naked T2.4 EnvLoggers deployed on rock surfaces were kindly provided by H. Parry-Wilson and N. N. Mieszkowska (MBA, UK). Data on T2.4 and T7.3 EnvLoggers embedded within rocks were compiled from various intertidal logger networks maintained by us since 2019. All loss rates are expressed as percentage loss per month or year.

2.3.3. Sampling frequency

The effect of reducing sampling frequency (i.e., sampling at increasingly long intervals) was evaluated on data from EnvLoggers deployed in holes in the rock, as described in section 4.1, at the rocky shore of Praia do Barreiro (41.2618º N, -8.7268º W), in Lavra, Portugal. Loggers recorded data at one-minute intervals from 24 May to 15 November 2024. A total of 64 EnvLoggers were deployed: 10 each at low, high, and supratidal levels (3 facing North, 3 South, 2 East, and 2 West per level), 14 at mid-tide level (5 North, 5 South, 2 East, and 2 West), and 20 in tide pools (8 mid-tide, 8 high-tide, and 4 supratidal). Increasingly rarefied datasets were generated by sampling the original one-minute data at intervals of 5, 10, 15, 30, 60, 90, 120, 240, and 360 minutes. Maximum and minimum daily temperatures were extracted from each rarefied dataset and compared to the extremes from the original dataset, quantifying the *temperature* error. Additionally, we evaluated the timing (day of the week) of the hottest and coldest days in the original dataset and compared them to the rarefied datasets, quantifying the *temporal* error of those extreme events.

2.4. Results

2.4.1. Performance of temperature loggers

The overall performance of the nine types of temperature loggers was relatively similar, with all satisfactorily matching the reference thermocouples, despite some variability (**Table 2.2**, **Fig. 2.2**).

Table 2.2: Overall performance of the temperature loggers, combined across replicates (n= 3) and rocks (n= 3). Metrics include Pearson's correlation coefficient (R), normalised standard deviation (NSD), centred root mean square error (cRMSE), root mean square error (RMSE) and mean bias (MB).

	R	NSD	cRMSE (ºC)	RMSE (ºC)	MB (ºC)
Black EnvLoggers	0.95	0.99	1.70	2.25	-1.47
Grey 25 EnvLoggers	0.94	1.02	1.79	2.58	-1.86
Grey 50 Envloggers	0.94	0.99	1.83	2.38	-1.52
Grey 75 EnvLoggers	0.95	0.97	1.59	1.82	-0.88
White EnvLoggers	0.96	0.83	1.60	2.01	1.22
Transparent Envloggers	0.94	0.96	1.79	2.24	-1.34
EnvLoggers Inside the Rock	0.95	0.94	1.64	1.64	-0.01
iButtons	0.95	0.92	1.75	1.75	-0.03
Robolimpets	0.95	0.84	1.79	1.86	0.51
Other Thermocouples	0.98	1.00	0.98	0.98	-0.05

Correlations (R) were consistently high, ranging from 0.94 to 0.96, compared to 0.98 among thermocouples. Normalised Standard Deviations (NSD), indicating how well loggers captured temperature variability relative to thermocouples, ranged from 1.02 (Grey 25 EnvLoggers) to 0.83–0.84 (White EnvLoggers and Robolimpets). Centred Root Mean Squared Errors (cRMSE), reflecting data dispersion, varied from 1.59 °C (Grey 75 EnvLoggers) to 1.83 °C (Grey 50 EnvLoggers), compared to 0.98 °C among thermocouples. Mean Bias (MB) was worst in Grey 25 EnvLoggers (-1.86 °C) and best in EnvLoggers inside the rock (-0.01 °C), even outperforming other thermocouples (-0.05 °C). Root Mean Square Error (RMSE), which combines both bias (MB) and random error (cRMSE), was best for EnvLoggers inside the rock (1.64 °C) and worst for Grey 25 EnvLoggers (2.58 °C), with thermocouples achieving 0.98 °C.

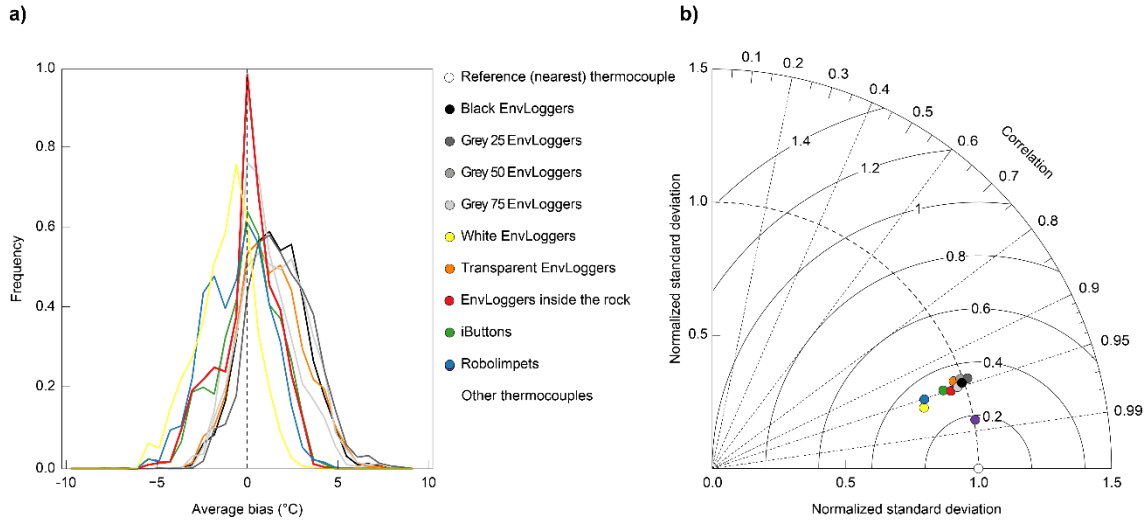


Figure 2.2: Overall performance of temperature loggers compared to reference thermocouple; a) Distribution of biases; b) Taylor diagram where each coloured circle represents a logger type, while the white circle at the bottom shows the reference thermocouple data. The azimuth angle of each coloured circle corresponds to its correlation coefficient with the reference (R). The radial distance from the graph's origin indicates Normalized Standard Deviation (NSD), and the concentric lines centred on the reference represent Centered Root Mean Square Error (cRMSE). The best-performing loggers are located at the same radial distance as the reference (indicating better NSD), lower on the graph (indicating higher R), and closer to the reference circle

The comparison of temperatures recorded by the tested loggers against reference thermocouples (**Fig. 2.3**) reveals distinct performance patterns across logger types. Black and Grey 25 EnvLoggers, along with Transparent Loggers to a lesser extent, exhibited a warm bias, consistently overestimating thermocouple readings across the whole temperature range. In contrast, White EnvLoggers and Robolimpets showed a cold bias, underestimating temperatures, especially at higher values. Grey 75 Envloggers (at the surface), iButtons and EnvLoggers inside the rock exhibited the closest agreement with their closest thermocouples, with data points closely aligned with the 1:1 line, indicating minimal bias and good accuracy across the whole temperature range, with performance only marginally below that of the other thermocouples (located a few centimetres away in the same rock).

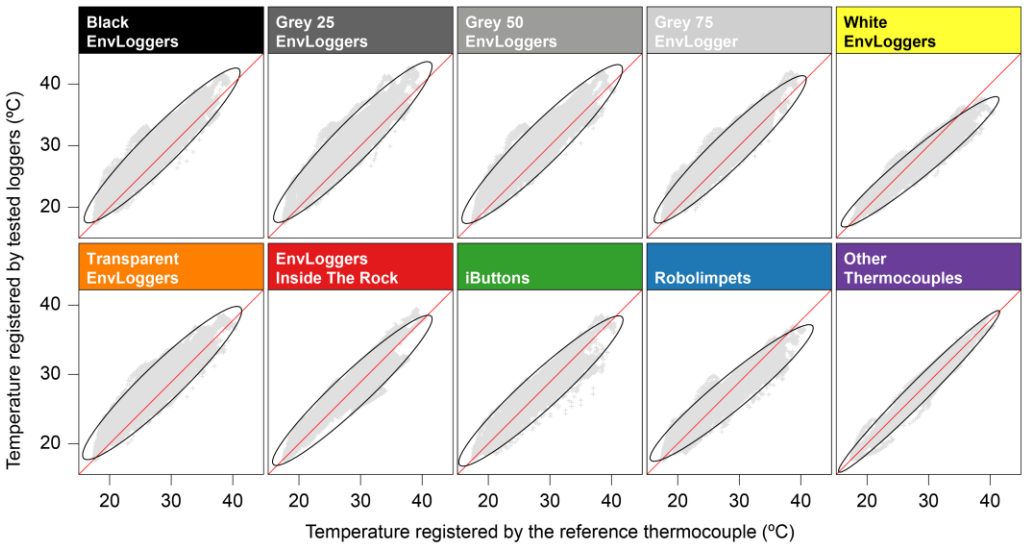


Figure 2.3: Overall temperature distribution between each type of temperature logger and its nearest thermocouple (reference). The 1:1 red line indicates perfect correspondence. Black ellipses enclose 95% of data points (grey crosses). Points above the red line represent loggers recording higher temperatures than their reference thermocouple ("running hot"), while points below indicate lower temperatures ("running cold") at specific values.

The cross-correlogram (**Fig. 2.4**) shows that all tested loggers exhibited peak correlations with reference thermocouples at a time lag of 0, with correlations decreasing symmetrically for both positive and negative lags, indicating that the thermal inertia of all loggers closely matched that of the reference thermocouples. Differences between loggers were negligible, at least at short time lags.

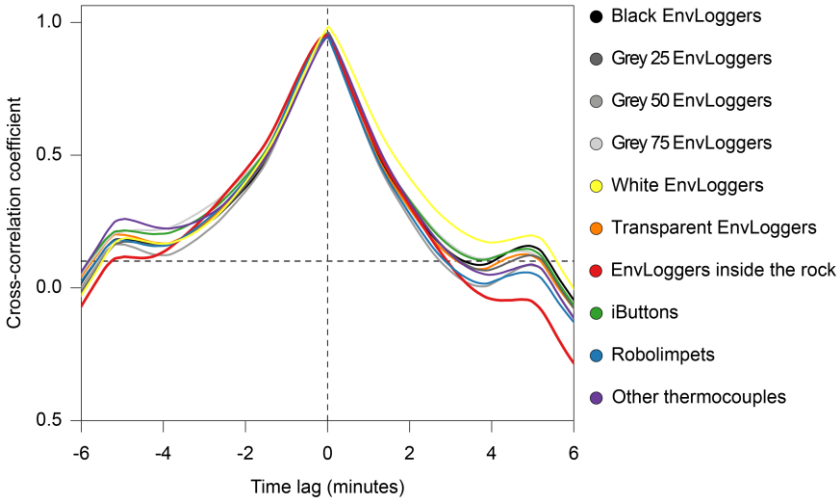


Figure 2.4: Cross-correlation analysis between each type of temperature logger and its nearest thermocouple (reference). A peak away from zero and in the negative half of the graph would indicate a lag of the logger behind the reference.

In summary, among the tested loggers, Grey 75 EnvLoggers, iButtons, and EnvLoggers inside the rock showed the highest accuracy and minimal bias compared to their nearest thermocouples, making them the most reliable options for estimating substrate temperatures in the top few millimetres of rock.

2.4.2. Long-term logger loss rate in challenging environments

Although long-term loss rates varied considerably across studies, three main categories emerged. First, naked iButtons deployed in aquatic or damp habitats exhibited the highest loss rates, ranging from 11% to 47% per month (**Table 2.3**). These were followed by surface-deployed EnvLoggers or biomimetic loggers such as robolimpets and robobarnacles, which, while still experiencing considerable loss rates, were an order of magnitude more resilient, with loss rates ranging from 8% to 37% per year. Lastly, EnvLoggers deployed inside the rock had negligible loss rates, two orders of magnitude lower, at approximately 0.1% per year.

Table 2.3: Loss rates of temperature loggers equivalent to those evaluated in this study, deployed in similar habitats. Note that while the loss rates of iButtons are expressed in % per month, the loss rates of all other loggers are expressed in % per year.

Dataloggers	Loss rate	n	Habitat	Geographical area	Deployment period	Reference
Naked DS1922L iButtons	46.67% per month	45	Rocky intertidal	7 locations in the East coast of USA, between MA and NC	May-June 2007	Authors of this study, unpub. data
Unspecified naked iButtons	21.43% per month	8	Freshwater springs, underwater	Coahuila, Mexico	June 2006	Wolaver and Sharp, 2007
Naked DS1921G iButtons	11.02% per month	387	Riparian habitats	Queensland, Australia	May-June 2007	Roznik and Alford, 2012
Robobarnacles based on DS1922L iButtons	15.00% per year	10	Rocky intertidal	NE Taiwan	2013-2014	Chan et al., 2016
Robolimpets based on DS1922L iButtons	36.78% per year	264	Rocky intertidal	16 locations between Scotland and Portugal	2017-2018	Salois et al., 2022

Robolimpets based on T2.4 Envloggers	18.33% per year	15	Rocky intertidal	13 locations between Scotland and Portugal	2019-2023	H. Parry-Wilson and N. Mieszkowska, pers. communication
Naked T2.4 EnvLogger at the rock surface	7.61% per year	46	Rocky intertidal	13 locations between Scotland and Portugal	2019-2023	H. Parry-Wilson and N. Mieszkowska, pers. communication
EnvLogger T2.4 within the rock	0.10% per year	444	Rocky intertidal	68 locations in Morocco, Portugal and Spain	2019-2024	Authors of this study, unpub. data
EnvLogger T7.3 within the rock	0.07% per year	299	Rocky intertidal	33 locations from Norway to Portugal, Brazil and Argentina	2021-2024	Authors of this study, unpub. data

2.4.3. Sampling frequency

The impact of reduced sampling frequency showed consistent patterns across the four intertidal levels (**Fig. 2.5** and **Supplementary Fig. S2.4**), with more pronounced differences at higher tidal levels. Average temperature differences increased with longer sampling intervals, resulting in underestimations of maximum daily temperatures and overestimations of daily minimum temperatures (see a detailed example in **Supplementary Fig. S2.5**). Notably, maximum temperature underestimations were always greater in magnitude than minimum temperature overestimations. Even at very low sampling rates (1 sample per 360 minutes), minimum temperature overestimations stayed below 1 °C, while maximum temperature underestimations reached -5 °C. Microhabitat comparisons revealed that maximum temperature underestimations were highest in the hottest microhabitats (facing south) and lowest in the coolest (facing north), with intermediate values in east- and west-facing orientations and tide pools. Differences in daily minimum temperatures among microhabitats were minimal. Across all microhabitats, tidal heights, and temperature targets, sampling frequencies of 1 sample per 60 minutes or higher resulted in average errors below 1 °C.

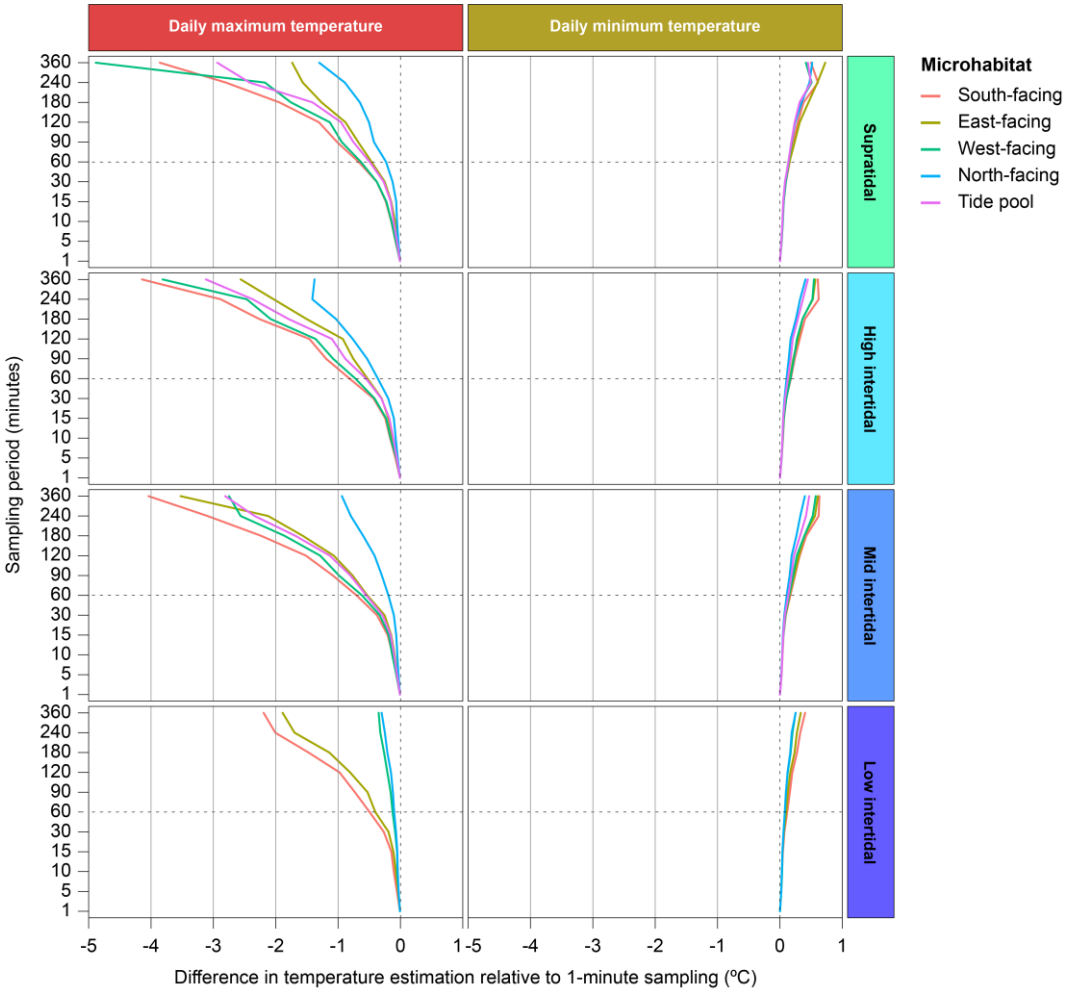


Figure 2.5: Average differences in daily maximum and minimum temperature estimations across various sampling rates relative to 1-minute sampling (reference) in distinct intertidal zones and microhabitats (supratidal, high, mid, and low intertidal zones across various compass orientations and tide pools). Since the study site is located in the northern hemisphere, south-facing loggers correspond to the warmest microhabitats, and north-facing loggers to the coolest. Negative values indicate underestimation, while positive values indicate overestimation relative to the 1-minute reference. For more details, see **Supplementary Figs. S2.4** and **S2.5**.

Reduced sampling also affected the identification of the hottest and coldest days within a week. As shown in **Fig. 2.6**, even slight rarefaction of the original 1-minute dataset (e.g., 1 sample every 5 minutes) caused errors in identifying the hottest or coldest day. For example, in 0.8% of cases, the hottest day was mistakenly identified as the next or previous day, and in 0.1% of cases, it was identified up to 5 days away. These errors likely occurred in weeks where consecutive daily maxima or minima differed only slightly, resulting in incorrect identification when the true extremes were not sampled. At intermediate sampling frequencies (e.g., 1 sample per 60 minutes), errors still remained

relatively low, with the hottest day correctly identified 90% of the time and the coldest day 94% of the time. However, at the maximum sampling interval (1 sample per 360 minutes), accuracy dropped significantly, with correct identification of the hottest day occurring only 69 % of the time and the coldest day 79% of the time.

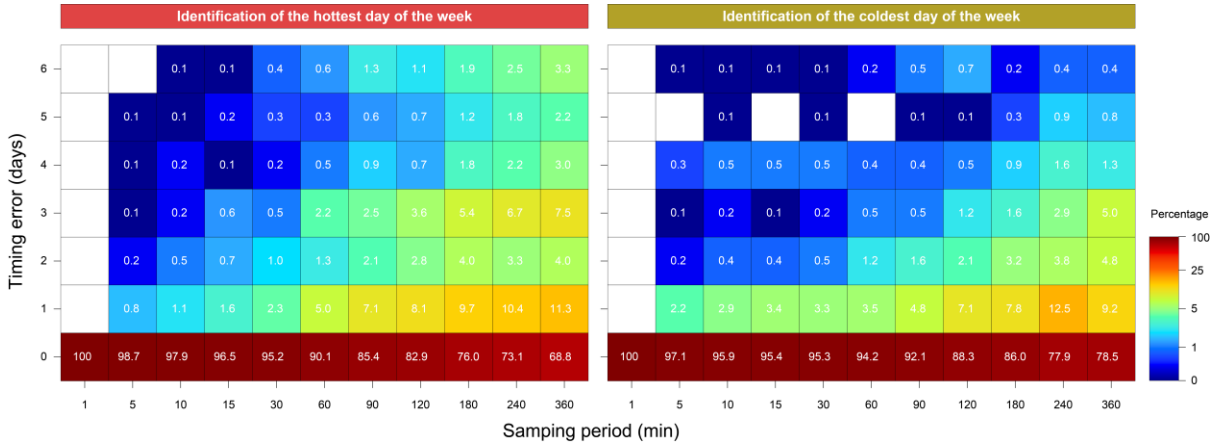


Figure 2.6: Percentage distribution of timing errors when using rarefied data to estimate the hottest or coldest day of the week. The x-axis represents the sampling intervals tested, from the 1-minute reference to every 360 minutes. The y-axis shows the absolute timing error in days. Each box's colour intensity indicates the percentage of occurrences for a given timing error at each sampling interval (also shown as white text inside each box), with warmer (reddish) colours representing higher percentages. The closer to 100% on the lower row, the fewer errors are being introduced in the identification of the days when the extremes occurred. For a breakdown of timing errors across intertidal zones and orientations, see **Supplementary Fig. S2.6**.

2.5. Discussion

Long-term monitoring is crucial and requires careful methodological decisions. While accuracy is arguably the main concern, other considerations include durability, ease of use, and cost-effectiveness, which determine representativity and replication.

This study demonstrates that embedding T7.3 EnvLoggers within the rock substrate provides comparable or superior performance to surface deployments for accurately quantifying intertidal rocky surface temperatures. Surface-deployed loggers often exhibit greater bias, likely associated with their colour and material properties. For instance, black and dark grey EnvLoggers tend to record temperatures higher than those of the rock (likely due to increased absorption of solar radiation), whereas white EnvLoggers and robolimpets underestimate higher rock temperatures (likely due to higher reflectivity). Moreover, the accuracy of surface-deployed loggers is more dependent on the specific rock type where they were deployed (**Table S2.1**). In contrast, rock-embedded loggers exhibit more consistent performance across different rock types,

presumably because their energy balance is primarily driven by conductive heat transfer. Hence, although the logger's thermal conductivity and heat capacity may differ from those of the rock, the much smaller mass and volume render its thermal inertia nearly indistinguishable from that of the surrounding substrate, and the thermal trajectory of an embedded logger remains closely coupled to that of the rock in which it is embedded. This feature is particularly beneficial when the goal is to obtain a broad, standardised estimate of the thermal environment of a rocky microhabitat over time, i.e., not limited to a specific species. Surface-deployed loggers are more exposed to external factors such as wind, evaporative cooling, enhanced convective heat transfer, and differential solar radiation, under which their physical properties (e.g., albedo, shape) exert a stronger influence. Consequently, they are more thermally decoupled from the rock. Hence, surface-deployed loggers should only be used after careful consideration of their thermal properties relative to those of the substrate or when the goal is explicitly to mimic a particular species. In such cases, the logger encapsulation should be fine-tuned and validated against temperatures measured in live animals (Lima & Wethey, 2019).

While the primary motivation for embedding loggers was to improve accuracy and standardization, a key secondary benefit emerged: significantly longer monitoring durations, at least one order of magnitude longer than other currently available options. With an observed loss rate of only ~0.1 % per year, most rock-embedded EnvLoggers can effectively realise their full 15-year battery life and data-storage capacity. This has profound logistical and budgetary implications, reducing the need for frequent servicing or replacement, especially in challenging environments like ice-scoured areas or locations prone to wave-hauled debris. Unlike loggers protruding from the rock, embedded loggers are naturally protected by it. Reliability is enhanced by non-volatile memory and communication powered solely by the smartphone, enabling data retrieval even after battery depletion. The inconspicuous deployment also ensures loggers remain as hidden from passersby as possible, seamlessly integrated into the environment, which not only contributes to their longevity but also preserves the natural aesthetic of the deployment location, an especially important consideration inside protected area. These advantages, although already important at small-scale deployments, are crucial when establishing long-term, large-scale monitoring networks.

This study also shows that a sampling frequency of 1-hour captures most of the information required to characterise intertidal thermal landscapes. Such a frequency minimizes logistical burdens, supports long-term monitoring even during periods of restricted site access (e.g., the COVID-19 pandemic), and produces volumes of data that

are still manageable. While shorter sampling intervals can be advantageous and are recommended for specific experiments, they should not be used as the default unless absolutely necessary.

The ease of use and durability of T7.3 EnvLoggers open additional opportunities for collaborative and large-scale monitoring initiatives. Embedded loggers can remain in place for extended periods, with data easily downloaded via regular NFC-enabled smartphones. Both iOS and Android Apps are freely available at the respective App stores (Envloggers Viewer, v6.1). The user-friendly interface of the smartphone App, initially developed to improve usability even in adverse weather conditions, also facilitates the adoption of this technology by researchers, students, park rangers (Bravo et al., 2024), and citizen science initiatives with minimal training (for example, it minimizes human errors by saving and backing up data automatically). This setup also supports "data-vault" deployments, where loggers passively record data until specific events (e.g., marine heatwaves or temperature thresholds) prompt data retrieval, reducing the need for routine site visits.

The validation of T7.3 EnvLoggers in the rocky intertidal – a thermally dynamic, harsh, yet accessible environment – can be used as a benchmark for other ecosystems, such as deserts or tropical forests. The simplicity of the methodology, its operational advantages, and its scalability make it suitable to be adapted for use in other contexts with only minor adjustments.

The proposed method does have limitations. Embedded loggers are permanently installed and cannot be relocated for new experiments, as removing them destroys the devices. Batteries cannot be replaced due to the design and deployment methods, but their sturdiness nearly eliminates the risk of early failure from water ingress, a common issue in loggers with replaceable batteries. Data download requires site visits (i.e., cannot be done remotely), and the initial deployment is complex, involving relatively heavy drilling equipment and additional time. Depending on the number of loggers to be installed, deployment may need to be spread across multiple low tides. In addition, some microhabitats, such as narrow cracks, high vertical walls, or deep tide pools, may be challenging or impossible to drill into. However, submersible drillers can address some of these limitations. Despite these challenges, this study highlights that embedding T7.3 EnvLoggers in rocky intertidal substrates provides an optimal solution for accurate, long-term temperature monitoring. This approach ensures accurate measurement of surface temperatures while enabling extended monitoring durations, significantly longer than most other currently available options.

2.6. Acknowledgements

This work was supported by Fundação para a Ciência e Tecnologia (FCT) through the projects ThermalBuffer (POCI-01-0145-FEDER-31088) and OceanLog (PTDC/BIA-BMA/4848/2021), and by Luso-American Development Foundation (FLAD) through the project CCTBON (Science Award Atlantic 2020). LFP received support from FCT through a PhD grant (SFRH/BD/136924/2018), and FPL, RdS and RS through CEECInd contracts (10.54499/CEECIND/03185/2018/CP1546/CP1648/CT0004, 10.54499/2021.03268.CEECIND/CP1668/CT0001,10.54499/CEECIND/01424/2017/CP1423/CP1645/CT0006, respectively).

2.7. References

Bravo, G., Bigatti, G., Bagur, M., Macaya, E. C., Valdivia, N., Rodriguez, A., Gauna, M., Walker, I., Livore, J. P., Mendez, M. M., Nieto Vilela, R., Lima, F. P., Seabra, R., & Montes, E. (2024). Implementing biodiversity monitoring of rocky shores using photo-quadrats and artificial intelligence in support of data-driven decision-making of marine living resources. Research Ideas and Outcomes, 10, e126660. https://doi.org/10.3897/rio.10.e126660

Carslaw, D. C., & Ropkins, K. (2012). openair—An R package for air quality data analysis. Environmental Modelling & Software, 27–28, 52–61. https://doi.org/10.1016/j.envsoft.2011.09.008

Chan, B. K. K., Lima, F. P., Williams, G. A., Seabra, R., & Wang, H.-Y. (2016). A simplified biomimetic temperature logger for recording intertidal barnacle body temperatures. Limnology and Oceanography: Methods, 14(7), 452–462. https://doi.org/10.1002/lom3.10103

Christidis, N., Jones, G., & Stott, P. (2015). Dramatically increasing chance of extremely hot summers since the 2003 European heatwave. Nature Climate Change, 5, 46–50. https://doi.org/10.1038/nclimate2468

Comte, L., & Olden, J. D. (2017). Climatic vulnerability of the world's freshwater and marine fishes. Nature Climate Change, 7, 718–722. https://doi.org/10.1038/nclimate3382

Dillon, M. E., Woods, H. A., & Pincebourde, S. (2019, March). Sampling frequency in thermal ecology: Do missed extremes and interpolated means matter? In Integrative and Comparative Biology, 59, E54–E54. Oxford University Press.

Gandra, M., Seabra, R., & Lima, F. P. (2015). A low-cost, versatile data logging system for ecological applications. Limnology and Oceanography: Methods, 13(3), 115–126. https://doi.org/10.1002/lom3.10012

Gilbert, D. E., Morris, J. E., Kaveney, A. R., & Déry, S. J. (2022). Sub-hourly water temperature data collected across the Nechako Watershed, 2019-2021. Data in Brief, 43, 108425. https://doi.org/10.1016/j.dib.2022.108425

Helmuth, B. S., & Hofmann, G. E. (2001). Microhabitats, thermal heterogeneity, and patterns of physiological stress in the rocky intertidal zone. Biological Bulletin, 201(3), 374–384. https://doi.org/10.2307/1543615

Helmuth, B., Mieszkowska, N., Moore, P., & Hawkins, S. J. (2006). Living on the edge of two changing worlds: Forecasting the responses of rocky intertidal ecosystems to climate change. Annual Review of Ecology, Evolution, and Systematics, 37(1), 373–404. https://doi.org/10.1146/annurev.ecolsys.37.091305.110149

Hobday, A. J., Alexander, L. V., Perkins, S. E., Smale, D. A., Straub, S. C., Oliver, E. C. J., ... Wernberg, T. (2016). A hierarchical approach to defining marine heatwaves. Progress in Oceanography, 141, 227–238. https://doi.org/10.1016/j.pocean.2015.12.014

Kemppinen, J., Lembrechts, J. J., Van Meerbeek, K., Carnicer, J., Chardon, N. I., Kardol, P., ... De Frenne, P. (2024). Microclimate, an important part of ecology and biogeography. Global Ecology and Biogeography, 33, e13834. https://doi.org/10.1111/geb.13834

Lembrechts, J. J., Aalto, J., Ashcroft, M. B., et al. (2020). SoilTemp: A global database of near-surface temperature. Global Change Biology, 26, 6616–6629. https://doi.org/10.1111/gcb.15123

Lima, F. P., & Wethey, D. S. (2009). Robolimpets: Measuring intertidal body temperatures using biomimetic loggers. Limnology and Oceanography: Methods, 7, 347–353. https://doi.org/10.4319/lom.2009.7.347

Lima, F. P., Gomes, F., Seabra, R., Wethey, D. S., Seabra, M. I., Cruz, T., ... Hilbish, T. J. (2016). Loss of thermal refugia near equatorial range limits. Global Change Biology, 22(1), 254–263. https://doi.org/10.1111/gcb.13115

Ma, L.-X., Wang, J., Denny, M., & Dong, Y.-W. (2024). Hindcasted body temperatures reveal underestimated thermal stress faced by intertidal species. Global Ecology and Biogeography, 33, e13908. https://doi.org/10.1111/geb.13908

Maloney, M. E., Buckley, K. M., & Strader, M. E. (2024). Appendage pigmentation and temperature acclimation correlate with survival during acute heat stress in the upside-down jellyfish, Cassiopea xamachana. Frontiers in Ecology and Evolution, 12, 1409379. https://doi.org/10.3389/fevo.2024.1409379

Meneghesso, C., Seabra, R., Broitman, B. R., Wethey, D. S., Burrows, M. T., Chan, B. K. K., ... Lima, F. P. (2020). Remotely-sensed L4 SST underestimates the thermal fingerprint of coastal upwelling. Remote Sensing of Environment, 237, 111588. https://doi.org/10.1016/j.rse.2019.111588

Montalto, V., Sará, G., Ruti, P., Dell'Aquila, A., & Helmuth, B. (2014). Testing the effects of temporal data resolution on predictions of bivalve fitness in the context of global warming. Ecological Modelling, 278, 1–8. https://doi.org/10.1016/j.ecolmodel.2014.01.019

Parry-Wilson, H. M., Fenberg, P. B., Hawkins, S. J., & Mieszkowska, N. (2024). Lethal and sub-lethal responses of rocky shore gastropods to extreme temperatures. Journal of Experimental Marine Biology and Ecology, 579, 152044. https://doi.org/10.1016/j.jembe.2024.152044

Pfister, C. A., Wootton, J. T., & Neufeld, C. J. (2007). The relative roles of coastal and oceanic processes in determining physical and chemical characteristics of an intensively sampled nearshore system. Limnology and Oceanography, 52(5), 1767–1775. https://doi.org/10.4319/lo.2007.52.5.1767

Pincebourde, S., & Salle, A. (2020). On the importance of getting fine-scale temperature records near any surface. Global Change Biology, 26(11), 6025–6027. https://doi.org/10.1111/gcb.15210

Potter, K. A., Woods, H. A., & Pincebourde, S. (2013). Microclimatic challenges in global change biology. Global Change Biology, 19, 2932–2939. https://doi.org/10.1111/gcb.12257

Rich, W. A., Glanz, J. S., Mele, G., Burt, N. J., Carvalho, S., Doo, S. S., ... Suggett, D. J. (2024). Widespread inconsistency in logger deployment methods in coral reef studies may bias perceptions of thermal regimes. PLOS Climate, 3(12), e0000517. https://doi.org/10.1371/journal.pclm.0000517

Ripple, W. J., Wolf, C., Gregg, J. W., Rockström, J., Newsome, T. M., Law, B. E., ... King, S. D. A. (2023). The 2023 state of the climate report: Entering uncharted territory. BioScience, 73(12), 841–850. https://doi.org/10.1093/biosci/biad080

R Development Core Team. (2024). R: A language and environment for statistical computing (Version 4.4.2). R Foundation for Statistical Computing. https://www.r-project.org/

Roznik, E. A., & Alford, R. A. (2012). Does waterproofing Thermochron iButton dataloggers influence temperature readings? Journal of Thermal Biology, 37(4), 260–264. https://doi.org/10.1016/j.jtherbio.2012.02.004

Salois, S. L., Gouhier, T. C., Helmuth, B., Choi, F., Seabra, R., & Lima, F. P. (2022). Coastal upwelling generates cryptic temperature refugia. Scientific Reports, 12(1), 19313. https://doi.org/10.1038/s41598-022-23717-5

Seabra, R., Wethey, D. S., Santos, A. M., & Lima, F. P. (2011). Side matters: Microhabitat influence on intertidal heat stress over a large geographical scale. Journal of Experimental Marine Biology and Ecology, 400(1–2), 200–208. https://doi.org/10.1016/j.jembe.2011.02.010

Spurgeon, E., Thompson, M. L., Alexander, M. D., Anderson, J. M., Rex, P. T., Stirling, B., ... Lowe, C. G. (2024). The influence of micro-scale thermal habitat on the movements of juvenile white sharks in their Southern California aggregation sites. Frontiers in Marine Science, 11. https://doi.org/10.3389/fmars.2024.1290769

Sun, Y. X., Hu, L. S., & Dong, Y. W. (2023). Surviving hot summer: Roles of phenotypic plasticity of intertidal mobile species considering microhabitat environmental

heterogeneity. Journal of Thermal Biology, 117, 103686. https://doi.org/10.1016/j.jtherbio.2023.103686

Taylor, K. E. (2001). Summarizing multiple aspects of model performance in a single diagram. Journal of Geophysical Research: Atmospheres, 106(D7), 7183–7192. https://doi.org/10.1029/2000JD900719b

Wolaver, B. D., & Sharp, J. M. (2007). Thermochron iButton: Limitation of this inexpensive and small-diameter temperature logger. Ground Water Monitoring & Remediation, 27(3), 129–133. https://doi.org/10.1111/j.1745-6592.2007.00158.x

2.8. Supplementary Figures

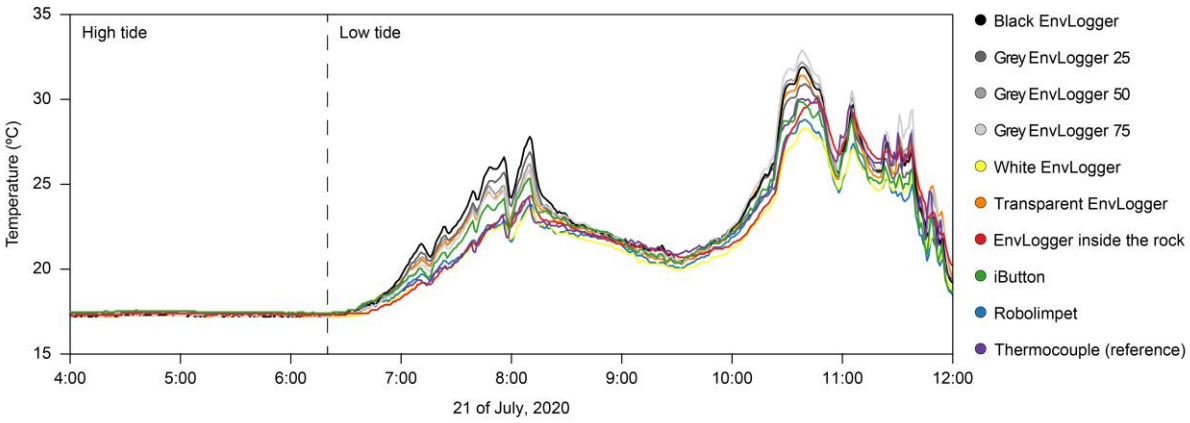
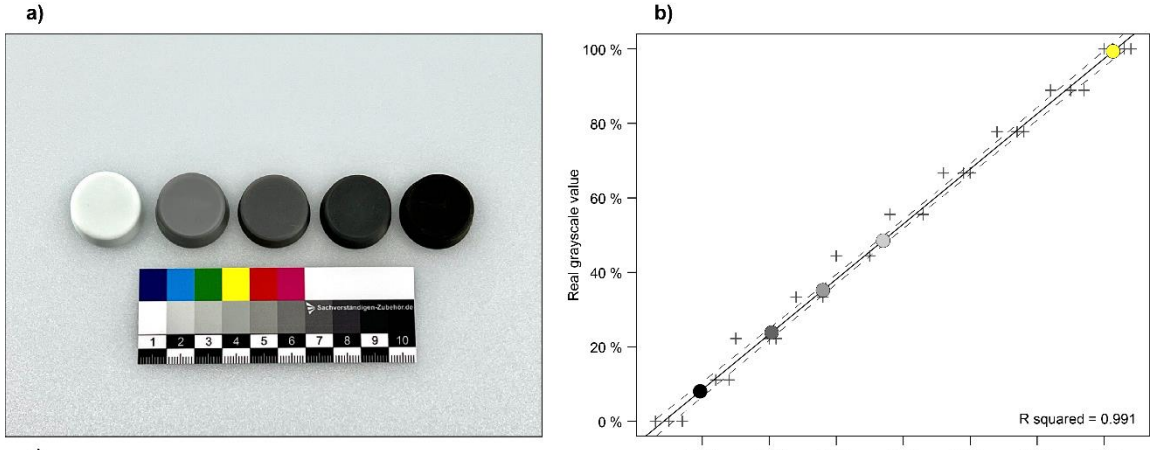


Figure S2.1: Typical temperature profiles recorded by different types of loggers, illustrated by the set of loggers nearest to thermocouple on the fine-grain granite rock during low tide on July 21, 2020. Temperatures in the period up to around 6:20, on the left side of the graph, were recorded underwater, while the rest was recorded during low tide.



c)

Reference name	Colour proportion	Real greyscale
White EnvLogger	4:0 white/black	99 %
Grey 75 EnvLogger	3:1 white/black	49 %
Grey 50 EnvLogger	2:2 white/black	35 %
Grey 25 EnvLogge	1:3 white/black	24 %
Black EnvLogger	0:4 white/black	8 %

Figure S2.2: Determination of the greyscale tone for white, grey, and black EnvLoggers. The color gradient was obtained by varying the proportions of black and white opaque acrylic paint during logger manufacturing; a) Sample image of the loggers with a calibration greyscale from https://sachverstaendigen-zubehoer.de; b) Linear regression (with 95% confidence intervals) between pixel values from the calibration scale images and their actual greyscale values (cross symbols), using three replicate images taken under slightly different lighting conditions. Pixel measurements were obtained using Affinity Photo software; c) Proportions of acrylic paint used in each logger type and their corresponding absolute greyscale values.

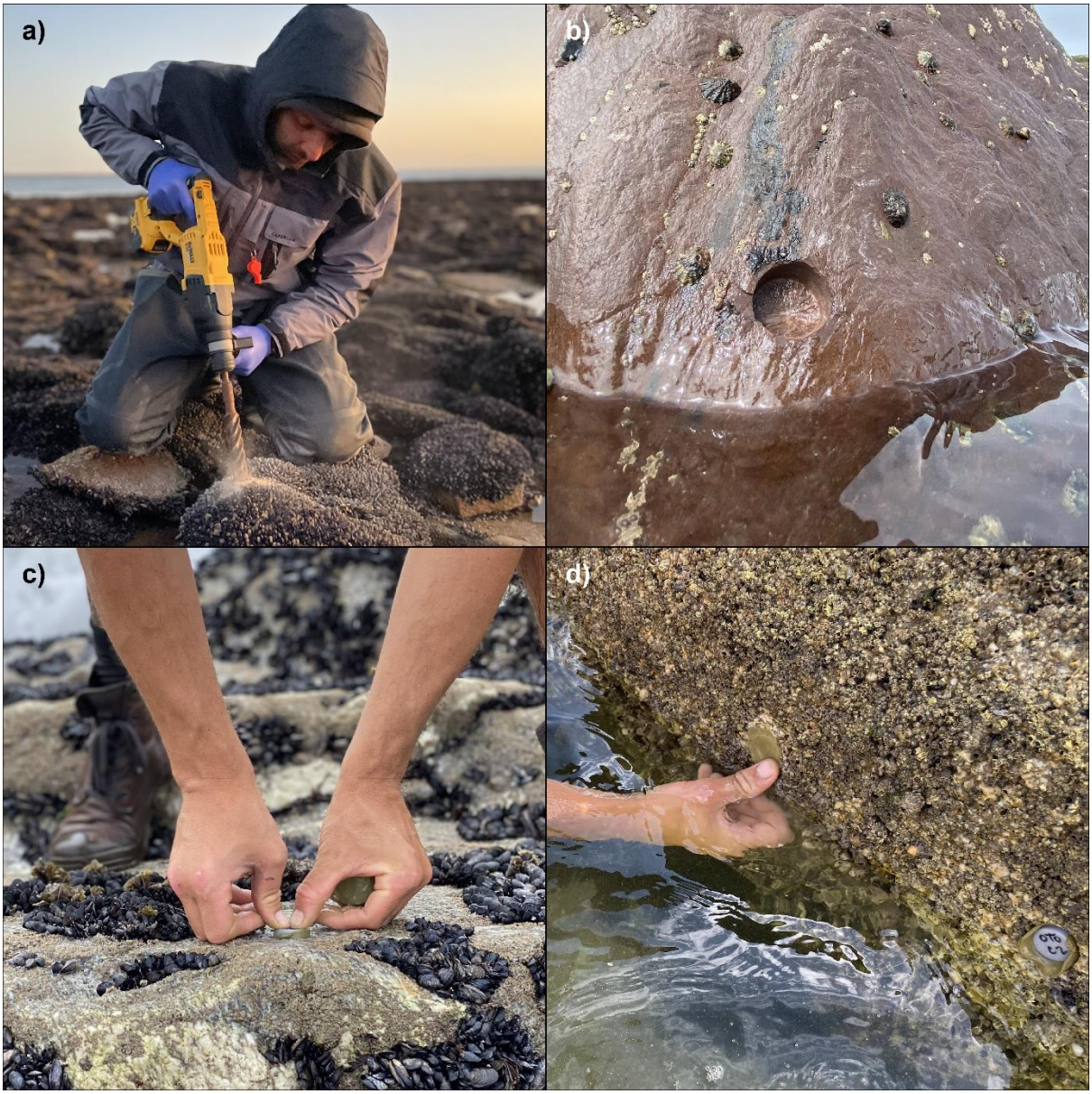


Figure S2.3: Process of embedding EnvLoggers into the rock; a) Using a battery-powered DCH133M1 DeWALT driller with a 30 mm DeWALT DT9618-QZ drill bit to make a hole in the rock; b) A 30 mm wide and 15 mm deep hole in the rock; c) Pressing an EnvLogger against the rock with A-788 Z-Spar Splash Zone Compound (Carboline, USA. The antenna side of the logger must be kept facing up; d) On the left, covering a EnvLogger with a ~1 mm layer of the same compound; on the right, a logger still to be covered.

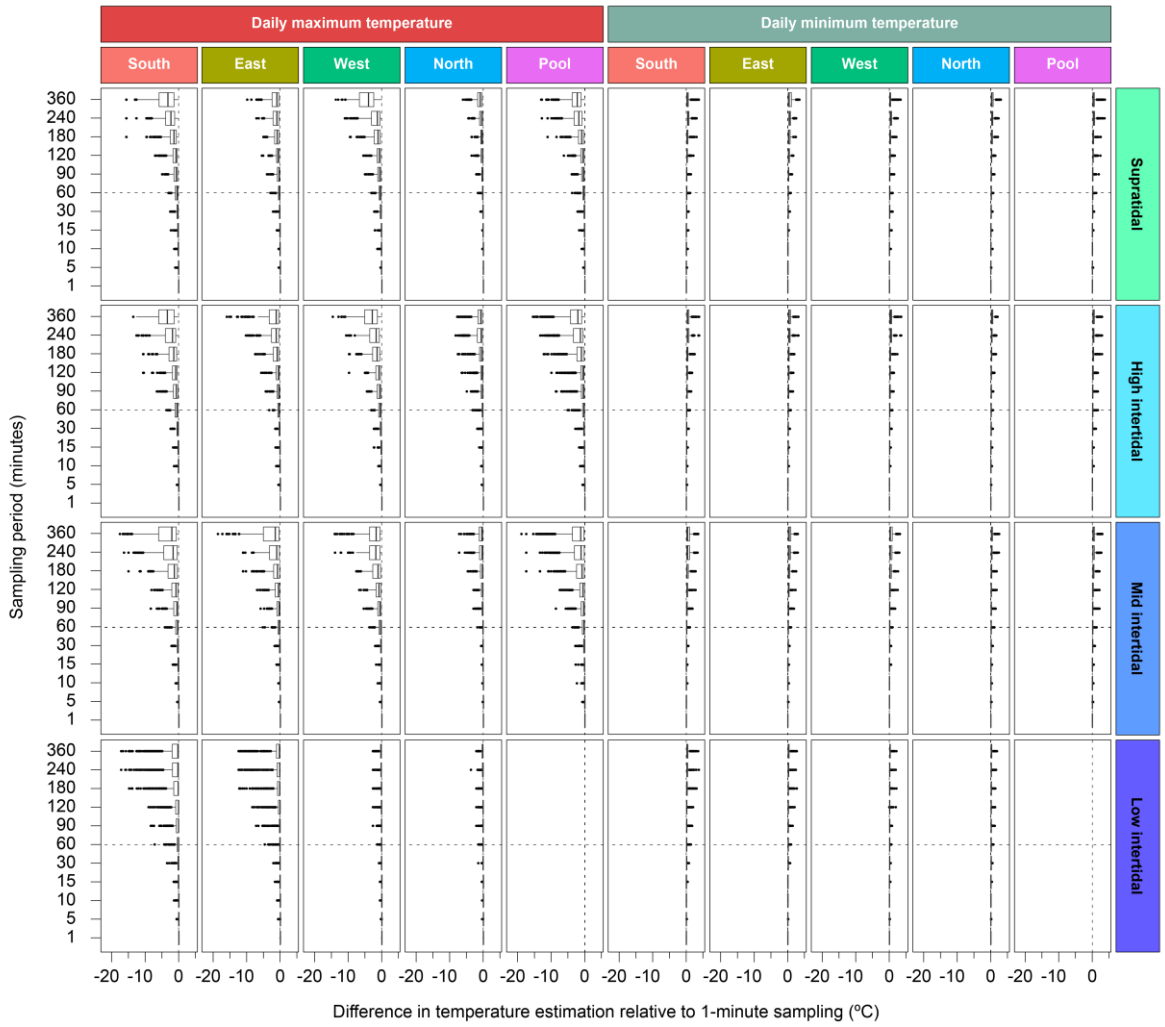


Figure S2.4: Box plots (with outliers) showing differences in daily maximum and daily minimum temperature estimates at various sampling intervals compared to the 1-minute sampling reference across intertidal zones and orientations. Sampling intervals range from 1 to 360 minutes, with results shown for supratidal, high, mid, and low intertidal zones in south, east, west, and north orientations, as well as for a tide pool microhabitat. Since the study site is located in the northern hemisphere, south-facing loggers correspond to the warmest microhabitats, and north-facing loggers are representative of the coolest. Negative values indicate underestimations, and positive values indicate overestimations relative to the 1-minute reference, highlighting how sampling frequency impacts temperature accuracy in each zone and orientation.

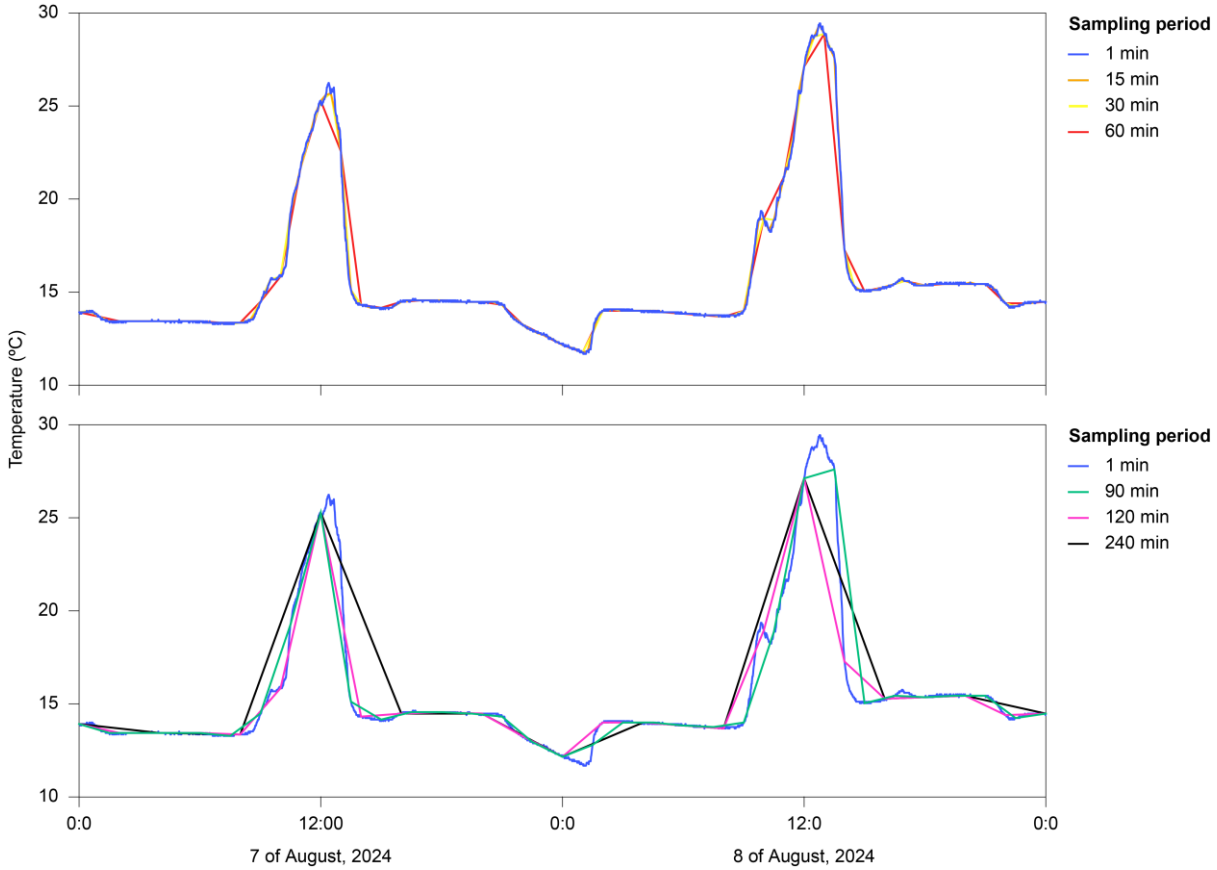


Figure S2.5: Impact of reduced sampling rates on temperature estimates, with 1-minute sampling at one of the high-intertidal, south-facing loggers as the reference (where temperature fluctuates the most). To enhance clarity, only selected sampling rates are shown, separated into two plots. Sampling intervals include 15, 30, 60, 90, 120, and 240 minutes. It can be clearly seen that reduced frequency reduces the details that can be extracted from the data. In particular, estimations of the daily extremes can include large biases at the lowest sampling frequencies.

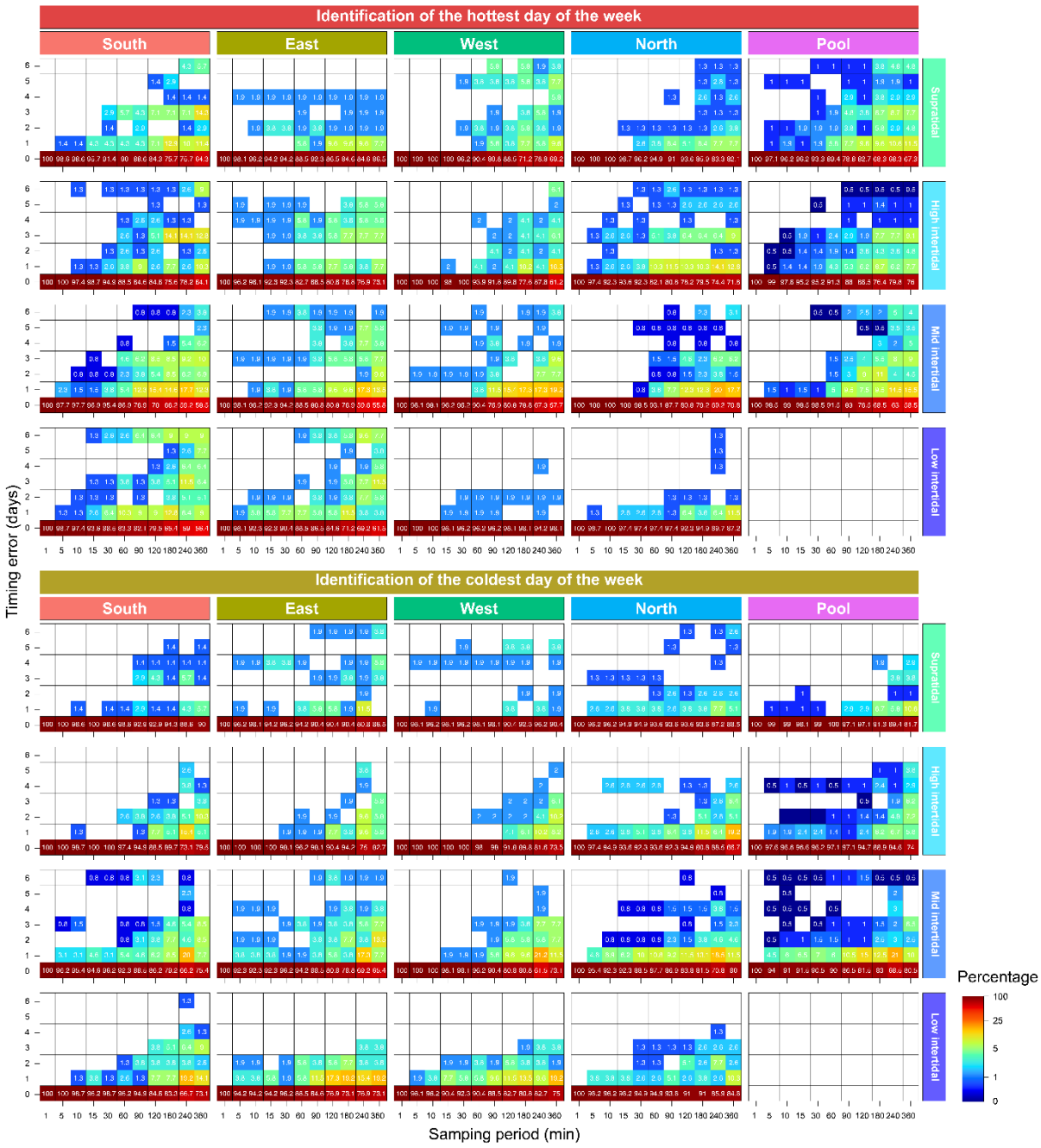


Figure S2.6: Percentage distribution of timing errors when using rarefied data to estimate the hottest or coldest day of the week, across intertidal zones and orientations. The x-axis represents the sampling intervals tested, from the 1-minute reference to every 360 minutes. The y-axis shows the absolute timing error in days. Each box's colour intensity indicates the percentage of occurrences for a given timing error at each sampling interval, with warmer (reddish) colours representing higher percentages. The closer to 100% on the lower row, the fewer errors are being introduced in the identification of the days when the extremes occurred.

2.9. Supplementary Tables

Table S2.1: Combined performance of the replicate temperature loggers (n= 3), separately for each type of rock. Metrics include mean bias (MB), centred root mean square error (cRMSE), root mean square error (RMSE), Pearson's correlation coefficient (R), and normalised standard deviation (NSD). Rock albedo was roughly estimated by quantifying brightness in ImageJ (Schneider et al., 2012) from standardised, replicated areas (n= 3) in digital photographs of the rocks, using a reference A4 sheet of office paper (with a known albedo of ~0.65) included in each image.

		MB (ºC)	cRMSE (ºC)	RMSE (ºC)	R	NSD
Fine-grain granite (albedo ~0.246)	**Black EnvLoggers**	-1.00	1.60	1.89	0.95	0.99
	Grey 25 EnvLoggers	-1.66	1.33	2.13	0.97	1.04
	Grey 50 Envloggers	-0.89	1.47	1.72	0.96	1.00
	Grey 75 EnvLoggers	-0.41	1.61	1.66	0.94	0.97
	White EnvLoggers	1.58	1.46	2.15	0.96	0.86
	Transparent Envloggers	-0.71	1.63	1.78	0.95	0.94
	EnvLoggers Inside Rock	-0.11	1.46	1.46	0.96	0.98
	iButtons	0.17	1.65	1.66	0.96	0.94
	Robolimpets	0.78	1.77	1.93	0.95	0.85
	Other Thermocouples	-0.06	1.23	1.23	0.97	1.01
Medium-grain granite (albedo ~0.285)	**Black EnvLoggers**	-1.79	1.54	2.36	0.96	1.04
	Grey 25 EnvLoggers	-1.80	1.86	2.59	0.94	1.02
	Grey 50 Envloggers	-2.14	1.49	2.61	0.97	1.09
	Grey 75 EnvLoggers	-1.06	1.68	1.99	0.95	0.97
	White EnvLoggers	0.96	1.65	1.91	0.96	0.83
	Transparent Envloggers	-1.85	1.50	2.38	0.96	1.04
	EnvLoggers Inside Rock	-0.25	1.68	1.70	0.95	0.97
	iButtons	-0.66	1.41	1.56	0.96	0.97
	Robolimpets	0.17	1.54	1.55	0.96	0.87
	Other Thermocouples	-0.09	0.78	0.79	0.99	1.00
Coarse-grain granite (albedo ~0.278)	**Black EnvLoggers**	-1.59	1.84	2.43	0.94	0.95
	Grey 25 EnvLoggers	-2.07	2.03	2.90	0.93	1.00
	Grey 50 Envloggers	-1.38	2.17	2.57	0.92	0.9
	Grey 75 EnvLoggers	-1.14	1.39	1.80	0.96	0.99
	White EnvLoggers	1.17	1.61	1.99	0.97	0.81
	Transparent Envloggers	-1.41	1.99	2.44	0.92	0.92
	EnvLoggers Inside Rock	0.29	1.69	1.71	0.95	0.88
	iButtons	0.20	1.92	1.93	0.94	0.86
	Robolimpets	0.67	1.97	2.08	0.95	0.79
	Other Thermocouples	0.00	0.93	0.93	0.98	1.00

2.10. Supplementary References

Schneider, C. A., Rasband, W. S., & Eliceiri, K. W. (2012). NIH Image to ImageJ: 25 years of image analysis. *Nature Methods,* *9*(7), 671–675. https://doi.org/10.1038/nmeth.2089

Chapter 3

Intertidal Environmental Chamber: an automatic system to accurately simulate the thermal complexity of intertidal environments

3.1. Abstract

Climate change is increasing the frequency of extreme temperature events, often causing sub-lethal stress or mass mortalities in organisms. This has raised the interest in assessing species' thermal performance under current and future climates. Common-garden experiments are widely used to assess species' heat tolerance across populations from different origins under standardised conditions. Replicating realistic conditions, especially for intertidal environments, where both marine and terrestrial stressors are involved, is technically challenging. Consequently, ecologists often develop custom-built systems that are either too simplistic (e.g., ignoring emersion) or difficult to replicate, leading to inconsistencies between studies. To address this challenge, we developed the Intertidal Environmental Chamber: a modular, open-source system designed to realistically simulate the complex thermal environment of intertidal habitats with independent control of tides, immersion and emersion temperatures, light intensity, and water exchange. Here, we showcase the system's capabilities and evaluate its accuracy in replicating field data. We also offer recommendations for running long-term, remote-controlled, geographically distributed, and synchronised experiments.

Keywords

Intertidal environment, immersion, emersion, temperature, heatwaves, common-garden experiments.

Open source repository

Complete bill of materials, instructions on how to operate the Intertidal Environmental Chamber and scripts to support preparation of experiments can be found in the following GitHub repository: https://anonymous.4open.science/r/Intertidal_chamber.

3.2. Introduction

Climate change is increasing the frequency of temperature extremes across many ecosystems (Pörtner et al., 2019), often exceeding species' tolerance and causing mass mortalities (Hesketh & Harley, 2023). This has sparked interest in assessing the thermal performance of species and populations under current and future climate conditions (Bennett et al., 2021) to gain mechanistic insights that improve predictions of climate change impacts (Seabra et al., 2016). Typically, researchers evaluate species' thermal limits by transplanting the organisms to other regions or conducting laboratory common-garden experiments (King et al., 2018). The latter method has significant advantages, as it minimises logistical complexity and allows exposure to environmental conditions beyond those of the experimental location. However, assembling and operating common-garden systems to realistically simulate environmental conditions can involve considerable technical complexity. Consequently, ecologists often resort to custom-built systems that commonly have two fundamental limitations: Firstly, experimental conditions tend to oversimplify heat stress by applying constant or steadily ramping temperatures or isolating heat stress into single thermal events, which can overlook compounded stress responses (Pasparakis et al., 2016). This issue is particularly true for intertidal environments, where organisms are periodically exposed to marine and terrestrial conditions. Additionally, physiological studies frequently neglect tidal cycles and air exposure, focusing solely on water temperature (Wilson et al., 2015). Such approaches can yield inaccurate predictions by ignoring emersion, which can be a moment when organisms experience the highest thermal stress (Davison & Pearson, 1996; Seuront et al., 2019). Secondly, custom-built systems are often assembled iteratively using locally sourced parts, with new components and software added on an ad-hoc basis, frequently resulting in one-of-a-kind apparatuses that are difficult for other researchers to replicate. This lack of standardisation is problematic, as it hampers replicability — a critical requirement in empirical science (Baker, 2016).

To address these issues, we developed a self-contained system that simulates intertidal heat stress, controlling tides, water and air temperatures, light intensity, and water exchange. Its compact design allows for multiple independent units to operate simultaneously within a lab. Featuring automatic water renewal, the system can be programmed for months-long experiments with minimal supervision. Environmental conditions can either follow a repeating cycle or vary continuously over time. Additionally, all parameters can be monitored and adjusted remotely, ensuring both high repeatability and flexibility. This feature also enables researchers to conduct "virtual common-garden

experiments" across geographically distant locations, enabling synchronised studies without transporting organisms to a central location.

3.3. Design and features

3.3.1. Architecture

The Intertidal Environmental Chamber consists of two tanks and a lid supported by an aluminium frame (**Fig. 3.1a**), managed by an Electronic Control Unit (ECU) interfacing with sensors and actuators. The ECU continuously monitors environmental conditions using wired water level and temperature sensors for water, substrate, and room temperature (RT), comparing them to target values. It adjusts the output of visible light, infrared (IR) lamps, water chillers, water heaters, air-circulation fans, valves, and pumps to maintain set parameters. The tanks and lid are made from off-the-shelf polypropylene (PP) containers. The Water Storage Tank (65 L) serves as a sump and pre-conditions water temperature, while the Experiment Tank (35 L) simulates the intertidal environment and holds the organisms (**Fig. 3.1b**). The lid, an inverted 15 L tank reinforced with a steel sheet, supports the lamps and fans. The ECU, located on the left side, features a colour LCD displaying the chamber's status, environmental conditions, sensor/actuator activity, and alarms. It includes manual switches to override the chamber's automatic operation, facilitating maintenance and organism handling. The ECU can also be connected to Wi-Fi for remote monitoring and control. Sensor data and actuator status are continuously logged on a micro-SD and can be stored online.

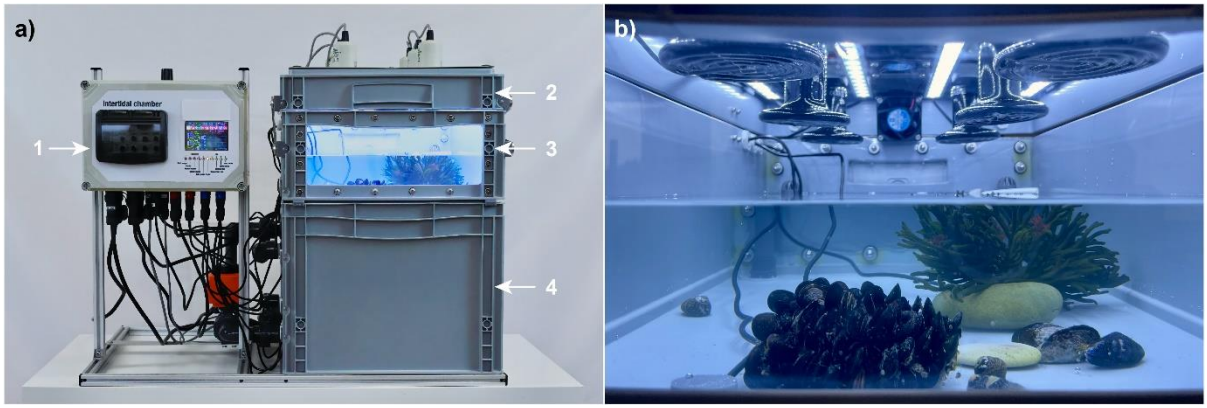


Figure 3.1: a) The Intertidal Environmental Chamber: 1 - ECU with manual override switches and LCD display, 2 – Experimental Tank's Lid, 3 – Experimental Tank, 4 – Water Storage Tank; b) Detail of the Experimental Tank at high tide, showing the LED strips, black IR lamps and air-circulating fans at the top, various mollusc specimens and seaweed underwater, and temperature sensors.

3.3.2. Water control

The Experiment Tank has two clean 8 mm holes at the bottom, as well as two other holes fitted with polyvinyl chloride (PVC) vertical tubes, all fitted with filters to prevent clogging and passively draining water to the Water Storage Tank. To simulate a high tide, a Tide Pump (**Fig.3.2**) is activated, pumping water from the Water Storage Tank into the Experiment Tank faster than it drains, raising the water level. Once the water reaches the height of the PVC tubes, excess water drains through them, balancing the inflow and outflow, hence maintaining the high tide. The tube length sets the high tide level, adjustable up to 14 cm. Water flow can be slightly controlled via the pump's inlet adjustment bracket or changed entirely by using a different AC pump. However, we found that a flow rate of 800 L h^{-1} ensures sufficient mixing between both tanks during high tide while minimizing the risk of overflow in the event of partial clogs affecting the water drainage valves. Water in the Water Storage Tank can be manually or automatically renewed via two valves (In and Out Valves, **Fig. 3.2**). The In Valve lets new water from a pressurized or gravity-fed source into the system. If using an external reservoir, an inlet pump can replace the valve. The Out Valve at the bottom drains water, while the Safeguard Outlet prevents overfilling.

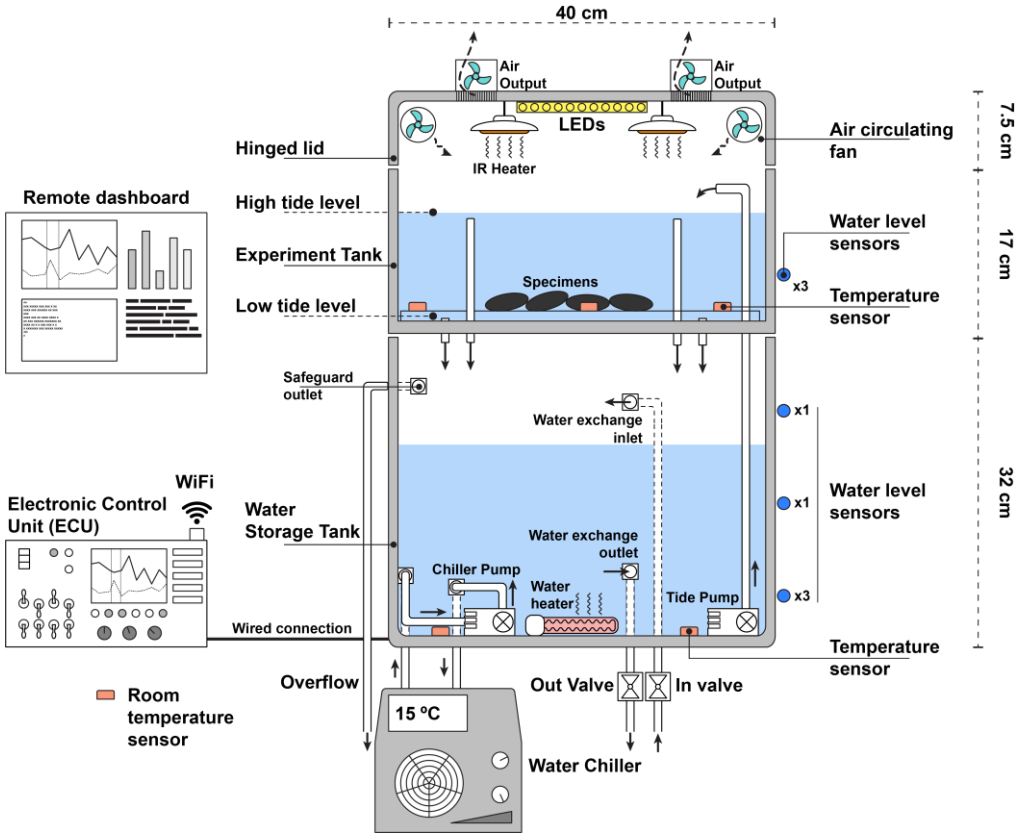


Figure 3.2: Schematic illustration of an Intertidal Environmental Chamber.

3.3.3. Temperature and visible light control

Temperature is monitored by six waterproof DS18B20 sensors (Maxim Integrated, USA): three in the Experiment Tank, two in the Water Storage Tank, and one outside the system (pink rectangles; **Fig. 3.2**). The Experiment Tank sensors provide feedback to the ECU, ensuring the experimental monitoring. Depending on the experiment, these sensors can be attached to or embedded in the substrate. For the rocky intertidal validation described here, sensors were attached to granite tiles, mirroring the field deployment method.

During low tide, the ECU regulates temperature via six 50 W IR lamps and two cooling fans. IR lamps are controlled by a PID algorithm (Ziegler & Nichols, 1942) calibrated for this system, which adjusts the intensity of a response based on real-time feedback, considering the current error, its rate of change, and accumulated past errors, enabling smooth, precise control instead of binary on/off actions. Heating or cooling intensity is calculated every second based on sensor input and target temperature. Note that cooling fans can only lower the Experiment Tank's temperature to match the ambient RT, so additional cooling may require external air conditioning. Additionally, two air-circulating fans inside the lid activate with the IR lamps to homogenise air temperature and minimise heat spots.

Water temperature is controlled by a Water Chiller (Titan 200, 160W, Aqua medic, DE) and a Water Heater (Titanium heater, 500W, Aqua medic, DE), with water homogenisation managed by the Chiller Pump (**Fig. 3.2**). As chillers typically lack precision, the system chills the water slightly below the target temperature, with the Water Heater fine-heating it to the desired level. During low tide, when all water is in the Water Storage Tank, the ECU pre-conditions the water temperature for the next high tide. Visible light is provided by four LED bars (AquaBar T-Series 590mm, Ultra Daylight, Tropical Marine Center, UK) mounted on the lid. The ECU adjusts the light in 1% increments, but it can also be manually controlled via override switches.

3.3.4. Control panel, display, and online mirroring

The ECU features a 3.5-inch colour LCD screen for real-time monitoring of the chamber's operational status, displaying both actual and target environmental conditions (e.g., current vs desired temperature), along with a sensor, actuator, manual override, connectivity, and alarm status (**Fig. 3.3**). This information is also relayed to a third-party website (Blynk IoT platform, USA). Users can quickly check key experimental

parameters (e.g., water levels, heating/cooling intensity, LED brightness), which is vital for long-term experiments where timely detection of malfunctions is critical.

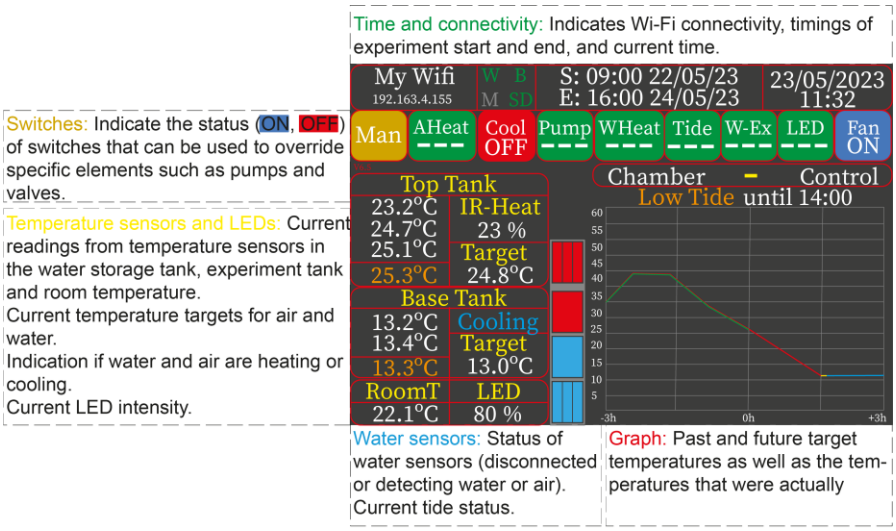


Figure 3.3: Example of the display on the Electronic Control Unit.

To improve system resilience, key components like temperature and water sensors are installed in redundant pairs or triplets, ensuring continued operation even if one fails. Faulty components can be detected early, allowing proactive maintenance without disrupting ongoing experiments. The system also has manual switches on the ECU to cut power to specific elements, enabling safe interventions. The statuses of these switches are displayed on the LCD (**Fig. 3.3**), and most components are designed for easy replacement.

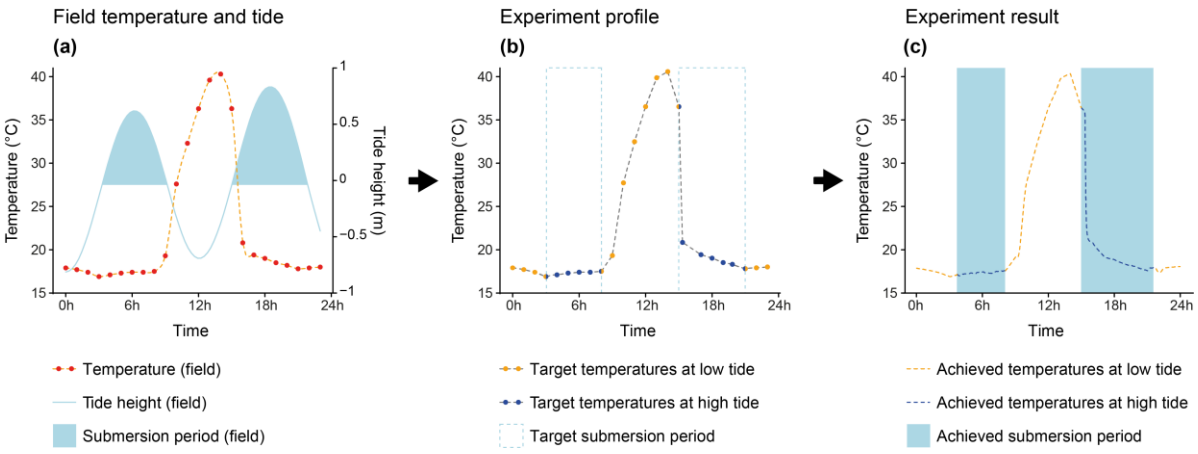


Figure 3.4: a) Hourly temperature data from a temperature logger deployed in a rocky intertidal environment; b) Simplified experiment profile replicating the field conditions. Key experimental steps and their respective temperatures are marked, with submerged steps shown in blue and immersed steps in yellow; c) Actual experiment results from an Intertidal Environmental Chamber. In all plots, submersion periods are highlighted in light blue.

3.3.5. How to run an experiment

Running an experiment in the Intertidal Environmental Chamber requires creating a set of sequential instructions, referred to as the experiment profile, defining environmental conditions at specific times. This profile is a simple text file saved in the root directory of a microSD card and inserted into the ECU (detailed instructions in **Supplementary Text S3.1** and **Fig. S3.1**). Alternatively, it can be uploaded via FTP or a web app (detailed instructions on GitHub repo). An R script is available (provided GitHub repo) to generate the experiment profile from a spreadsheet, converting timestamps to Unix format and calculating LED intensities based on required Photosynthetically Active Radiation (PAR) or Lux levels.

To replicate realistic conditions, field temperature data should be analysed together with tide levels (**Fig. 3.4a**). An instruction line should be created whenever there is a change in temperature, tide status, light intensity, or there is the need to perform a water renewal cycle. In each case, the target for all parameters at that moment must also be specified. Furthermore, instruction lines should be added at critical temperature milestones (e.g., daily peak temperature during low tide) or at any inflexion points in the temperature profile (**Fig. 3.4b**). Between these instructions, the ECU interpolates temperature linearly, generating an internal instruction list at one-second resolution (**Fig. 3.4c**). The tide status flag directs the ECU on whether to control temperature via water-based cooling/heating or IR lamps, as appropriate.

3.3.6. Protection and safety

The Intertidal Environmental Chamber includes safety features to minimize risks associated with its electrical, mechanical, and thermal components, especially in an environment where water and electricity coexist. These features fall into two categories: electrical protections and programmed safeguards.

Electrical protections include: (i) A circuit breaker integrated into the ECU that cuts power to the entire chamber in case of overcurrent or short-circuit conditions, preventing hazards and equipment damage. (ii) Individual fuses protecting major actuators (e.g., chiller, fans, lamps, pumps, heaters), which isolate faulty components by blowing if a short-circuit occurs, allowing the rest of the system to continue operating safely. (iii) A lid-activated safety interlock that disconnects mains power to the IR lamps when the lid is opened, protecting users from burns or electric shocks caused by accidental contact with the IR lamps.

Programmed safeguards include redundant water level sensors (blue circles; **Fig. 3.2**) in both the Experiment Tank and the Water Storage Tank. In the Experiment Tank, these sensors ensure the IR lamps only activate when the tank has no water. If the ECU attempts to simulate a hot low tide but the tank failed to drain (e.g., due to a clog), the lamps could ramp up to full power, as submerged temperature sensors won't detect the heat. This can damage components, create fire risks, or harm organisms when the water eventually drains. Another safeguard caps user-requested temperatures at 60 ºC during low tide and 45 ºC during high tide, preventing overheating and ensuring safe operation. By preventing lamp operation during immersion and limiting temperature settings, the system safeguards both equipment and experiments.

In the Water Storage Tank, sensors monitor the water level to ensure there is sufficient water for safe pump and heater operation. If the water level drops below a safe threshold (e.g., due to a leak), the ECU automatically stops these devices from running dry, preventing potential damage. Detailed information regarding maintenance recommendations and the handling of water circulation problems can be found in the user's manual available on the GitHub repo.

3.4. Benchmarking and validation

We conducted three tests on the Intertidal Environmental Chamber to benchmark its ability to control visible light and temperature during simulated high and low tide periods. All tests were performed at a room temperature of 15 ºC, maintained by an A/C system.

3.4.1. Light performance

The first test assessed the light environment inside the experiment tank. Illuminance was measured using an ILM-01 light meter (ISO-TECH, UK), and Photosynthetically Active Radiation (PAR) was measured with an MQ-510 sensor (Apogee Instruments, USA). LED intensities ranged from 0% to 100%, increasing in 10% increments, and light was measured at 15 evenly spaced points (3 x 5 grid) inside the tank. At 100% LED intensity, the average values were 8.82 ± 1.46 LUX and 259.9 ± 40.9 µmol m^{-2} s^{-1} (PAR) (**Fig. 3.5**).

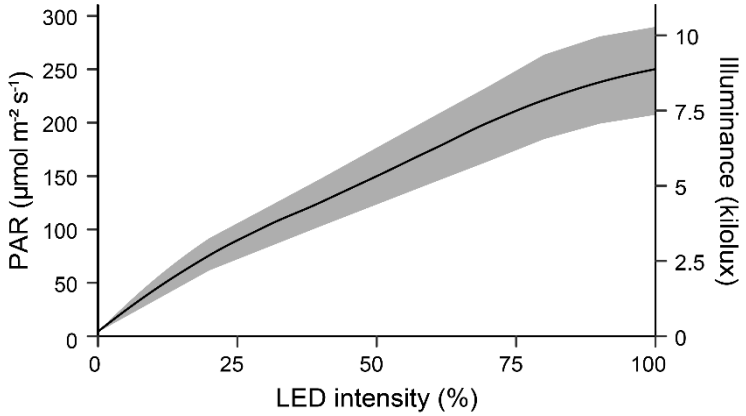


Figure 3.5: Visible light intensity in PAR (µmol m^{-2} s^{-1} photons) and LUX (klx) measured at low tide, showing similar average response curves (black line) ± SD (grey shade).

Although the LED bars were arranged for optimal distribution, the light was more intense at the centre of the tank (**Table S3.1**). Variability was greater at lower LED intensities: at 10%, light in the centre was 39 ± 5% higher than at the edges, while at 100%, the difference decreased to 12 ± 4%, similar for both PAR and LUX. Fine-scale PAR data measured in situ across tidal cycles are rarely available due to the technical challenges involved. However, this system can simulate such profiles if these data become accessible, providing researchers with the flexibility to incorporate precise light regimes into their experiments.

3.4.2. Temperature limits and performance benchmarks

The second test evaluated the maximum warming and cooling rates, as well as the peak water temperatures during high tide. The ECU was programmed to maintain continuous high tide, alternating between 1 ºC and 50 ºC every 12 hours for 3 consecutive days. Water temperature varied between 4.95 ± 0.18 ºC and 39.06 ± 0.42 ºC in 12-hour cycles (**Fig. 3.6**). Following an initial 20-minute delay caused by the equipment's thermal inertia, the warming and cooling processes exhibited near logarithmic patterns. The highest heating rate was 7.33 ± 0.13 ºC h^{-1}, and the highest cooling rate was -8.83 ± 0.08 ºC h^{-1}, both observed early in the test. Cyclic oscillations at 3h 35m and 9h 35m were caused by the air conditioning system entering its defrost cycle, temporarily raising the RT.

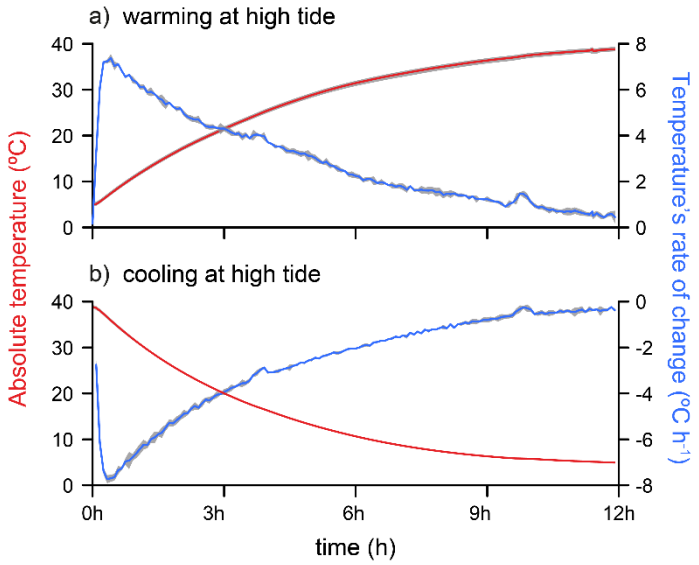


Figure 3.6: a) Water temperature and warming rate in the Experiment Tank during 12 h of constant heating; b) Water temperature and cooling rate during 12 h of constant cooling. Red lines represent the average temperature, and blue lines represent the average rate of change. The shaded grey area indicates the standard deviation (SD) between the three sensors.

The final test evaluated temperature extremes during low tide. Three consecutive cycles targeted 50 ºC for 1h 30m (warming phase; **Fig. 3.7a**), followed by 1 ºC for 4 hours (cooling phase; **Fig. 3.7b**).

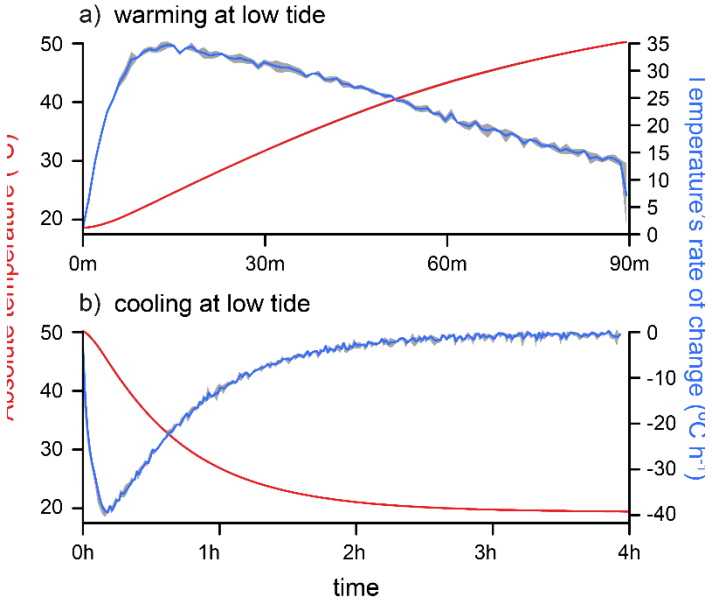


Figure 3.7: a) Low-tide temperature and warming rate in the Experiment Tank during 1h30m warming up to 50 ºC. b) Low-tide temperature and cooling rate during 4h of constant cooling. Red lines represent the average temperature, and blue lines represent the average rate of temperature change. The shaded grey area indicates the standard deviation (SD) between the three sensors.

Maximum temperatures (50.28 ± 0.07 ºC) were reached at the end of the warming cycle, with a peak warming rate of 34.16 ± 0.30 ºC h^{-1} around the 15-minute mark, suggesting even higher temperatures could be reached with longer cycles. The lowest temperature recorded was 14.98 ± 0.04 ºC, close to RT (15.32 ± 1.21 ºC), as cooling was achieved by directing exterior air into the tank. The minimum cooling rate was -41.63 ± 0.45 ºC h^{-1}, again limited by RT.

3.4.3. Validation

The system's performance was validated by replicating a five-day temperature profile recorded by a Envlogger T7.3 sensor (ElectricBlue, CRL, Portugal) deployed at mid-tide level in the rocky intertidal zone at Odeceixe, Portugal (37.432 ºN, -8.806 ºW) configured at 0.1 ºC resolution and hourly sampling rate. Tide data was calculated using the FES2014 global ocean tide model (Lyard et al., 2021) based on the sensor height, measured with centimetre-level precision using a GPS with RTK (RTK Facet L-Band, SparkFun, USA). A warm week (June 22–26, 2023) was selected, during which the rocky surface reached 40.3 ºC at low tide and was submerged by cold water (~16 ºC) at high tide. Visible light was applied in a Gaussian-like pattern, simulating sunrise and sunset times for the field site (light from 5:20 to 19:50 local time). The experiment was conducted simultaneously in four Intertidal Environmental Chambers, again with the RT maintained at ~15 ºC by an AC system.

The Intertidal Environmental Chamber successfully replicated the experimental temperature profile without malfunctions or significant deviations (**Fig. 3.8a, b**). Each day included two low and high tide periods, with average durations of 6h 14m for high tide and 5h 46m for low tide. Though the binary tide simulation is abrupt, it closely mirrors tidal transitions at a specific shore elevation. Target temperatures were closely followed, with a Pearson's correlation of >0.996 between measured and target temperatures across all four chambers. The average difference between target and observed temperatures was -0.05 ± 0.046 ºC, with a root-mean-squared error (RMSE) of 0.56 ± 0.024 ºC. This performance stems from a finely tuned PID for this system. For example, the integrative constant (I) of the PID was set to 0.096, and even slight deviations (e.g., 0.09 or 0.10) would induce notable temperature overshoot or undershoot.

Tide transitions involved rapid shifts in the temperature target, causing brief error spikes between the target and experimental temperatures that reached up to 15.3 ºC but were quickly corrected, lasting less than 10 minutes (**Fig. 3.8c**). Temperature variation among sensors averaged 0.37 ± 0.21 ºC during high tide and 2.35 ± 1.31 ºC at low tide (**Fig. 3.8d**), with greater variability at higher temperatures (Pearson's correlation = 0.97).

Overall, average biases (i.e., the mean deviation between the environmental chamber's set points and the actual temperatures) were -0.17 ºC at low tide and -0.02 ºC at high tide (**Fig. 3.8e**).

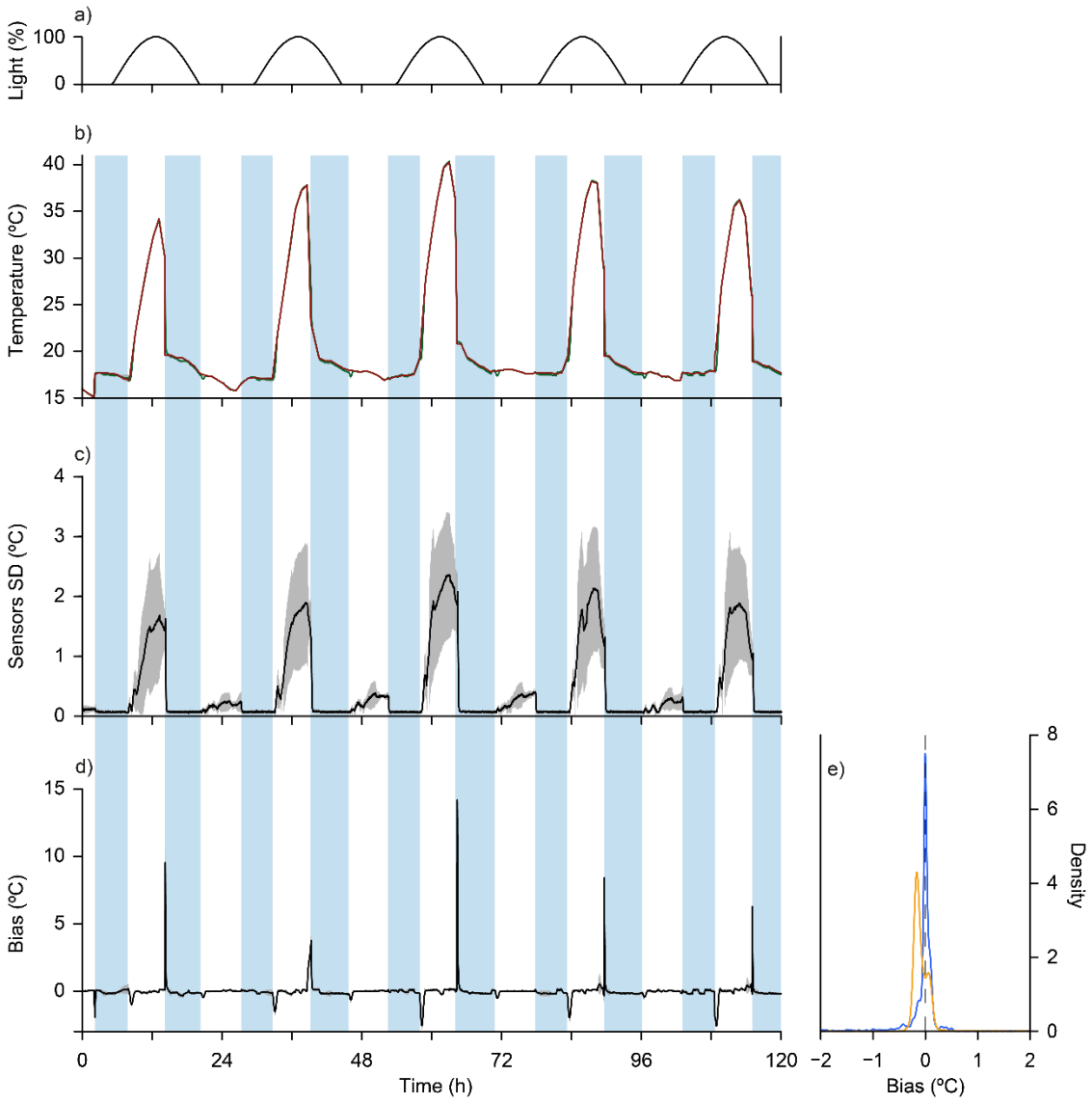


Figure 3.8: a) Light intensity; b) Measured experimental temperatures; c) Standard deviation among the temperature sensors within the Experimental tanks (n=3 per chamber). d) Instantaneous difference between experimental and target temperatures (Error). e) Mean bias between experimental and target temperatures during low-tide (yellow) and high-tide (blue) periods. Vertical blue bars on plots b, c, and d indicate high tide periods.

3.5. Discussion and conclusions

The Intertidal Environmental Chamber system described here represents a relevant advance in the ability to conduct long-term experiments that accurately replicate the thermal environment of intertidal habitats. These chambers provide precise control over light, tide timing, and temperatures during both submersion and emersion. The system's performance exceeds the warming and cooling rates observed in the field, which typically do not exceed 1 ºC per day at high tide and 15 ºC per hour during low tide (Salois et al., 2022).

Safety features minimize risks to operators and experiments, while system redundancy allows for easy maintenance without stopping operation, reducing downtime. Remote monitoring introduces a new approach for "virtual common-garden experiments", enabling geographically distant labs to simulate complementary experiments without transporting organisms. Although primarily designed for small marine and intertidal organisms such as limpets (Seabra et al., 2016), bivalves (Seuront et al., 2019), and juvenile macrophytes (Martinez et al., 2012), the system's capacity for independent control of all variables also makes it adaptable for experiments on terrestrial organisms.

While the system does not introduce new concepts — tide and thermal control during water immersion and emersion are well-established (Pincebourde et al., 2008), it addresses the critical need for standardization. We aimed to consolidate empirical insights from previous work (Seabra et al., 2016) and provide a standardized platform for future experiments. Other systems offer precise temperature control for small chambers with dynamic settings (Greenspan et al., 2016) and even commercial systems that control tide height, water temperature, and pH (Tide Chambers, AquaBioTech Inc.). However, none integrate all the features of this system or allow for open-source modifications or improvements.

Maintaining thermal stability within and around the chambers during experiments is crucial. Our testing results show that RT significantly affects the system's temperature control. Additionally, opening the experimental tank lid during low tide can compromise temperature regulation. We also registered some thermal heterogeneity during low tide, likely due to minor differences in heat emitted by the IR lamps, their beam angles, and radiation overlap. Although we used air-circulation fans to mitigate this issue, it was not completely eliminated. Hence, we recommend regularly rotating experimental organisms within the tank to balance out heat stress.

Building this system involves a considerable investment (~3800 € per unit; GitHub repo). However, many components, such as water pumps, coolers, and heaters, are already commonly found in experimental biology labs. Finally, the open-source nature of this chamber allows for future development by the scientific community, enabling modifications to incorporate new features (e.g., pH, humidity, thermal imaging), which can then be shared and improved collaboratively.

3.6. Acknowledgements

This work was supported by Fundação para a Ciência e Tecnologia (FCT) through the projects ThermalBuffer (POCI-01-0145-FEDER-31088) and EU H2020 FutureMARES (contract no. 869300). LFP received support from a FCT PhD grant (SFRH/BD/136924/2018). FPL and RS received support from FCT through CEECInd contracts (10.54499/CEECIND/03185/2018/CP1546/CT0004, 10.54499/CEECIND/01424/2017/CP1423/CP1645/CT0006).

3.7. References

Baker, M. (2016). 1,500 scientists lift the lid on reproducibility. *Nature*, *533*(7604). https://doi.org/10.1038/533452a

Bennett, J. M., Sunday, J., Calosi, P., Villalobos, F., Martinez, B., Molina-Venegas, R., Araujo, M. B., Algar, A. C., Clusella-Trullas, S., Hawkins, B. A., Keith, S. A., Kuhn, I., Rahbek, C., Rodriguez, L., Singer, A., Morales-Castilla, I., & Olalla-Tarraga, M. A. (2021). The evolution of critical thermal limits of life on Earth. *Nature Communications*, *12*(1), 1198. https://doi.org/10.1038/s41467-021-21263-8

Davison, I. R., & Pearson, G. A. (1996). Stress tolerance in intertidal seaweeds. *Journal of Phycology*, *32*(2), 197-211. https://doi.org/10.1111/j.0022-3646.1996.00197.x

Greenspan, S. E., Morris, W., Warburton, R., Edwards, L., Duffy, R., Pike, D. A., Schwarzkopf, L., Alford, R. A., & Golding, N. (2016). Low-cost fluctuating-temperature chamber for experimental ecology. *Methods in Ecology and Evolution*, *7*(12), 1567-1574. https://doi.org/10.1111/2041-210x.12619

Hesketh, A. V., & Harley, C. D. (2023). Extreme heatwave drives topography-dependent patterns of mortality in a bed-forming intertidal barnacle, with implications for associated community structure. *Global Change Biology*, *29*(1), 165-178. https://doi.org/10.1111/gcb.16390

King, N. G., McKeown, N. J., Smale, D. A., & Moore, P. J. (2018). The importance of phenotypic plasticity and local adaptation in driving intraspecific variability in thermal niches of marine macrophytes. *Ecography*, *41*(9), 1469-1484. https://doi.org/10.1111/ecog.03186

Lyard, F. H., Allain, D. J., Cancet, M., Carrère, L., & Picot, N. (2021). FES2014 global ocean tide atlas: design and performance. *Ocean Science*, *17*(3), 615-649. https://doi.org/10.5194/os-17-615-2021

Pasparakis, C., Davis, B. E., & Todgham, A. E. (2016). Role of sequential low-tide-period conditions on the thermal physiology of summer and winter laboratory-acclimated fingered limpets, Lottia digitalis. *Marine Biology*, *163*(2). https://doi.org/10.1007/s00227-015-2779-5

Pincebourde, S., Sanford, E., & Helmuth, B. (2008). Body temperature during low tide alters the feeding performance of a top intertidal predator. *Limnology and Oceanography*, *53*(4), 1562-1573. https://doi.org/10.4319/lo.2008.53.4.1562

Pörtner, H.-O., Roberts, D. C., Masson-Delmotte, V., Zhai, P., Tignor, M., Poloczanska, E., & Weyer, N. (2019). The ocean and cryosphere in a changing climate. *IPCC special report on the ocean and cryosphere in a changing climate*, *1155*, 10.1017. https://doi.org/10.1017/9781009157964

Salois, S. L., Gouhier, T. C., Helmuth, B., Choi, F., Seabra, R., & Lima, F. P. (2022). Coastal upwelling generates cryptic temperature refugia. *Scientific reports*, *12*(1), 19313. https://doi.org/10.1038/s41598-022-23717-5

Seabra, R., Wethey, D. S., Santos, A. M., Gomes, F., & Lima, F. P. (2016). Equatorial range limits of an intertidal ectotherm are more linked to water than air temperature. *Global Change Biology*, *22*(10), 3320-3331. https://doi.org/10.1111/gcb.13321

Seuront, L., Nicastro, K. R., Zardi, G. I., & Goberville, E. (2019). Decreased thermal tolerance under recurrent heat stress conditions explains summer mass mortality of the blue mussel Mytilus edulis. *Scientific reports*, *9*(1), 17498. https://doi.org/10.1038/s41598-019-53580-w

Wilson, K., Kay, L., Schmidt, A., & Lotze, H. (2015). Effects of increasing water temperatures on survival and growth of ecologically and economically important seaweeds in Atlantic Canada: implications for climate change. *Marine Biology*, *162*. https://doi.org/10.1007/s00227-015-2769-7

Ziegler, J. G., & Nichols, N. B. (1942). Optimum settings for automatic controllers. *Transactions of the American society of mechanical engineers*, *64*(8), 759-765. https://doi.org/10.1115/1.4019264

3.8. Supplementary Texts

Supplementary Text S3.1: Technical details regarding the experimental profile

To run an experiment using the Intertidal Environmental Chamber, the user must create a text file named **Profile.txt** and place it on the micro-SD card of the Electronic Control Unit (ECU). This file consists of a series of sequential instructions, each with a timestamp, one instruction per line. When the Chamber is powered on, it reads the **Profile.txt** and identifies the start and end of the experiment from the first and last rows of the file. It then checks its internal clock to determine which line of **Profile.txt** corresponds to the current time. Based on this, it sets its initial state, which is displayed on the ECU LCD (e.g., “Waiting to start”, “Experiment Finished”, “Low tide until 14:00”). If **Profile.txt** is not found on the micro-SD card, the display shows “No experiment”. In that case, the temperature will not be controlled (neither manually nor automatically), but certain functions, such as adjusting the tide height, lights, fans, and performing water changes, remain available via the ECU’s manual switches.

To edit the **Profile.txt** on the micro-SD card, the user may (i) physically remove the card from the ECU and insert it into a computer, (ii) connect via File Transfer Protocol (FTP; see User Manual section 5.1), or (iii) send the profile remotely through the Node-RED application (see User Manual section 5.3.3).

Each line in **Profile.txt** must have 19 characters and represent a set of required experimental setpoints. The system currently supports up to 1,000 lines. Given that each day typically requires about 50 lines to capture variations in temperature, tide, and lighting, 1,000 lines suffice for approximately 20 days of experimentation. However, the text file can be replaced at any time, even during an ongoing experiment, so in practice, there is no limit to the experiment’s duration.

Each line of **Profile.txt** contains two numbers separated by a dash. For example:

167257440-25010500

- The left-hand number (**1672574400**) is a Unix epoch timestamp. Here, it corresponds to 01 January 2023 at 12:00:00.
- The right-hand number encodes four instructions:
    - Target temperature (first three digits). For instance, **250** corresponds to 25.0 °C. If the target temperature were 26.7 °C, these three digits would be **267**.
    - Binary tide state (fourth digit): **1** for high tide or **0** for low tide.

- LED intensity (digits five through seven): a number from **000** (0%) to **100** (100%). In the example, **050** means 50% intensity.
- Binary water change state (eighth digit): **0** if no water change is triggered, or **1** if a water change is triggered at that timestamp.

To execute an experiment, a series of these instruction lines is required. The ECU continuously checks its internal clock (shown on the ECU display) and looks for the nearest previous and next setpoints in **Profile.txt** relative to the current time. Tides and LED intensities change only at their specified timestamps and remain at those settings until the next timestamp. Temperatures, in contrast, are linearly interpolated between their consecutive setpoints. Thus, if a constant temperature plateau is desired, two consecutive instructions with the same temperature must be provided. Water changes occur exactly at their scheduled timestamp and last until the system has finished draining and refilling.

For illustration, consider the following profile, also shown in **Supplementary Fig. S3.1**:

1672574400-20000800

1672581600-20001000

1672588800-25011000

1672596000-25010600

1672599600-20010400

1672603200-20010300

1672606800-15010100

1672610400-15010001

1672614000-15010000

- The first row indicates that the experiment begins on 01 January 2023 at 12:00:00, with a low tide, 80% LED, and no water change.
- The last row indicates that the experiment ends on 01 January 2023 at 23:00:00, with a high tide, 0% LED, and no water change.
- Between the second and third rows (two hours), the target temperature transitions from 20.0 °C to 25.0 °C. Therefore, one hour after the second timestamp, the system aims for 22.5 °C, and 1 hour 30 minutes after the second timestamp, it aims for 23.75 °C, reaching 25.0 °C at the third timestamp.

- Light and tide remain constant between timestamps. For example, the LED remains at 80% from the first to the second timestamp, and only when the second timestamp arrives does it change to 100%. Similarly, the tide remains low until the third timestamp arrives, at which point it switches to high and remains high thereafter. Tide changes take approximately 15 minutes. Note that infrared heating is suspended while water is still detected in the experimental tank's water sensors, which may slightly delay the start of heating after the tide switches from high to low.
- Water changes occur only when their scheduled timestamp is reached. The duration of each water change depends on how long it takes to drain and refill the system and may be shorter or longer than the time interval until the next setpoint. In this example, the water change occurs at 22:00 and finishes in about 15 minutes (depending on the water flow rate).

An R script is available (check the provided GitHub repo) to conveniently generate the experiment profile from a spreadsheet, converting timestamps to Unix format and calculating LED intensities based on required Photosynthetically Active Radiation (PAR) or Lux levels.

3.9. Supplementary Figures

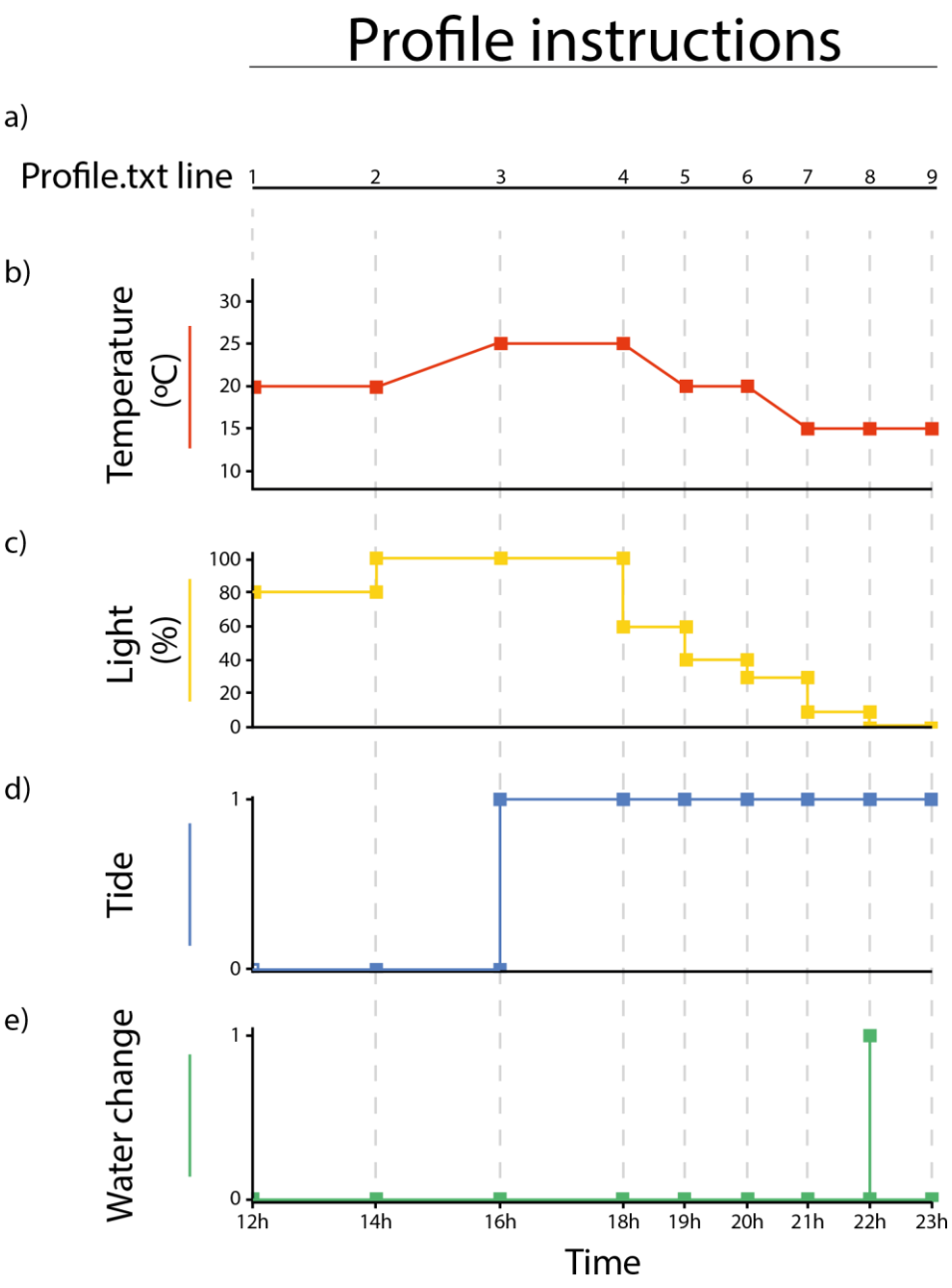


Figure S3.1: Visual representation of the experiment profile instructions provided above; a) Profile.txt lines (1 to 9); b) Temperature targets and in-between interpolation; c) Light intensities (%); d) Tide states (1=High, 0=Low); e) Water change states (instantaneous, 1=On, 0=Off).

3.10. Supplementary Tables

Table S3.1: Distribution of visible light intensity in PAR (µmol m-2 s-1 photons) and LUX (lx) at low tide inside the Experimental Chamber. Illuminance was measured using an ILM-01 light meter (ISO-TECH, UK), and Photosynthetically Active Radiation (PAR) was measured with an MQ-510 sensor (Apogee Instruments, USA). LED intensities ranged from 0% to 100%, increasing in 10% increments, and light was measured at 15 evenly spaced points (3 x 5 grid) inside the Experimental Chamber. Colour gradients represent PAR or LUX (10 to 100%) values separately.

PAR				LUX		
			10%			
41	54	37		1450	1950	1190
55	72	51		1850	2345	1750
53	76	52		1900	2550	1800
54	70	51		1850	2300	1800
35	52	36		1350	1800	1300
			20%			
65	79	56		2220	2850	1820
84	104	80		2800	3500	2600
84	109	80		2900	3700	2800
83	102	78		2800	3500	2750
57	75	56		2050	2600	2000
			30%			
82	103	76		2900	3700	2450
113	134	106		3750	4500	3600
112	141	107		3900	4700	3750
111	131	105		3700	4500	3600
76	98	77		2700	3400	2650
			40%			
111	126	97		3700	4550	3050
143	165	132		4650	5600	4350
142	174	135		4800	5900	4650
139	162	130		4600	5400	4500
98	120	97		3450	4200	3350
			50%			
132	150	115		4400	5400	3700
171	195	159		5550	6650	5300
170	206	162		5800	7000	5550
168	191	158		5500	6600	5350
117	143	116		4100	4900	4050

60%						
155	173	136		5200	6300	4300
201	228	187		6500	7750	6100
199	239	190		6800	8100	6450
196	222	185		6450	7600	6250
137	166	137		4700	5700	4700
70%						
179	196	155		5900	7100	4850
229	256	212		7450	8800	7000
227	270	216		7800	9200	7250
224	252	209		7400	8650	7150
157	188	155		5400	6500	5375
80%						
200	220	174		6650	8000	5450
259	288	240		8400	9900	7850
255	304	244		8750	10400	8250
252	283	236		8300	9750	8100
177	211	176		6100	7350	6050
90%						
217	231	189		7210	8450	5860
260	303	258		9000	10460	8500
277	319	263		9450	10990	8900
271	297	254		8980	10310	8680
192	222	190		6550	7770	6600
100%						
227	236	197		7500	8670	6120
290	310	269		9420	10720	8820
290	326	274		9850	11270	9260
282	303	266		9340	10590	9030
201	228	200		6860	7990	6870

Chapter 4

Intertidal Fucales response to low tide heat stress at their southern distribution edge

4.1. Abstract

The increasing intensity and frequency of atmospheric heatwaves threaten the physiological capabilities of intertidal canopy-forming macroalgae, especially at their southern range, where species live closer to their upper thermal limits. Although heat stress experiments on these species are becoming more common, few have incorporated realistic intertidal conditions. This study assessed the physiological responses of key intertidal macroalgae across the intertidal range, at their southern distribution limit in the NW Iberian Peninsula (Fucus serratus, Fucus spiralis, Ascophyllum nodosum, and Pelvetia canaliculata) to simulated heat stress using a custom setup that replicated realistic conditions, including tidal cycles and temperature patterns. Performance was measured after 10 and 20 consecutive days of diurnal emersion stress. Additionally, temperature data from in-situ loggers placed at different tide levels were used to correlate lab results with real intertidal temperatures experienced by each species. Growth and PSII maximum quantum yield (Fv/Fm) supported heat tolerance theory for intertidal zonation, indicating F. serratus as the most vulnerable and F. spiralis as the next most susceptible. Mortality primarily affected Fucus spp. and increased with the duration of the experiment. Although lipid peroxidation was responsive to thermal stress, it did not directly reflect overall performance. The alignment between in-situ temperatures and lab-measured thermal resilience underscores the importance of accounting for species' thermal niches and the often-overlooked role of emersion in thermal stress experiments. Our findings reiterate the maladaptation of Fucus spp. to emersion heat stress at their southern limits and highlight the critical role of emersion exposure when assessing species' responses to climate change.

Keywords

Macroalgae, Canopy-forming species, Intertidal thermal stress, emersion, Rocky shore, Intertidal Vertical zonation, Iberian Peninsula

4.2. Introduction

Marine coastal ecosystems are particularly susceptible to climate change due to exposure to multiple stressors, including rising seawater temperature, ocean acidification, sea level rise, and increasingly intense and frequent heatwaves, all of which are intensified by additional human-induced pressures (Bindoff et al., 2019; Oliver et al., 2019). The latest decade was the warmest on record, with surface global temperature 0.82 ºC above the 20th century average (NOAA, 2022). Additionally, global warming is not homogenous, as it shows significant differences at various geographical scales (Lima & Wethey, 2012; Seabra et al., 2011; Varela et al., 2023). The Atlantic Ocean for example, has been warming faster than any other ocean basin (Cheng et al., 2021; Ren et al., 2024), with likely impacts on species distributions. In the East Atlantic, various intertidal cold-water species have their southern distribution limit along the Northwest (NW) coast of the Iberian Peninsula (Ardré, 1970; Casado-Amezúa et al., 2019; Hawkins et al., 2019). There, coastal air and surface water temperatures have increased by 0.5 ºC and 0.24 ºC per decade since 1974, respectively (Barton et al., 2013; Gómez-Gesteira et al., 2011). These observations drove a series of studies that revealed a distributional shift in several intertidal species (Araujo et al., 2014; Cheung et al., 2009; Lima et al., 2007), including some habitat-forming species such as fucoids and kelps (Casado-Amezúa et al., 2019; Monteiro et al., 2022; Viejo et al., 2024). While there is a general consensus that warming is a primary driver of distributional contractions of some species, this trend is particularly evident at their meridional range edge (Andrews et al., 2014; de Bettignies et al., 2018; Ferreira et al., 2015).

Macroalgae, in particular canopy-forming species, play essential ecological roles in intertidal ecosystems, serving as primary producers and key habitat providers. These foundation species support diverse communities, often enhancing biodiversity and ecosystem stability (Lüning, 1990; Straub et al., 2019). Being ectotherms and sessile organisms, they are strongly affected by environmental temperature, which directly influences growth, reproduction, and even survival (Breeman, 1988; Wernberg et al., 2016). Research on the tolerance of intertidal macroalgae to current and future warming is increasingly common in the ecological literature (Graiff et al., 2015; Jueterbock et al., 2014; Liesner et al., 2020; Marbà et al., 2017; Piñeiro-Corbeira et al., 2018). Many studies use experimental designs of varying complexity to replicate natural conditions realistically (Duarte & Viejo, 2018; Ji et al., 2016). However, studies on intertidal species often neglect — either partially or entirely — the impact of tidal cycles and the associated exposure to aerial conditions, focusing instead solely on water temperature (Graiff et al.,

2015; Nepper-Davidsen et al., 2019; Wilson et al., 2015). These approaches can lead to unreliable predictions, as they disregard the effects of emersion — precisely when these organisms encounter the highest temperatures and potentially face the greatest thermal stress (Davison & Pearson, 1996; Dring & Brown, 1982). Nonetheless, an increasing number of studies are including treatments featuring aerial exposure (Román et al., 2020; Seabra et al., 2016), sometimes in association with marine heat waves (Thomsen et al., 2019) or other variables such as solar radiation or air humidity (Bischof & Rautenberger, 2012; Fernández et al., 2015; Martinez et al., 2012). Studies show that, under normal stress conditions, some seaweeds can withstand prolonged desiccation and quickly recover after the following high tide (Fierro et al., 2017). However, when exposed to abnormally high temperatures or prolonged emersions, macroalgae can experience decreases in photosynthesis rate, limited rehydration capability, pigment loss, and damage to cell membranes and the photosynthetic apparatus due to the accumulation of reactive oxygen species (ROS; (Flores Molina et al., 2014; Nepper-Davidsen et al., 2019; Sampath-Wiley et al., 2008). These effects may be more significant for populations at the species' warm trailing edge, as those are the locations where extreme emersion temperatures are more likely to occur (Duarte & Viejo, 2018; Pearson et al., 2009).

Brown algae of the Order Fucales play a critical role as ecosystem engineers in temperate regions. However, conservation threats to these canopy-forming species have received significantly less attention than those affecting subtidal kelps (Coleman & Wernberg, 2017). Southern-range populations of *Fucus serratus* have been shown to be particularly sensitive to low tide conditions, exhibiting reduced growth and overall maladaptation to heat stress (Martinez et al., 2012; Pearson et al., 2009). Similarly, populations of *Fucus spiralis* and *Fucus vesiculosus* show decreased photosynthetic rates after stressful emersion conditions at the same locations (Ferreira et al., 2014). Although these studies mark a substantial advancement beyond research focusing solely on elevated water temperatures, the logistical and experimental constraints of more complex studies often limit the range of thermal treatments that can be applied (Fernández et al., 2015; Jueterbock et al., 2014; Román et al., 2020). Consequently, there is still uncertainty regarding how intertidal brown algae respond to increasingly stressful conditions during emersion periods.

Earlier research established that species located lower on the shore typically have a lower tolerance to heat and desiccation during emersion (Dorgelo, 1976; Zaneveld, 1937; Zaneveld, 1969). However specific thresholds and correlations with experienced

temperatures have not yet been fully determined and understood. To explore this topic further, we assessed the resilience of four canopy-forming macroalgae — *Fucus serratus*, *Fucus spiralis*, *Ascophyllum nodosum*, and *Pelvetia canaliculata* — collected from the NW Iberian Peninsula (Viana do Castelo, Portugal), a biogeographic stronghold for cold-adapted species and close to the southern limit of *F. serratus*, *A. nodosum* and *P. canaliculata* (Jueterbock et al., 2013; Lalegerie & Stengel, 2022; Pereira et al., 2020). Importantly, these four species exhibit distinct vertical distributions that cover the majority of the intertidal range available at the study site. We subjected fronds to repeated realistic low tide heat stress events derived from in-situ temperature data collected by temperature loggers previously deployed at the study site and evaluated physiological responses by measuring survival, growth, maximum quantum yield of PSII (F_v/F_m) and lipid peroxidation (LPO). The heat stress treatments spanned 20 days, with physiological measurements conducted at two intervals during the experimental period. We argue that while resilience to low tide heat stress in intertidal species is expected to align with their natural emersion exposure, further research is essential to fully understand their limits and avoid overlooking potential vulnerabilities.

4.3. Materials and methods

4.3.1. Sample collection

Vegetative fronds of *Fucus serratus*, *Fucus spiralis*, *Ascophyllum nodosum* and *Pelvetia canaliculata* were collected in January 2021 at low tide in northern Portugal, Viana do Castelo (Latitude: 41.697; Longitude: -8.851). At the collection site, the selected species exhibit sequential tidal zonation, with *P. canaliculata* occurring highest on the shore, followed by *A. nodosum*, *F. spiralis* and *F. serratus* (**Fig. 4.1**). This region represents the south-eastern distributional limit for the selected species, with the possible exception being *F. spiralis,* which until Almeida et al. (2022) redefinition, was considered to extend until Morocco (Moalic et al., 2011; Neiva et al., 2016). The diversity of genetic entities within the former *F. spiralis* taxa along the Atlantic shores has been a subject of research over the past decade (Almeida et al., 2022). We collected fronds from *Fucus* patches located directly below the *A. nodosum* patches. Based on recent literature and the species observed at the collection site, these patches are composed of *F. spiralis*.



Figure 4.1: Photos showing the typical morphology of the four target seaweeds species at the collection site (Viana do Castelo; Portugal).

Experimental fronds were collected based on species-specific morphology. For *Ascophyllum nodosum* and *Pelvetia canaliculata*, whole juvenile fronds less than 10 cm in length were gathered, while for *Fucus* species, non-fertile apical fronds of a similar size (<10 cm) were sampled. After collection, the algae were transported to the Interdisciplinary Centre of Marine and Environmental Research (CIIMAR, Portugal) and acclimated in an open seawater intake facility for two weeks at 15 ºC in 30-litre polyvinyl chloride tanks. Acclimation conditions were kept constant at 150-175 µmol photon $m^{-2}s^{-1}$ PAR irradiance (US-SQS/L PAR sensor, WALZ, Germany), 12h:12h (light/dark) photoperiod (maintained using LED strips; model 5630 Led-Pol, PL) with continuous aeration and a tide cycle of 8/4 hours (high/low).

4.3.2. Experimental design

We designed the experiment as an exposure to short-term heat stress during diurnal low tides under a realistic tidal cycle (**Fig. 4.2**). The emersion exposure duration (4 hours) was limited to the maximum observed on the lower-level species (i.e., *Fucus serratus*) to maintain focus on thermal stress, rather than the impact of over-extended desiccation periods.

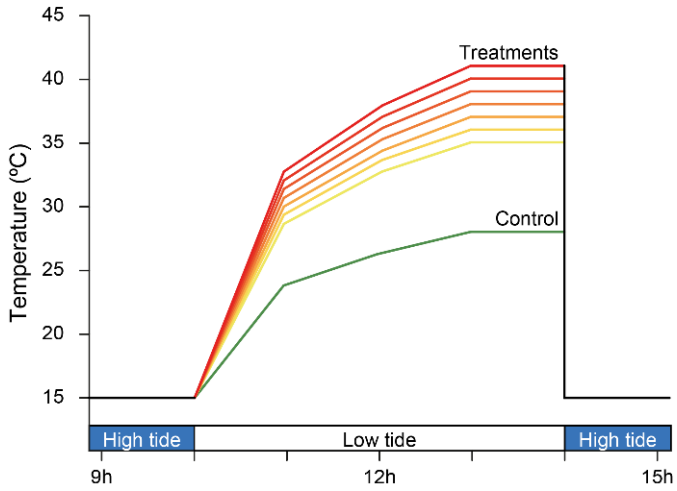


Figure 4.2: Diurnal heat stress treatment profiles. Coloured lines depict temperature profiles during daily low tides (10h-14h). Control treatment (28 ºC) is shown as a green line and experimental treatments (35 ºC to 41 ºC) are represented by lines ranging from yellow to red, respectively. High tide periods (14h-22h and 02h-10h) were identical in all treatments (15 ºC). Temperature during nocturnal low tides (22h-02h) was kept around 15 °C, remaining close to water temperature. Tidal cycle (8:4; high:low) and heat stress profiles were repeated daily for the whole 20 days of the experiment.

Diurnal low tide periods lasted four hours and were characterized by emersion accompanied by a realistic temperature increase provided by two 125 W ceramic infrared lamps (IR, RS, UK) on each experimental tank. Temperature control during low tide was achieved by a fine control over the IR lamps with a customized Proportional-Integral-Derivative (PID) algorithm and two circulation fans to prevent thermal stratification (60 mm wide fans with 43.9 $m^3 h^{-1}$ air flow). Peak temperatures of each treatment (28, 35, 36, 37, 38, 39, 40 and 41 ºC) were achieved for only one hour (± 0.25 ºC). Two temperature loggers (DS18B20, Analog Devices, USA) were placed inside each tank, attached to granite tiles, providing temperature feedback to a microcontroller (ATMEGA2560), which coordinated all electrical functions (Seabra et al., 2016). The low

tide temperature profiles employed here reflect the average thermal progression registered by temperature loggers (Envlogger T2.4, Electricblue CRL, Portugal) previously deployed in a nearby intertidal rocky shore (Latitude: 41.840; Longitude: -8.874), configured to collect data at one-hour intervals and 0.1 ºC resolution (n= 3).

To determine experimental peak temperatures, we analysed a 7-year-long temperature dataset (2010-2017) from the same site to find an approximation of the local climatology. Control peak temperature was based on the average maximum temperatures observed during summer low tides (28 ºC). The experimental temperature levels (35 ºC to 41 ºC) were determined based on a pilot study in which fronds of the same Fucales species were exposed to 1st and 2nd category heatwaves (peak temperature of 35 ºC and 44 ºC, respectively), corresponding to temperatures exceeding the overall 90th percentile, following the definition from Hobday et al. (2016). These temperatures resulted either in 100% survival in the lower heatwave category group (35 ºC) or complete mortality at 44 ºC. To zoom in on this thermal interval, we designed this experiment with peak temperatures ranging from 35 to 41 ºC at 1 ºC intervals. Water temperature during the experiment was kept constant at 15 ºC, as this corresponds to the average sea surface temperature (SST) we observed during summer in northern Portugal during high tide, as determined using the in-situ temperature dataset.

The experiment was conducted in an open seawater system, and all treatments were made in duplicated tanks with individual temperature control (totalling 16 independent mesocosms; Pereira et al. (in press)). Each high-low tide transition cycle involved a complete water exchange, which helped maintain stable water quality throughout the experiment. Room temperature was kept at 17 ºC to minimize temperature fluctuations during nocturnal low tide (15.71 ± 0.32 ºC). Specimens from the four species were subjected to two low-tide events per day for 20 days, with only the diurnal low tide involving warming treatment. Photoperiod during the experiment was kept as in acclimation. Each tank initially contained 12 individual fronds per species. However, due to destructive sampling conducted and the mortalities recorded after 10 days, only six fronds per species remained by the end of the experiment (20 days).

4.3.3. Field intertidal zonation

To better characterize the maximum daily temperature to which the four seaweed species are exposed in the site where they were collected, *in-situ* temperature data were obtained using temperature loggers (Envlogger T2.4, Electricblue CRL, Portugal) deployed in duplicates or triplicates at three tidal levels (low-tide, mid-tide, and high-tide).

Loggers were deployed in 30 mm wide and 15 mm deep holes drilled into the rocky substrate and sealed with marine epoxy (Z-Spar™ Splash Zone Compound A-788). All sensors were oriented identically, facing south on ~45 º angled rocks for maximum solar exposure to effectively capture the maximum rock temperature at each height during low tide. Loggers were programmed to record hourly temperatures with a 0.1 ºC resolution between February 26th, 2023, and February 25th, 2024. Data were collected using an Android smartphone with the application Envlogger Viewer v5.3 (Electricblue CRL), which communicated with the loggers via near-field communication (NFC).

Height relative to mean sea level (MSL) was measured for the targeted species and loggers using a centimetre-precision Global Navigation Satellite Systems (GNSS) receiver (SparkFun RTK Facet L-Band, Sparkfun, USA) with Real-Time Kinematic (RTK) corrections obtained from the NTRIP-broadcasting station of Paredes de Coura, from the ReNEP network (Direção-Geral do Território, Portugal). Elevations above Earth's ellipsoid were converted into elevations above the geoid using the most accurate geoid model available for the region (GeodPT08, Direção-Geral do Território, Portugal). Field positioning had an average precision of 13 mm horizontally and 26 mm vertically.

Species vertical ranges were measured at a minimum of 16 points per species. Average immersion and emersion periods were calculated using tide data from the FES2014 global ocean tide model (Lyard et al., 2021). FES2014 was produced by LEGOS, NOVELTIS and CLS Ocean and Climate Division, was interfaced through the R package Rfes2014 (https://github.com/avsdev-uk/Rfes2014) and obtained from AVISO (http://www.aviso.altimetry.fr). Astronomical tide heights were calculated for the study location at a 10 min resolution over a ten-year period (2015–2024).

4.3.4. Growth, chlorophyll fluorescence and mortality

Growth was calculated as a proportional fresh weight (FW) change of fully hydrated fronds relative to the initial FW. Fronds were weighted on the day prior to the experiment start (initial FW) and then again on the 10^{th} and 20^{th} day (T1 and T2, respectively). For measurement, individuals (n= 12 and 6 per tank, for T1 and T2, respectively) were gently soaked from excess water with a paper towel before weight measure with 0.01 g precision in a Kern EG 220-eNM scale (Mechanikus Gottlieb KERN, Germany). Chlorophyll fluorescence images of each seaweed were measured by using a FluorCAM 800MF imaging fluorometer (Photon System Instruments, Brno, Czech Republic), comprising a computer-operated control unit (SN-FC800-082; Photon System Instruments) and a CCD camera (CCD381; PSI) with a f1.2 objective (2.8–6 mm; Eneo,

Rödermark, Germany), as described by (Serôdio & Campbell, 2021). Images of chlorophyll fluorescence parameters F_0 and F_m (dark-level and maximum fluorescence level, respectively) were captured on fronds (n= 6 per tank for both T1 and T2) samplings, respectively) after a minimum of 20 min of dark-acclimation followed by a modulated measuring light and saturation pulses (<0.1 and >7500 µmol photons m^{-2} s^{-1}, respectively), provided by red LED panels (612 nm emission peak, 40-nm bandwidth). Images (512×512 pixels) were analysed with the FluorCam7 software (Photon System Instruments, spol. s r.o., Drasov, Czech Republic); here we defined areas of interest (AOIs) matching the whole area of each seaweed by excluding the non-fluorescent background signal (outside the seaweed surface). The maximum quantum yield of photosystem II (PSII) was calculated for each pixel of AOI individually as F_v/F_m = (F_m-F_o)/F_m (Schreiber et al., 1986). Survival was determined after T1 and T2, and individuals were considered dead if their pictures showed no pixels with fluorescence above the background.

4.3.5. Lipid peroxidation

Lipid peroxidation (LPO) was evaluated after T1 (n= 3 per tank) in accordance to Hodges et al. (1999) via quantification of malondialdehyde levels, as it is an end product formed from polyunsaturated fatty acids peroxidation in the cells, permitting an evaluation of membrane damage with interference correction from non-malondialdehyde compounds absorbing at 532 nm. Briefly, frozen seaweed tissue samples were homogenized with inert sand in 1:25 (g FW:ml) 80:20 (v:v) ethanol:water, followed by centrifugation at 3000 g for 10 min. Incubations were made at 95 ºC in a block heater (Multiblok, Lab-Line Instruments, Ill., USA) for 25 min in two reaction buffers with 20% (w/v) trichloroacetic acid and 0.01% butylated hydroxytoluene, differing only in TBA presence (0.65% TBA). The absorbance of cleared supernatant was read at 440, 532 and 600 nm. Finally, the levels of malondialdehyde were estimated through the extinction coefficient of 155 mM^{-1} cm^{-1} and expressed as $nmol^{-1}$ g FW.

4.3.6. Statistical analysis

Statistical analysis for growth, F_v/F_m and LPO (T1 or T2) were made by linear mixed models fit to analyse the effect of each treatment. Models were fitted to the full model composed of two fixed factors: low tide aerial temperature (8 levels: 28, 35, 36, 37, 38, 39, 40 and 41 ºC) and species (4 levels: *F. serratus*, *F. spiralis*, *P. canaliculata*, *A. nodosum*,). The tank was included as a random factor. The survival rate was analysed using a generalized linear model (GLM) with binomial distribution with a logit-link function

(Zuur et al., 2009). When the inclusion of random effects did not improve model quality (assessed using AIC and BIC criteria), it was removed. When pertinent, model normality was checked by visual inspection of Q-Q plots, and heteroscedasticity was assessed through residual plots. To investigate pairwise differences between treatment groups, we used estimated marginal means (library emmeans). A significance threshold of 0.05 was used for testing treatment effects. We adopted 0.05 as the threshold value when testing for significant treatment effects with GLMs. All statistical analyses were done in R4.3.1 (R Core Team, 2023). Packages used for statistical analysis were lme4 (v1.1-35.1; Bates et al. (2015)) for mixed models and generalized linear models, and estimated marginal means were calculated with emmeans (v1.8.7; Lenth et al. (2021)).

4.4. Results

Daily maximum temperatures differed greatly at each different intertidal level during spring and summer, whereas winter temperatures were markedly more similar (**Fig. 4.3a**). Nonetheless, the hours per year spent above the experimental temperatures analysed in this work were significantly different between intertidal levels (**Fig. 4.3b**; ANOVA $P<0.001$). At low tide level, temperatures surpassed 28 ºC for eight hours but never reached 35 ºC, while at mid tide temperature, hours per year spent above 28 ºC were 227, above 39 ºC were three, and 40 ºC never occurred. At the high-tide level, temperatures surpassed 28 ºC for 948 hours, above 39 ºC for 132 hours, and above 41 ºC for 50 hours.

Intertidal height above MSL for the target species (**Fig. 4.3b**) showed a single sympatric relationship between *A. nodosum* and *F. spiralis,* sharing over 40% of their vertical range (-0.33 to 0.04 m above MSL). *P. canaliculata* was found to be allopatric, not sharing habitat with any other fucoid at the study site (0.71 to 1.19 m above MSL). Daily average emersion periods (**Fig. 4.3c**) revealed different patterns for each species, with *F. serratus* at 1 h 31 min ± 2 h 31 min, *F. spiralis* at 4 h 40 min ± 1 h 29 min, *A. nodosum* at 6 h 34 min ± 1 h 57 min, and *P. canaliculata* at 10 h 18 min ± 52 min.

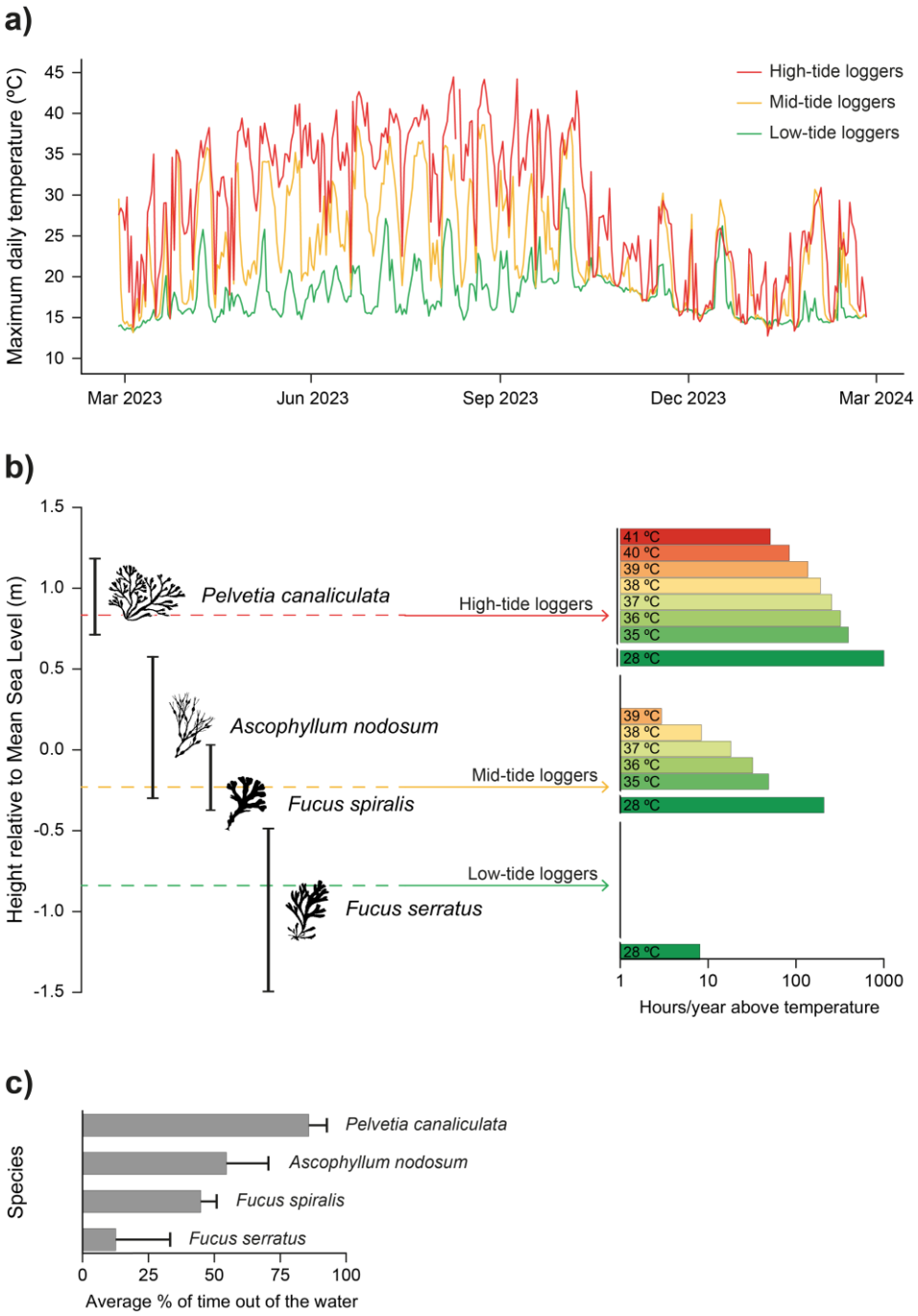


Figure 4.3: a) Daily temperature maximum observed at the sampling site at low, mid and high tide levels (n= 2 or 3; green, orange and red lines, respectively). Sensors were placed at a height of -0.81 ± 0.25, -0.18 ± 0.04 and 0.84 ± 0.05 meters relative to mean sea level (MSL) for low, mid and high tide, respectively; b) Intertidal heights for target species and loggers relative to MSL, and temperature occurrences at each intertidal level in hours/year above experimental temperatures. Target species height at Viana do Castelo (Portugal) was measured as: *P. canaliculata* (0.71 ± 0.09 to 1.19 ± 0.13 m), *A. nodosum* (-0.33 ± 0.16 to 0.58 ± 0.06 m), *F. spiralis* (-0.37± 0.04 to 0.04 ± 0.18 m) and *F. serratus* (-1.51 ± 0.10 to -0.48 ± 0.15 m).

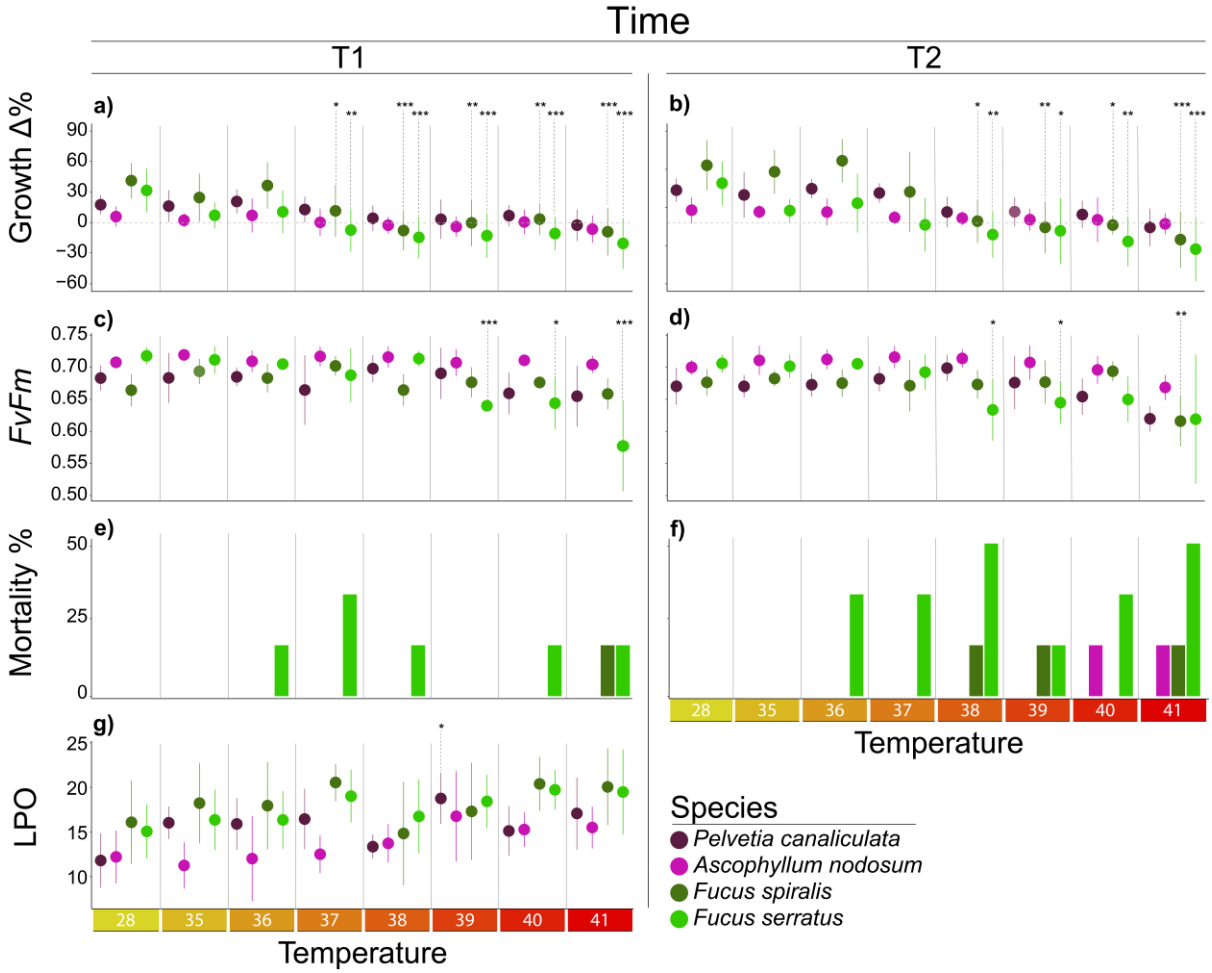


Figure 4.4: a, b) Growth at instants T1 and T2 expressed as percentage relative to initial weight (mean ± SD); c,d) F_v/F_m at instants T1 and T2 (mean ± SD); e, f) Mortality as percentage of total individuals at instants T1 and T2; g) Lipid Peroxidation at instant T1 (mean ± SD); Bottom axes indicate low tide (emersion) temperatures for all eight treatments (28 [control], 35, 36, 37, 38, 39, 40 and 41 ºC). Significance asterisks refer to pair-wise comparisons within the same species and sampling instant (T1 or T2) against respective control treatments (28 ºC). Significance levels: * $P < 0.05$, ** $P < 0.01$, *** $P < 0.001$.

Table 4.1: Summarised results of GLMs used to test the effects of low tide temperatures and species. Significant effects are in bold (*P*-value < 0.05). Models presented are for growth, F_v/F_m and LPO at the 10th and 20th day separately (T1 and T2, respectively).

	T1			T2		
Growth	***F***	**df**	***P*-value**	***F***	**df**	***P*-value**
Temperature	8.39	7	**0.004**	6.63	7	**0.008**
Species	32.85	3	**<0.001**	24.42	3	**<0.001**
Temperature x Species	4.45	21	**<0.001**	3.71	21	**<0.001**
F_v/F_m						
Temperature	8.53	7	**<0.001**	10.71	7	**<0.001**
Species	19.52	3	**<0.001**	16.43	3	**<0.001**
Temperature x Species	4.32	21	**<0.001**	2.09	21	**0.006**
Mortality		Df			Df	
Temperature	8.11	7	0.322	15.57	7	**0.029**
Species	14.70	3	**0.002**	26.01	3	**<0.001**
Temperature x Species	3.10	21	0.999	7.58	21	0.997
LPO						
Temperature	19.13	7	**0.007**			
Species	8.72	3	**0.033**			
Temperature x Species	24.75	21	0.258			

All physiological responses showed a significant Temperature response and/or Temperature x Species interaction (**Table 4.1**). After instant T1, the growth of *F. serratus* and *F. spiralis* was already significantly reduced at 37 ºC (**Fig. 4.3a**). A similar growth reduction as a consequence of the severity of aerial heatwaves was not found for the two species that occur higher on the shore (*A. nodosum* and *P. canaliculata*). At the end of the experiment (after 20 days; instant T2), among the fronds that survived, only *F. serratus* and *F. spiralis* showed reduced growth in response to the increased intensity of aerial heatwaves (**Supplementary Table S4.1**). Both species experienced a reduction in their growth rate at temperatures of 38 ºC and above (**Fig. 4.3b**). No significant decrease in growth was observed in *P. canaliculata* and *A. nodosum* at the end of the experiment compared to the control treatment for any of the temperature treatments (28 ºC; **Supplementary Table S4.2**).

Although temperature and species were significant factors in F_v/F_m response at T1 and T2 (**Table 4.1**), pairwise comparisons revealed small significant differences (**Fig. 4.3c, d**). F_v/F_m remained overall stable at instant T1 and even T2 (between 0.65-0.75; **Fig. 4.3c**) for all species except *F. serratus*, for which a slight but significant decrease was observed from 39 ºC on.

Mortality was significantly different between species at instant T1 (P = 0.033; **Table 4.1**), as only individuals of *Fucus spp.* succumbed to the treatments, starting at 36 ºC (8 %) for *F. serratus* and only at 41 ºC for *F. spiralis* (8%) (**Fig. 4.3e**). Mortality increased at instant T2, with a significant impact of the factors of temperature and species. Similarly to T1, mortalities occurred only at temperatures of 36 ºC or higher (**Fig. 4.3f**). Mortality peaked at 50 % for *F. serratus* at temperatures as low as 36 ºC, while for *F. spiralis* it reached 17% at 38 ºC. *A. nodosum* also showed 17% mortality at T2 but only at the higher temperature treatments (40 ºC and 41 ºC). All individuals of *P. canaliculata* survived the entire experiment.

Both temperature and species were significant factors in LPO response (**Table 4.1**), but not their interaction. Although there is a general trend for increasing LPO at higher temperatures, no significant differences were detected, except for *P. canaliculata* at 39 ºC (**Fig. 4.3g**). The highest values were detected on individuals of *Fucus spp.*, with *F. serratus* showing the highest values (20.6 ± 2.1 $nmol^{-1}$ g FW) from 37 ºC on.

4.5. Discussion

The fucoid species examined in this study often dominate rocky shores in the northeast Atlantic, providing crucial ecological services (Cotas et al., 2023; Whitaker et al., 2023). Despite past research on these species (Álvarez-Losada et al., 2020; Lalegerie & Stengel, 2022; Pereira et al., 2020), their resilience to ongoing climate change remains poorly understood (Harley et al., 2012). In addition, research frequently concentrates on the consequences of increasing seawater temperatures, disregarding the influence of heat stress during emersion periods. Although factors delimiting vertical zonation in intertidal communities have been identified in earlier studies, regional variations in abiotic (e.g. wave exposure and water clarity) and biotic (competition and grazing pressure) conditions can affect these limits (Chappuis et al., 2014; Coleman et al., 2006). In fact, vertical zonation for the target species at their distribution centre (Brittany and the British Isles) has been reported to be mostly above the mean sea level (MSL; (Feldmann, 1978; Hiscock, 1979), while at our sampling site, only *P. canaliculata* was found completely above MSL. Naturally, this is reflected in different emersion

periods and consequent heat stress exposures. As our temperature data reveals, temperatures experienced at each intertidal level can be drastically different. Hence, pairing species' vertical zonation with their realistic exposure to atmospheric temperatures can be crucial when interpreting results from thermal stress experiments. We found it particularly interesting that *A. nodosum* and *F. spiralis* displayed an opposite vertical distribution pattern at our sampling site (*A. nodosum* occurring higher than *F. spiralis*) compared to what is typically reported at their distribution centre (*F. spiralis* occurring higher than *A. nodosum*, (Bizien et al., 2024; Evans, 1949; Schrofner-Brunner et al., 2023)). The observed shift in shore position may be driven by a balance between species-specific thermal resilience and interspecific competition. The expected lower temperatures during low tide on higher latitudes could benefit *F. spiralis* more than *A. nodosum*. Although the vertical layout we observed has been reported before (Santos, 2000), it is not always as explicit. In fact, the vertical overlap between these species appears to be greater along the shores near our sampling site (unpublished data), but without ever reverting to the pattern of *A. nodosum* below *F. spiralis*. Vertical retractions at warmer edge populations have been observed in *F. serratus* (Álvarez-Losada et al., 2020; Pearson et al., 2009), suggesting that populations there may not be locally adapted and could, therefore, be more vulnerable to climate change. An alternative possibility, suggesting a top-down effect where increased grazing intensity limits the height of fucoids along these shores, seems unlikely as it has been previously shown that limpet grazing does not significantly control biomass in these edge populations in southern Europe (Coleman et al., 2006). Further studies focusing on other common grazers are needed to further elucidate this aspect.

In our laboratory experiment, we observed a significant interaction between temperature and species, affecting growth rates. Control treatments exhibited a cumulative growth ranging from 8 to 41% over the first ten days, consistent with the reported daily growth rates of 1 to 4% for these species (Fortes & Lunning, 1980; Schonbeck & Norton, 1979; Schrofner-Brunner et al., 2023; Strömgren, 1977). We observed a decline in growth across all species as the intensity of aerial heatwaves increased; however, only the two *Fucus* species exhibited significant differences compared to their respective control treatments. The sharp decline in growth seen in *F. serratus* and the stable growth of *A. nodosum* under higher low tide temperatures are both consistent with previous vertical transplant experiments in the intertidal zone (Schrofner-Brunner et al., 2023). Contrastingly, this pattern does not hold for *F. spiralis*, which also exhibited a decline in growth despite previously having been reported to maintain growth across different tide height levels. However, that study was conducted near the northern distribution edge

(Sweden), where low tide temperatures observed during summer are considerably lower than at the southern limit.

The mortality of *Fucus spp.* was predominantly influenced by higher temperatures, especially those that were uncommon to their intertidal zones. This result is expected, as performance traits often decline as the species approach their lethal temperature limits (Eggert, 2012). Notably, *P. canaliculata* exhibited no mortality and grew even at the highest temperature tested (41 ºC). Known to be highly tolerant to desiccation, *P. canaliculata* can endure consecutive days of emersion (Pereira et al., 2020), and fully recover within just 2 hours (Dring & Brown, 1982). However, there's still uncertainty regarding how much low tide thermal stress it can endure. In fact, the ability of *P. canaliculata* to cope with emersion stress might be at its limit, as studies have found that necrosis and mortality can occur at its upper limits after warm summers (Hawkins & Hartnoll, 1984), and a decrease in biomass has been linked to rising air and water temperatures (Lamela-Silvarrey et al., 2012). Ultimately, the presence of *P. canaliculata* in the Cantabrian Sea, where SSTs can reach 20 ºC, and its absence from the centre of Portugal (Monteiro et al., 2022), where colder summer SSTs are the norm (Neiva et al., 2014), further suggests that warmer aerial climate might be a key factor determining this species' distribution range, and highlights the need to account for emersion thermal stress during experiments testing the impacts of climate change on this and similar species.

Maximum quantum yield of PSII (F_v/F_m) reflects the maximum efficiency of PSII photochemistry (Anderson et al., 1997). This important physiological metric can be jeopardized by various factors present during emersion, such as desiccation, high temperature and excessive light (Fernández-Marín et al., 2011). In the present study, F_v/F_m results revealed a species-specific response to temperature, with notable sensitivity observed in *Fucus* species—particularly *F. serratus*, followed by *F. spiralis*. Additionally, lower F_v/F_m values were detected at instant T2 compared to T1, indicating cumulative stress at higher temperatures. These findings suggest that *F. spiralis* may be increasingly vulnerable to emersion stress under future warming scenarios. Such a response is likely due to the inability to fully recover the photosynthetic performance between tide cycles, as this has been shown to depend on the intensity and duration of the emersion period on both *F. serratus* and *F. spiralis* (Fernández et al., 2015; Zardi et al., 2011). In addition to the negative effects of desiccation*, F. serratus* appears inefficient at dealing with increased light exposure, failing to meet the photosynthetic performance of *A. nodosum* while emersed (Olabarria et al., 2018) and *P. canaliculata* when immersed

(Migné et al., 2015). Combined with our findings, these studies confirm that the effects of desiccation and thermal stress on the photosynthetic performance of both *Fucus* species tested are closely linked to their vertical positioning within the intertidal zone. However, in the case of *Ascophyllum nodosum* and *Pelvetia canaliculata*, these species typically exhibit a large photosynthetic resilience despite exposure to desiccation and heat stress.

The suboptimal conditions experienced during low tides, such as extreme temperatures and elevated light exposure, are known to trigger unbalanced ROS production in seaweed (Kumar et al., 2020; Taenzer et al., 2024). A widely used proxy to account for ROS-induced damage is lipid peroxidation (LPO), as it reflects ROS damage to cell membranes (Bischof & Rautenberger, 2012; Collén & Davison, 2002). In this study, LPO showed a significant response to temperature across all seaweed species, and although higher LPO levels were consistently observed in *Fucus spp.*, and the lowest in *A. nodosum* and *P. canaliculata*, it remained unclear whether lipid peroxidation could be a valuable proxy for intertidal heat stress experiments. Our LPO results are consistent with those reported by Martins et al. (2021) for the same species and region. However, in both studies, LPO values did not correlate with tolerance to emersion. In fact, Martins et al. (2021) observed similar LPO values for *F. serratus* and *P. canaliculata* at low tide. Together with our results, this suggests that oxidative stress at low tide might not follow the intertidal level gradient.

The highest temperature levels tested in this study (41 ºC) already occur in the field at the high-tide zone, and up to 39 ºC for the mid-tide zone. Considering the increased frequency of heatwaves and temperature extremes experienced in the last decades (Berthou et al., 2024; Dunstone et al., 2024), and more acutely in the last two years, the decreased growth and mortality revealed here for some seaweeds might be experienced in the field sooner than expected, with evident consequences for these species' chances of survival at their southern distributional range. Additionally, species retraction towards higher immersion periods might not represent a simple niche shift but more likely a compression, as high tide species can be easily outgrown by their lower-level competitors when submerged.

In conclusion, our findings support the thermal tolerance theory for the intertidal zonation for intertidal seaweeds (Dorgelo, 1976; Zaneveld, 1937; Zaneveld, 1969). The correlation between *in-situ* temperatures and thermal resilience observed in laboratory experiments underscores the importance of emersion temperature for the species'

zonation (Pearson et al., 2009; Román et al., 2020). Finally, despite the differential responses of the species to aerial heat stress, the projected temperature increases associated with climate change are likely to affect these southernmost populations.

4.6. Acknowledgements

This work was supported by the Blue Growth program - EEA grants BLUEFORESTING (PT-INNOVATION-0077) and the Fundação para a Ciência e Tecnologia (FCT) through the projects ThermalBuffer (POCI-01-0145-FEDER-31088), NorteRocks (NORTE-01-0145-FEDER-031053), CCTBON (FLAD Science Award Atlantic 2020), OceanLog (PTDC/BIA-BMA/4848/202) and the EU H2020 FutureMARES (contract no. 869300). CESAM (UIDP/50017/2020 + UIDB/50017/2020 + LA/P/0094/2020), GreenUPorto (UIDB/05748/2020 + UIDP/05748/2020), funded by national funds (OE) through FCT/MCTES. LFP received support from a FCT PhD grant (SFRH/BD/136924/2018). CM was supported through the abovementioned OceanLog and Thermalbuffer, as well as the EU H2020 project ANERIS (no. 101094924). FPL, RS, RdS and SF received support from FCT through CEECInd contracts (10.54499/CEECIND/03185/2018/CP1546/CT0004, 0.54499/CEECIND/01424/2017/CP1423/CP1645/CT0006, 10.54499/2021.03268.CEECIND/CP1668/CT0001, 10.54499/2021.02653.CEECIND/CP1659/CT0012). FA received additional support by the strategic funding UIDB/04423/2020 (https://doi.org/10.54499/UIDB/04423/2020) and UIDP/04423/2020 (https://doi.org/10.54499/UIDP/04423/2020) and LA/P/0101/2020 (https://doi.org/10.54499/LA/P/0101/2020) through national funds provided by FCT – Fundação para a Ciência e a Tecnologia".

4.7. References

Almeida, S. C., Neiva, J., Sousa, F., Martins, N., Cox, C. J., Melo-Ferreira, J., Guiry, M. D., Serrão, E. A., & Pearson, G. A. (2022). A low-latitude species pump: Peripheral isolation, parapatric speciation and mating-system evolution converge in a marine radiation. *Molecular Ecology*, *31*(18), 4797-4817. https://doi.org/10.1111/mec.16623

Álvarez-Losada, Ó., Arrontes, J., Martínez, B., Fernández, C., & Viejo, R. M. (2020). A regime shift in intertidal assemblages triggered by loss of algal canopies: A multidecadal survey. *Marine environmental research*, *160*, 104981. https://doi.org/10.1016/j.marenvres.2020.104981

Anderson, J. M., Park, Y. I., & Chow, W. S. (1997). Photoinactivation and photoprotection of photosystem II in nature. https://doi.org/10.1111/j.1399-3054.1997.tb04777.x

Andrews, S., Bennett, S., & Wernberg, T. (2014). Reproductive seasonality and early life temperature sensitivity reflect vulnerability of a seaweed undergoing range reduction. *Marine Ecology Progress Series*, *495*, 119-129. https://doi.org/10.3354/meps10567

Araujo, R. M., Serrao, E. A., Sousa-Pinto, I., & Åberg, P. (2014). Spatial and temporal dynamics of fucoid populations (*Ascophyllum nodosum* and *Fucus serratus*): a comparison between central and range edge populations. *PLoS One*, *9*(3), e92177. https://doi.org/10.1371/journal.pone.0092177

Ardré, F. (1970). Contribution à l'étude des algues marines du Portugal. *Portugaliae Acta Biologica (B)*, *10*. https://doi.org/10.1007/978-3-642-61398-2_12

Barton, E. D., Field, D., & Roy, C. (2013). Canary current upwelling: more or less? *Progress in Oceanography*, *116*, 167-178. https://doi.org/10.1016/j.pocean.2013.07.007

Bates, D., Mächler, M., Bolker, B., & Walker, S. (2015). Fitting Linear Mixed-Effects Models Using lme4. *Journal of Statistical Software*, *67(1)*, 1-48. https://doi.org/10.18637/jss.v067.i01

Berthou, S., Renshaw, R., Smyth, T., Tinker, J., Grist, J. P., Wihsgott, J. U., Jones, S., Inall, M., Nolan, G., Berx, B., Arnold, A., Blunn, L. P., Castillo, J. M., Cotterill, D., Daly, E., Dow, G., Gómez, B., Fraser-Leonhardt, V., Hirschi, J. J. M., . . . Worsfold, M. (2024). Exceptional atmospheric conditions in June 2023 generated a northwest European marine heatwave which contributed to breaking land temperature records. *Communications Earth & Environment*, *5*(1). https://doi.org/10.1038/s43247-024-01413-8

Bindoff, N. L., Cheung, W. W., Kairo, J. G., Arístegui, J., Guinder, V. A., Hallberg, R., Hilmi, N., Jiao, N., Karim, S., & Levin, L. (2019). Changing ocean, marine ecosystems, and dependent communities. *Cambridge University Press*, 447-587. https://doi.org/10.1017/9781009157964.007.

Bischof, K., & Rautenberger, R. (2012). Seaweed Responses to Environmental Stress: Reactive Oxygen and Antioxidative Strategies. In *Seaweed Biology* (pp. 109-132). https://doi.org/10.1007/978-3-642-28451-9_6

Bizien, A., Toumi, C., Boyé, A., Sturbois, A., Le Duff, M., Grall, J., Helias, M., Gauthier, O., & Burel, T. (2024). Contrasted trends of intertidal macroalgal communities and sharp decline of canopy-forming species across two decades. *Marine Ecology Progress Series*, *742*, 73-86. https://doi.org/10.3354/meps14652

Breeman, A. (1988). Relative importance of temperature and other factors in determining geographic boundaries of seaweeds: experimental and phenological evidence. *Helgoländer Meeresuntersuchungen*, *42*, 199-241. https://doi.org/10.1007/BF02366043

Casado-Amezúa, P., Araújo, R., Bárbara, I., Bermejo, R., Borja, Á., Díez, I., Fernández, C., Gorostiaga, J., Guinda, X., & Hernández, I. (2019). Distributional shifts of canopy-forming seaweeds from the Atlantic coast of Southern Europe. *Biodiversity and Conservation*, *28*(5), 1151-1172. https://doi.org/10.1007/s10531-019-01716-9

Chappuis, E., Terradas, M., Cefalì, M. E., Mariani, S., & Ballesteros, E. (2014). Vertical zonation is the main distribution pattern of littoral assemblages on rocky shores at a regional scale. *Estuarine, Coastal and Shelf Science*, *147*, 113-122. https://doi.org/10.1016/j.ecss.2014.05.031

Cheng, L., Abraham, J., Trenberth, K. E., Fasullo, J., Boyer, T., Locarnini, R., Zhang, B., Yu, F., Wan, L., & Chen, X. (2021). Upper Ocean Temperatures Hit Record High in 2020. *38*, 523-530. https://doi.org/10.1007/s00376-021-0447-x

Cheung, W. W., Lam, V. W., Sarmiento, J. L., Kearney, K., Watson, R., & Pauly, D. (2009). Projecting global marine biodiversity impacts under climate change scenarios. *Fish and fisheries*, *10*(3), 235-251. https://doi.org/10.1111/j.1467-2979.2008.00315.x

Coleman, M. A., & Wernberg, T. (2017). Forgotten underwater forests: the key role of fucoids on Australian temperate reefs. *Ecology and Evolution*, *7*(20), 8406-8418. https://doi.org/10.1002/ece3.3279

Coleman, R. A., Underwood, A. J., Benedetti-Cecchi, L., Aberg, P., Arenas, F., Arrontes, J., Castro, J., Hartnoll, R. G., Jenkins, S. R., Paula, J., Della Santina, P., &

Hawkins, S. J. (2006). A continental scale evaluation of the role of limpet grazing on rocky shores. *Oecologia*, *147*(3), 556-564. https://doi.org/10.1007/s00442-005-0296-9

Collén, J., & Davison, I. (2002). Reactive oxygen metabolism in intertidal Fucus spp.(Phaeophyceae). *Journal of Phycology*, *35*, 62-69. https://doi.org/10.1046/j.1529-8817.1999.3510062.x

Cotas, J., Gomes, L., Pacheco, D., & Pereira, L. (2023). Ecosystem Services Provided by Seaweeds. *Hydrobiology*, *2*(1), 75-96. https://doi.org/10.3390/hydrobiology2010006

Davison, I. R., & Pearson, G. A. (1996). Stress tolerance in intertidal seaweeds. *Journal of Phycology*, *32*(2), 197-211. https://doi.org/10.1111/j.0022-3646.1996.00197.x

de Bettignies, T., Wernberg, T., & Gurgel, C. F. D. (2018). Exploring the influence of temperature on aspects of the reproductive phenology of temperate seaweeds. *Frontiers in Marine Science*, *5*, 218. https://doi.org/10.3389/fmars.2018.00218

Dorgelo, J. (1976). Intertidal fucoid zonation and desiccation. *Aquatic Ecology*, *10(2)*, 115-122. https://doi.org/10.1007/BF02282219

Dring, M., & Brown, F. A. (1982). Photosynthesis of Intertidal Brown Algae During and After Periods of Emersion: A Renewed Search for Physiological Causes of Zonation. *Marine Ecology-Progress Series*, *8*, 301-308. https://doi.org/10.3354/meps008301

Duarte, L., & Viejo, R. M. (2018). Environmental and phenotypic heterogeneity of populations at the trailing range-edge of the habitat-forming macroalga Fucus serratus. *Marine environmental research*, *136(2)*, 16-26. https://doi.org/10.1016/j.marenvres.2018.02.004

Dunstone, N. J., Smith, D. M., Atkinson, C., Colman, A., Folland, C., Hermanson, L., Ineson, S., Killick, R., Morice, C., Rayner, N., Seabrook, M., & Scaife, A. A. (2024). Will 2024 be the first year that global temperature exceeds 1.5°C? *Atmospheric Science Letters*, *25*(9). https://doi.org/10.1002/asl.1254

Eggert, A. (2012). Seaweed Responses to Temperature. In C. Wiencke & K. Bischof (Eds.), *Seaweed Biology: Novel Insights into Ecophysiology, Ecology and Utilization* (pp. 47-66). Springer Berlin Heidelberg. https://doi.org/10.1007/978-3-642-28451-9_3

Evans, R. G. (1949). The intertidal ecology of rocky shores in South Pembrokeshire. *The Journal of Ecology*, 120-139. https://doi.org/10.2307/2256736

Feldmann, J. (1978). Les algues. *Précis de Botanique. Les végétaux inférieurs.*, *1*, 95-320. (Masson)

Fernández-Marín, B., Míguez, F., Becerril, J. M., & García-Plazaola, J. I. (2011). Activation of violaxanthin cycle in darkness is a common response to different abiotic stresses: a case study in Pelvetia canaliculata. *BMC Plant Biology*, *11*, 1-11. https://doi.org/10.1186/1471-2229-11-181

Fernández, Á., Arenas, F., Trilla, A., Rodríguez, S., Rueda, L., & Martínez, B. (2015). Additive effects of emersion stressors on the ecophysiological performance of two intertidal seaweeds. *Marine Ecology Progress Series*, *536*, 135-147. https://doi.org/10.3354/meps11401

Ferreira, J. G., Arenas, F., Martínez, B., Hawkins, S. J., & Jenkins, S. R. (2014). Physiological response of fucoid algae to environmental stress: comparing range centre and southern populations. *New Phytologist*, *202*(4), 1157-1172. https://doi.org/10.1111/nph.12749

Ferreira, J. G., Hawkins, S. J., & Jenkins, S. R. (2015). Physical and biological control of fucoid recruitment in range edge and range centre populations. *Marine Ecology Progress Series*, *518*, 85-94. https://doi.org/10.3354/meps11016

Fierro, C., López-Cristoffanini, C., Meynard, A., Lovazzano, C., Castañeda, F., Guajardo, E., & Contreras-Porcia, L. (2017). Expression profile of desiccation tolerance factors in intertidal seaweed species during the tidal cycle. *Planta*, *245*(6), 1149-1164. https://doi.org/10.1007/s00425-017-2673-0

Flores Molina, M., Thomas, D., Lovazzano Bravo, C., Núñez, A., Zapata, J., Kumar, M., Correa, J., & Contreras-Porcia, L. (2014). Desiccation stress in intertidal seaweeds: Effects on morphology, antioxidant responses and photosynthetic performance. *Aquatic Botany*, *113*, 90-99. https://doi.org/10.1016/j.aquabot.2013.11.004

Fortes, M. D., & Lunning, K. (1980). Growth rates of North Sea macroalgae in relation to temperature, irradiance and photoperiod. https://doi.org/10.1007/BF01983538

Gómez-Gesteira, M., Gimeno, L., Decastro, M., Lorenzo, M., Alvarez, I., Nieto, R., Taboada, J., Crespo, A., Ramos, A., & Iglesias, I. (2011). The state of climate in NW Iberia. *Climate Research*, *48*(2-3), 109-144. https://doi.org/10.3354/cr00967

Graiff, A., Liesner, D., Karsten, U., & Bartsch, I. (2015). Temperature tolerance of western Baltic Sea Fucus vesiculosus – growth, photosynthesis and survival. *Journal of Experimental Marine Biology and Ecology*, *471*. https://doi.org/10.1016/j.jembe.2015.05.009

Hawkins, J., & Hartnoll, R. G. (1984). Factors determining the upper limits of intertidal canopy-forming algae. *Marine Ecology Progress Series*, *20(3)*, 265-271. https://doi.org/10.3354/meps020265

Hawkins, S., Pack, K., Firth, L., Mieszkowska, N., Evans, A., Martins, G., Aberg, P., Adams, L., Arenas, F., Boaventura, D., Bohn, K., Borges, D., Castro, J., Coleman, R., Crowe, T., Cruz, T., Davies, M., Epstein, G., Faria, J., & Jenkins, S. (2019). The Intertidal Zone of the North-East Atlantic Region: Pattern and Process. In (pp. 7-46). https://doi.org/10.1017/9781108235792.003

Hiscock, S. (1979). A field key to the British brown seaweeds (Heterokontophyta). *Field Studies*, *5*, 1-44.

Hobday, A. J., Alexander, L. V., Perkins, S. E., Smale, D. A., Straub, S. C., Oliver, E. C. J., Benthuysen, J. A., Burrows, M. T., Donat, M. G., Feng, M., Holbrook, N. J., Moore, P. J., Scannell, H. A., Sen Gupta, A., & Wernberg, T. (2016). A hierarchical approach to defining marine heatwaves. *Progress in Oceanography*, *141*, 227-238. https://doi.org/10.1016/j.pocean.2015.12.014

Hodges, D. M., DeLong, J. M., Forney, C. F., & Prange, R. K. (1999). Improving the thiobarbituric acid-reactive-substances assay for estimating lipid peroxidation in plant tissues containing anthocyanin and other interfering compounds. *Planta*, *207*(4), 604-611. https://doi.org/10.1007/s004250050524

Ji, Y., Xu, Z., Zou, D., & Gao, K. (2016). Ecophysiological responses of marine macroalgae to climate change factors. *Journal of Applied Phycology*, *28*(5), 2953-2967. https://doi.org/10.1007/s10811-016-0840-5

Jueterbock, A., Kollias, S., Smolina, I., Fernandes, J. M., Coyer, J. A., Olsen, J. L., & Hoarau, G. (2014). Thermal stress resistance of the brown alga Fucus serratus along the North-Atlantic coast: acclimatization potential to climate change. *Marine Genomics*, *13*, 27-36. https://doi.org/10.1016/j.margen.2013.12.008

Jueterbock, A., Tyberghein, L., Verbruggen, H., Coyer, J. A., Olsen, J. L., & Hoarau, G. (2013). Climate change impact on seaweed meadow distribution in the North Atlantic rocky intertidal. *Ecology & Evolution*, *3*(5), 1356-1373. https://doi.org/10.1002/ece3.541

Kumar, Y. N., Poong, S. W., Gachon, C., Brodie, J., Sade, A., & Lim, P. E. (2020). Impact of elevated temperature on the physiological and biochemical responses of Kappaphycus alvarezii (Rhodophyta). *PLoS One*, *15*(9), e0239097. https://doi.org/10.1371/journal.pone.0239097

Lalegerie, F., & Stengel, D. B. (2022). Concise review of the macroalgal species Pelvetia canaliculata (Linnaeus) Decaisne & Thuret. *Journal of Applied Phycology*, *34*(6), 2807-2825. https://doi.org/10.1007/s10811-022-02830-y

Lamela-Silvarrey, C., Fernández, C., Anadón, R., & Arrontes, J. (2012). Fucoid assemblages on the north coast of Spain: past and present (1977–2007). *Botanica Marina*, *55*(3), 199-207. https://doi.org/10.1515/bot-2011-0081

Lenth, R., Singmann, H., Love, J., Buerkner, P., & Herve, M. (2021). Emmeans: Estimated marginal means, aka least-squares means (R package version 1.8. 7). *The Comprehensive R Archive Network.* https://CRAN.R-project.org/package=emmeans

Liesner, D., Fouqueau, L., Valero, M., Roleda, M., Pearson, G., Bischof, K., Valentin, K., & Bartsch, I. (2020). Heat stress responses and population genetics of the kelp Laminaria digitata (Phaeophyceae) across latitudes reveal differentiation among North Atlantic populations. *Ecology & Evolution*, *10*. https://doi.org/10.1002/ece3.6569

Lima, F. P., Ribeiro, P. A., Queiroz, N., Hawkins, S. J., & Santos, A. M. (2007). Do distributional shifts of northern and southern species of algae match the warming pattern? *Global Change Biology*, *13*(12), 2592-2604. https://doi.org/10.1111/j.1365-2486.2007.01451.x

Lima, F. P., & Wethey, D. S. (2012). Three decades of high-resolution coastal sea surface temperatures reveal more than warming. *Nature Communications*, *3*(1), 704. https://doi.org/10.1038/ncomms1713

Lüning, K. (1990). Seaweeds: their environment, biogeography, and ecophysiology. *Journal of the Marine Biological Association of the United Kingdom*, *71*(1), 246-246. https://doi.org/10.1017/S0025315400037632

Lyard, F. H., Allain, D. J., Cancet, M., Carrère, L., & Picot, N. (2021). FES2014 global ocean tide atlas: design and performance. *Ocean Science*, *17*(3), 615-649. https://doi.org/10.5194/os-17-615-2021

Marbà, N., Krause-Jensen, D., Olesen, B., Christensen, P. B., Merzouk, A., Rodrigues, J., Wegeberg, S., & Wilce, R. T. (2017). Climate change stimulates the growth of the intertidal macroalgae Ascophyllum nodosum near the northern distribution limit. *Ambio*, *46*(1), 119-131. https://doi.org/10.1007/s13280-016-0873-7

Martinez, B., Arenas, F., Rubal, M., Burgues, S., Esteban, R., Garcia-Plazaola, I., Figueroa, F. L., Pereira, R., Saldana, L., Sousa-Pinto, I., Trilla, A., & Viejo, R. M. (2012). Physical factors driving intertidal macroalgae distribution: physiological stress of a dominant fucoid at its southern limit. *Oecologia*, *170*(2), 341-353. https://doi.org/10.1007/s00442-012-2324-x

Martins, M., Soares, C., Figueiredo, I., Sousa, B., Torres, A. C., Sousa-Pinto, I., Veiga, P., Rubal, M., & Fidalgo, F. (2021). Fucoid Macroalgae Have Distinct

Physiological Mechanisms to Face Emersion and Submersion Periods in Their Southern Limit of Distribution. *Plants (Basel)*, *10*(9). https://doi.org/10.3390/plants10091892

Migné, A., Delebecq, G., Davoult, D., Spilmont, N., Menu, D., & Gévaert, F. (2015). Photosynthetic activity and productivity of intertidal macroalgae: In situ measurements, from thallus to community scale. *Aquatic Botany*, *123*, 6-12. https://doi.org/10.1016/j.aquabot.2015.01.005

Moalic, Y., Arnaud-Haond, & S., P., C. et al. (2011). Travelling in time with networks: Revealing present day hybridization versus ancestral polymorphism between two species of brown algae, Fucus vesiculosus and F. spiralis. *BMC Ecology and Evolution*, *11*, 33 https://doi.org/10.1186/1471-2148-11-33

Monteiro, C., Pereira, J., Seabra, R., & Lima, F. P. (2022). Fine-scale survey of intertidal macroalgae reveals recent changes in a cold-water biogeographic stronghold. *Frontiers in Marine Science*, *9*. https://doi.org/10.3389/fmars.2022.880074

Neiva, J., Assis, J., Fernandes, F., Pearson, G. A., Serrão, E. A., & Maggs, C. (2014). Species distribution models and mitochondrial DNA phylogeography suggest an extensive biogeographical shift in the high-intertidal seaweed Pelvetia canaliculata. *Journal of Biogeography*, *41*(6), 1137-1148. https://doi.org/10.1111/jbi.12278

Neiva, J., Serrão, E. A., Assis, J., Pearson, G. A., Coyer, J. A., Olsen, J. L., Hoarau, G., & Valero, M. (2016). Climate oscillations, range shifts and phylogeographic patterns of North Atlantic Fucaceae. In *Seaweed phylogeography* (pp. 279-308). Springer. https://doi.org/10.1007/978-94-017-7534-2_11

Nepper-Davidsen, J., Andersen, D. T., & Pedersen, M. (2019). Exposure to simulated heatwave scenarios causes long-term reductions in performance in Saccharina latissima. *Marine Ecology Progress Series*, *630*, 25-39. https://doi.org/10.3354/meps13133

NOAA. (2022). *Global Climate Report for Annual 2022* (State of the Climate, Issue. https://www.ncdc.noaa.gov/sotc/global/202013

Olabarria, C., Arenas, F., Fernandez, A., Troncoso, J. S., & Martinez, B. (2018). Physiological responses to variations in grazing and light conditions in native and invasive fucoids. *Marine environmental research*, *139*, 151-161. https://doi.org/10.1016/j.marenvres.2018.05.016

Oliver, E. C. J., Burrows, M. T., Donat, M. G., Sen Gupta, A., Alexander, L. V., Perkins-Kirkpatrick, S. E., Benthuysen, J. A., Hobday, A. J., Holbrook, N. J., Moore, P. J., Thomsen, M. S., Wernberg, T., & Smale, D. A. (2019). Projected Marine

Heatwaves in the 21st Century and the Potential for Ecological Impact. *Frontiers in Marine Science*, *6*, 734. https://doi.org/10.3389/fmars.2019.00734

Pearson, G. A., Lago-Leston, A., & Mota, C. (2009). Frayed at the edges: selective pressure and adaptive response to abiotic stressors are mismatched in low diversity edge populations. *Journal of Ecology*, *97*(3), 450-462. https://doi.org/10.1111/j.1365-2745.2009.01481.x

Pereira, L., Morrison, L., Shukla, P. S., & Critchley, A. T. (2020). A concise review of the brown macroalga Ascophyllum nodosum (Linnaeus) Le Jolis. *Journal of Applied Phycology*, *32*(6), 3561-3584. https://doi.org/10.1007/s10811-020-02246-6

Pereira, L. F., Seabra, R., Loureiro, B., Arenas, F., & Lima, F. P. (in press). Intertidal Environmental Chamber: an automatic system to accurately simulate the thermal complexity of intertidal environments. *Methods in Ecology and Evolution*.

Piñeiro-Corbeira, C., Barreiro, R., Cremades, J., & Arenas, F. (2018). Seaweed assemblages under a climate change scenario: Functional responses to temperature of eight intertidal seaweeds match recent abundance shifts. *Scientific reports*, *8*(1), 1-9. https://doi.org/10.1038/s41598-018-31357-x

Ren, Q., Kwon, Y.-O., Yang, J., Huang, R. X., Li, Y., & Wang, F. (2024). Substantial Warming of the Atlantic Ocean in CMIP6 Models. *Journal of Climate*, *37*(11), 3073-3091. https://doi.org/10.1175/JCLI-D-23-0418.1

Román, M., Román, S., Vázquez, E., Troncoso, J., & Olabarria, C. (2020). Heatwaves during low tide are critical for the physiological performance of intertidal macroalgae under global warming scenarios. *Scientific reports*, *10*(1), 1-14. https://doi.org/10.1038/s41598-020-78526-5

Sampath-Wiley, P., Neefus, C. D., & Jahnke, L. S. (2008). Seasonal effects of sun exposure and emersion on intertidal seaweed physiology: Fluctuations in antioxidant contents, photosynthetic pigments and photosynthetic efficiency in the red alga Porphyra umbilicalis Kützing (Rhodophyta, Bangiales). *Journal of Experimental Marine Biology and Ecology*, *361*(2), 83-91. https://doi.org/10.1016/j.jembe.2008.05.001

Santos, A. M. (2000). Intertidal ecology of northern Portuguese rocky shores.

Schonbeck, M. W., & Norton, T. A. (1979). Drought-hardening in the uppershore seaweeds Fucus spiralis and Pelvetia canaliculata. *Journal of Ecology*, *67(2)*, 687. https://doi.org/10.2307/2259120

Schreiber, U., Schliwa, U., & Bilger, W. (1986). Continuous recording of photochemical and non-photochemical chlorophyll fluorescence quenching with a new type of

modulation fluorometer. *Photosynth Res*, *10*(1-2), 51-62. https://doi.org/10.1007/BF00024185

Schrofner-Brunner, B., Hagan, J. G., Cappelatti, L., Hassellöv, J., Wißmann, M., & Gamfeldt, L. (2023). Macroalgae maintain growth outside their observed distributions: Implications for biodiversity-ecosystem functioning at landscape scales. *Journal of Ecology*, *111*(6), 1362-1373. https://doi.org/10.1111/1365-2745.14103

Seabra, R., Wethey, D. S., Santos, A. M., Gomes, F., & Lima, F. P. (2016). Equatorial range limits of an intertidal ectotherm are more linked to water than air temperature. *Global Change Biology*, *22*(10), 3320-3331. https://doi.org/10.1111/gcb.13321

Seabra, R., Wethey, D. S., Santos, A. M., & Lima, F. P. (2011). Side matters: Microhabitat influence on intertidal heat stress over a large geographical scale. *Journal of Experimental Marine Biology and Ecology*, *400*(1-2), 200-208. https://doi.org/10.1016/j.jembe.2011.02.010

Serôdio, J., & Campbell, D. A. (2021). Photoinhibition in optically thick samples: Effects of light attenuation on chlorophyll fluorescence-based parameters. *Journal of Theoretical Biology*, *513*, 110580. https://doi.org/10.1016/j.jtbi.2021.110580

Straub, S. C., Wernberg, T., Thomsen, M. S., Moore, P. J., Burrows, M. T., Harvey, B. P., & Smale, D. A. (2019). Resistance, extinction, and everything in between–The diverse responses of seaweeds to marine heatwaves. *Frontiers in Marine Science*, *6*, 763. https://doi.org/10.3389/fmars.2019.00763

Strömgren, T. (1977). Short-term effects of temperature upon the growth of intertidal Fucales. *Journal of Experimental Marine Biology and Ecology*, *29(2)*, 181-195. https://doi.org/10.1016/0022-0981(77)90047-8

Taenzer, L., Toth, G., & Hansel, C. M. (2024). Assessment of hydrogen peroxide as a bioindicator of stress in seaweed aquaculture. *Sci Rep*, *14*(1), 1956. https://doi.org/10.1038/s41598-024-52182-5

Thomsen, M., Mondardini, L., Alestra, T., Gerrity, S., Tait, L., South, P., Lilley, S., & Schiel, D. (2019). Local Extinction of Bull Kelp (Durvillaea spp.) Due to a Marine Heatwave. *Frontiers in Marine Science*, *6*, 84. https://doi.org/10.3389/fmars.2019.00084

Varela, R., de Castro, M., Dias, J. M., & Gómez-Gesteira, M. (2023). Coastal warming under climate change: Global, faster and heterogeneous. *Science of the total environment*, *886(3)*. https://doi.org/10.1016/j.scitotenv.2023.164029

Viejo, R. M., Des, M., & Gutiérrez, D. (2024). Drivers of the fine-scale distribution of a canopy-forming seaweed at the southern edge of its range. *Marine Ecology Progress Series*, *727*, 91-109. https://doi.org/10.3354/meps14499

Wernberg, T., de Bettignies, T., Joy, B. A., & Finnegan, P. M. (2016). Physiological responses of habitat-forming seaweeds to increasing temperatures. *Limnology and Oceanography*, *61*(6), 2180-2190. https://doi.org/10.1002/lno.10362

Whitaker, S. G., Ambrose, R. F., Anderson, L. M., Fales, R. J., Smith, J. R., Sutton, S., & Miller, R. J. (2023). Ecological restoration using intertidal foundation species: Considerations and potential for rockweed restoration. *Ecosphere*, *14*(3). https://doi.org/10.1002/ecs2.4411

Zaneveld. (1937). The Littoral Zonation of Some Fucaceae in Relation to Desiccation. *The Journal of Ecology*, *25(2)*, 431-468. https://doi.org/10.2307/2256204

Zaneveld, J. S. (1969). Factors Controlling the Delimitation of Littoral Benthic Marine Algal Zonation. *Integrative and Comparative Biology*, *9(2)*, 367-391. https://doi.org/10.1093/icb/9.2.367

Zardi, G. I., Nicastro, K. R., Canovas, F., Costa, J. F., Serrao, E. A., & Pearson, G. A. (2011). Adaptive traits are maintained on steep selective gradients despite gene flow and hybridization in the intertidal zone. *PLoS One*, *6*(6), e19402. https://doi.org/10.1371/journal.pone.0019402

Zuur, A. F., Ieno, E. N., Walker, N. J., Saveliev, A. A., & Smith, G. M. (2009). Mixed effects models and extensions in ecology with R. *574*. https://doi.org/10.1007/978-0-387-87458-6

4.8. Supplementary Tables

Table S4.1: Pairwise contrasts summary of GLM model for growth described in **Table 4.1**. Analysis was performed for T1 and T2 separate models with a focus on species contrast within each temperature treatment (Degrees of freedom: T1= 728 and T2= 341). Significant effects are indicated in bold (*P*-value < 0.05), and * indicates marginal significance. The t-ratio test is represented as *t*.

		T1		T2	
Temperature (ºC)	**Species contrast**	***t***	***P*-value**	***t***	***P*-value**
28	*A .nodosum* vs *F. serratus*	-4.29	**0.001**	-2.64	**0.043**
	A .nodosum vs *F. spiralis*	-5.86	**<0.001**	-4.18	**<0.001**
	A .nodosum vs *P. canaliculata*	-2.18	0.131	-2.10	0.154
	F. serratus vs *F. spiralis*	-1.57	0.398	-1.54	0.414
	F. serratus vs *P. canaliculata*	2.11	0.1497	0.54	0.949
	F. spiralis vs *P. canaliculata*	3.68	**0.001**	2.08	0.162
35	*A .nodosum* vs *F. serratus*	-0.87	0.822	-0.11	0.999
	A .nodosum vs *F. spiralis*	-3.70	**0.001**	-3.71	**0.001**
	A .nodosum vs *P. canaliculata*	-2.50	0.061*	-.1.63	0.3624
	F. serratus vs *F. spiralis*	-2.83	**0.025**	-3.69	**0.001**
	F. serratus vs *P. canaliculata*	-1.63	0.362	-1.56	0.406
	F. spiralis vs *P. canaliculata*	1.20	0.628	2.13	0.146
36	*A .nodosum* vs *F. serratus*	-0.49	0.961	-0.68	0.905
	A .nodosum vs *F. spiralis*	-4.90	**<0.001**	-4.79	**<0.001**
	A .nodosum vs *P. canaliculata*	-2.58	**0.049**	-2.46	0.068*
	F. serratus vs *F. spiralis*	-4.41	**<0.001**	-4.11	**<0.001**
	F. serratus vs *P. canaliculata*	-2.09	0.157	-1.78	0.283
	F. spiralis vs *P. canaliculata*	2.32	0.095	2.32	0.095
37	*A .nodosum* vs *F. serratus*	1.99	0.191	1.34	0.540
	A .nodosum vs *F. spiralis*	-1.87	0.241	-2.28	0.104
	A .nodosum vs *P. canaliculata*	-2.48	0.065*	-2.62	**0.046**
	F. serratus vs *F. spiralis*	-3.86	**<0.001**	-3.62	**0.002**
	F. serratus vs *P. canaliculata*	-4.47	**<0.001**	-3.95	**<0.001**
	F. spiralis vs *P. canaliculata*	0.60	0.931	-0.33	0.987
38	*A .nodosum* vs *F. serratus*	3.21	**0.008**	2.51	0.061*
	A .nodosum vs *F. spiralis*	1.54	0.414	0.61	0.928
	A .nodosum vs *P. canaliculata*	-1.32	0.552	-0.61	0.928
	F. serratus vs *F. spiralis*	-1.67	0.340	-1.89	0.233
	F. serratus vs *P. canaliculata*	-4.53	**<0.001**	-3.12	**0.011**
	F. spiralis vs *P. canaliculata*	2.86	**0.023**	-1.22	0.612

		T1		T2	
Temperature (ºC)	**Species contrast**	***t***	***P*-value**	***t***	***P*-value**
39	*A .nodosum* vs *F. serratus*	2.46	0.068*	2.10	0.153
	A .nodosum vs *F. spiralis*	-0.36	0.985	1.33	0.544
	A .nodosum vs *P. canaliculata*	-1.29	0.568	-0.90	0.805
	F. serratus vs *F. spiralis*	-2.81	**0.026**	-0.79	0.858
	F. serratus vs *P. canaliculata*	-3.75	**0.001**	-3.07	**0.012**
	F. spiralis vs *P. canaliculata*	-0.936	0.785	-2.28	0.105
40	*A .nodosum* vs *F. serratus*	2.66	**0.040**	3.02	**0.015**
	A .nodosum vs *F. spiralis*	-0.49	0.961	0.29	0.991
	A .nodosum vs *P. canaliculata*	-1.29	0.573	-0.92	0793
	F. serratus vs *F. spiralis*	-3.15	**0.009**	-2.79	**0.029**
	F. serratus vs *P. canaliculata*	-3.95	**0.001**	-4.03	**<0.001**
	F. spiralis vs *P. canaliculata*	-0.79	0.857	-1.24	0.60
41	*A .nodosum* vs *F. serratus*	3.98	**<0.001**	4.58	**<0.001**
	A .nodosum vs *F. spiralis*	0.96	0.772	2.69	**0.038**
	A .nodosum vs *P. canaliculata*	-0.82	0.845	0.62	0.927
	F. serratus vs *F. spiralis*	-3.02	**0.014**	-1.89	0.232
	F. serratus vs *P. canaliculata*	-4.80	**<0.001**	-3.97	**<0.001**
	F. spiralis vs *P. canaliculata*	-1.78	0.284	-2.07	0.164

Table S4.2: Pairwise contrasts summary of GLM model for growth described in **Table 4.1**. Analysis performed for T1 and T2 separate models with a focus on each species response at various temperatures (Degrees of freedom: T1 = 728 and T2=341). Contrasts towards control temperature (28 ºC) are as indicated in **Fig. 4.1**. Significant effects are indicated in bold (*P*-value < 0.05), and * indicates marginal significance. The t-ratio test is represented as *t*.

		T1		T2	
Species	**Temperature contrast**	***t***	***P*-value**	***t***	***P*-value**
A. nodosum	28 ºC vs 35 ºC	0.46	1	0.09	1
	28 ºC vs 36 ºC	-0.07	1	0.14	1
	28 ºC vs 37 ºC	0.83	0.989	0.54	0.999
	28 ºC vs 38 ºC	1.16	0.934	0.59	0.999
	28 ºC vs 39 ºC	1.4	0.848	0.77	0.993
	28 ºC vs 40 ºC	0.76	0.994	1	0.97
	28 ºC vs 41 ºC	1.83	0.609	1.12	0.945
	35 ºC vs 36 ºC	-0.53	0.999	0.05	1
	35 ºC vs 37 ºC	0.37	1	0.44	1
	35 ºC vs 38 ºC	0.7	0.996	0.49	1
	35 ºC vs 39 ºC	0.94	0.978	0.67	0.997
	35 ºC vs 40 ºC	0.3	1	0.89	0.984
	35 ºC vs 41 ºC	1.37	0.858	1.01	0.967
	36 ºC vs 37 ºC	0.9	0.982	0.4	1
	36 ºC vs 38 ºC	1.23	0.912	0.45	1
	36 ºC vs 39 ºC	1.47	0.813	0.63	0.998
	36 ºC vs 40 ºC	0.83	0.989	0.86	0.987
	36 ºC vs 41 ºC	1.9	0.565	0.98	0.973
	37 ºC vs 38 ºC	0.33	1	0.06	1
	37 ºC vs 39 ºC	0.57	0.999	0.24	1
	37 ºC vs 40 ºC	-0.07	1	0.47	1
	37 ºC vs 41 ºC	1	0.968	0.58	0.999
	38 ºC vs 39 ºC	0.24	1	0.18	1
	38 ºC vs 40 ºC	-0.4	1	0.41	1
	38 ºC vs 41 ºC	0.67	0.997	0.52	0.999
	39 ºC vs 40 ºC	-0.64	0.998	0.23	1
	39 ºC vs 41 ºC	0.43	1	0.34	1
	40 ºC vs 41 ºC	1.07	0.955	0.11	1

		T1		T2	
Species	**Temperature contrast**	***t***	***P*-value**	***t***	***P*-value**
F. serratus	28 ºC vs 35 ºC	2.81	0.151	1.85	0.595
	28 ºC vs 36 ºC	2.54	0.239	1.51	0.795
	28 ºC vs 37 ºC	5.14	**0.001**	3.31	0.058*
	28 ºC vs 38 ºC	6.31	**<0.001**	4.18	**0.009**
	28 ºC vs 39 ºC	6.03	**<0.001**	4.11	**0.011**
	28 ºC vs 40 ºC	5.53	**0.001**	4.99	**0.002**
	28 ºC vs 41 ºC	7.51	**<0.001**	6.15	**<0.001**
	35 ºC vs 36 ºC	-0.27	1	-0.35	1
	35 ºC vs 37 ºC	2.34	0.325	1.45	0.822
	35 ºC vs 38 ºC	3.5	**0.04**	2.32	0.331
	35 ºC vs 39 ºC	3.22	0.069*	2.26	0.362
	35 ºC vs 40 ºC	2.72	0.175	3.14	**0.08**
	35 ºC vs 41 ºC	4.71	**0.003**	4.29	**0.007**
	36 ºC vs 37 ºC	2.61	0.212	1.8	0.628
	36 ºC vs 38 ºC	3.78	**0.023**	2.67	0.191
	36 ºC vs 39 ºC	3.5	**0.04**	2.6	0.213
	36 ºC vs 40 ºC	3	0.107	3.49	**0.04**
	36 ºC vs 41 ºC	4.98	**0.002**	4.64	**0.003**
	37 ºC vs 38 ºC	1.17	0.931	0.87	0.986
	37 ºC vs 39 ºC	0.89	0.984	0.81	0.991
	37 ºC vs 40 ºC	0.39	1	1.69	0.695
	37 ºC vs 41 ºC	2.37	0.309	2.84	0.141
	38 ºC vs 39 ºC	-0.28	1	-0.06	1
	38 ºC vs 40 ºC	-0.78	0.992	0.82	0.99
	38 ºC vs 41 ºC	1.2	0.922	1.97	0.524
	39 ºC vs 40 ºC	-0.5	1	0.88	0.984
	39 ºC vs 41 ºC	1.48	0.807	2.03	0.486
	40 ºC vs 41 ºC	1.98	0.517	1.15	0.936

		T1		T2	
Species	**Temperature contrast**	***t***	***P*-value**	***t***	***P*-value**
F. spiralis	28 ºC vs 35 ºC	1.94	0.542	0.36	1
	28 ºC vs 36 ºC	0.58	0.999	-0.28	1
	28 ºC vs 37 ºC	3.57	**0.035**	1.86	0.591
	28 ºC vs 38 ºC	6.24	**<0.001**	3.93	**0.016**
	28 ºC vs 39 ºC	5.18	**0.001**	4.63	**0.004**
	28 ºC vs 40 ºC	4.44	**0.005**	4.13	**0.01**
	28 ºC vs 41 ºC	6.51	**0**	5.9	**<0.001**
	35 ºC vs 36 ºC	-1.36	0.865	-0.64	0.998
	35 ºC vs 37 ºC	1.62	0.731	1.5	0.799
	35 ºC vs 38 ºC	4.3	**0.007**	3.57	**0.034**
	35 ºC vs 39 ºC	3.24	0.068*	4.27	**0.008**
	35 ºC vs 40 ºC	2.5	0.252	3.77	**0.023**
	35 ºC vs 41 ºC	4.57	**0.004**	5.54	**0.001**
	36 ºC vs 37 ºC	2.98	0.11	2.14	0.427
	36 ºC vs 38 ºC	5.66	**<0.001**	4.21	**0.009**
	36 ºC vs 39 ºC	4.59	**0.004**	4.91	**0.002**
	36 ºC vs 40 ºC	3.86	**0.019**	4.4	**0.006**
	36 ºC vs 41 ºC	5.93	**0**	6.18	**<0.001**
	37 ºC vs 38 ºC	2.68	0.19	2.07	0.465
	37 ºC vs 39 ºC	1.61	0.739	2.77	0.159
	37 ºC vs 40 ºC	0.88	0.985	2.27	0.358
	37 ºC vs 41 ºC	2.95	0.117	4.04	**0.013**
	38 ºC vs 39 ºC	-1.06	0.957	0.7	0.996
	38 ºC vs 40 ºC	-1.8	0.629	0.2	1
	38 ºC vs 41 ºC	0.27	1	1.97	0.524
	39 ºC vs 40 ºC	-0.73	0.995	-0.51	1
	39 ºC vs 41 ºC	1.34	0.873	1.27	0.9
	40 ºC vs 41 ºC	2.07	0.465	1.77	0.643

		T1		T2	
Species	**Temperature contrast**	***t***	***P*-value**	***t***	***P*-value**
P. canaliculata	28 ºC vs 35 ºC	0.24	1	0.4	1
	28 ºC vs 36 ºC	-0.35	1	-0.11	1
	28 ºC vs 37 ºC	0.62	0.998	0.18	1
	28 ºC vs 38 ºC	1.75	0.659	1.63	0.727
	28 ºC vs 39 ºC	2	0.504	1.6	0.745
	28 ºC vs 40 ºC	1.37	0.86	1.82	0.618
	28 ºC vs 41 ºC	2.76	0.163	3.01	0.103
	35 ºC vs 36 ºC	-0.59	0.999	-0.51	1
	35 ºC vs 37 ºC	0.39	1	-0.22	1
	35 ºC vs 38 ºC	1.51	0.792	1.24	0.911
	35 ºC vs 39 ºC	1.77	0.647	1.2	0.922
	35 ºC vs 40 ºC	1.13	0.941	1.42	0.839
	35 ºC vs 41 ºC	2.53	0.243	2.61	0.209
	36 ºC vs 37 ºC	0.97	0.973	0.29	1
	36 ºC vs 38 ºC	2.1	0.448	1.74	0.664
	36 ºC vs 39 ºC	2.36	0.315	1.71	0.683
	36 ºC vs 40 ºC	1.72	0.675	1.92	0.553
	36 ºC vs 41 ºC	3.12	0.086*	3.12	0.084
	37 ºC vs 38 ºC	1.13	0.943	1.45	0.823
	37 ºC vs 39 ºC	1.38	0.854	1.42	0.839
	37 ºC vs 40 ºC	0.75	0.994	1.63	0.726
	37 ºC vs 41 ºC	2.14	0.426	2.83	0.144
	38 ºC vs 39 ºC	0.26	1	-0.03	1
	38 ºC vs 40 ºC	-0.38	1	0.18	1
	38 ºC vs 41 ºC	1.01	0.967	1.38	0.856
	39 ºC vs 40 ºC	-0.64	0.998	0.22	1
	39 ºC vs 41 ºC	0.76	0.994	1.41	0.842
	40 ºC vs 41 ºC	1.39	0.849	1.2	0.924

Chapter 5

Heat stress on the brown seaweed *Ascophyllum nodosum*: differential population sensitivity to future climate

5.1. Abstract

Accurate forecasts of the biological impacts of climate change require a better understanding of how small-scale temperature variability affects individual physiology and population dynamics. However, doing so for intertidal species with large distribution ranges while accounting for the effects of local adaptation presents numerous technical challenges. Here, we assessed the macroecological consequences of thermal stress on the cold-adapted brown seaweed *Ascophyllum nodosum* across its European distribution. We collected specimens from ten populations spanning latitudes 41°N to 60°N and subjected them to simulated intertidal heat stress using a novel, custom-built experimental setup that replicated realistic conditions, including tidal cycles, light conditions, and temperature trajectories based on in-situ data. Results indicate that thermal stress is more closely associated with the magnitude of temperature change between high and low tides rather than the absolute maximum temperatures reached. Notwithstanding, algae exposed to warmer water temperatures (20.5 °C) consistently outperformed those in colder water (15 °C), suggesting that cold upwelled waters at the species' southern limit may not be essential for survival. By integrating empirical physiological observations with state-of-the-art climate projections, we found that some populations, though more resilient to thermal stress, could still be overwhelmed by the pace of warming, leading to uneven impacts across the European distribution of the species.

Keywords

Ascophyllum nodosum, Habitat-forming species, Rocky shore, Intertidal thermal stress, Population sensitivity, Climate change, Macroecology, Thermal ecotype, European distribution

5.2. Introduction

Temperatures have been following alarming trends in both atmospheric and marine domains (Kemp et al., 2022; Oliver et al., 2019). These trends are expected to intensify, with global air temperatures predicted to rise between 1 ºC and 5 ºC and sea surface temperatures between 1.6 ºC and 4 ºC until the end of the century (Pörtner et al., 2022). Importantly, since warming patterns differ among the two domains, temporal and spatial heterogeneity at smaller scales may also be on the rise (Coumou et al., 2013). Understanding how this small-scale temperature variability affects the individual's physiology and subsequent population resilience is, therefore, critical for accurately predicting the biotic impacts of climate change (Choi et al., 2019). Species inhabiting intertidal rocky shores provide exceptional opportunities for these studies. Despite their marine origin, they periodically endure terrestrial conditions during low tide, when body temperatures can fluctuate by as much as 20 ºC in a couple of hours (Seabra et al., 2011). Consequently, rocky shore organisms are considered sensitive indicators of climate change (Mislan et al., 2014; Wethey & Woodin, 2008). Yet, the explicit incorporation of the thermal complexity of intertidal zones within experimental studies presents substantial challenges.

First, the identification of appropriate experimental temperature treatments isn't always trivial. A common framework is identifying heatwaves and cold snaps, defined as significant deviations from typical climate conditions (Domeisen et al., 2023; Hobday et al., 2016), and using them to characterise and quantify weather anomalies. But although extreme events are evidently correlated with mass mortality events among algae (Thomsen et al., 2019), seagrass (Strydom et al., 2020), and benthic invertebrates (Le Nohaic et al., 2017; Traiger et al., 2022), mild but realistic temperature changes can also lead to meaningful impacts. For example, survivability in mussels (*Perna canaliculus*) following field transplants was found to be correlated with time spent in not-so-extreme heat (>25 ºC) during emersion periods (Benjamin et al., 2024), a detail that could only be properly captured with in-situ temperature sensors. Additionally, these impacts can be more severe when habitat-forming species are affected, triggering cascading effects on biodiversity, community structure, and ecosystem services (Garrabou et al., 2022; Hesketh & Harley, 2023; Smale, 2017).

Second, environmental data must be acquired at scales relevant to the organisms under study (Potter et al., 2013), and that can be very hard to accomplish. Obtaining long-term and accurate data for the coastal fringe is already difficult during high tides (Brewin et al., 2018; Castillo & Lima, 2010) because remotely sensed data often lack the spatial

and temporal resolution needed to capture sharp gradients in sea temperature near the coast (Meneghesso et al., 2020). This task becomes even more challenging during low tides when even data from nearby weather stations have been shown to overlook extreme variations in intertidal air temperature (Lathlean et al., 2011). However, ignoring those temperatures altogether may result in the mischaracterisation of critical thermal limits for some species. Crucially, while still a logistically complex task, this challenge has now been largely resolved through the development of small, sturdy, and autonomous temperature loggers (e.g., Lima and Wethey (2009)) that can consistently record hourly temperature data over extended periods of time and at the scale of the study organisms both during high and low tides (Lima et al., 2016).

Third, the potential geographical variability in the physiological responses of the organisms themselves must be accounted for. This is particularly concerning in species with broad geographic ranges and low mobility (Straub et al., 2019), such as macroalgae, which are likely to exhibit phenotypic plasticity or local adaptation (Hernández et al., 2023; King et al., 2018). One of the most usual methods to detect population-level variability in heat tolerance involves conducting common-garden experiments where populations from different origins are tested under uniform environmental conditions (King et al., 2018). So far, results have varied across species and experiments, with findings sometimes pointing to heat-adapted distribution edges and other times uncovering unexpectedly tolerant central populations (DuBois et al., 2022; King et al., 2019). Regardless, it is important to recognise that even heat-tolerant populations may face future challenges if the temperatures they experience eventually exceed their adaptive thresholds (Pearson et al., 2009). Thus, the significance of a population's heat resilience can only be fully understood within the context of the projected climate it will endure.

With these challenges in mind, we aimed to assess the macroecological consequences of the physiological responses of the fucoid *Ascophyllum nodosum* (Fucales, Phaeophyeceae) to simulated intertidal heat stress across its distributional range. *A. nodosum* is an important habitat-forming species present along both North Atlantic coastlines, commonly found in sheltered intertidal rocky shores from Norway to Portugal in the East and from Baffin Island, Canada to New York, USA in the West. It is a relatively slow-growing, long-lived species with an estimated maximum lifespan of 60 years, and it is capable of producing clonal individuals through vegetative sprouting from its base (Åberg, 1992b). Commonly referred to as a cold-adapted species, summer temperatures are thought to be a limiting factor for its southern populations (Lüning, 1990). Importantly,

these southern populations are not contiguous to the rest of the species range. Instead, they are geographically separated and restricted to the NW corner of the Iberian Peninsula, a biogeographic stronghold for cold-adapted species due to the upwelling of cold water during the summer months (Monteiro et al., 2022).

We used a custom-built experimental set-up to realistically simulate tides, light, and, importantly, daily submersion and emersion temperature trajectories through the fine control of water temperature, infrared (IR) radiation, and air circulation. Sampled populations span a latitudinal range from 41º to 60º N, encompassing most of the species' latitudinal range across Europe. Realistic temperature trajectories were based on hourly temperature data from in-situ loggers deployed in the sampled populations. To understand the importance of cold water in the upwelling-dominated southern distribution limit, we simulated two water temperature scenarios, one typical of a period of strong upwelling (colder) and another corresponding to upwelling relaxation (warmer). We then evaluated physiological performance through growth, mortality, and oxygen production. From the collected data, we inferred evidence of local adaptation to thermal stress. We combined current population-specific physiological responses with future temperature projections and ran demographic models (David R. Schiel, 2013) parameterised to the specific populations under study (Åberg, 1992b) so as to produce long-term population forecasts across the European range of this species.

5.3. Materials and methods

5.3.1. Sample collection

Juvenile vegetative fronds of *A. nodosum* measuring 6 to 10 cm in length were collected between 15 and 25 of August 2021 at low tide from ten populations (**Fig. 5.1a**; **Supplementary Table S5.1**) across the species' vertical distribution and capturing most of its European latitudinal range (Pereira et al., 2020). Sampling avoided nearby individuals, minimising the chance of collecting clones. After collection, fronds were transported to the Interdisciplinary Center of Marine and Environmental Research (CIIMAR, Porto, Portugal) within 24 hours in refrigerated boxes. Upon arrival, they were acclimated separately for two weeks at constant aeration and at 150-175 µmol photon m^{-2} s^{-1} PAR irradiance (US-SQS/L PAR sensor, WALZ, Germany) with 12h/12h photoperiod (light/dark) under 5032 LED stripes.

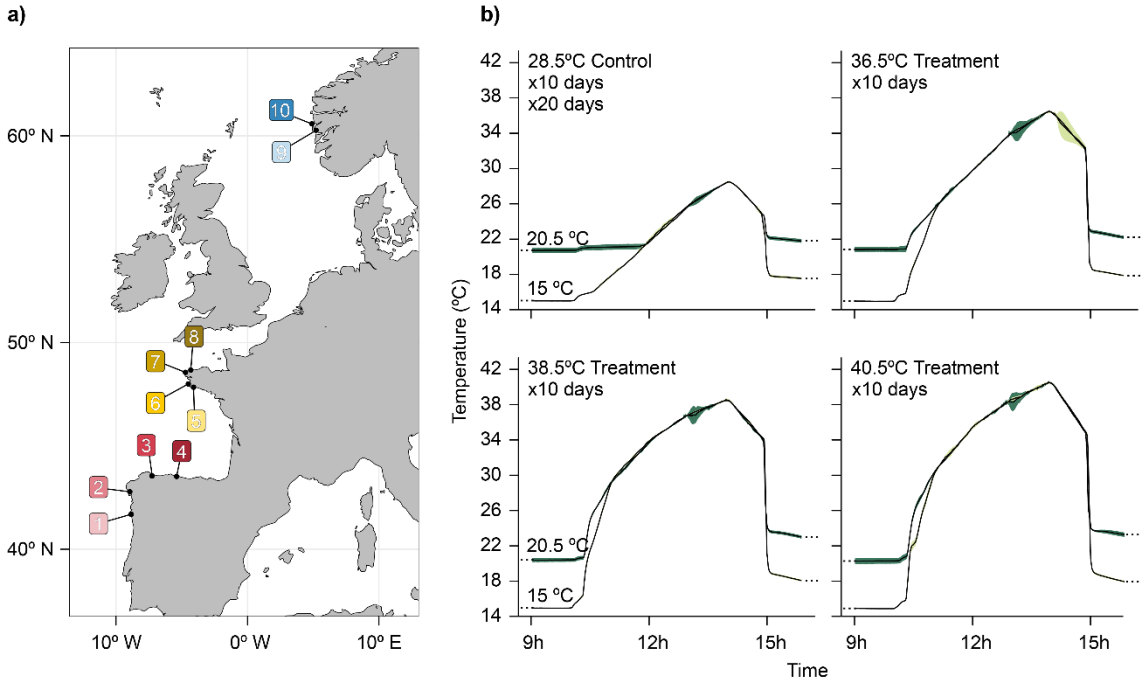


Figure 5.1: a) Map of the study area. Numbers 1–10 indicate the locations of the ten populations sampled (1– Viana do Castelo, PT; 2- Ría de Muros, ES; 3- Ría de Foz, ES; 4- Ría de Villaviciosa, ES; 5- Île-Tudy, FR; 6- Penmarch, FR; 7- Landunvez, FR; 8- Soulougan, FR; 9- Blomsterdalen, NO; 10- Straumøyna, NO). b) Average diurnal low tide temperatures within each experimental tank for the 8 treatments (black line) ± SD (light green and dark green for cold- and warm-water treatments, 15 ºC and 20.5 ºC, respectively). Nocturnal low tide temperatures remained close to their respective water temperatures. The tide cycle of 7:5 (high: low) was repeated twice daily for the whole 20 days of the experiment. Map created in R (R Development Core Team, 2023) using the Rnaturalearth library v1.0.0.

Acclimation followed an intertidal cycle of 7/5 hours (high/low), simulating the observed tides at the vertical niche of *A. nodosum* in Viana do Castelo (Portugal). During acclimation, water temperature was slowly brought from the water temperature observed at the collection site to the targeted treatment at a daily maximum rate of 1 ºC.

5.3.2. Experimental design

The experiment (**Fig. 5.1b**) was designed to provide short-term exposure to heat stress during low tides while simulating realistic tidal cycles with two different high tide temperatures. A 7/5 h (high/low) tide cycle was applied to all treatments during the whole experiment. The experimental design had four low tide and two high tide temperatures, composing a full factorial design of 4x2 levels. Water temperature during the experiment was fixed at 15 ºC (cold) or 20.5 ºC (warm), depending on the treatment. These water temperatures correspond to the summer average values at the southern edge population (Viana do Castelo, Portugal) during strong and weak upwelling events, respectively, and were obtained from an hourly in-situ temperature dataset collected between 2010 and 2020. Although seasonal upwelling keeps seawater around 15 ºC during most of the summer, occasional relaxation of upwelling promotes warming periods, providing insight into the conditions of a weakened upwelling system.

Low tide periods were characterised by emersion accompanied by realistic heating simulated with infrared-emitting lamps. To assess the effect of an acute heatwave on *A. nodosum* performance, we selected the most extreme hot days from the temperature record (i.e., those days whose temperatures exceeded the overall 90th percentile). We then determined that peak temperatures were typically reached four hours after the emersion began and calculated the average temperature trajectory slopes leading to and from this peak point. These data were used to generate four diurnal low-tide temperature profiles with similar shapes but reaching different temperature peaks (**Fig. 5.1b**). The lowest peak, set at 28.5 ºC, was used as the control treatment and corresponded to the average summer temperature at the southern edge population. The other three experimental peak temperatures were chosen based on preliminary tests that indicated a peak temperature of approximately 38.5 ºC as a potential tipping point for *A. nodosum'*s growth performance. To capture any critical tipping performance point, which could occur at slightly lower or higher temperatures due to the broader selection of populations under test, we added the peak temperature treatments of 36.5 ºC and 40.5 ºC alongside the 38.5 ºC treatment. In summary, the experiment involved eight treatments in a 4x2 factorial design, combining four low-tide peak temperatures (28.5 ºC, 36.5 ºC, 38.5 ºC, and 40.5 ºC) with two high-tide water temperatures (15 ºC and 20.5 ºC). These eight

temperature profiles (**Fig. 5.1b**) were applied for 10 consecutive days, followed by an additional 10-day period during which all experimental conditions were set to the control treatment, allowing any delayed stress or recovery effects to manifest.

5.3.3. Experimental common-garden system

The common-garden system was composed of 16 polycarbonate 30-liter tanks (n = 2 per treatment), maintained in a water bath system to regulate water temperatures. Water bath temperature was controlled using a combination of three 500 W titanium heaters and a water chiller (TECO TR15). Room temperature was maintained at 17 ºC to reduce temperature fluctuations during nocturnal low tides. Light was kept constant at 150-175 µmol photon m^{-2} s^{-1} PAR in a 12-hour light/dark photoperiod cycle. Tide control was achieved via automatisation of valves (U.S. Solid, USA). At low tide, seawater was discarded from each tank, and at high tide, new seawater was pumped in. Separated filling system, complete water replacement during each tidal cycle, and continuous aeration ensured independent systems and prevented water deterioration effects. Low tide temperatures were controlled using two 125 W IR lamps per experimental tank, regulated by a customised Proportional-Integral-Derivative (PID) algorithm. To prevent temperature stratification during low tide, a 60 mm wide fan with 43.9 m^3 h^{-1} air flow was turned at low tides. Two temperature loggers (Lima & Wethey, 2009) were deployed inside each tank attached to granite tiles, providing temperature feedback to a microcontroller (ATMEGA2560), which coordinated all electrical functions (Seabra et al., 2016). All algae were identified with wire markers and held on the granite tile surface with an elastic fabric cord (10 individuals per population on each tank; n=20 per treatment).

5.3.4. Relative growth rates

Relative growth rates (RGR), expressed as the percentage change in fresh weight (FW) per day, (Hurd et al., 2014) were calculated on day 10 and day 20 of the experiment (n = 20 per population).

$$RGR[\%\, day^{-1}] = \frac{ln\left(\frac{N_1}{N_2}\right)}{(t_2 - t_1)} \times 100 \quad (1)$$

Where N_1 and N_2 represent the initial and final fresh weight, respectively, and t_1 and t_2 are the time points in days. Only fronds determined as whole and alive were considered in RGR results. Fragmented fronds, although they could be considered alive, were not

reliable for growth measurements. For measurement, individuals were briefly dried on paper cloth before weighing with a 0.01 g precision scale (Kern EG 220-eNM, Mechanikus Gottlieb KERN, Germany).

5.3.5. Survival

Survival was determined by chlorophyll fluorescence imaging on day 10 and day 20 of the experiment. Individuals were considered dead if their images showed no pixels with fluorescence above the background level. Chlorophyll fluorescence was measured for all individuals using a FluorCAM 800MF imaging fluorometer (Photon System Instruments, Brno, Czechia), as described by Serôdio and Campbell (2021). Images of chlorophyll fluorescence parameters (dark-level fluorescence) were captured for all seaweeds after a minimum of 20 minutes of dark adaptation, followed by a modulated measuring light and saturation pulses (< 0.1 and > 7500 µmol photons m^{-2} s^{-1}, respectively), provided by red LED panels (612 nm emission peak, 40-nm bandwidth). Images (512×512 pixels) were analysed using FluorCam7 software (Photon System Instruments, spol. s r.o., Drasov, Czechia). Areas of interest (AOIs) were defined to match the whole area of each seaweed, excluding the non-fluorescent background signal.

5.3.6. Primary productivity

Primary productivity was quantified in all treatments at day 10 and day 20 of the experiment by measuring oxygen production and respiration. Fronds (n = 6 per population) were placed in 60 ml acrylic chambers filled with filtered seawater (1 µm polypropylene filter) and kept in a water bath at the respective treatment temperature (15 ºC or 20.5 ºC) for productivity-irradiance curve analysis (P-I curves). Each chamber contained a magnetic stirring bead to ensure seawater homogenisation, separated by an acrylic mesh to avoid damaging the algae. To measure oxygen production and consumption (respiration), light intensity followed a gradient of 0 (dark), 50, 180, 330, 550, and 1000 µE m^{-2} s^{-1}. Light intensity was measured with a calibrated quantum irradiance meter (US-SQS/L, ULM-500; Waltz GmbH, Effeltrich, Germany). Light intensities were obtained from cool white LED strips (model 5032), assembled in five groups, and controlled by an ATMEGA 328p microcontroller with a 5-relay setup. Light periods started with 15 minutes of darkness, followed by sequential 10-minute steps at each light intensity. The water volume in each chamber, used for posterior oxygen rate calculations, was specific to each individual, with the frond's volume subtracted from the total chamber volume. Oxygen content was measured once per minute by an optical

fiber probe (DP-PSt7, Oxy-4 SMA, PreSens Precision Sensing GmbH, Germany). Productivity measurements were conducted in sets of eight chambers at a time, with one being a control blank chamber. Oxygen rates were calculated in μmol O^2 ww g^{-1} h^{-1} in 5-minute intervals. Dark respiration (R_d) and net primary productivity (NPP) rates were estimated as the slope of the linear regression between oxygen concentration and time. Gross photosynthesis (GP) was calculated by adding the absolute value of R_d to the NPP estimates at each light intensity. The maximum rate of gross photosynthesis at saturating light (GP_{max}) was determined by fitting the model of Eilers and Peeters (1988):

$$\mathrm{GP} = 1/[(\mathrm{E}^2/\alpha \times {\mathrm{E}_{\mathrm{opt}}}^2) + (\mathrm{E}/\mathrm{Gp}_{\max}) - (2\mathrm{E}/\alpha \times \mathrm{E}_{\mathrm{opt}}) + (1/\alpha)] \quad (2)$$

where E is irradiance, E_{opt} is the optimum irradiance, and α is photosynthetic efficiency at low irradiance. The maximum rate of net primary production (NPP_{max}) was calculated as GPmax—R_d. Model fitting was performed by non-linear regression using the Phytotools package for R (Silsbe & Malkin, 2015).

5.3.7. Statistical analysis

We used generalised linear mixed models (GLMMs; **Supplementary Table S5.2**) with a Gaussian distribution to analyse the effect of each treatment on growth and oxygen production (Zuur et al., 2009). Analyses were made separately for the results on day 10 and day 20. The best model for each parameter was found by gradual simplification of the full model until the lowest Akaike Information Criterion (AIC) was found (Burnham & Anderson, 2004). The full model included high-tide temperature (two levels: 15 ºC and 20.5 ºC), low-tide temperature (four levels: 28.5 ºC, 36.5 ºC, 38.5 ºC, and 40.5 ºC), and region (three levels: South, Center, and North) as fixed factors. The population was included as a random effect nested within the region, and the tank was included as a cross-random effect. Model normality was checked by visual inspection of Q-Q plots, and heteroscedasticity was assessed through residual plots. Random effects showed negligible contributions to the model's variance for all the models. To investigate pairwise differences between treatment groups, we used estimated marginal means (emmeans). A significance threshold of 0.05 was used for testing treatment effects. The survival rate was analysed using GLMM as well but with binomial distribution with a logit-link function. For direct analysis of survival after 10 and 20 days, the factors low- and high-tide temperatures were replaced by a continuous variable representing the temperature difference between the two (8 ºC to 26.5 ºC). While population survival models used in forecasting mortalities followed the lower AIC method described for

growth for the simplest model (**Supplementary Table S5.3**). Statistical analyses were done in R4.3.1 (R Core Team, 2023), with the lme4 (v1.1-35.1) and the emmeans (v1.8.7) (Lenth et al., 2021) packages.

5.3.8. Modelling strategy

To predict survival and population size as a consequence of the physiological responses observed here, we required temperature data for low and high tides that would be analogous to in-situ measurements. Although in-situ measurements are accurate, their availability is limited in both space and time due to substantial costs and logistical challenges involved in data collection. Additionally, these measurements are influenced by local-scale factors, making it difficult to extrapolate them to future climate scenarios. To address this limitation, we developed a model relating in-situ daily maximum temperature of intertidal rock (T_{max}) to weather model data and used it to obtain forecasts of low tide maximum temperatures from fine-scale climatic data.

5.3.9. Forecasting in-situ data

In-situ, data was obtained from autonomous temperature loggers (Envloggers, Electricblue,CRL, Portugal) deployed at the centre of the tidal range of *A. nodosum* at ten population sites for 2 years (August 2021 to October 2023). Temperature data were collected hourly at 0.1 ºC resolution (n = 2 per site). Loggers were deployed in 30-mm wide and 15- mm deep drilled holes and sealed with marine epoxy (Z-Spar™ Splash Zone Compound A-788). All sensors were facing south on ~45º angled rocks for maximum sun exposure to effectively capture the low tide maximum rock temperature.

Weather data were gathered from ERA5 reanalysis datasets (Hersbach, 2023; Muñoz-Sabater et al., 2021), produced by the European Centre for Medium-Range Weather Forecasts (ECMWF). Variables included 2 m temperature (t2m), 10 m u and v wind components (10u and 10v, respectively), total precipitation (tp), and sea surface temperature (SST). All variables were provided as hourly values with spatial resolutions of 0.1 x 0.1 arc degrees (with the exception of SST, available as a 0.25 arc degree grid). Data pre-processing involved summarising temperature to daily maximum for both in-situ loggers and ERA5 t2m ($t2m_{max}$), calculating the daily SST average (SST_{mean}), converting total precipitation from m h^{-1} to mm s^{-1} (tp_{mean}), and converting wind speed from scalar to magnitude by applying the square root of the sum of the squares of its u and v components ($wind_{mean}$). All climatic variables were accessed through Copernicus Climate Data Store (CDS), at coordinates closest to each of the ten sites (**Supplementary Table S5.4**). Environmental variables for predicting temperature were

selected based on their availability across the reanalysis and forecasted datasets (ERA5 re-analysis and CMIP6 projections) and their informative value for the model. Since violations of linear model assumptions can compromise reliable predictions, we used a Generalized Least Square (GLS) model, which provides more efficient estimates when the residuals exhibit heteroscedasticity or autocorrelation. In the GLS model, temporal dependency in the residuals was corrected using an autoregressive model (corAR1), and heteroscedasticity was addressed by applying a variance function to fix variance weights. The power of a variance covariate function was selected based on the lowest AIC. The resulting model accuracy was evaluated using the adjusted coefficient of determination (adj R2) and residual standard error (RSE).

5.3.10. Model projection

Climatic data forecasts were obtained from the Coupled Model Intercomparison Project Phase 6 (CMIP6) (Eyring et al., 2016). Data were also accessed via CDS website at coordinates closest to each of the ten sites (**Supplementary Table S5.5**). We used daily maximum near-surface air temperature, near-surface wind speed, and precipitation data from the climate model CMCC-ESM2 (Cherchi et al., 2019), and monthly sea surface temperature from UKESM1-0-LL (Sellar et al., 2019). All data were retrieved for historical and future projections for three main shared socio-economic pathways: SSP26, SSP45 and SSP85.

5.3.11. Yearly cumulative-product survival

Future survival projections were made by applying survivability linear equations obtained in this study for mortalities observed on day 20. These equations were derived for each population using water and low tide peak temperatures from the experiments as predictors (**Supplementary Table S5.3**). Since there were no deaths in the control treatments throughout the whole experiment, the mortalities observed on day 20 were considered a delayed consequence of the 10-day heat stress event.

To adapt the daily predicted T_{max} data to the 10-day survival outcomes obtained in this experiment, daily T_{max} temperatures were averaged using a 10-day moving average algorithm. This approach enabled us to project physiological outcomes over different temporal periods and scenarios (historical, SSP26, SSP45 and SSP85). Using a 10-day average prediction showed better correlation with in-situ measurements, improving correlations from 0.81 (daily) to 0.91 (10-day average) predictions. To account for stress accumulation in populations, a cumulative product approach was applied, generating a minimal survival rate per year.

Additionally, we simulated the yearly cumulative survival of all populations under two sets of future climate scenarios. The first set was used to evaluate the relative performance of different populations under the same environmental conditions, similar to a common-garden experiment. This approach allowed us to assess the potential of each population to cope with the same heat stress levels. Specifically, we simulated the fate of all populations under the projected climate of Viana do Castelo, the southernmost limit of the species, and presumably the most stressful location.

The second set of scenarios predicted the yearly cumulative survival of each population based on the specific climate conditions of their respective geographical locations. This allowed us to assess the likelihood of their survival in their own, realised climate.

5.3.12. Population size projection

Population size at 2100 was projected by an iterative stochastic process described by a first-order Markov chain (Caswell, 2001). This process covered the period from 2014 to 2100, corresponding to the start and ending of the CMIP6 SSP projections. The probabilistic matrices used in this projection were size-stage-classed, comprising five classes ranging from < 5 g to ≥ 190 g. Since our experimental data pertain only to fronds that fall into the first class (< 5 g), to project survivability of larger size classes, survival ratios relative to frond survival were assigned based on local demographic matrices (**Supplementary Table S5.6**). We used the Iberian matrix for the southern region (populations 1 to 4) and the Brittany matrix for the central region (populations 5 to 8), both developed by Araujo et al. (2014), and the Swedish demographic matrices Åberg (1992a) for the northern region (populations 9 and 10).

To model the population growth, the number of individuals n(*t*+1) was calculated by multiplying each stage-class matrix probability vector (A_t) by the yearly survival vector (S) and the previous year's number of individuals n(*t*). The resulting stochastic matrix population model can be expressed as:

$$n(t+1) = A_t \cdot S \cdot n(t) \tag{3}$$

Survival (**S**) is the product of the yearly survival rate (0 to 1) with the proportional survival vector. A limiting aspect of these demographic matrices is the reduced stochastic growth rate (λ_s) (Leslie, 1945). To balance this, we followed Åberg (1992b) approach, and scaled fertility across all classes. The scaling factor used aimed for a stable population between the years of 1850 and 2014. This was achieved by applying Equation 3 with **S** obtained

from survival modelled with CMIP6 historical data from 1850-2014. This can be seen as an optimistic perspective, assuming there has not been a notorious contraction in recent decades, thereby highlighting the importance of any negative outcome we might predict.

5.4. Results

5.4.1. Experimental heat stress simulations

After 10 days of simulated heat stress, average growth rates tended to decrease as the temperature difference between high tides and low tides increased (**Fig. 5.2**). In other words, growth appeared to be inversely proportional to the experimental daily warming rates.

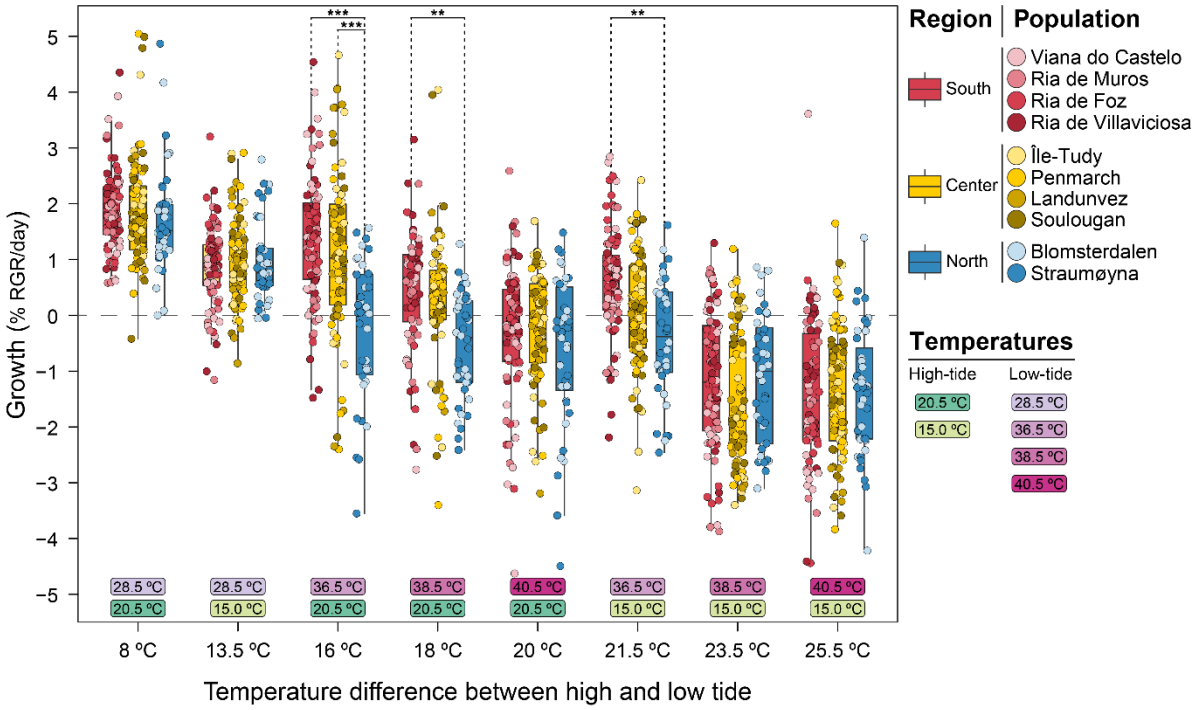


Figure 5.2: Average relative growth rate per day (% RGR day^{-1}) (mean ± SD; n = 20 per population) after ten days of thermal stress. Experimental treatments are arranged from left to right based on the absolute temperature difference between lower temperatures at high tide and peak heating temperatures at low tide. Therefore, absolute differences ranged from 8 ºC to 25.5 ºC. Experimental temperatures are represented in shades of green (high-tide temperatures) and pink (low-tide peak temperatures). Points show individual growth rates, while bars show the overall interquartile distribution for each region, color-coded as blue (north populations), yellow (center populations), and red (south populations). Statistical analysis focused only on pairwise comparisons between regions within the same treatment. Significance

In treatments with a low temperature difference between high and low tide, *A. nodosum* exhibited faster growth (e.g., an average of 1.83 ± 0.88% RGR per day in the control treatment with 8 °C temperature increase, from 20.5 °C at high tide to a maximum of 28.5 °C at low tide). Conversely, growth was inhibited in treatments with the steepest daily temperature increases (e.g., an average of -1.38 ± 1.23% RGR per day in the treatment where temperatures increased by 25.5 °C, from 15 °C at high tide to a maximum of 40.5 °C at low tide).

Generally, growth rates varied inversely with the latitude of source populations. These differences were statistically significant at intermediate temperature differences of 16 ºC ($p < .001$ for both), 18 ºC ($p < .02$), and 21.5 ºC ($p < .001$). Under these conditions, southern populations showed significantly higher growth rates compared to northern populations. At the 16 °C-increase treatment, central populations also differed significantly from their northern counterparts ($p < .001$).

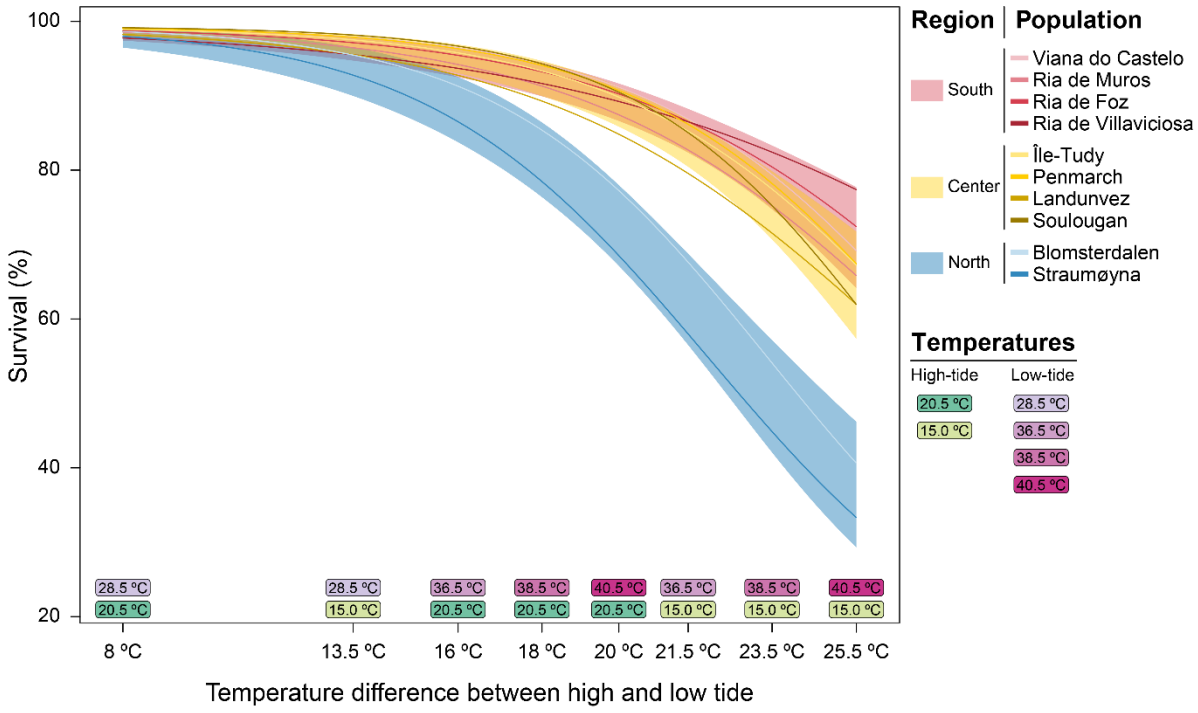


Figure 5.3: Linear model of survival rate of *A. nodosum* fronds at the end of the experiment (day 20). Treatments are arranged from left to right based on the absolute temperature difference between lower temperatures at high tide and peak heating temperatures at low tide. Treatment temperatures are represented in shades of green (high-tide temperatures) and pink (low-tide temperatures). Shaded areas show the model's regional predictions with 95% confidence intervals, and lines represent the survival of each population. Populations from the north are shown in blue, the centre in yellow, and the south in red.

By day 20 of the experiment, after the recovery period, the trend of decreasing performance from south to north persisted, particularly at intermediate temperature differences (20°C, $p < .001$ and $p < .02$; 21.5°C, $p < .05$), where differences were statistically significant (**Supplementary Fig. S5.1**). However, the inverse relationship between growth and daily warming rate, which was evident on day 10 immediately following the heat stress period, was no longer as clear. Additionally, survival rates were not evenly distributed across regions nor experimental temperatures (**Fig. 5.3**). The potential bias introduced by differential survival rates likely affected extreme temperatures and northern populations the most, followed by milder temperature increases and central and southern populations.

Survival rates, assessed immediately after the heat stress period on day 10 (**Supplementary Fig. S5.2**), were reduced across all treatments and did not differ significantly between regions. However, by the end of the experiment (day 20), survival rates were also inversely proportional to the absolute temperature difference between temperatures at high tide and the peak heating temperatures at low tide (**Fig. 5.3**). The highest mortality occurred with the highest temperature increases, and, consistent with growth rate trends, mortality was highest in algae from the northern populations. The lack of overlap confidence intervals in **Fig. 5.3** (coloured shades) indicates significant differences between those populations and the centre and south populations for treatments with temperature differences of >16 °C. At the highest temperature difference (25.5 °C), mortality rates were 68.9 ± 5.4% for the populations from the southern region, 56.3 ± 2.2% for those from the central region, and 42.5 ± 2.5% for those from the northern region (regional averages ± SD). No mortality was observed in the control treatments, regardless of the source population.

The oxygen production and respiration of *A. nodosum* (**Fig. 5.4)** shows from different regions on day 10 across a range of low-high tide temperature differences. The overall trend indicates that as the low-high tide temperature difference increases, maximum net primary production (NPP_{max}, upper portion of each coloured bar in **Fig. 5.4**) declines across all regions, with a more pronounced decline in the central and northern regions, suggesting greater sensitivity to heat stress.

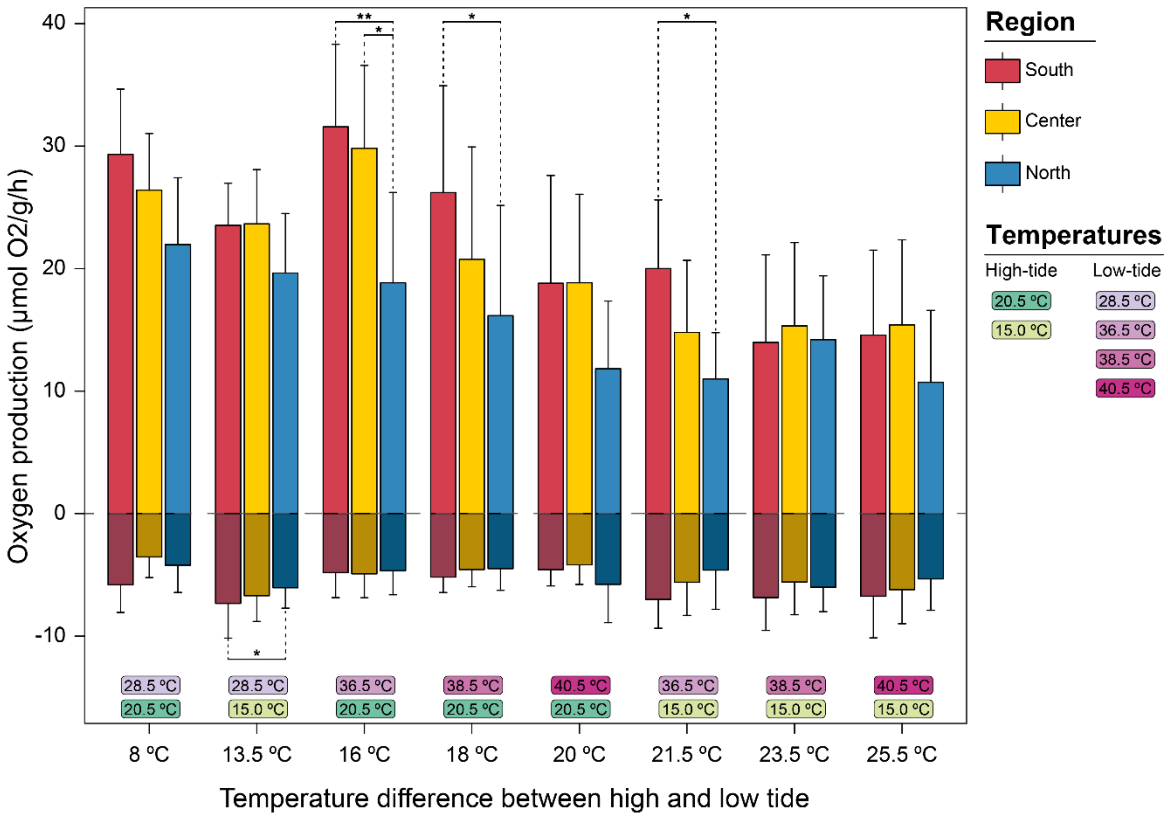


Figure 5.4: Maximum net primary production (Nppmax; µmol O2 g^{-1} h^{-1}) and maximum respiration rate (Rmax; µmol O2 g^{-1} h^{-1}) (mean + SD; n = 24 per region for south and centre; n=12 for north) after the heatwave stress (on the day 10). Regions are colour-coded as blue (north populations), yellow (centre populations), and red (south populations). Nppmax is shown as positive values, while Rmax is shown as negative values (and indicates consumption). The treatments are arranged from left to right based on the absolute temperature difference between lower temperatures at high tide and peak heating temperatures at low tide. Therefore, absolute differences ranged from 8 ºC to 25.5 ºC. Treatment temperatures are represented in shades of green (high-tide temperatures) and pink (low-tide temperatures). Statistical analysis focused only on pairwise comparisons between regions within the same treatment. Significance levels: * p < .05, ** p < .01, *** p < .001.

Regarding regional differences, NPPmax was higher in southern populations at most temperature ranges, particularly at 16 °C ($p < .001$), 18 °C, and 21.5 °C ($p < .05$ for both), where the differences from the northern population were significant. At a temperature difference of 16 °C, algae from central populations also showed significantly higher net production compared to those from the north ($p < .04$). Maximum respiration rates (R_d), indicated by the lower portion of each bar, showed some variability and a slight increase at the highest low-high tide temperature differences, but were generally lower for algae

from the north, with statistically significant differences only in the control treatment at 13.5 °C ($p < .05$).

On day 20, NPP_{max} followed a similar but less pronounced pattern (**Supplementary Fig. S5.3**). While the northern populations continued to show a tendency for lower NPP_{max}, significant differences were only found in the treatment with a warming rate of 16 °C, but only between the southern and northern populations ($p < 0.05$). R_d showed little variation and no significant regional differences in any of the treatments.

5.4.2. Population forecasts

The GLS model, designed to predict in-situ daily maximum temperatures of intertidal rock from weather data, explained 56% of the variability observed in temperature logger data between 2021 and 2023 (Pearson's correlation = 0.75, RMSE = 1.40 °C). The model showed that air t2m and SST had the strongest positive correlations with in-situ temperature readings, while wind velocity and tp were negatively correlated.

Under the same climatic conditions as those in the southernmost limit of *A. nodosum* distribution (**Fig. 5.5**, left panel), the results suggest that northern populations would be severely affected. These populations show low yearly survival rates, even in the mildest scenario (SSP26), accounting 189 years (of the 250 analysed) with reduced survivability. In contrast, central and southern populations performed much better, although they experienced increased mortality under the most severe climate scenarios (SSP45 and SSP85), particularly after the 2040s.

On the other hand, the cumulative survival rates simulated for the specific climate conditions of each population showed a markedly different outcome (**Fig. 5.5**, right panel). Populations from northern and central Europe appeared to perform relatively well, with only a slight decline in survival rates projected by the end of the century, particularly in populations 5 and 7. A similar pattern was observed for the two southernmost populations (1 and 2), which are unlikely to experience increased heat-associated mortality over the next century. However, a different trend was seen for populations 3 and 4.

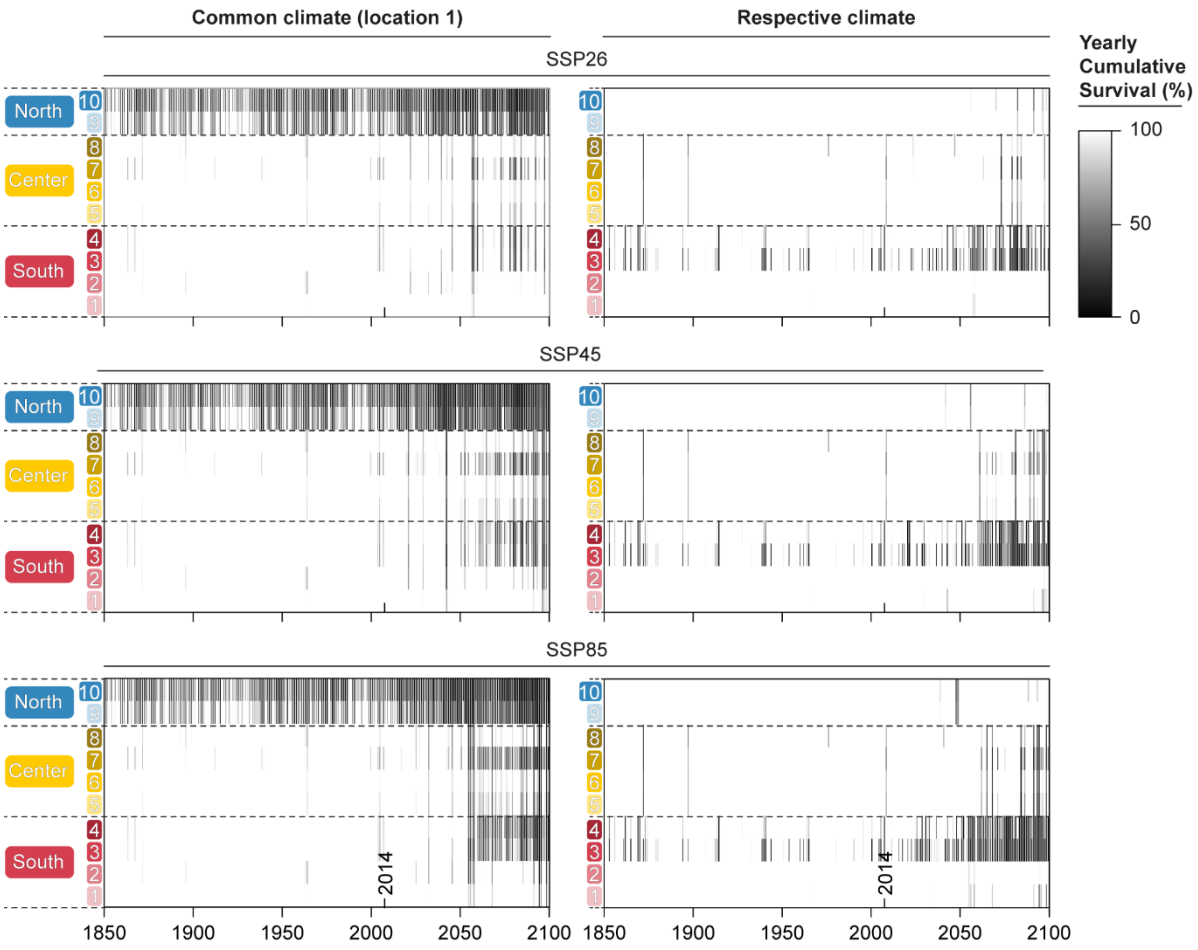


Figure 5.5: Yearly cumulative-product survival results for all ten populations from 1850 to 2100 under different SSP scenarios (SSP26, SSP45, and SSP85). The x axis represents time in yearly increments, while the vertical axis shows the regions and their respective populations. Final survival rates for each year are depicted as heatmap bars in grayscale (black represents 0% survival, and white represents 100% survival). Survival rates are reset to 100% at the beginning of each year. Plots in the left column, labelled "common climate," show survival rates based on population-specific survivability equations applied to a single common climate (in this case, the climate experienced by the southernmost population, at Viana do Castelo, population 1, Portugal). Plots in the right column, labelled "respective climates," indicate survival rates based on population-specific survivability equations applied to their own local climates.

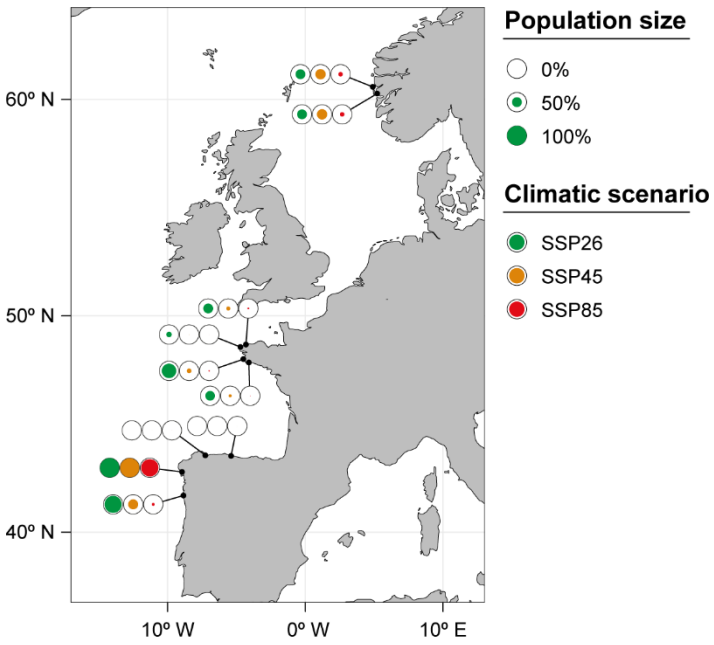


Figure 5.6: Projected population sizes for all ten populations by the end of 2100 under different SSP scenarios (SSP26, SSP45, and SSP85). Black circumferences represent the population size in 2014, while coloured filled circles indicate the expected population size in 2100, with the size of each circle proportional to the population size. Filled circles smaller than the black circumference indicate population contraction, while empty circumferences represent population extinction. Each projection considers respective climate conditions (based on CMIP6 climatic data), yearly survival rates, and regional demographic matrices. The map was created in R (R Development Core Team, 2023) using the Rnaturalearth library v1.0.0.

Projections in relative population sizes from 2014 to 2100 under three SSP scenarios (SSP26, SSP45, and SSP85) are shown in **Fig. 5.6**. This simulation assumes stable populations throughout the historical period of the CMIP6 hindcasts (1850 to 2014), meaning that if the frequency and intensity of heatwaves were to remain constant in the future (2014 to 2100), the populations would retain their 2014 sizes.

Firstly, it is observed that, for some locations, population sizes are expected to remain mostly stable. The most positive forecast is for the population of 2 (Ría de Muros) in NE Iberia, where the resilience of local individuals, combined with projected local warming, suggests that the population will likely maintain a relatively good demographic condition across all SSP scenarios. Relatively high population sizes are also expected for other locations, such as population 1 (Viana do Castelo) in NE Iberia and populations 5 (Île-Tudy), 6 (Penmarch), and 8 (Soulougan) in Brittany, but only under the mildest warming

scenario (SSP26). Significant population size reductions are predicted under the two more severe SSP scenarios in all these locations, suggesting vulnerability to extreme climate change conditions. Secondly, the two northernmost populations, 9 and 10 (Blomsterdalen and Straumøyna), exhibit intermediate and similar responses under the SSP26 and SSP45 scenarios but are also projected to be strongly affected under the SSP85 climate scenario. Thirdly, there are populations projected to face severe reductions or even extinction, irrespective of the climate scenario, emphasizing their heightened susceptibility to climate change. These include populations 3 (Ría de Foz) and 4 (Ría de Villaviciosa) in northern Iberia and population 7 (Landunvez) in northern Brittany. While a few populations may demonstrate resilience and maintain stable sizes under moderate climate change scenarios, others, particularly those in northern Iberia and Brittany, are at risk of significant decline or extinction.

5.5. Discussion

This study aimed to investigate the physiological responses of the brown seaweed *A. nodosum* to simulated intertidal heat stress across its distributional range. By replicating realistic intertidal thermal conditions, with precise control over tides, light, and daily temperatures, we were able to (i) assess the significance of upwelling events at the southern limit of the species distribution; (ii) identify thermal patterns with physiological stress; (iii) demonstrate population-specific tolerance to thermal stress; and (iv) produce long-term population forecasts throughout the European range of this species.

5.5.1. The importance of cold, upwelled waters

Our data suggest that *A. nodosum* does not directly benefit from the relatively cold waters associated with upwelling pulses at its southern distribution limit. Given its Arctic-Boreal distribution, to approximately 42° latitude in northern Portugal (Pereira et al., 2020), one could expect this species to be limited by warm waters . However, our findings indicate that *A. nodosum* performs better at all treatments with water temperatures of 20.5 °C compared to 15 °C, suggesting that, unlike other cold-water species (Wilson et al., 2015), it may grow better during upwelling relaxation. A similar conclusion was reached by Keser et al. (2005), who studied the growth of *A. nodosum* in the field at the southern distribution limit of the species in Connecticut, USA. More recently, it was demonstrated in the lab that growth increased with temperatures up to ~25 ºC, although these experiments did not include any period of aerial exposure (Hernández et al., 2023; Wilson et al., 2015)

In *A. nodosum*, as anticipated from its growth rates, productivity has also been shown to improve with increasing water temperatures up to approximately 22 °C under natural field conditions (Chock & Mathieson, 1979). Laboratory studies by Piñeiro-Corbeira et al. (2018) have demonstrated that mild increases in water temperature can enhance photosynthesis and respiration in other Fucales, although this positive effect is quickly reversed at critical temperatures between 21 °C and 22 °C. The warmest seawater temperature in our experiments (20.5 °C) remained below these thresholds, which likely accounts for the lack of observed detrimental effects of warm water on net primary productivity.

Overall, our findings may explain why the southern limit of *A. nodosum* has remained stable in northern Portugal, where sea temperatures rarely exceed 22 ºC (Seabra et al., 2011), while other cold-water species have experienced significant range contraction northwards (Casado-Amezúa et al., 2019; Lima et al., 2006). This realisation raises the question of what actually sets its distribution limit. One contributing factor may be the scarcity of suitable habitat. *A. nodosum* forms dense populations only on wave-protected to moderately protected rocky shores (Scrosati & Heaven, 2008). South of Viana do Castelo, in northern Portugal, such protected shores are rare, and the few that do exist are located deep inside river mouths or coastal lagoons. Our results, however, also point to another potential limiting factor: thermal stress resulting from the temperature difference between each consecutive high and low tide.

5.5.2. Thermal stress response from high to low tides

Given their relatively high position on the shore, many intertidal fucoids have developed physiological adaptations to cope with stressors such as increased ultraviolet radiation, elevated temperatures, and desiccation during low tide. In fact, the upper distribution limits of intertidal algae are believed to be primarily determined by their capacity to withstand and recover from low-tide emersion (Dring & Brown, 1982; Schonbeck & Norton, 1978). However, not all the effects of low tide are detrimental. As documented by Dring and Brown (1982), Nitschke et al. (2012) and Ryzhik et al. (2018), for various brown algae species, increased light exposure during emersion can enhance photosynthetic activity, at least during the initial stages of exposure.

Although important, realistic experiments involving low tides remain rare and, to our knowledge, have never been conducted with *A. nodosum*. Consequently, directly comparable data from low-tide assessments are lacking. Nonetheless, our growth control results align with previously reported optimal daily growth rates of 2% to 3%

(Fortes & Lunning, 1980). The inhibited growth observed in the treatments featuring higher low-tide temperatures was likely due to damage to the photosynthetic system caused by stress factors. This is supported by the observed decrease in oxygen production, indicating limited carbon fixation, lower ATP production, and, consequently, reduced growth (Takahashi & Murata, 2008). Additionally, this inhibition is unlikely to be due to increased metabolic costs, as this would typically result in higher respiration rates (Hurd et al., 2014), which were not observed. Instead, the results suggest an overall compromise of the photosynthetic apparatus (Eggert, 2012).

Experiments with other species also suggest that high temperatures during emersion may impair growth more severely than when seaweeds are submerged. Román et al. (2020) demonstrated that even mild low-tide heat stress can reduce growth in macroalgae far more than marine heatwaves. Similarly, experiments on *Fucus serratus* found that low-tide treatments at 34 °C had a greater impact on growth than hot water treatments at 22 °C (Martinez et al., 2012).

Although our results indicate a general decrease in performance with increasing low-tide thermal stress, this relationship was not entirely linear. The treatments in which the algae showed the poorest performance — whether measured by survivability, growth, or respiration — were not necessarily those with the highest temperature peaks. Instead, the lowest performance occurred in treatments where the algae experienced the most temperature increase, from the time when the tide receded until the temperature peak at low tide. Interestingly, similar research on a cold-adapted intertidal gastropod (*Patella vulgata*) by Seabra et al. (2016), found that heat stress over a 30-day period was directly linked to elevated water temperatures, with high air temperatures causing stress only when water temperatures were also high. Hence, one cannot assume that being repeatedly exposed to upwelling relaxation has no deleterious consequences for *A. nodosum* since longer-term effects (i.e.,> 20 days) in performance and survival remain to be tested. However, because realistic simulations of the entire tidal cycle are rarely done, connecting these findings to broader ecological implications remains challenging, and further research is needed to determine whether these patterns can be generalised to other species and geographic locations.

Nonetheless, our study underscores the importance of designing laboratory experiments that accurately simulate the complex thermal environments experienced by intertidal species. Undeniably, laboratory simulation deemed realistic can be challenging, as these require fine control of both marine and terrestrial conditions. Moreover, the technical challenges extend beyond the experimental setup to the data collection phase, as it is

crucial to gather long-term temperature data across both high and low tides at the scale of the studied organisms (Lima & Wethey, 2009). Given these complexities, it is unsurprising that many studies focus only on simulating high tide conditions, overlooking the thermal stress experienced during low tide. This approach carries the risk of overestimating the ecological niche of intertidal species. In the case of *A. nodosum*, this may help explain the large-scale discrepancies between its predicted and actual observed range reported by Hernández et al. (2023).

5.5.3. Thermal sensitivity across the species distribution

Common-garden experiments, in which different populations of a species are exposed to the same environmental conditions, are often used to determine which populations are better adapted to specific climatic conditions (Schwinning et al., 2022). In this context, our results were quite clear: across all evaluated parameters — survival, growth, and oxygen production — a consistent performance gradient emerged from northern populations performing the poorest and southern populations exhibiting the highest performance. Differences were most pronounced in the mid-range treatments, likely because, at the most benign levels, the stress was not severe enough to elicit strong responses, while at higher stress levels, organisms were already experiencing damage, regardless of their population origin (i.e., photosystem damage, oxidative stress, Allakhverdiev et al. (2008), Takahashi and Murata (2008)).

While regional differences were found in both growth and oxygen production, the most significant differences in thermal sensitivity were registered in survival rates, in agreement with other studies that compared survival and growth performance (Bennett et al., 2015; Mohring et al., 2014). Interestingly, in our experiment, most mortality did not occur immediately following heat stress but emerged later in a delayed manner. This is also in agreement with previous reports by Edwards (2004), Raymond et al. (2022), and Speare et al. (2022).

Our results have some inherent limitations that should be acknowledged. First, they do not provide insight into the mechanisms underlying the latitudinal cline in performance (King et al., 2018). Thus, we cannot distinguish between local adaptation (where natural selection causes changes in allele frequencies, leading to a shift towards local optimal traits) and phenotypic plasticity (where individuals adjust their phenotype in response to local conditions through changes in gene expression), although, within the scope of this study, this distinction is not critical. Secondly, our laboratory trials, despite efforts to closely simulate the thermal environment of the intertidal zone, cannot fully replicate the

complex natural conditions these organisms face in the wild. Field thermal stress depends on the resilience, recovery, and recolonisation traits of the affected species, along with interactions with other stressors such as eutrophication, altered currents, salinity, or modified grazing pressure (Straub et al., 2019), none of which were simulated in this study.

5.5.4. Population hindcasts, forecasts, and extinction risk

The modelled survival of populations under a hypothetical common climate reflects the results of the common-garden experiment. It indicates that northern populations, if exposed to the warmer temperatures typical of Viana do Castelo, Portugal, would have experienced frequent mortality events in the past and would likely continue to do so in the future. In contrast, central and southern populations would have remained largely unaffected in the past and would only begin to show differences starting in the mid-2040s. This suggests that while central and southern populations are adapted to the warmer conditions they have been experiencing, northern populations would struggle if exposed to those same temperatures. Such heterogeneous responses are expected in highly isolated populations. *A. nodosum* is well-known for its limited dispersal (Vadas et al., 1990), and genetic evidence indicates that southern populations may have drifted apart due to low gene flow (Olsen et al., 2010).

These patterns were substantially different when survival was simulated under each population's respective climate. Northern and central populations appear to have been well-adapted to the climates they have recently experienced. Looking ahead, northern populations show moderate declines under the milder scenarios, with slightly better performance in SSP45 than in SSP26. This aligns with other studies suggesting that mild warming may expand the ecological niche for *A. nodosum* at higher latitudes (Jueterbock et al., 2013; Westmeijer et al., 2019). Central populations, on the other hand, show moderate contractions under the SSP26 scenario but experience a sharp collapse under harsher scenarios, consistent with the partial extinction projected for Brittany by Jueterbock et al. (2013).

In the southern region, there was greater variability among populations. While population 1 is predicted to experience moderate losses under the most severe conditions, population 2 is expected to perform the best across all SSP scenarios. This may be a consequence of its geographical setting (i.e., inside a large Ría, a high-relief drowned river valley), and hints at the importance of such enclosed environments, which may buffer coastal water temperatures (Sousa et al., 2020). On the other hand, the two

remaining southern populations, 3 (Ría de Foz) and 4 (Ría de Villaviciosa), seem to have experienced frequent mortality events in the past, and these are expected to worsen rapidly within this century. This result matches recent biogeographic changes in this region, where several fucoid species have been retreating westward to the relatively cooler northwest corner of the Iberian Peninsula (Casado-Amezúa et al., 2019; Fernández, 2011). For instance, the distributions of *Fucus serratus* and *Himanthalia elongata* have contracted, respectively, by 197 km and by 330 km since the end of the 19th century in northern Spain (Duarte et al., 2013). The distribution of *A. nodosum* has similarly shifted westward. Our survey found the easternmost population of *A. nodosum*, consisting of only five individuals, in Niembru, northern Spain — approximately 218 km from Pedernales, the distribution limit documented by Fischer-Piette in the 1950s (Fischer-Piette, 1955). Furthermore, populations 3 and 4 are currently inhabited by smaller individuals that occupy only a few tens of square meters, in contrast to the other populations, which cover hundreds of square meters and consist of much larger (and seemingly healthier) individuals (L. F. Pereira, pers. observation). This scenario contradicts the general forecasts made by Jueterbock et al. (2013) and Westmeijer et al. (2019) of an overall northward contraction of the species' range at its southern limit. However, their correlative approach did not account for the importance of local ecotypes, which may explain these discrepancies.

This modelling exercise is based on several assumptions and should, therefore, be interpreted with caution. First, the model relies solely on the mortality rates observed in this study and does not account for any sub-lethal effects of heat stress. Second, converting CMIP6 projections to actual maximum temperatures in the intertidal zone relied on a correlational relationship between meteorological data and in-situ observations, with inherent uncertainties. Despite these potential limitations, the model performed extremely well during the hindcast period (1850–2014) when we simulated the yearly cumulative survival of each population under its respective observed climate. This provided an opportunity for model validation as it showed that, during the 20th century, no populations appeared to be severely impacted by heat stress except for populations 3 and 4, precisely in the region where distribution retractions have been observed.

Even if we take a cautious approach and refrain from interpreting the modelling results in absolute terms, they still offer valuable insights. They illustrate how varying sensitivities of populations across a species' range, combined with region-specific climate forecasts, can create a geographic mosaic of outcomes. Range contractions may

occur at the warm edge of the distribution, where populations, though more resilient to thermal stress, can still be overwhelmed by the rapid pace of warming. In contrast, despite being more sensitive to heat stress, northern populations may be less negatively affected by future climate.

In conclusion, this study underscores the importance of conducting realistic experiments when evaluating a species' thermal tolerance. Our findings indicate that *Ascophyllum nodosum* populations exhibit a fairly latitudinal cline in sensitivity to heat stress. By integrating empirical physiological observations with state-of-the-art climate projections, we were able to significantly refine forecasts at the population level. Our results show that future climate conditions can, in some situations, outweigh the differences in thermal stress resilience, potentially leading to uneven impacts on various populations along the species' current distribution.

5.6. Acknowledgements

This work was supported by Fundação para a Ciência e Tecnologia (FCT) through the projects ThermalBuffer (POCI-01-0145-FEDER-31088) and OceanLog (PTDC/BIA-BMA/4848/202), Blue Growth program - EEA grants BLUEFORESTING (PT-INNOVATION-0077), EU H2020 FutureMARES (contract no. 869300), and CESAM (UIDP/50017/2020 + UIDB/50017/2020 + LA/P/0094/2020), funded by national funds (OE) through FCT/MCTES. LFP received support from a FCT PhD grant (SFRH/BD/136924/2018). CM was supported through the abovementioned OceanLog and Thermalbuffe, as well as the EU H2020 project ANERIS (no. 101094924). FPL, RS, RdS and SF received support from FCT through CEECInd contracts (10.54499/CEECIND/03185/2018/CP1546/CT0004, 10.54499/CEECIND/01424/2017/CP1423/CP1645/CT0006, 10.54499/2021.03268.CEECIND/CP1668/CT0001, 10.54499/2021.02653.CEECIND/CP1659/CT0012). We want to thank Consolación Fernández for directions to populations of A. nodosum, Kjersti Sjøtun for her support in Norway, Hugo Meyer and Óscar Gómez for their help with the lab experiments, and Per Åberg and Rita Araújo for their support and sharing of unpublished demographic matrixial data.

5.7. References

Åberg, P. (1992a). A demographic study of two populations of the seaweed Ascophyllum nodosum. *Ecology*, *73*(4), 1473-1487. https://doi.org/10.2307/1940691

Åberg, P. (1992b). Size-based demography of the seaweed ascophyllum nodosum in stochastic environments. *Ecology*, *73(4)*, 1488-1501. https://doi.org/10.2307/1940692

Allakhverdiev, S. I., Kreslavski, V. D., Klimov, V. V., Los, D. A., Carpentier, R., & Mohanty, P. (2008). Heat stress: an overview of molecular responses in photosynthesis. *Photosynth Res*, *98*(1-3), 541-550. https://doi.org/10.1007/s11120-008-9331-0

Araujo, R. M., Serrao, E. A., Sousa-Pinto, I., & Åberg, P. (2014). Spatial and temporal dynamics of fucoid populations (*Ascophyllum nodosum* and *Fucus serratus*): a comparison between central and range edge populations. *PLoS One*, *9*(3), e92177. https://doi.org/10.1371/journal.pone.0092177

Benjamin, E. D., Toone, T. A., Hillman, J. R., Handley, S. J., & Jeffs, A. (2024). Aerial exposure and critical temperatures limit the survival of restored intertidal mussels. *Restoration Ecology*, *32*(4). https://doi.org/10.1111/rec.14105

Bennett, S., Wernberg, T., Arackal Joy, B., de Bettignies, T., & Campbell, A. H. (2015). Central and rear-edge populations can be equally vulnerable to warming. *Nature Communications*, *6*, 10280. https://doi.org/10.1038/ncomms10280

Brewin, R., Smale, D., Moore, P., Dall'Olmo, G., Miller, P., Taylor, B., Smyth, T., Fishwick, J., & Yang, M. (2018). Evaluating Operational AVHRR Sea Surface Temperature Data at the Coastline Using Benthic Temperature Loggers. *Remote Sensing*, *10*(6). https://doi.org/10.3390/rs10060925

Burnham, K., P., & Anderson, D., R. (2004). Multimodel inference: understanding AIC and BIC in model selection. *Sociological methods & research*, *33*(2), 261-304.

Casado-Amezúa, P., Araújo, R., Bárbara, I., Bermejo, R., Borja, Á., Díez, I., Fernández, C., Gorostiaga, J., Guinda, X., & Hernández, I. (2019). Distributional shifts of canopy-forming seaweeds from the Atlantic coast of Southern Europe. *Biodiversity and Conservation*, *28*(5), 1151-1172. https://doi.org/10.1007/s10531-019-01716-9

Castillo, K. D., & Lima, F. P. (2010). Comparison of in situ and satellite-derived (MODIS-Aqua/Terra) methods for assessing temperatures on coral reefs. *Limnology and Oceanography: Methods*, *8*(3), 107-117. https://doi.org/10.4319/lom.2010.8.0107

Caswell, H. (2001). *Matrix population models: construction, analysis, and interpretation. 2nd edn Sinauer Associates* (2 ed.).

Cherchi, A., Fogli, P. G., Lovato, T., Peano, D., Iovino, D., Gualdi, S., Masina, S., Scoccimarro, E., Materia, S., Bellucci, A., & Navarra, A. (2019). Global Mean Climate and Main Patterns of Variability in the CMCC-CM2 Coupled Model. *Journal of Advances in Modeling Earth Systems*, *11*(1), 185-209. https://doi.org/10.1029/2018MS001369

Chock, J. S., & Mathieson, A. C. (1979). Physiological ecology of Ascophyllum nodosum (L.) Le Jolis and its detached ecad scorpioides (Hornemann) Hauck (Fucales, Phaeophyta).

Choi, F., Gouhier, T., Lima, F., Rilov, G., Seabra, R., & Helmuth, B. (2019). Mapping physiology: biophysical mechanisms define scales of climate change impacts. *Conserv Physiol*, *7*(1), coz028. https://doi.org/10.1093/conphys/coz028

Coumou, D., Robinson, A., & Rahmstorf, S. (2013). Global increase in record-breaking monthly-mean temperatures. *Climatic Change*, *118*(3), 771-782. https://doi.org/10.1007/s10584-012-0668-1

David R. Schiel, M. S. F. (2013). The Population Biology of Large Brown Seaweeds: Ecological Consequences of Multiphase Life Histories in Dynamic Coastal Environments. *Annu. Rev. Ecol. Evol. Syst.*, *37*(1), 343-372. https://doi.org/10.2307/annurev.ecolsys.37.091305.30000014

Domeisen, D. I. V., Eltahir, E. A. B., Fischer, E. M., Knutti, R., Perkins-Kirkpatrick, S. E., Schär, C., Seneviratne, S. I., Weisheimer, A., & Wernli, H. (2023). Prediction and projection of heatwaves. *Nature Reviews Earth & Environment*, *4*(1), 36-50. https://doi.org/10.1038/s43017-022-00371-z

Dring, M., & Brown, F. A. (1982). Photosynthesis of Intertidal Brown Algae During and After Periods of Emersion: A Renewed Search for Physiological Causes of Zonation. *Marine Ecology-Progress Series*, *8*, 301-308. https://doi.org/10.3354/meps008301

Duarte, L., Viejo, R. M., Martínez, B., deCastro, M., Gómez-Gesteira, M., & Gallardo, T. (2013). Recent and historical range shifts of two canopy-forming seaweeds in North Spain and the link with trends in sea surface temperature. *Acta Oecologica*, *51*, 1-10. https://doi.org/10.1016/j.actao.2013.05.002

DuBois, K., Pollard, K. N., Kauffman, B. J., Williams, S. L., & Stachowicz, J. J. (2022). Local adaptation in a marine foundation species: Implications for resilience to future global change. *Global Change Biology*, *28*(8), 2596-2610. https://doi.org/10.1111/gcb.16080

Edwards, M. S. (2004). Estimating scale-dependency in disturbance impacts: El Ninos and giant kelp forests in the northeast Pacific. *Oecologia*, *138*(3), 436-447. https://doi.org/10.1007/s00442-003-1452-8

Eggert, A. (2012). Seaweed Responses to Temperature. In C. Wiencke & K. Bischof (Eds.), *Seaweed Biology: Novel Insights into Ecophysiology, Ecology and Utilization* (pp. 47-66). Springer Berlin Heidelberg. https://doi.org/10.1007/978-3-642-28451-9_3

Eilers, P. H. C., & Peeters, J. C. H. (1988). A model for the relationship between light intensity and the rate of photosynthesis in phytoplankton. *Ecological Modelling*. https://doi.org/10.1016/0304-3800(88)90057-9

Eyring, V., Bony, S., Meehl, G. A., Senior, C. A., Stevens, B., Stouffer, R. J., & Taylor, K. E. (2016). Overview of the Coupled Model Intercomparison Project Phase 6 (CMIP6) experimental design and organization. *Geoscientific Model Development*, *9*(5), 1937-1958. https://doi.org/10.5194/gmd-9-1937-2016

Fernández, C. (2011). The retreat of large brown seaweeds on the north coast of Spain: the case ofSaccorhiza polyschides. *European Journal of Phycology*, *46*(4), 352-360. https://doi.org/10.1080/09670262.2011.617840

Fischer-Piette, E. (1955). *Répartition, le long des côtes septentrionales de l'Espagne, des principales espèces peuplant les rochers intercotidaux.* (Vol. 31). Masson et Cie.

Fortes, M. D., & Lunning, K. (1980). Growth rates of North Sea macroalgae in relation to temperature, irradiance and photoperiod. https://doi.org/10.1007/BF01983538

Garrabou, J., Gomez-Gras, D., Medrano, A., Cerrano, C., Ponti, M., Schlegel, R., Bensoussan, N., Turicchia, E., Sini, M., Gerovasileiou, V., Teixido, N., Mirasole, A., Tamburello, L., Cebrian, E., Rilov, G., Ledoux, J. B., Souissi, J. B., Khamassi, F., Ghanem, R., . . . Harmelin, J. G. (2022). Marine heatwaves drive recurrent mass mortalities in the Mediterranean Sea. *Global Change Biology*, *28*(19), 5708-5725. https://doi.org/10.1111/gcb.16301

Hernández, S., García, A. G., Arenas, F., Escribano, M. P., Jueterbock, A., De Clerck, O., Maggs, C. A., Franco, J. N., & Martínez, B. D. C. (2023). Range-edge populations of seaweeds show niche unfilling and poor adaptation to increased temperatures. *Journal of Biogeography*, *50*(4), 780-791. https://doi.org/10.1111/jbi.14572

Hersbach, H., Bell, B., Berrisford, P., Biavati, G., Horányi, A., Muñoz Sabater, J., Nicolas, J., Peubey, C., Radu, R., Rozum, I., Schepers, D., Simmons, A., Soci, C., Dee, D., Thépaut, J-N. . (2023). ERA5 hourly data on single levels from 1940 to

present. *Copernicus Climate Change Service (C3S) Climate Data Store (CDS)*. https://doi.org/10.24381/cds.adbb2d47

Hesketh, A. V., & Harley, C. D. (2023). Extreme heatwave drives topography-dependent patterns of mortality in a bed-forming intertidal barnacle, with implications for associated community structure. *Global Change Biology*, *29*(1), 165-178. https://doi.org/10.1111/gcb.16390

Hobday, A. J., Alexander, L. V., Perkins, S. E., Smale, D. A., Straub, S. C., Oliver, E. C. J., Benthuysen, J. A., Burrows, M. T., Donat, M. G., Feng, M., Holbrook, N. J., Moore, P. J., Scannell, H. A., Sen Gupta, A., & Wernberg, T. (2016). A hierarchical approach to defining marine heatwaves. *Progress in Oceanography*, *141*, 227-238. https://doi.org/10.1016/j.pocean.2015.12.014

Hurd, C. L., Harrison, P. J., Bischof, K., & Lobban, C. S. (2014). *Seaweed Ecology and Physiology* (2 ed.). Cambridge University Press. https://doi.org/DOI: 10.1017/CBO9781139192637

Jueterbock, A., Tyberghein, L., Verbruggen, H., Coyer, J. A., Olsen, J. L., & Hoarau, G. (2013). Climate change impact on seaweed meadow distribution in the North Atlantic rocky intertidal. *Ecology and Evolution*, *3*(5), 1356-1373. https://doi.org/10.1002/ece3.541

Kemp, L., Xu, C., Depledge, J., Ebi, K. L., Gibbins, G., Kohler, T. A., Rockstrom, J., Scheffer, M., Schellnhuber, H. J., Steffen, W., & Lenton, T. M. (2022). Climate Endgame: Exploring catastrophic climate change scenarios. *Proceedings of the National Academy of Sciences*, *119*(34), e2108146119. https://doi.org/10.1073/pnas.2108146119

Keser, M., Swenarton, J. T., & Foertch, J. F. (2005). Effects of thermal input and climate change on growth of Ascophyllum nodosum (Fucales, Phaeophyceae) in eastern Long Island Sound (USA). *Journal of Sea Research*, *54*(3), 211-220. https://doi.org/10.1016/j.seares.2005.05.001

King, N. G., McKeown, N. J., Smale, D. A., & Moore, P. J. (2018). The importance of phenotypic plasticity and local adaptation in driving intraspecific variability in thermal niches of marine macrophytes. *Ecography*, *41*(9), 1469-1484. https://doi.org/10.1111/ecog.03186

King, N. G., McKeown, N. J., Smale, D. A., Wilcockson, D. C., Hoelters, L., Groves, E. A., Stamp, T., & Moore, P. J. (2019). Evidence for different thermal ecotypes in range centre and trailing edge kelp populations. *Journal of Experimental Marine Biology and Ecology*, *514*, 10-17. https://doi.org/10.1016/j.jembe.2019.03.004

Lathlean, J. A., Ayre, D. J., & Minchinton, T. E. (2011). Rocky intertidal temperature variability along the southeast coast of Australia: comparing data from in situ loggers, satellite-derived SST and terrestrial weather stations. *Marine Ecology Progress Series*, *439*, 83-95. https://doi.org/10.3354/meps09317

Le Nohaic, M., Ross, C. L., Cornwall, C. E., Comeau, S., Lowe, R., McCulloch, M. T., & Schoepf, V. (2017). Marine heatwave causes unprecedented regional mass bleaching of thermally resistant corals in northwestern Australia. *Scientific reports*, *7*(1), 14999. https://doi.org/10.1038/s41598-017-14794-y

Lenth, R., Singmann, H., Love, J., Buerkner, P., & Herve, M. (2021). Emmeans: Estimated marginal means, aka least-squares means (R package version 1.8. 7). *The Comprehensive R Archive Network.* . https://CRAN.R-project.org/package=emmeans

Leslie, P. H. (1945). On the use of matrices in certain population mathematics. *Biometrika*, *33*, 183-212.

Lima, F. P., Gomes, F., Seabra, R., Wethey, D. S., Seabra, M. I., Cruz, T., Santos, A. M., & Hilbish, T. J. (2016). Loss of thermal refugia near equatorial range limits. *Global Change Biology*, *22*(1), 254-263. https://doi.org/10.1111/gcb.13115

Lima, F. P., Queiroz, N., Ribeiro, P. A., Hawkins, S. J., & Santos, A. M. (2006). Recent changes in the distribution of a marine gastropod, Patella rustica Linnaeus, 1758, and their relationship to unusual climatic events. *Journal of Biogeography*, *33*(5), 812-822. https://doi.org/10.1111/j.1365-2699.2006.01457.x

Lima, F. P., & Wethey, D. S. (2009). Robolimpets: measuring intertidal body temperatures using biomimetic loggers. *Limnology and Oceanography: Methods*, *7*(5), 347-353. https://doi.org/10.4319/lom.2009.7.347

Lüning, K. (1990). Seaweeds: their environment, biogeography, and ecophysiology. *Journal of the Marine Biological Association of the United Kingdom*, *71*(1), 246-246. https://doi.org/10.1017/S0025315400037632

Martinez, B., Arenas, F., Rubal, M., Burgues, S., Esteban, R., Garcia-Plazaola, I., Figueroa, F. L., Pereira, R., Saldana, L., Sousa-Pinto, I., Trilla, A., & Viejo, R. M. (2012). Physical factors driving intertidal macroalgae distribution: physiological stress of a dominant fucoid at its southern limit. *Oecologia*, *170*(2), 341-353. https://doi.org/10.1007/s00442-012-2324-x

Meneghesso, C., Seabra, R., Broitman, B. R., Wethey, D. S., Burrows, M. T., Chan, B. K. K., Guy-Haim, T., Ribeiro, P. A., Rilov, G., Santos, A. M., Sousa, L. L., & Lima, F. P. (2020). Remotely-sensed L4 SST underestimates the thermal fingerprint of

coastal upwelling. *Remote Sensing of Environment*, *237*, 111588. https://doi.org/10.1016/j.rse.2019.111588

Mislan, K. A. S., Helmuth, B., & Wethey, D. S. (2014). Geographical variation in climatic sensitivity of intertidal mussel zonation. *Global Ecology and Biogeography*, *23*(7), 744-756. https://doi.org/10.1111/geb.12160

Mohring, M. B., Wernberg, T., Wright, J. T., Connell, S. D., & Russell, B. D. (2014). Biogeographic variation in temperature drives performance of kelp gametophytes during warming. *Marine Ecology Progress Series*, *513*, 85-96. https://doi.org/10.3354/meps10916

Monteiro, C., Pereira, J., Seabra, R., & Lima, F. P. (2022). Fine-scale survey of intertidal macroalgae reveals recent changes in a cold-water biogeographic stronghold. *Frontiers in Marine Science*, *9*. https://doi.org/10.3389/fmars.2022.880074

Muñoz-Sabater, J., Dutra, E., Agustí-Panareda, A., Albergel, C., Arduini, G., Balsamo, G., Boussetta, S., Choulga, M., Harrigan, S., & Hersbach, H. (2021). ERA5-Land: A state-of-the-art global reanalysis dataset for land applications. *Earth System Science Data*, *13*(9), 4349-4383. https://doi.org/10.5194/essd-13-4349-2021

Nitschke, U., Connan, S., & Stengel, D. B. (2012). Chlorophyll a fluorescence responses of temperate Phaeophyceae under submersion and emersion regimes: a comparison of rapid and steady-state light curves. *Photosynthesis research*, *114*, 29-42. https://doi.org/10.1007/s11120-012-9776-z

Oliver, E. C. J., Burrows, M. T., Donat, M. G., Sen Gupta, A., Alexander, L. V., Perkins-Kirkpatrick, S. E., Benthuysen, J. A., Hobday, A. J., Holbrook, N. J., Moore, P. J., Thomsen, M. S., Wernberg, T., & Smale, D. A. (2019). Projected Marine Heatwaves in the 21st Century and the Potential for Ecological Impact. *Frontiers in Marine Science*, *6*, 734. https://doi.org/10.3389/fmars.2019.00734

Olsen, J. L., Zechman, F. W., Hoarau, G., Coyer, J. A., Stam, W. T., Valero, M., & Åberg, P. (2010). The phylogeographic architecture of the fucoid seaweed Ascophyllum nodosum: an intertidal 'marine tree' and survivor of more than one glacial-interglacial cycle. *Journal of Biogeography*, *37*(5), 842-856. https://doi.org/10.1111/j.1365-2699.2009.02262.x

Pearson, G. A., Lago-Leston, A., & Mota, C. (2009). Frayed at the edges: selective pressure and adaptive response to abiotic stressors are mismatched in low diversity edge populations. *Journal of Ecology*, *97*(3), 450-462. https://doi.org/10.1111/j.1365-2745.2009.01481.x

Pereira, L., Morrison, L., Shukla, P. S., & Critchley, A. T. (2020). A concise review of the brown macroalga Ascophyllum nodosum (Linnaeus) Le Jolis. *Journal of Applied Phycology*, *32*(6), 3561-3584. https://doi.org/10.1007/s10811-020-02246-6

Piñeiro-Corbeira, C., Barreiro, R., Cremades, J., & Arenas, F. (2018). Seaweed assemblages under a climate change scenario: Functional responses to temperature of eight intertidal seaweeds match recent abundance shifts. *Scientific reports*, *8*(1), 1-9. https://doi.org/10.1038/s41598-018-31357-x

Pörtner, H.-O., Roberts, D. C., Poloczanska, E., Mintenbeck, K., Tignor, M., Alegría, A., Craig, M., Langsdorf, S., Löschke, S., & Möller, V. (2022). *IPCC, 2022: Summary for policymakers* (9291691593). (IPCC, Issue.

Potter, K. A., Arthur Woods, H., & Pincebourde, S. (2013). Microclimatic challenges in global change biology. *Global Change Biology*, *19*(10), 2932-2939. https://doi.org/10.1111/gcb.12257

Raymond, W. W., Barber, J. S., Dethier, M. N., Hayford, H. A., Harley, C. D. G., King, T. L., Paul, B., Speck, C. A., Tobin, E. D., Raymond, A. E. T., & McDonald, P. S. (2022). Assessment of the impacts of an unprecedented heatwave on intertidal shellfish of the Salish Sea. *Ecology*, *103*(10), e3798. https://doi.org/10.1002/ecy.3798

Román, M., Román, S., Vázquez, E., Troncoso, J., & Olabarria, C. (2020). Heatwaves during low tide are critical for the physiological performance of intertidal macroalgae under global warming scenarios. *Scientific reports*, *10*(1), 1-14. https://doi.org/10.1038/s41598-020-78526-5

Ryzhik, I., Kosobryukhov, A., Markovskaya, E., & Makarov, M. (2018). Physiological Parameters of Fucus vesiculosus and Fucus serratus in the Barents Sea during a Tidal Cycle: Adaptation and Tolerance to Extreme Environments. In (pp. 439-459). https://doi.org/10.1002/9781119510390.ch10

Schonbeck, M., & Norton, T. A. (1978). Factors controlling the upper limits of fucoid algae on the shore. *Journal of Experimental Marine Biology and Ecology*, *31*(3), 303-313. https://doi.org/10.1016/0022-0981(78)90065-5

Schwinning, S., Lortie, C. J., Esque, T. C., & DeFalco, L. A. (2022). What common-garden experiments tell us about climate responses in plants. In (Vol. 110, pp. 986-996): Wiley Online Library.

Scrosati, R., & Heaven, C. (2008). Trends in abundance of rocky intertidal seaweeds and filter feeders across gradients of elevation, wave exposure, and ice scour in eastern Canada. *Hydrobiologia*, *603*, 1-14. https://doi.org/10.1007/s10750-007-9160-8

Seabra, R., Wethey, D. S., Santos, A. M., Gomes, F., & Lima, F. P. (2016). Equatorial range limits of an intertidal ectotherm are more linked to water than air temperature. *Global Change Biology*, *22*(10), 3320-3331. https://doi.org/10.1111/gcb.13321

Seabra, R., Wethey, D. S., Santos, A. M., & Lima, F. P. (2011). Side matters: Microhabitat influence on intertidal heat stress over a large geographical scale. *Journal of Experimental Marine Biology and Ecology*, *400*(1-2), 200-208. https://doi.org/10.1016/j.jembe.2011.02.010

Sellar, A. A., Jones, C. G., Mulcahy, J. P., Tang, Y., Yool, A., Wiltshire, A., O'Connor, F. M., Stringer, M., Hill, R., Palmieri, J., Woodward, S., de Mora, L., Kuhlbrodt, T., Rumbold, S. T., Kelley, D. I., Ellis, R., Johnson, C. E., Walton, J., Abraham, N. L., . . . Zerroukat, M. (2019). UKESM1: Description and Evaluation of the U.K. Earth System Model. *Journal of Advances in Modeling Earth Systems*, *11*(12), 4513-4558. https://doi.org/10.1029/2019MS001739

Serôdio, J., & Campbell, D. A. (2021). Photoinhibition in optically thick samples: Effects of light attenuation on chlorophyll fluorescence-based parameters. *Journal of Theoretical Biology*, *513*, 110580. https://doi.org/10.1016/j.jtbi.2021.110580

Silsbe, G., & Malkin, S. (2015). Phytotools: phytoplankton production tools. *The Comprehensive R Archive Network.* https://cran.r-project.org/web/packages/phytotools/index.html

Smale, D. A., Thomas Wernberg, and Mathew A. Vanderklift. (2017). Regional-scale variability in the response of benthic macroinvertebrate assemblages to a marine heatwave. *Marine Ecology Progress Series*, *568*, 17-30. https://doi.org/10.3354/meps12080

Sousa, M. C., Ribeiro, A., Des, M., Gomez-Gesteira, M., deCastro, M., & Dias, J. M. (2020). NW Iberian Peninsula coastal upwelling future weakening: Competition between wind intensification and surface heating. *Science of the total environment*, *703*, 134808. https://doi.org/10.1016/j.scitotenv.2019.134808

Speare, K. E., Adam, T. C., Winslow, E. M., Lenihan, H. S., & Burkepile, D. E. (2022). Size-dependent mortality of corals during marine heatwave erodes recovery capacity of a coral reef. *Glob Chang Biol*, *28*(4), 1342-1358. https://doi.org/10.1111/gcb.16000

Straub, S. C., Wernberg, T., Thomsen, M. S., Moore, P. J., Burrows, M. T., Harvey, B. P., & Smale, D. A. (2019). Resistance, extinction, and everything in between–The diverse responses of seaweeds to marine heatwaves. *Frontiers in Marine Science*, *6*, 763. https://doi.org/10.3389/fmars.2019.00763

Strydom, S., Murray, K., Wilson, S., Huntley, B., Rule, M., Heithaus, M., Bessey, C., Kendrick, G. A., Burkholder, D., Fraser, M. W., & Zdunic, K. (2020). Too hot to handle: Unprecedented seagrass death driven by marine heatwave in a World Heritage Area. *Global Change Biology*, *26*(6), 3525-3538. https://doi.org/10.1111/gcb.15065

Takahashi, S., & Murata, N. (2008). How do environmental stresses accelerate photoinhibition? *Trends Plant Sci*, *13*(4), 178-182. https://doi.org/10.1016/j.tplants.2008.01.005

Thomsen, M., Mondardini, L., Alestra, T., Gerrity, S., Tait, L., South, P., Lilley, S., & Schiel, D. (2019). Local Extinction of Bull Kelp (Durvillaea spp.) Due to a Marine Heatwave. *Frontiers in Marine Science*, *6*, 84. https://doi.org/10.3389/fmars.2019.00084

Traiger, S. B., Bodkin, J. L., Coletti, H. A., Ballachey, B., Dean, T., Esler, D., Iken, K., Konar, B., Lindeberg, M. R., Monson, D., Robinson, B., Suryan, R. M., & Weitzman, B. P. (2022). Evidence of increased mussel abundance related to the Pacific marine heatwave and sea star wasting. *Marine Ecology*, *43*(4), e12715. https://doi.org/10.1111/maec.12715

Vadas, R., Wright, W. A., & Miller, S. L. (1990). Recruitment of Ascophyllum nodosum_ wave action as a source of mortality. *Marine Ecology-Progress Series*, *61(3)*, 263. https://doi.org/10.3354/meps061263

Westmeijer, G., Everaert, G., Pirlet, H., De Clerck, O., & Vandegehuchte, M. B. (2019). Mechanistic niche modelling to identify favorable growth sites of temperate macroalgae. *Algal Research*, *41*. https://doi.org/10.1016/j.algal.2019.101529

Wethey, D. S., & Woodin, S. A. (2008). Ecological hindcasting of biogeographic responses to climate change in the European intertidal zone. *Hydrobiologia*, *606*(1), 139-151. https://doi.org/10.1007/s10750-008-9338-8

Wilson, K., Kay, L., Schmidt, A., & Lotze, H. (2015). Effects of increasing water temperatures on survival and growth of ecologically and economically important seaweeds in Atlantic Canada: implications for climate change. *Marine Biology*, *162*. https://doi.org/10.1007/s00227-015-2769-7

Zuur, A. F., Ieno, E. N., Walker, N. J., Saveliev, A. A., & Smith, G. M. (2009). Mixed effects models and extensions in ecology with R. *574*. https://doi.org/10.1007/978-0-387-87458-6

5.8. Supplementary Figures

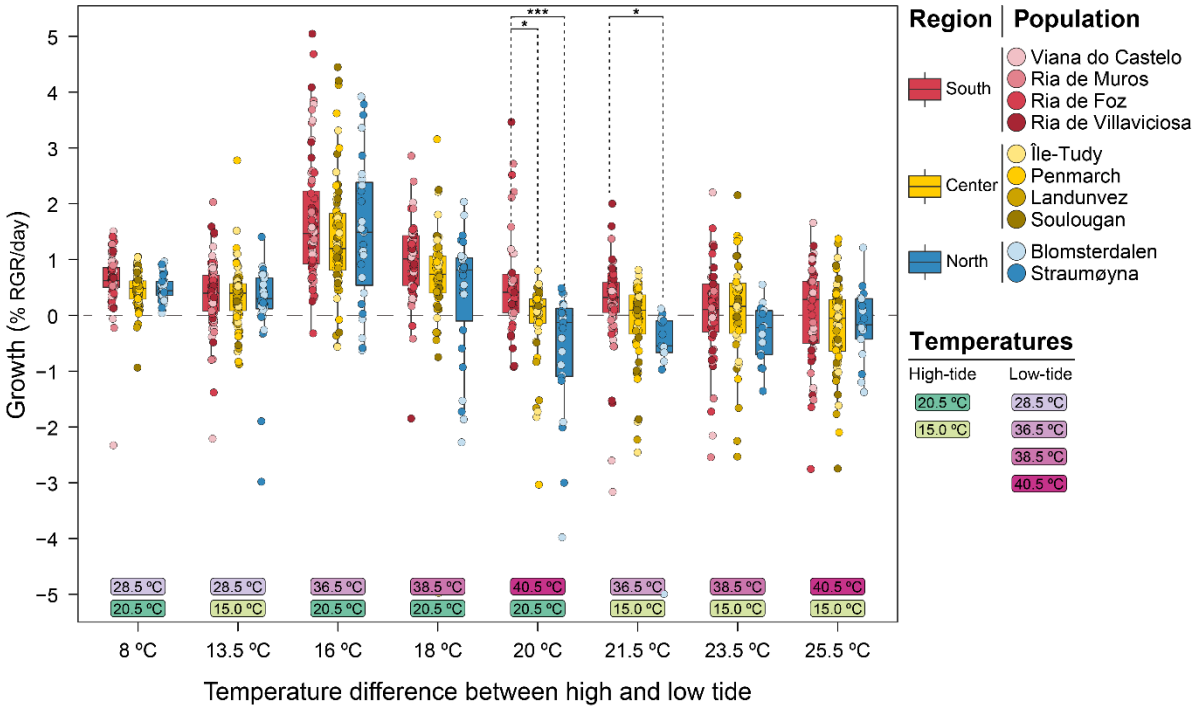


Figure S5.1: Average relative growth rate per day (% RGR day^{-1}) (mean ± SD; n = 20 per population) after the recovery period (on the day 20). The treatments are arranged from left to right based on the absolute temperature difference between lower temperatures at high tide and peak heating temperatures at low tide. Treatment temperatures are represented in shades of green (high-tide temperatures) and pink (low-tide temperatures). Points show individual growth rates, while bars show the overall interquartile distribution for each region, color-coded as blue (north populations), yellow (centre populations), and red (south populations). Statistical analysis focused only on pairwise comparisons between regions within the same treatment. Significance levels: * $p < 0.05$, ** $p < 0.01$, *** $p < 0.001$.

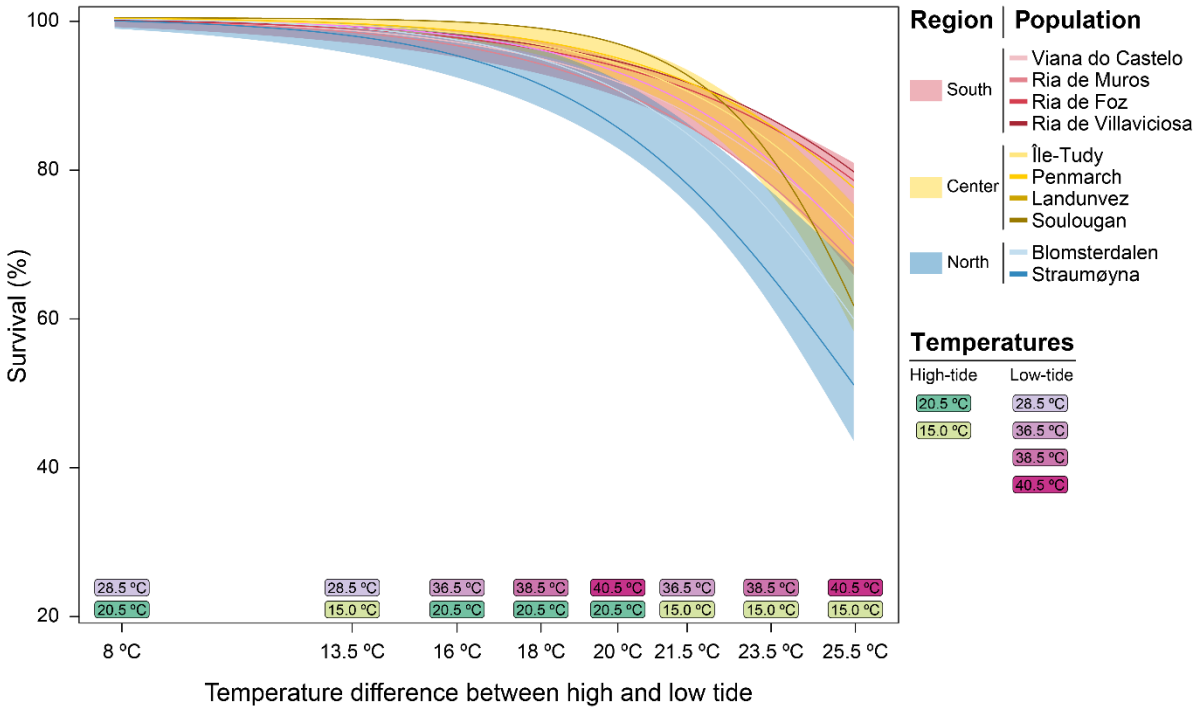


Figure S5.2: Linear model of survival rate of *A. nodosum* fronds after heat stress events (on the day 10). Treatments are arranged from left to right based on the absolute temperature difference between lower temperatures at high tide and peak heating temperatures at low tide. Treatment temperatures are represented in shades of green (high-tide temperatures) and pink (low-tide temperatures). Shaded areas show model's regional predictions with 95% confidence intervals and lines represent the survival of each population. Populations from Norway are shown in blue, France in yellow, and Iberian Peninsula in red.

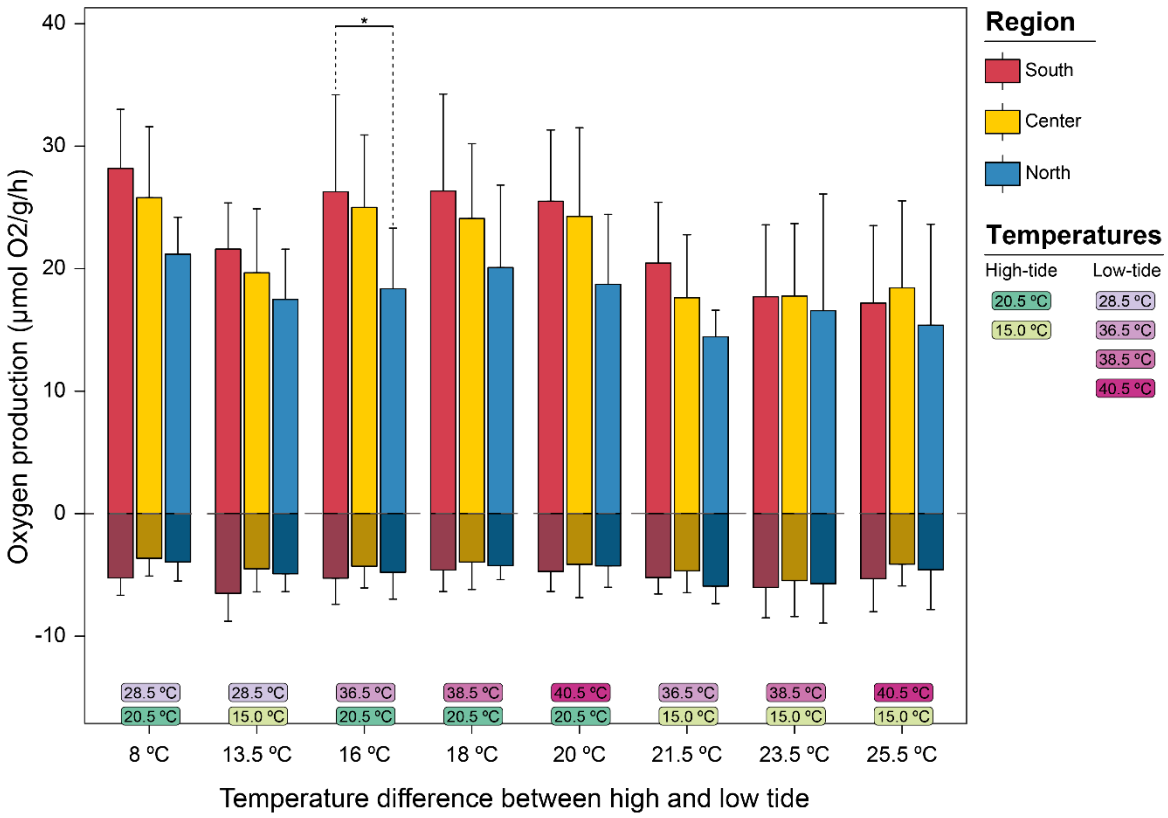


Figure S5.3: Maximum net primary production (Nppmax; µmol O2 g^{-1} h^{-1}) and maximum respiration rate (Rmax; µmol O2 g^{-1} h^{-1}) (mean + SD; n = 24 per region for South and Center; n=12 for North) after the recovery period (on the day 20). Regions are color-coded as blue (north populations), yellow (centre populations), and red (south populations). Nppmax is shown as positive values, while Rmax is shown as negative values (and indicates consumption). The treatments are arranged from left to right based on the absolute temperature difference between lower temperatures at high tide and peak heating temperatures at low tide. Treatment temperatures are represented in shades of green (high-tide temperatures) and pink (low-tide temperatures). Statistical analysis focused only on pairwise comparisons between regions within the same treatment. Significance levels: * p < .05, ** p < .01, *** p < .001.

5.9. Supplementary Tables

Table S5.1: Coordinates for the sampled populations.

Reference	Country	Location	Latitude	Longitude
1	Portugal	Viana do Castelo	41.696917	-8.851306
2	Spain	Ría de Muros	42.782500	-8.953278
3	Spain	Ría de Foz	43.550583	-7.260944
4	Spain	Ría de Villaviciosa	43.523389	-5.392167
5	France	Île-Tudy	47.839222	-4.169472
6	France	Penmarch	47.798417	-4.333472
7	France	Landunvez	48.558361	-4.715722
8	France	Soulougan	48.672389	-4.313694
9	Norway	Blomsterdalen	60.26875	5.219111
10	Norway	Straumøyna	60.582472	4.863333

Table S5.2: Summary of the results from generalized linear mixed models (GLMMs) testing the effects of low-tide temperatures (Air), hight-tide temperatures (Water), Region, Population as a nested random effect within Region (Population (Region)), Tank as cross-random effect, and their interactions for best model in each parameter. Significant effects ($p < 0.05$) are indicated in bold, while * denotes marginal significance. The models presented cover growth, net oxygen production and respiration, after the heat stress and the recovery periods.

Variable	**After heat stress**			**After recovery**		
Growth						
Best model	A x R + W x R + P(R) + T			A x W + A x R + P(R) + T		
Fixed effects	χ2	Df	p-value	χ2	Df	p-value
Air (A)	112.92	3	**<0.001**	149.05	3	**0.002**
Water (W)	37.07	1	**<0.001**	185.34	1	**<0.001**
Region (R)	19.23	2	**<0.001**	37.70	2	**<0.001**
A x W	-			90.90	3	0.076*
A x R	50.94	6	**<0.001**	13.06	6	**0.021**
W x R	21.28	4	**<0.001**	-		
A x W x R	-			-		
Random effects	Variance		Std. Dev.	Variance		Std. Dev.
Tank (T)	0.102		0.320	0.1312		0.044
Population (Region) (P(R))	0.001		0.001	0		0
Residual	1.179		1.086	0.925		0.9618

Net primary production						
Best model	A x W x R + P(R) + T			A x W x R + P(R) + T		
Fixed effects	χ2	Df	p-value	χ2	Df	p-value
Air (A)	76.950	3	**<0.001**	7.53	3	0.057*
Water (W)	65.170	1	**<0.001**	77.53	1	**<0.001**
Region (R)	16.300	2	**<0.001**	10.42	2	**0.005**
A x W	20.590	3	**<0.001**	0.29	3	0.962
A x R	14.530	6	**0.024**	7.69	6	0.262
W x R	7.910	2	**0.019**	12.24	2	**0.002**
A x W x R	12.290	6	0.055*	1.14	6	0.980
Random effects	Variance		Std. Dev.	Variance		Std. Dev.
Tank (T)	1.27		1.128	1.056		1.028
Population (Region) (P(R))	3.25		1.803	3.450		3.450
Residual	42.13		6.491	33.637		5.800
Respiration						
Best model	A x W x R + P(R) + T			A x W x R + P(R) + T		
Fixed effects	χ2	Df	p-value	χ2	Df	p-value
Air (A)	6.49	3	<0.089*	3.09	3	0.377
Water (W)	53.83	1	**<0.001**	9.80	1	**<0.001**
Region (R)	24.39	2	**<0.001**	9.49	2	**0.009**
A x W	11.84	3	**<0.001**	3.05	3	0.383
A x R	8.27	6	0.22	5.53	6	0.478
W x R	6.10	2	**0.047**	2.9	2	0.234
A x W x R	3.22	6	0.78	4.93	6	0.552
Random effects	Variance		Std. Dev.	Variance		Std. Dev.
Tank (T)	0.884		0.940	0.001		0.001
Population (Region) (P(R))	0		0	0		0
Residual	8.052		2.837	7.012		2.650

Table S5.3: Survival rate equation constants, per population. Equations followed the form "Survival rate = β_0 + β_1 LPT + β_2 SST + β_3 $Tank_R$" where LPT represents low tide peak temperature, SST represents water temperature (SST), and $Tank_R$ represents cross random effect of experimental tank. Models selected by their AIC.

Reference	Location	β_0	β_1	β_2	β_3	AIC
1	Viana do Castelo	16.731	-0.3975	1.6141	0.7429	99.50279
2	Ría de Muros	19.3459	-0.4684	1.2969	1.029	113.4228
3	Ría de Foz	19.276	-0.4588	1.0057	0.6357	101.4419
4	Ría de Villaviciosa	12.0576	-0.2702	0.5617	0.5105	109.5692
5	Île-Tudy	20.2749	-0.4902	1.1389	0.5104	104.0603
6	Penmarch	18.6274	-0.4491	1.2798	0	101.2708
7	Landunvez	21.4076	-0.5253	1.5058	0	102.4099
8	Soulougan	14.1529	-0.3434	0.9252	0	129.3407
9	Blomsterdalen	13.028	-0.339	1.753	0.102	145.6631
10	Straumøyna	12.1336	-0.3262	1.6163	0	160.0565

Table S5.4: Coordinates sampled on the ERA5 dataset. Data was accessed in January 2024.

Reference	Location	Country	ERA5 Inland Latitude	ERA5 Inland Longitude	ERA5 SST Latitude	ERA5 SST Longitude
1	Viana do Castelo	Portugal	41.94	351.25	41.70	351.15
2	Ría de Muros	Spain	42.88	351.25	42.78	350.86
3	Ría de Foz	Spain	42.88	352.50	43.66	352.84
4	Ría de Villaviciosa	Spain	42.88	355.00	43.61	354.61
5	Île-Tudy	France	48.53	356.25	47.84	355.85
6	Penmarch	France	48.53	356.25	47.87	355.62
7	Landunvez	France	48.53	356.25	48.54	355.29
8	Soulougan	France	48.53	356.25	48.67	355.68
9	Blomsterdalen	Norway	60.79	5.00	60.27	5.13
10	Straumøyna	Norway	60.79	5.00	60.58	5.04

Table S5.5: Coordinates sample on the CMIP6 dataset. Data was accessed in January 2024.

Reference	Location	Country	CMIP6 Inland Latitude	CMIP6 Inland Longitude	CMIP6 SST Latitude	CMIP6 SST Longitude
1	Viana do Castelo	Portugal	41.70	351.15	41.70	350.15
2	Ría de Muros	Spain	42.46	351.75	42.46	350.74
3	Ría de Foz	Spain	43.14	352.80	44.14	352.80
4	Ría de Villaviciosa	Spain	43.35	354.79	43.08	354.83
5	Île-Tudy	France	48.53	356.25	47.26	356.19
6	Penmarch	France	48.53	356.25	47.26	356.19
7	Landunvez	France	48.53	356.25	48.66	353.32
8	Soulougan	France	48.53	356.25	48.66	353.32
9	Blomsterdalen	Norway	60.79	5.00	60.20	5.14
10	Straumøyna	Norway	60.79	5.00	60.20	5.14

Table S5.6: Survival ratio for the five size classes relative to size class 1, and fertility inflation ratios for all populations. Survival ratio values are organized by size class (1 to 5) and represent the natural survivability of each size class compared to size class 1. The equation used to determine a size class's survival is: Survival rate = 1 - ((1 - Size class 1 survival rate / respective size class ratio). Survival ratios are derived from demographic matrixes obtained from Åberg (1992a) and Araujo et al. (2014). Fertility inflation was calculated based on the population's requirement to maintain the same size in 2014 it had in 1850, using a stochastic approach with historical CMIP6 data (1850 to 2014).

Reference	Location	Survival ratios	Fertility inflation
1	Viana do Castelo	1, 1.77, 2.19, 2.25, 2.44, 1.84	1.84
2	Ría de Muros		1.84
3	Ría de Foz		3.84
4	Ría de Villaviciosa		2.41
5	Île-Tudy	1, 2, 3.25, 3.31, 3.30, 3.1	12.66
6	Penmarch		12.59
7	Landunvez		12.82
8	Soulougan		13.05
9	Blomsterdalen	1, 1.06, 1.11, 1.13, 1.15	1.376
10	Straumøyna		1.376

Chapter 6

General discussion

The characterisation of the thermal landscapes that a species occupies is key to understand its current and future distribution patterns. Historically, the numerous difficulties of accurately recording environmental conditions and then using that knowledge to simulate realistic conditions in the lab have hindered efforts to accurately evaluate species' physiological limits. This limitation becomes critical when studying species with broad geographic ranges, as they often occur in a wide range of environments and exhibit substantial intra-specific differences that are easily overlooked in large-scale predictive models. However, the correct characterisation of population-specific thermal limits holds significant potential for refining predictions. This thesis focuses on the development of novel tools that make it possible to collect fine-scale temperature data and integrate it with innovative approaches to assess species' heat tolerances and explore how population-specific sensitivities shape species' responses to climate change.

6.1. Developments in assessing and replicating intertidal heat stress

In **Chapter 2**, I assessed the performance of various temperature loggers. While these generally performed well in recording the intertidal thermal environment, I found that specific device features and deployment methods can maximise precision and address logistical challenges. For instance, the colour of surface-deployed loggers and the sampling rates used can greatly influence the accuracy of capturing daily thermal profiles. This is particularly critical when determining daily maximum temperatures, as insufficient sampling rates alone could lead to underestimations of up to 5 ºC — an error that often exceeds the natural variability within each microhabitat (Seabra et al., 2011) — and can exacerbate errors in assessing thermal stress experienced across different latitudes and seasons. Furthermore, temperature biases resulting from different deployment methods and sampling rates were most pronounced during emersion periods, which can lead to bias interpretations of thermal stress across intertidal levels, with implications for understanding ecological dynamics.

In this context, the improved resilience and memory storage capacity provided by the EnvLogger T7.3, coupled with the newly described deployment method involving embedding the logger into the rock substrate, provides a reliable alternative for capturing thermal profiles in intertidal rocky environments while offering numerous logistical advantages that enhance the cost-effectiveness of environmental monitoring networks.

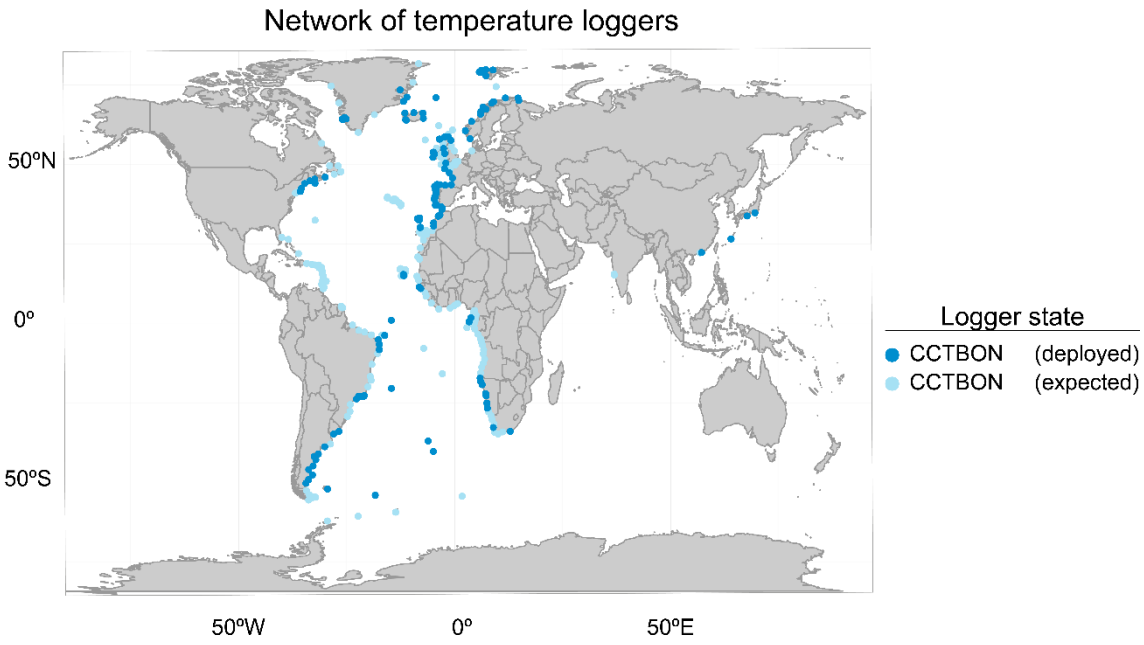


Figure 6.1: Current temperature logger deployment in global scale networks; Dark and light blue dots represent deployed and expected CCTBON temperature loggers respectively (225 deployed out of 412 total).

This combination of rugged logger design and rock-embedding deployment is already enabling unprecedently large networks of temperature loggers to be put in place, as is the case of the CCTBON network, with its more than 220 currently active sites (out of a target of 412; **Fig. 6.1**; Reese (2023)). Since at each CCTBON site, at least ten EnvLogger v7.3 have been deployed, using the methodology tested in this thesis, this amounts to more than 2200 temperature loggers actively collecting data from rocky shores as far apart as the Patagonian Argentina and Svalbard, in the Arctic. Crucially, the first assessment of the rate of logger losses seems to confirm the adequacy of this logger-deployment combination for very long-term monitoring applications. This is crucial because CCTBON aims to study the link between temperature and biodiversity patterns within the context of ongoing global warming, which can only be achieved at global and decadal scales.

In addition to the previously discussed technical and logistical advantages, the use of rock surface temperature as reference for designing laboratory experiments, provides a standardised approach to accurately replicate realistic thermal profiles without being constrained by species-specific methods (e.g., biomimetic loggers). Still, this approach is only valid if the organism's interaction with the rock surface is similar between field and laboratory conditions. Admittedly, for intertidal organisms that are in direct contact with

the rock surface (e.g., seaweed juvenile fronds: Román et al. (2020); limpets: Seabra et al. (2016)), meeting this requirement is relatively straightforward. However, for organisms associated with other substrates (e.g., sandy tidal flats: Román et al. (2023)) or inhabiting complex microhabitats (e.g., dense seaweed canopies: Scrosati and Ellrich (2018)), accurately replicating field conditions in laboratory settings poses significant technical challenges (e.g., maintaining large sand beds or seaweed assemblages). To surpass this, studies can adapt the thermal collection method to capture a field setup that can be replicated in the laboratory. For example, this could involve measuring temperature within the canopy in the field and using only a representative sub-sample of the canopy in the laboratory.

Independently of the target species, accurately replicating field conditions in the laboratory to study the impact of temperature on the physiological performance of intertidal species poses significant technical challenges. These difficulties are primarily linked to replicating tidal cycles and achieving precise temperature control during low tide. This has often led to the oversimplification of experimental conditions — compromising the ecological relevance of findings (Hernández et al., 2023; Jueterbock et al., 2014) — or the development of custom-built systems that are too complex to replicate (Fernández et al., 2015; Ferreira et al., 2014). To tackle these issues, in **Chapter 3** I developed the Intertidal Environmental Chamber, a modular system that provides a standardized and accessible framework for realistic and repeatable simulations of intertidal conditions. This system allows researchers with minimal technical expertise to conduct ecologically relevant experiments without compromising accuracy. Ultimately, it was only through the integration of the technological tools developed in this thesis that it became possible to perform the realistic experiment necessary to uncover the thermal stress experienced by the four key habitat-forming macrophyte species: *Fucus serratus*, *Fucus spiralis*, *Ascophyllum nodosum*, and *Pelvetia canaliculata*.

6.2. Impact of heat stress on intertidal species

The laboratory experiment conducted in **Chapter 4** corroborated the correlation between tidal level and stress tolerance, with species inhabiting lower in the shore exhibiting lower physiological tolerance to emersion stress. These results not only align with the already well-established theory for intertidal species' lower tolerance to heat during emersion (Dorgelo, 1976; Zaneveld, 1937; Zaneveld, 1969), but also provide greater resolution to the thermal thresholds of these species. While the methodologies

developed in this thesis facilitated the execution and replicability of intertidal thermal stress experiments, various studies had already performed laboratory experiments encompassing high and low tide periods on all four macrophyte species (Fernández et al., 2015; Harker et al., 2010; Nitschke et al., 2012). Still, the technical challenges involved in accurately controlling both marine and terrestrial stressors have led to oversimplifications, potentially limiting the conclusions of those studies. This has become evident in various incongruences in reports of the physiological tolerance of *Fucus* spp. to sudden emersion exposure. For example, Pearson et al. (2009) reported that immediate emersion of *F. serratus* at 25 – 29 ºC (from water temperature at 18 ºC) for three hours caused severe, irrecoverable damage to photosynthetic performance (*Fv/Fm*) while also indicating that those temperatures did occur in the field at *F. serratus*' zone (13 occurrences in a single summer >28 ºC, similar to the eight observed in **Chapter 4** - **Fig. 4.3**). Similarly, Ferreira et al. (2014) found *F. spiralis* struggling to recover from exposure to an air temperature of 32 ºC (for 75 min; and partial mortality after 90 min of exposure) — conditions that not only appeared tolerable in my experiment, but also occurred frequently at the species tidal level. Beyond unrealistic emersion profiles, the complete overlooking of emersion during heat stress experiments has also led to intriguing ecological projections for *A. nodosum*, suggesting that its suitable habitat could extend as far south as the rocky shores of Morocco, even under the most severe climatic projections (SSP85; Hernández et al. (2023)), well beyond its current or the historical distribution range. While these comparisons appear informative, they are not perfectly aligned, as experimental methodologies often differ substantially. For instance, Ferreira et al. (2014) conducted experiments outdoors, which adds realistic solar radiation, and Hernández et al. (2023) experiments lasted twice as long as mines (42 vs 20 days).

The decision to concentrate the experiments on evaluating thermal stress in various populations of *A. nodosum* (**Chapter 5**) rather than *Fucus spp*. or *P. canaliculata* was driven by three key factors. Firstly, the intertidal zone inhabited by *A. nodosum* was particularly well-suited for the realistic experiments envisioned here. Its relatively high exposure to emersion conditions broadens the range of intertidal temperatures differing across its extensive latitudinal span, potentially harbouring contrasting thermal tolerances among populations. Secondly, the findings in **Chapter 4** suggested some susceptibility to emersion stress within the tested temperatures, which was not as apparent in *P. canaliculata*. Thus, opting for *P. canaliculata* would risk necessitating further preliminary experiments to assess its physiological thresholds. Notwithstanding, realistic tidal experiments on *P. canaliculata* could greatly benefit our current

understanding over the factors limiting its geographic distribution, especially as SST alone did not explain its presence on the Cantabrian Sea, where SST can reach 20 ºC, and absence in central Portugal (Monteiro et al., 2022), where colder summer temperatures prevail (Neiva et al., 2014). Thirdly, *Fucus spp*. are known for extensive hybridisation among sister species, involving parental pairs in which one is a hermaphrodite (e.g., *F. spiralis*, F. *distichus*, *F. evanescens*), and the other is dioecious (e.g., *F. serratus*, *F. vesiculosus*) (Coyer et al., 2007; Hatchett et al., 2022). Although hybrids between *F. serratus* and *F. spiralis* have not been reported, and the crossing *F. serratus x F. distichus* is unlikely to be found in the Iberian Peninsula as *F. distichus* is not found there (Neiva et al., 2016), crossed exemplars of *F. spiralis vs F. vesiculosus* are possible (Billard et al., 2010). Additionally, *F. spiralis* in northern Iberia presents two potentially distinct genetic identities, occupying a partially separated vertical range (*F. spiralis*-High and *F. spiralis*-Low), where *F. spiralis*-Low was also commonly referred to as *F. guiryi* or *F. spiralis* var *platycarpus*, and more recently referred as *F. macroguiryi* (Almeida et al., 2022). Although these species are reported to be separated in the shore (~1 meter on vertical range; Almeida et al. (2022)) and the fronds sampled in **Chapter 4** were close to their highest distribution, the still potentially extensive gene flow across these individuals creates uncertainty about the presence of both species and their hybrids at *F. spiralis* high shore level. These hybridisations, while potentially advantageous for adaptation, would greatly complicate the interpretation of results from the cross-populational thermal stress experiments.

The ecological consequences of miscalculating the realistic thermal stress experienced at different intertidal levels may vary across the vertical range, especially since environmental stress models for benthic species suggest that biodiversity declines toward the upper intertidal zones (Bruno et al., 2003; Scrosati et al., 2011). Field surveys on *F. serratus* canopies, for example, have documented hundreds (to thousands) of associated epifaunal species (Christie et al., 2009; Fredriksen et al., 2005) — a richness that far exceeds that observed in mid-to-high shore *Fucales* canopies, such as those of *F. spiralis* and *A. nodosum*. Notably, the diversity and abundance of these species are more strongly correlated with the vertical shore level being analysed rather than the canopy-forming species itself (Colman, 1940; Dunstone et al., 1979; Pereira et al., 2020). At the highest shore levels, *P. canaliculata* is typically associated with a few other macroscopic species, dominated primarily by amphipods, *Littorina*, and mussels (Dunstone et al., 1979; Lalegerie & Stengel, 2022). However, it is precisely at these higher intertidal levels that the thermal buffering provided by algal canopies becomes most critical for the survival of understory species (Umanzor et al., 2019; Watt & Scrosati,

2013). Although this thesis cannot indicate which species loss would have greater impact on the ecological community, it highlights that misjudging emersion stress can have complex ecological implications, influencing not only our ability to interpret species distributions and interactions within the intertidal zone but also the accuracy of models predicting biodiversity patterns across the vertical gradient.

6.3. Heat stress on *Ascophyllum nodosum*

The southern distribution limit of *A. nodosum* is thought to be primarily constrained by summer temperatures (Lüning, 1990). Notably, the thermal pattern that emerges from the upwelling of cold waters off northern Portugal and the warmer conditions in the Bay of Biscay align closely with the distribution of various cold-water species (Ardré, 1970; Fischer-Piette, 1963). However, until now, technical challenges have made the execution of laboratory experiments with enough detail and precision to test the thermal thresholds behind species distribution too complex to implement. For instance, and in agreement with results in C**hapter 5**, *A. nodosum*'s growth and productivity have been recurrently reported to benefit from warmer temperatures (Hernández et al., 2023; Wilson et al., 2015), a finding that challenges the generalisation that increased SST is the main driver behind this species' range contraction observed in northern Spain (Casado-Amezúa et al., 2019). By incorporating tidal cycles and realistic emersion exposure conditions into laboratory simulations, the results in **Chapter 5** suggest that thermal stress experienced by *A. nodosum* may correlate not only with emersion temperatures but also with the temperature difference experienced during consecutive tides.

Foundational theory on ectothermic species suggests they are particularly sensitive to daily temperature fluctuations, as these can be more metabolic demanding than stable temperature conditions (Kern et al., 2015; Paaijmans et al., 2013). Additionally, species' thermal limits show a time-intensity relationship, where shorter, more intense temperature contrasts can decrease the critical temperature maxima (Rezende et al., 2011). Expectedly, this is especially pertinent for intertidal species, which are regularly subjected to substantial temperature variations between tidal cycles (Vafeiadou et al., 2018; Vajedsamiei et al., 2021).

Although not studied in this thesis, quantifying the expression of heat-shock protein (HSP) is a valuable proxy for assessing thermal stress in other experiments. HSP levels typically rise initially as part of the organism's response to mitigate protein degradation (Collins et al., 2023). However, these abruptly decline when the organism becomes overwhelmed and cannot counteract the escalating thermal stress (Jeyachandran et al.,

2023). While HSPs have been recurrently reported for macrophytes to support thermal tolerance (Henkel & Hofmann, 2008; Jueterbock et al., 2014; King et al., 2019), there is generally no direct association with heating rates — but rather abrupt temperature changes. However, complementary thermal stress studies on *F. vesiculosus* have suggested an HSP rapid depression could happen at 32 ºC when transitioning from 10 ºC control treatments (22 ºC temperature difference Mota et al. (2018)) or at 36 ºC when transitioning from 15 ºC (21 ºC temperature difference, Mota et al. (2014)). While these studies recognise these temperature shocks to be well beyond what the species could experience naturally during high tide periods, that is not true when considering both high and low tide periods. This was evident in the temperature data presented in **Chapters 4** and **5**, where temperatures often exceed 25.5 ºC. Therefore, more than peak temperatures, *A. nodosum's* response to temperature change is likely related to natural limitations to maintain the required physiological response to broad temperature ranges, as main damage mitigators like HSP expression can begin to fail at sustaining overall protein structure and functionality. However, most studies do not consider the impact of peak temperatures vs temperature changes, and different mechanistic studies rarely complement each other's results properly, as these usually employ different experimental temperatures, heat stress durations, and acclimatisation conditions. In contrast, experiments on intertidal animals have historically been more contemplating of the complexity of thermal stress throughout the tidal cycle (Pincebourde et al., 2008; Seabra et al., 2016; Yamane & Gilman, 2009). For instance, a study on the intertidal copepod *Tigriopus californicus* showed that gradual (and more realistic) heat increase promotes greater HSP expression and survivability than abrupt heat contrasts (Harada & Burton, 2019).

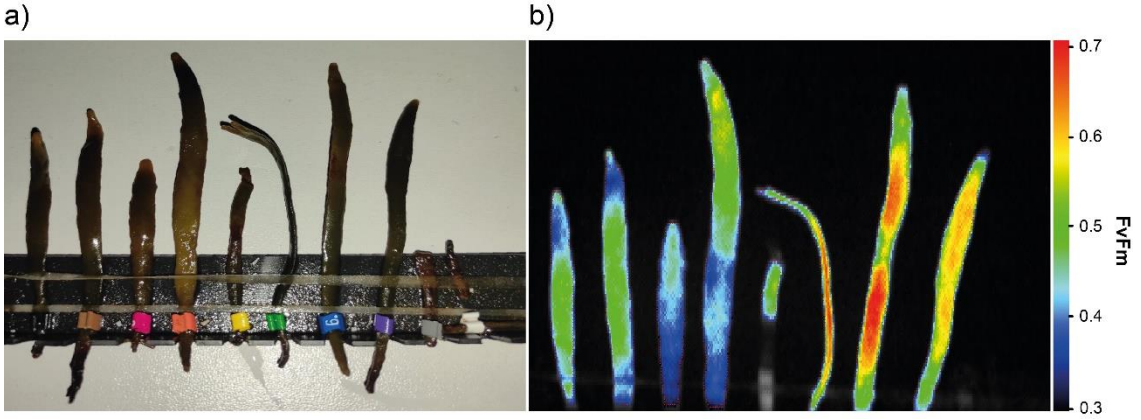


Figure 6.2: a) Set of ten *A. nodosum* fronds from 25.5 ºC in **Chapter 5** temperature difference treatment after 20 days, distributed and marked according to each population (cable tags numbered 0 to 9, from left to right); b) *Fv/Fm* ratio picture of the same set of fronds, displaying variation within South and Centre populations but no detection of any chlorophyll-a fluorescence in the northern populations (two fronds at the right).

In this thesis, photosynthetic performance (*Fv/Fm*) proved to have surprisingly limited informative value in assessing the response of *A. nodosum* to thermal stress. In fact, *A. nodosum* was observed to be species with the most stable *Fv/Fm*, varying just 4 % between treatments (0.67 to 0.70 FvFm; **Chapter 4** - **Fig. 4.4c, d**), considerably less than the other species (>8 %) — which is still comparably lower than the 50-80 % range regularly reported on other studies (Fernández et al., 2015; Ferreira et al., 2014). However, these studies usually access chlorophyll fluorescence via optic Fiber PAM devices (MiniPAM or Water-PAM devices), which can be far more susceptible to the heterogenous photosynthetic damage across the algae that an imaging fluorometer (**Fig.6.2a, b**). Hence, in **Chapter 5** *Fv/Fm* was used as proxy of survival rather than for performance. Notably, the *Fv/Fm* ratio in *A. nodosum* has been described to be more stable than in other fucoids (Kim & Garbary, 2009), and most comparative stress experiments generally fail to report significant *Fv/Fm* changes in *A. nodosum* (Garbary et al., 2014; Olabarria et al., 2018; Sanz-Martín et al., 2019). A possible reason might be the individual's morphology, as PAM techniques primarily capture fluorescence from the outermost cell layers (Lichtenthaler et al., 2005), leading to the mischaracterisation of thick-leaved specimens (Nielsen & Nielsen, 2008).

6.4. The future of *Ascophyllum nodosum*

In **Chapter 5** I found that the thermal tolerance of *A. nodosum* to vary across populations. However, this does not appear to be the primary factor shaping its future. Instead, the populations' future depended mostly on the local climatic forecast for the main performance driver — temperature difference between low and high tide. By integrating fine-scale temperature data with climatic projection models, I found this driver to show a latitudinal gradient (**Fig. 6.3a-d**), but more importantly, to promote differences between southern populations in the NW and NE Iberian Peninsula (**Fig. 6.3a, b**).

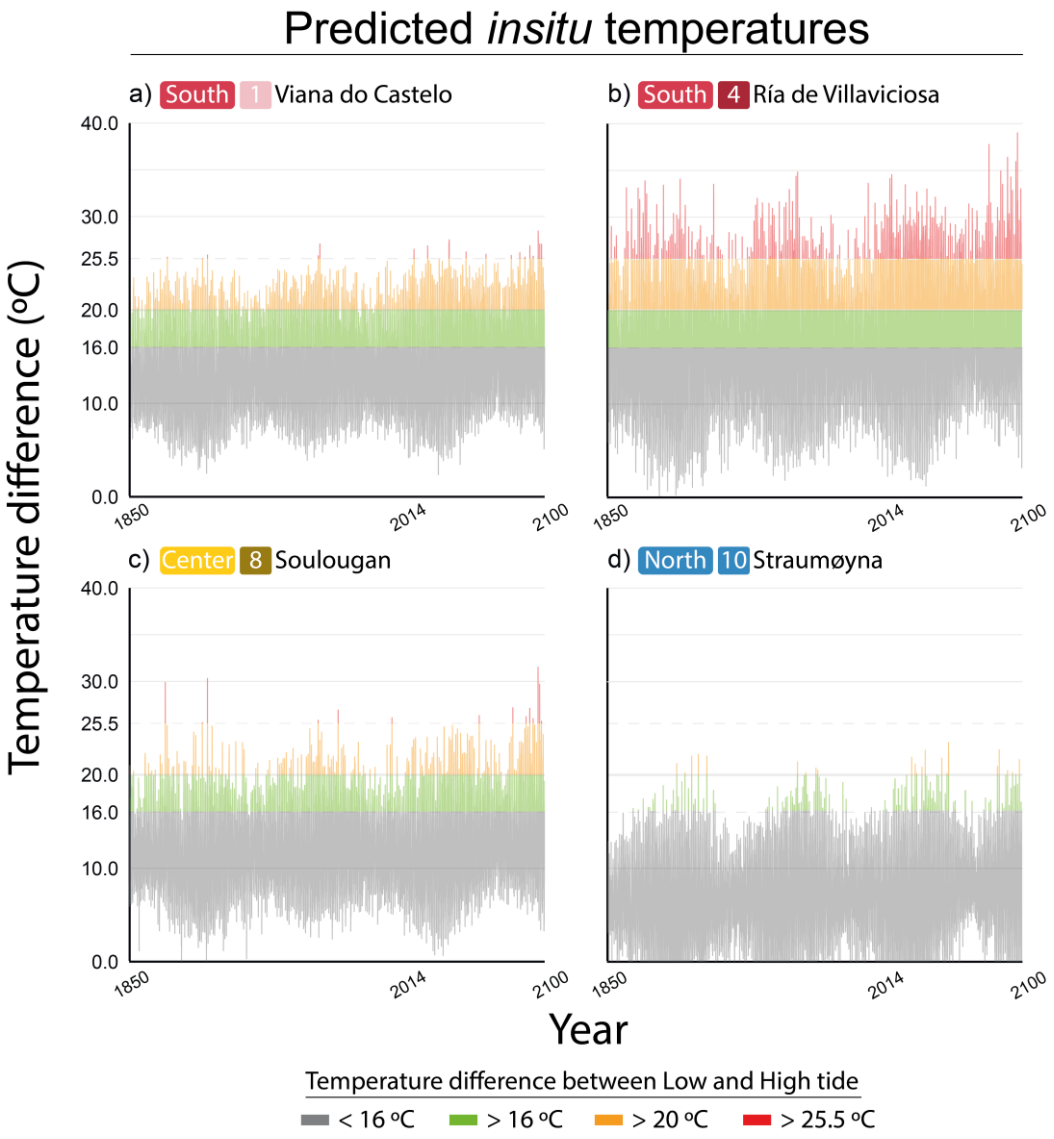


Figure 6.3: Predicted in-situ temperature difference data according to SSP45 at four populations; Lines are coloured according to three temperature differences tested in **Chapter 5** (grey for < 16 ºC, green for >16 ºC, yellow for >20 ºC and red > 25.5 ºC); a) Population 1, Viana do Castelo (Portugal); b) Population 2, Ría de Villaviciosa (Spain); c) Population 8, Soulougan (France) and d) Population 10, Straumøyna (Norway).

Various studies have suggested that the coast of northern Spain is experiencing a steady SST increase and that population shifts match the coastal macroalgae (Chefaoui et al., 2024; Izquierdo et al., 2022). However, the impact of emersion periods on species distribution has received far less attention than sea SST, even though marine heatwaves are often linked to persistent atmospheric highs (Capotondi et al., 2024). More importantly, this thesis showed that the typically hypothesised heat-tolerant populations at the southern edge can still be overwhelmed by future climate, corroborating the physiological responses observed here and the range contraction already observed (218 km westward since the 1950s (Fischer-Piette, 1955)). Notably, the populations sampled in NE Iberian Peninsula during this thesis exhibited signs of stress and decline, characterised by reduced individual size of 29.7 cm average length compared to the 49.9 cm in the NW Iberian Peninsula populations.

Despite the population projections for *A. nodosum* indicating a localised extinction at the southern distribution edge, its overall distribution will ultimately depend on more than its current (and regional) thermal thresholds. The capacity of a species to mitigate extinction risk under climate change hinges on its ability to adapt through three key mechanisms: 1) distributional range shifts (moving to habitats with more favourable thermal conditions), 2) genetic adaptation (involving the positive selection of alleles that enhance thermal tolerance) and 3) phenotypic plasticity (gaining increased resilience to thermal stress via acclimatisation) (Somero, 2010; Straub et al., 2019).

The geographical distribution of *A. nodosum* is largely attributed to its rafting capabilities, facilitated by its air bladders, which enable fragments to float for up to 45 weeks and cross vast distances (Pereira et al., 2020; Vandendriessche et al., 2007). For example, photographic records on GBIF and iNaturalist document *A. nodosum* drift fragments reaching the Madeira archipelago, located 1220 km from the nearest population in Viana do Castelo (Portugal GBIF (2024)). Rafting may be its primary dispersal mechanism and should be particularly relevant to the upcoming colonisation of higher latitudes (Jueterbock et al., 2013; Westmeijer et al., 2019). In contrast, dispersal through reproduction is highly inefficient, as fertilised zygotes lack buoyancy and typically settle within 8 meters of their parental source (Dudgeon et al., 2001).

The success of genetic adaptation depends on two paths: a severe selection over its current genetic diversity or its ability to rapidly accumulate beneficial mutations into the population — typically observed in species with short generations (O'Brien et al., 2022), like sea snails (*Littorina saxatilis*), guppies (*Poecilia reticulata*) and fruit flies (*Drosophila*

melanogaster) (Daborn et al., 2002; Garcia Castillo et al., 2024; Reznick et al., 1997). In both scenarios, *A. nodosum* does not present the greatest adaptation potential. Although this thesis did not contemplate genetic analysis, it did establish a collaboration with other teams to assess its genetic diversity and structure. Samples from all three regions (Iberian Peninsula, Brittany, and Norway) were analysed by the Genotyping-by-Sequencing approach, identifying Single Nucleotide Polymorphism (SNPs) markers that could hint at population genetic structure. The results suggested a low genetic diversity in the Iberian populations compared to the central and northern regions (Ledoux, 2024). These results agree with the genetic drift reported for the Iberian populations (Olsen et al., 2010) and match the general assertion that peripheral populations exhibit low genetic diversity. This is typically consequence of low effective population size and the effects of genetic drift — consequent of a reduced gene flow between populations (Eckert et al., 2008; Liesner et al., 2020; Maneiro Estraviz et al., 2011).

Rapid adaptation is just as unlikely as its generation time is long. It can take up to five years to start developing fertile plants (Pereira et al., 2020), even longer than *Fucus* spp. and *P. canaliculata,* which usually take about two years (De Wreede & Klinger, 1988; Lalegerie & Stengel, 2022). Additionally, their long lifespan (up to 60 years vs 5-10 years for *Fucus* spp. and *P. canaliculata*) can harm population adaptation, as it extends the genetic influence of less-fit individuals over new offspring.

On the other hand, phenotypic plasticity is perhaps the most recognised factor driving divergent responses in macroalgae, particularly to seasonal variation (Andrews et al., 2014; Collén & Davidson, 2001; Schmid et al., 2021), leading to increased thermal tolerance in summer (Gauci et al., 2022; Lüning, 1984). Despite having collected *A. nodosum* fronds from Viana do Castelo (southernmost population) in different seasons (winter for Chapter 4 and summer for Chapter 5), survival and growth did not differ substantially between both experiments. However, tidal cycles differed between these two experiments (4 h emersion in Chapter 4 and 5 h in Chapter 5), hampering a clear comparison, as heat stress and desiccation could have differed. Although this is typically perceived as a temporary and limited coping mechanism (Murren et al., 2015), it can benefit future generations. While rarely demonstrated, transgenerational plasticity is possible, as not all adjustments are reset in subsequent generations. Demonstrating this, however, requires multiple thermal experiments throughout several generations, hardly feasible for most studies. As a result, most evidence for transgenerational plasticity comes from short-lived organisms, such as fruit flies (*D.* melanogaster) and sea snails (*Ilyanassa obsoleta*) (Cavieres et al., 2019; Goulding, 2024; van Heerwaarden et al.,

2016). Whereas evidence for macroalgae remains limited and is typically derived from short-term laboratory studies focused on the early developmental stages of embryos (Hays, 2007; Li & Brawley, 2004; Sanchez de Pedro et al., 2023). Nevertheless, the historical thermal contexts of the ten *A. nodosum* populations assessed here varied between regions and even within the southern region (NW vs. NE Iberian coasts). Therefore, this thesis could not fully determine whether the observed increased thermal resilience in the southern populations results from phenotypic plasticity driven by prolonged exposure to warmer climates or genetic adaptation. However, even if I refute the latter, the critical finding is that the heat-tolerant populations can still be associated with a high extinction risk. Combined with the evident contraction of *A. nodosum* populations (Fischer-Piette, 1955), fine-scale temperature assessments could be critical for understanding and addressing the species' future.

6.5. Conclusions and future prospects

This thesis focused on developing and applying methodologies for assessing thermal stress in the intertidal environment. Combining fine-scale temperature data with a novel experimental system and realistic thermal stress treatments demonstrates that thermal stress impacts species at both micro-scales (intertidal levels) and macro-scales (broadly distributed populations).

While temperature loggers provided critical insights into the thermal stress experienced across the intertidal gradient, temperature is only one of many factors influencing resident species. Notably, the literature identifies desiccation in seaweed as a primary determinant of emersion tolerance, driven by factors such as atmospheric humidity, wind, and solar radiation. Therefore, frequent and continuous logging of desiccation and its contributing factors (likely more technically feasible) could yield valuable insights into species resilience to thermal stress. Similarly, the Intertidal Environmental Chamber offers further potential for refinement; incorporating controls for humidity, wave impact, or pH could expand its applicability, providing a more comprehensive understanding of intertidal species' responses to environmental stressors.

Using the exemplar case of brown seaweed at a contracting distribution edge, this thesis demonstrates that incorporating realistic emersion stress in experiments with intertidal organisms can produce physiological responses more closely aligned with the temperatures experienced at their vertical range. Here, future experiments focused on each species could explore in greater detail how different tidal cycles, peak temperatures, and cool/heat rates delimit a species' thermal thresholds.

Through a detailed analysis of *Ascophyllum nodosum* thermal stress responses, this thesis suggests that temperature differences between high and low tide periods can reveal thermally resilient ecotypes at the southern distribution limit. Still, population-specific survivability models based on fine-scale intertidal temperature data indicate that even heat-tolerant populations may struggle to keep pace with rapid warming, resulting in uneven impacts across the European distribution of this species.

The concepts addressed in this thesis provide a solid foundation for developing future ecological studies to improve our understanding of species limits at the intertidal and other environments. This knowledge is key to better inform policy-making efforts to protect ecosystems and biodiversity, guiding conservation strategies and prioritising actions that mitigate the impacts of climate change on vulnerable intertidal species and their associated communities.

6.6. References

Almeida, S. C., Neiva, J., Sousa, F., Martins, N., Cox, C. J., Melo-Ferreira, J., Guiry, M. D., Serrão, E. A., & Pearson, G. A. (2022). A low-latitude species pump: Peripheral isolation, parapatric speciation and mating-system evolution converge in a marine radiation. *Molecular Ecology*, *31*(18), 4797-4817. https://doi.org/10.1111/mec.16623

Andrews, S., Bennett, S., & Wernberg, T. (2014). Reproductive seasonality and early life temperature sensitivity reflect vulnerability of a seaweed undergoing range reduction. *Marine Ecology Progress Series*, *495*, 119-129. https://doi.org/10.3354/meps10567

Ardré, F. (1970). Contribution à l'étude des algues marines du Portugal. *Portugaliae Acta Biologica (B)*, *10*. https://doi.org/10.1007/978-3-642-61398-2_12

Billard, E., Serrão, E., Pearson, G., Destombe, C., & Valero, M. (2010). Fucus vesiculosus and spiralis species complex: a nested model of local adaptation at the shore level. *Marine Ecology Progress Series*, *405*, 163-174. https://doi.org/10.3354/meps08517

Bruno, J. F., Stachowicz, J. J., & Bertness, M. D. (2003). Inclusion of facilitation into ecological theory. *Trends in Ecology & Evolution*, *18*(3), 119-125. https://doi.org/10.1016/S0169-5347(02)00045-9

Capotondi, A., Rodrigues, R. R., Sen Gupta, A., Benthuysen, J. A., Deser, C., Frölicher, T. L., Lovenduski, N. S., Amaya, D. J., Le Grix, N., Xu, T., Hermes, J., Holbrook, N. J., Martinez-Villalobos, C., Masina, S., Roxy, M. K., Schaeffer, A., Schlegel, R. W., Smith, K. E., & Wang, C. (2024). A global overview of marine heatwaves in a changing climate. *Communications Earth & Environment*, *5*(1), 701. https://doi.org/10.1038/s43247-024-01806-9

Casado-Amezúa, P., Araújo, R., Bárbara, I., Bermejo, R., Borja, Á., Díez, I., Fernández, C., Gorostiaga, J., Guinda, X., & Hernández, I. (2019). Distributional shifts of canopy-forming seaweeds from the Atlantic coast of Southern Europe. *Biodiversity and Conservation*, *28*(5), 1151-1172. https://doi.org/10.1007/s10531-019-01716-9

Cavieres, G., Alruiz, J. M., Medina, N. R., Bogdanovich, J. M., & Bozinovic, F. (2019). Transgenerational and within-generation plasticity shape thermal performance curves. *Ecology & Evolution*, *9*(4), 2072-2082. https://doi.org/10.1002/ece3.4900

Chefaoui, R. M., Martinez, B. D., & Viejo, R. M. (2024). Temporal variability of sea surface temperature affects marine macrophytes range retractions as well as gradual

warming. *Scientific reports*, *14*(1), 14206. https://doi.org/10.1038/s41598-024-64745-7

Christie, H., Norderhaug, K. M., & Fredriksen, S. (2009). Macrophytes as habitat for fauna. *Marine Ecology Progress Series*, *396*, 221-233. https://doi.org/10.3354/meps08351

Collén, J., & Davidson, R. (2001). Seasonality and Thermal Acclimation of Reactive Oxygen Metabolism in fucus Vesiculosus (Phaeophyceae). Jonas Collen. *Journal of Phycology*, *37(4)*, 474–481. https://doi.org/10.1046/j.1529-8817.2001.037004474.x

Collins, M., Clark, M. S., & Truebano, M. (2023). The environmental cellular stress response: the intertidal as a multistressor model. *Cell Stress Chaperones*, *28*(5), 467-475. https://doi.org/10.1007/s12192-023-01348-7

Colman, J. (1940). On the faunas inhabiting intertidal seaweeds. *Journal of the Marine Biological Association of the United Kingdom*, *24*(1), 129-183. https://doi.org/10.1017/S0025315400054503

Coyer, J. A., Hoarau, G., Stam, W. T., & Olsen, J. L. (2007). Hybridization and introgression in a mixed population of the intertidal seaweeds Fucus evanescens and F. serratus. *Journal of Evolutionary Biology*, *20*(6), 2322-2333. https://doi.org/10.1111/j.1420-9101.2007.01411.x

Daborn, P. J., Yen, J. L., Bogwitz, M. R., Le Goff, G., Feil, E., Jeffers, S., Tijet, N., Perry, T., Heckel, D., Batterham, P., Feyereisen, R., Wilson, T. G., & ffrench-Constant, R. H. (2002). A single p450 allele associated with insecticide resistance in Drosophila. *Science*, *297*(5590), 2253-2256. https://doi.org/10.1126/science.1074170

De Wreede, R., & Klinger, T. (1988). Reproductive strategies in algae. *Plant reproductive ecology: patterns and strategies*, 267-284.

Dorgelo, J. (1976). Intertidal fucoid zonation and desiccation. *Aquatic Ecology*, *10(2)*, 115-122. https://doi.org/10.1007/BF02282219

Dudgeon, S., Kübler, J. E., Wright, W. A., Vadas Sr, R. L., & Petraitis, P. S. (2001). Natural variability in zygote dispersal of *Ascophyllum nodosum* at small spatial scales. *Functional Ecology*, *15*(5), 595-604. https://doi.org/10.1046/j.0269-8463.2001.00559.x

Dunstone, M., O'Connor, R., & Seed, R. (1979). The epifaunal communities of Pelvetia canaliculata and Fucus spiralis. *Ecography*, *2*(1), 6-11. https://doi.org/10.1111/J.1600-0587.1979.TB00676.X

Eckert, C. G., Samis, K. E., & Lougheed, S. C. (2008). Genetic variation across species' geographical ranges: the central-marginal hypothesis and beyond. *Molecular Ecology*, *17*(5), 1170-1188. https://doi.org/10.1111/j.1365-294X.2007.03659.x

Fernández, Á., Arenas, F., Trilla, A., Rodríguez, S., Rueda, L., & Martínez, B. (2015). Additive effects of emersion stressors on the ecophysiological performance of two intertidal seaweeds. *Marine Ecology Progress Series*, *536*, 135-147. https://doi.org/10.3354/meps11401

Ferreira, J. G., Arenas, F., Martínez, B., Hawkins, S. J., & Jenkins, S. R. (2014). Physiological response of fucoid algae to environmental stress: comparing range centre and southern populations. *New Phytologist*, *202*(4), 1157-1172. https://doi.org/10.1111/nph.12749

Fischer-Piette, E. (1955). *Répartition, le long des côtes septentrionales de l'Espagne, des principales espèces peuplant les rochers intercotidaux.* (Vol. 31). Masson et Cie.

Fischer-Piette, E. (1963). La distribution des principaux organisms nord-ibériques en 1954-55. *Annales de l'Institut Océanographique Paris 40*(3), 165-311.

Fredriksen, S., Christie, H., & Andre Sæthre, B. (2005). Species richness in macroalgae and macrofauna assemblages on Fucus serratus L. (Phaeophyceae) and Zostera marina L. (Angiospermae) in Skagerrak, Norway. *Marine Biology Research*, *1*(1), 2-19. https://doi.org/10.1080/17451000510018953

Garbary, D. J., Miller, A. G., & Scrosati, R. A. (2014). *Ascophyllum nodosum* and its symbionts: XI. The epiphyte Vertebrata lanosa performs better photosynthetically when attached to *Ascophyllum* than when alone. *Algae*, *29*(4), 321-331. https://doi.org/10.4490/algae.2014.29.4.321

Garcia Castillo, D., Barton, N., Faria, R., Larsson, J., Stankowski, S., Butlin, R., Johannesson, K., & Westram, A. M. (2024). Predicting rapid adaptation in time from adaptation in space: A 30-year field experiment in marine snails. *Science Advances*, *10*(41). https://doi.org/10.1126/sciadv.adp2102

Gauci, C., Bartsch, I., Martins, N., & Liesner, D. (2022). Cold Thermal Priming of Laminaria digitata (Laminariales, Phaeophyceae) Gametophytes Enhances Gametogenesis and Thermal Performance of Sporophytes. *Frontiers in Marine Science*, *9*. https://doi.org/10.3389/fmars.2022.862923

GBIF. (2024). *iNaturalist community. Observations of Ascophyllum nodosum from Madeira Archipelago, Portugal.* https://www.gbif.org/species/3196524; https://www.inaturalist.org/observations/12987333

Goulding, M. Q. (2024). Acclimation of intertidally reproducing sea-snails protects embryos from lethal effects of transient hyperthermia. *Journal of Experimental Zoology Part B: Molecular and Developmental Evolution*, *342*(2), 101-105. https://doi.org/10.1002/jez.b.23240

Harada, A. E., & Burton, R. S. (2019). Ecologically Relevant Temperature Ramping Rates Enhance the Protective Heat Shock Response in an Intertidal Ectotherm. *Physiol Biochem Zool*, *92*(2), 152-162. https://doi.org/10.1086/702339

Harker, M., Berkaloff, C., Lemoine, Y., Britton, G., Young, A., Duval, J.-C., Rmiki, N.-E., & Rousseau, B. (2010). Effects of high light and desiccation on the operation of the xanthophyll cycle in two marine brown algae. *European Journal of Phycology*, *34*(1), 35-42. https://doi.org/10.1080/09670269910001736062

Hatchett, W. J., Coyer, J. A., Sjøtun, K., Jueterbock, A., & Hoarau, G. (2022). A review of reproduction in the seaweed genus Fucus (Ochrophyta, Fucales): Background for renewed consideration as a model organism [Review]. *Frontiers in Marine Science*, *9*. https://doi.org/10.3389/fmars.2022.1051838

Hays, C. G. (2007). Adaptive phenotypic differentiation across the intertidal gradient in the alga Silvetia compressa. *Ecology*, *88*(1), 149-157. https://doi.org/10.1890/0012-9658(2007)88[149:apdati]2.0.co;2

Henkel, S. K., & Hofmann, G. E. (2008). Thermal ecophysiology of gametophytes cultured from invasive Undaria pinnatifida (Harvey) Suringar in coastal California harbors. *Journal of Experimental Marine Biology and Ecology*, *367*(2), 164-173. https://doi.org/10.1016/j.jembe.2008.09.010

Hernández, S., García, A. G., Arenas, F., Escribano, M. P., Jueterbock, A., De Clerck, O., Maggs, C. A., Franco, J. N., & Martínez, B. D. C. (2023). Range-edge populations of seaweeds show niche unfilling and poor adaptation to increased temperatures. *Journal of Biogeography*, *50*(4), 780-791. https://doi.org/10.1111/jbi.14572

Izquierdo, P., Rico, J. M., Taboada, F. G., González-Gil, R., & Arrontes, J. (2022). Characterization of marine heatwaves in the Cantabrian Sea, SW Bay of Biscay. *Estuarine, Coastal and Shelf Science*, *274*, 107923. https://doi.org/10.1016/j.ecss.2022.107923

Jeyachandran, S., Chellapandian, H., Park, K., & Kwak, I. S. (2023). A Review on the Involvement of Heat Shock Proteins (Extrinsic Chaperones) in Response to Stress Conditions in Aquatic Organisms. *Antioxidants (Basel)*, *12*(7). https://doi.org/10.3390/antiox12071444

Jueterbock, A., Kollias, S., Smolina, I., Fernandes, J. M., Coyer, J. A., Olsen, J. L., & Hoarau, G. (2014). Thermal stress resistance of the brown alga Fucus serratus

along the North-Atlantic coast: acclimatization potential to climate change. *Marine Genomics*, *13*, 27-36. https://doi.org/10.1016/j.margen.2013.12.008

Jueterbock, A., Tyberghein, L., Verbruggen, H., Coyer, J. A., Olsen, J. L., & Hoarau, G. (2013). Climate change impact on seaweed meadow distribution in the North Atlantic rocky intertidal. *Ecology and Evolution*, *3*(5), 1356-1373. https://doi.org/10.1002/ece3.541

Kern, P., Cramp, R. L., & Franklin, C. E. (2015). Physiological responses of ectotherms to daily temperature variation. *Journal of Experimental Biology*, *218*(19), 3068-3076. https://doi.org/10.1242/jeb.123166

Kim, K.-Y., & Garbary, D. j. (2009). Form, Function and Longevity in Fucoid Thalli: Chlorophyll a Fluorescence Differentiation of *Ascophyllum nodosum, Fucus vesiculosus* and *F. distichus* (Phaeophyceae). *Algae*, *24*(2), 93-104. https://doi.org/10.4490/algae.2009.24.2.093

King, N. G., McKeown, N. J., Smale, D. A., Wilcockson, D. C., Hoelters, L., Groves, E. A., Stamp, T., & Moore, P. J. (2019). Evidence for different thermal ecotypes in range centre and trailing edge kelp populations. *Journal of Experimental Marine Biology and Ecology*, *514*, 10-17. https://doi.org/10.1016/j.jembe.2019.03.004

Lalegerie, F., & Stengel, D. B. (2022). Concise review of the macroalgal species Pelvetia canaliculata (Linnaeus) Decaisne & Thuret. *Journal of Applied Phycology*, *34*(6), 2807-2825. https://doi.org/10.1007/s10811-022-02830-y

Ledoux, J.-B. (2024). *Project Deliverable Report D1.3*. www.blueforesting.com

Li, R., & Brawley, S. H. (2004). Improved survival under heat stress in intertidal embryos (Fucus spp.) simultaneously exposed to hypersalinity and the effect of parental thermal history. *Marine Biology*, *144*(2), 205-213. https://doi.org/10.1007/s00227-003-1190-9

Lichtenthaler, H. K., Buschmann, C., & Knapp, M. (2005). How to correctly determine the different chlorophyll fluorescence parameters and the chlorophyll fluorescence decrease ratio RFd of leaves with the PAM fluorometer. *Photosynthetica*, *43*(3), 379-393. https://doi.org/10.1007/s11099-005-0062-6

Liesner, D., Fouqueau, L., Valero, M., Roleda, M., Pearson, G., Bischof, K., Valentin, K., & Bartsch, I. (2020). Heat stress responses and population genetics of the kelp Laminaria digitata (Phaeophyceae) across latitudes reveal differentiation among North Atlantic populations. *Ecology & Evolution*, *10*. https://doi.org/10.1002/ece3.6569

Lüning, K. (1984). Temperature tolerance and biogeography of seaweeds: The marine algal flora of Helgoland (North Sea) as an example. *Helgoländer Meeresuntersuchungen 38*, 305–317. https://doi.org/10.1007/BF01997486

Lüning, K. (1990). Seaweeds: their environment, biogeography, and ecophysiology. *Journal of the Marine Biological Association of the United Kingdom*, *71*(1), 246-246. https://doi.org/10.1017/S0025315400037632

Maneiro Estraviz, I., Couceiro, L., Criado, I., Cremades, J., Ruiz, J., & Barreiro, R. (2011). Low genetic variation and isolation of northern peripheral populations of a red seaweed (Grateloupia lanceola). *Aquatic Conservation: Marine and Freshwater Ecosystems*, *21*, 590-600. https://doi.org/10.1002/aqc.1216

Monteiro, C., Pereira, J., Seabra, R., & Lima, F. P. (2022). Fine-scale survey of intertidal macroalgae reveals recent changes in a cold-water biogeographic stronghold. *Frontiers in Marine Science*, *9*. https://doi.org/10.3389/fmars.2022.880074

Mota, C., Engelen, A., Serrao, E., & Pearson, G. (2014). Some don't like it hot: Microhabitat-dependent thermal and water stresses in a trailing edge population. *Functional Ecology*, *29*. https://doi.org/10.1111/1365-2435.12373

Mota, C. F., Engelen, A. H., Serrao, E. A., Coelho, M. A., Marbà, N., Krause-Jensen, D., & Pearson, G. A. (2018). Differentiation in fitness-related traits in response to elevated temperatures between leading and trailing edge populations of marine macrophytes. *PLoS One*, *13*(9). https://doi.org/10.1371/journal.pone.0203666

Murren, C. J., Auld, J. R., Callahan, H., Ghalambor, C. K., Handelsman, C. A., Heskel, M. A., Kingsolver, J. G., Maclean, H. J., Masel, J., Maughan, H., Pfennig, D. W., Relyea, R. A., Seiter, S., Snell-Rood, E., Steiner, U. K., & Schlichting, C. D. (2015). Constraints on the evolution of phenotypic plasticity: limits and costs of phenotype and plasticity. *Heredity (Edinb)*, *115*(4), 293-301. https://doi.org/10.1038/hdy.2015.8

Neiva, J., Assis, J., Fernandes, F., Pearson, G. A., Serrão, E. A., & Maggs, C. (2014). Species distribution models and mitochondrial DNA phylogeography suggest an extensive biogeographical shift in the high-intertidal seaweed Pelvetia canaliculata. *Journal of Biogeography*, *41*(6), 1137-1148. https://doi.org/10.1111/jbi.12278

Neiva, J., Serrão, E. A., Assis, J., Pearson, G. A., Coyer, J. A., Olsen, J. L., Hoarau, G., & Valero, M. (2016). Climate oscillations, range shifts and phylogeographic patterns of North Atlantic Fucaceae. In *Seaweed phylogeography* (pp. 279-308). Springer. https://doi.org/10.1007/978-94-017-7534-2_11

Nielsen, H. D., & Nielsen, S. (2008). Evaluation of imaging and conventional PAM as a measure of photosynthesis in thin- and thick-leaved marine macroalgae. *Aquatic Biology*, *3*, 121-131. https://doi.org/10.3354/ab00069

Nitschke, U., Connan, S., & Stengel, D. B. (2012). Chlorophyll a fluorescence responses of temperate Phaeophyceae under submersion and emersion regimes: a comparison of rapid and steady-state light curves. *Photosynthesis research*, *114*, 29-42. https://doi.org/10.1007/s11120-012-9776-z

O'Brien, E. K., Walter, G. M., & Bridle, J. (2022). Environmental variation and biotic interactions limit adaptation at ecological margins: lessons from rainforest Drosophila and European butterflies. *Philosophical Transactions of the Royal Society B*, *377*(1848), 20210017. https://doi.org/10.1098/rstb.2021.0017

Olabarria, C., Arenas, F., Fernandez, A., Troncoso, J. S., & Martinez, B. (2018). Physiological responses to variations in grazing and light conditions in native and invasive fucoids. *Marine environmental research*, *139*, 151-161. https://doi.org/10.1016/j.marenvres.2018.05.016

Olsen, J. L., Zechman, F. W., Hoarau, G., Coyer, J. A., Stam, W. T., Valero, M., & Åberg, P. (2010). The phylogeographic architecture of the fucoid seaweed Ascophyllum nodosum: an intertidal 'marine tree' and survivor of more than one glacial-interglacial cycle. *Journal of Biogeography*, *37*(5), 842-856. https://doi.org/10.1111/j.1365-2699.2009.02262.x

Paaijmans, K. P., Heinig, R. L., Seliga, R. A., Blanford, J. I., Blanford, S., Murdock, C. C., & Thomas, M. B. (2013). Temperature variation makes ectotherms more sensitive to climate change. *Global Change Biology*, *19*(8), 2373-2380. https://doi.org/10.1111/gcb.12240

Pearson, G. A., Lago-Leston, A., & Mota, C. (2009). Frayed at the edges: selective pressure and adaptive response to abiotic stressors are mismatched in low diversity edge populations. *Journal of Ecology*, *97*(3), 450-462. https://doi.org/10.1111/j.1365-2745.2009.01481.x

Pereira, L., Morrison, L., Shukla, P. S., & Critchley, A. T. (2020). A concise review of the brown macroalga Ascophyllum nodosum (Linnaeus) Le Jolis. *Journal of Applied Phycology*, *32*(6), 3561-3584. https://doi.org/10.1007/s10811-020-02246-6

Pincebourde, S., Sanford, E., & Helmuth, B. (2008). Body temperature during low tide alters the feeding performance of a top intertidal predator. *Limnology and Oceanography*, *53*(4), 1562-1573. https://doi.org/10.4319/lo.2008.53.4.1562

Reese, A. (2023). Shore patrol. *Science*, *382*(6670), 505-507.

Rezende, E. L., Tejedo, M., & Santos, M. (2011). Estimating the adaptive potential of critical thermal limits: methodological problems and evolutionary implications. *Functional Ecology*, *25*(1), 111-121. https://doi.org/10.1111/j.1365-2435.2010.01778.x

Reznick, D. N., Shaw, F. H., Rodd, F. H., & Shaw, R. G. (1997). Evaluation of the Rate of Evolution in Natural Populations of Guppies Poecilia reticulata. *Science*, *275*(5308), 1934-1937. https://doi.org/10.1126/science.275.5308.1934

Román, M., Román, S., Vázquez, E., Troncoso, J., & Olabarria, C. (2020). Heatwaves during low tide are critical for the physiological performance of intertidal macroalgae under global warming scenarios. *Scientific reports*, *10*(1), 1-14. https://doi.org/10.1038/s41598-020-78526-5

Román, S., Olabarria, C., Weidberg, N., Román, M., & Vázquez, E. (2023). Population structure and habitat assessment for two commercial clam species exploited in small-scale fisheries. *Reviews in Fish Biology and Fisheries*, *33*(4), 1483-1504. https://doi.org/10.1007/s11160-023-09791-6

Sanchez de Pedro, R., Fernández, A. N., García-Sánchez, M. J., Flores-Moya, A., & Bañares-España, E. (2023). Parental environment modulates offspring thermal tolerance in a foundational intertidal seaweed. *European Journal of Phycology*, *58*(2), 121-144. https://doi.org/10.1080/09670262.2022.2081731

Sanz-Martín, M., Hendriks, I. E., Carstensen, J., Marbà, N., Krause-Jensen, D., Sejr, M. K., & Duarte, C. M. (2019). Continuous photoperiod of the Artic summer stimulates the photosynthetic response of some marine macrophytes. *Aquatic Botany*, *158*. https://doi.org/10.1016/j.aquabot.2019.06.005

Schmid, M., Guihéneuf, F., Nitschke, U., & Stengel, D. B. (2021). Acclimation potential and biochemical response of four temperate macroalgae to light and future seasonal temperature scenarios. *Algal Research*, *54*. https://doi.org/10.1016/j.algal.2021.102190

Scrosati, R., & Ellrich, J. (2018). Thermal moderation of the intertidal zone by seaweed canopies in winter. *Marine Biology*, *165*. https://doi.org/10.1007/s00227-018-3374-3

Scrosati, R. A., Knox, A. S., Valdivia, N., & Molis, M. (2011). Species richness and diversity across rocky intertidal elevation gradients in Helgoland: testing predictions from an environmental stress model. *Helgoland Marine Research*, *65*(2), 91-102. https://doi.org/10.1007/s10152-010-0205-4

Seabra, R., Wethey, D. S., Santos, A. M., Gomes, F., & Lima, F. P. (2016). Equatorial range limits of an intertidal ectotherm are more linked to water than air

temperature. *Global Change Biology*, *22*(10), 3320-3331. https://doi.org/10.1111/gcb.13321

Seabra, R., Wethey, D. S., Santos, A. M., & Lima, F. P. (2011). Side matters: Microhabitat influence on intertidal heat stress over a large geographical scale. *Journal of Experimental Marine Biology and Ecology*, *400*(1-2), 200-208. https://doi.org/10.1016/j.jembe.2011.02.010

Somero, G. N. (2010). The physiology of climate change: how potentials for acclimatization and genetic adaptation will determine 'winners' and 'losers'. *Journal of Experimental Biology*, *213*, 912 - 920. https://doi.org/10.1242/jeb.037473

Straub, S. C., Wernberg, T., Thomsen, M. S., Moore, P. J., Burrows, M. T., Harvey, B. P., & Smale, D. A. (2019). Resistance, extinction, and everything in between–The diverse responses of seaweeds to marine heatwaves. *Frontiers in Marine Science*, *6*, 763. https://doi.org/10.3389/fmars.2019.00763

Umanzor, S., Ladah, L., Calderon-Aguilera, L. E., & Zertuche-González, J. A. (2019). Testing the relative importance of intertidal seaweeds as ecosystem engineers across tidal heights. *Journal of Experimental Marine Biology and Ecology*, *511*, 100-107. https://doi.org/10.1016/j.jembe.2018.11.008

Vafeiadou, A.-M., Bretaña, B. L. P., Van Colen, C., Dos Santos, G. A., & Moens, T. (2018). Global warming-induced temperature effects to intertidal tropical and temperate meiobenthic communities. *Marine environmental research*, *142*, 163-177. https://doi.org/10.1016/j.marenvres.2018.10.005

Vajedsamiei, J., Melzner, F., Raatz, M., Morón Lugo, S. C., & Pansch, C. (2021). Cyclic thermal fluctuations can be burden or relief for an ectotherm depending on fluctuations' average and amplitude. *Functional Ecology*, *35*(11), 2483-2496. https://doi.org/10.1111/1365-2435.13889

van Heerwaarden, B., Kellermann, V., & Sgrò, C. M. (2016). Limited scope for plasticity to increase upper thermal limits. *Functional Ecology*, *30*(12), 1947-1956. https://doi.org/10.1111/1365-2435.12687

Vandendriessche, S., Vincx, M., & Degraer, S. (2007). Floating seaweed and the influences of temperature, grazing and clump size on raft longevity — A microcosm study. *Journal of Experimental Marine Biology and Ecology*, *343*(1), 64-73. https://doi.org/10.1016/j.jembe.2006.11.010

Watt, C. A., & Scrosati, R. A. (2013). Bioengineer effects on understory species richness, diversity, and composition change along an environmental stress gradient:

experimental and mensurative evidence. *Estuarine, Coastal and Shelf Science*, *123*, 10-18. https://doi.org/10.1016/j.ecss.2013.02.006

Westmeijer, G., Everaert, G., Pirlet, H., De Clerck, O., & Vandegehuchte, M. B. (2019). Mechanistic niche modelling to identify favorable growth sites of temperate macroalgae. *Algal Research*, *41*. https://doi.org/10.1016/j.algal.2019.101529

Wilson, K., Kay, L., Schmidt, A., & Lotze, H. (2015). Effects of increasing water temperatures on survival and growth of ecologically and economically important seaweeds in Atlantic Canada: implications for climate change. *Marine Biology*, *162*. https://doi.org/10.1007/s00227-015-2769-7

Yamane, L., & Gilman, S. E. (2009). Opposite responses by an intertidal predator to increasing aquatic and aerial temperatures. *Marine Ecology Progress Series*, *393*, 27-36. https://doi.org/10.3354/meps08276

Zaneveld. (1937). The Littoral Zonation of Some Fucaceae in Relation to Desiccation. *The Journal of Ecology*, *25(2)*, 431-468. https://doi.org/10.2307/2256204

Zaneveld, J. S. (1969). Factors Controlling the Delimitation of Littoral Benthic Marine Algal Zonation. *Integrative and Comparative Biology*, *9(2)*, 367-391. https://doi.org/10.1093/icb/9.2.367

Appendix A

A fully automated heart frequency recording device and associated data processing R package

Fernando P. Lima, Luís F. Pereira, Bruno Loureiro, Mar Humet, and Rui Seabra.

A.1. Abstract

Measuring cardiac frequency provides a non-invasive approach to quantifying sublethal stress responses of invertebrates to environmental stressors, such as heat stress. Existing cardiac monitoring methods rely on limited-performance hardware with data processing still largely manual or semi-automated. These limitations make current approaches cumbersome, restricting the scalability and the complexity of experiments that can be done. To address these challenges, we developed a fully automated toolkit that integrates hardware, firmware, and the R package *heartbeatr* to streamline the collection and analysis of large volumes of heartbeat data. We validated the system's automated frequency detection against a curated database of 78,769 manually assessed heartbeats, demonstrating high its reliability. We provide recommendations for conducting long-term, high-throughput cardiac monitoring in ecological research.

Keywords

Cardiac frequency, Physiology, Invertebrate, Hardware, Software, Data analysis, Automated peak detection, R package

Open source repository

Complete bill of materials, hardware and firmware of the Mesocosm system can be found in the following GitHub repositories: https://github.com/coastalwarming/heartbeatr and https://github.com/coastalwarming/Heartbeat_device .

A.2. Introduction

As biodiversity (Díaz et al., 2019) and climate (Masson-Delmotte et al., 2021) crises intensify, understanding the mechanistic links between environmental conditions and organismal physiology has become increasingly central, including in non-model organisms such as marine invertebrates. Such knowledge is essential for effectively predicting how climate change will impact natural systems (Kearney and Porter, 2009). Consequently, there is growing interest in methods that assess organismal performance across diverse environmental conditions, both in situ and in the laboratory (e.g., Pereira et al., 2025).

At the experimental level, non-invasive physiological assessments offer several advantages over invasive methods. They are more consistent with ethical considerations, minimise stress levels (yielding more accurate data on an organism's natural physiological state), and enable real-time, continuous monitoring of physiological performance in the same organisms, allowing studying the effects of accumulated stress (e.g., Pasparakis et al., 2016). Respirometry is a prime example of a non-invasive technique used to evaluate performance via O2 or CO2 quantification (Innes and Houlihan, 1981). However, because it must be conducted in a confined environment (typically in vials only slightly larger than the organism itself), it severely limits environmental manipulation and affects behaviour. Hence, it is typically employed over relatively short periods (minutes to hours, Han et al., 2024).

An alternative method is photoplethysmography (PPG), which uses an illumination source and a photodetector to measure the volumetric changes in circulating blood (Ghamari, 2018), from which it is possible to calculate cardiac frequency. PPG has gained popularity due to its simplicity, cost-effectiveness, and ability to provide data in real-time. It is now commonplace in smartwatch designs, allowing for continuous heart frequency monitoring in humans. Animal physiologists have been using this technique since the late 1980s (Depledge and Andersen, 1990). Having received a much-needed update in 2013 by Burnett et al. (2013), the technique involves attaching a small, wired infrared (IR) emitter and detector to an animal's exoskeleton above the heart. IR light penetrates the shell, and heart contractions alter the reflected intensity. This is then converted into electrical signals, amplified, filtered by the device's hardware, and stored for later processing. Although the animal is not entirely free due to the thin connecting wire, the technique allows for movement while monitoring in open environments in the field and laboratory. It has been widely applied in studies on marine crustaceans and molluscs, from the factors determining the large-scale distribution of limpets (Seabra et al., 2016) to the effects of temperature on fiddler crab performance (Levinton et al., 2020), or the impacts of warming and hypoxia on scallops (Tomasetti et al., 2023).

While Burnett et al.'s (2013) methodology already allows for several weeks of continuous data collection, it has several limitations. It is bulky, prone to damage in wet-lab environments, and lacks a display, making sensor placement and mid-experiment adjustments difficult. The lack of amplification adjustment complicates its use across different species or life stages, as signals may become saturated or insufficiently amplified. Data must be pre-processed by an external analogue-to-digital converter (e.g., Picoscope 2200, Pico Technology, UK) and recorded on a personal computer. Furthermore, data processing remains largely manual, limiting the volume of data that can be analysed and thereby limiting replication and experiment duration. Finally, under certain conditions, internal electric noise could self-sustain through positive feedback, which could be misinterpreted as true signals by untrained observers.

To address these issues, we developed a fully automated toolkit that integrates improved hardware, firmware, and the R package heartbeatr for seamless analysis of large-scale heartbeat data. The hardware, which is self-sufficient and does not require the use of any external hardware, features a more powerful processor with WiFi and a redesigned amplification circuit that considerably reduces the likelihood of positive feedback artefacts. It has ten independent channels, each with individually adjustable amplification, allowing flexibility across species and life stages. The system can record data in continuous mode or at predefined intervals and is housed in a splash-proof enclosure designed for durability. A 3.5-inch LCD screen provides real-time feedback, simplifying sensor placement and system adjustments. The heartbeatr package includes functions to import, slice and condition data, to automatically determine heartbeat frequencies, to normalise heartbeat frequencies, and to handle oversampling. To validate the system, we compared its automated frequency detection against a curated database of 78,769 manually assessed heartbeats from Seabra et al. (2016), evaluating its accuracy and reliability.

A.3. Materials and Methods

A.3.1. Hardware

The system, represented in **Fig. A.1**, is built around an ESP32S3-WROOM-1 microcontroller module (U1, a) – the main control and data acquisition unit. A coin-cell-powered real-time clock (RTK, U2, b) maintains accurate time even when the primary power source is disconnected, providing a 1 Hz interrupt timing signal to the microcontroller. Non-volatile data storage is managed via a microSD card socket (U3, c), interfaced with the ESP32's MMC bus. The microcontroller and RTK operate at 3.3 V, regulated by a linear voltage regulator (Reg 1, d), while a separate 5 V regulator (Reg 2, e) powers the signal

acquisition circuitry. Both regulators are supplied by an external 12 V power source. A push-button switch (SW1, f) toggles system power, with an embedded red LED indicating status. Additional push buttons (SW2-SW4, g) allow users to scroll through displayed channels on the LCD screen (h) and pause data recording. Activating the pause function illuminates a blue LED (D2) embedded in the pause switch. Each of the ten signal acquisition channels uses a Vishay CNY70 reflective optical sensor (U5, j). The sensor's infrared LED is powered from the 5 V rail through an 82 Ω current-limiting resistor. The phototransistor output is amplified and filtered using three signal processing stages implemented with a quad-operational amplifier (MCP6044, i). Low-pass and bandpass filters, formed by capacitors and resistors, stabilise the heartbeat waveform for reliable digitisation by the microcontroller. Variable resistors allow fine-tuning of offset and gain for each channel. A Zener diode clamp (D3, k) provides a stabilised reference voltage (Vref 1-10, i) for each amplification circuit. The processed signals are fed into the ESP32's analogue inputs, where they are digitised and time-stamped using the RTK before being written to the microSD card for offline analysis.

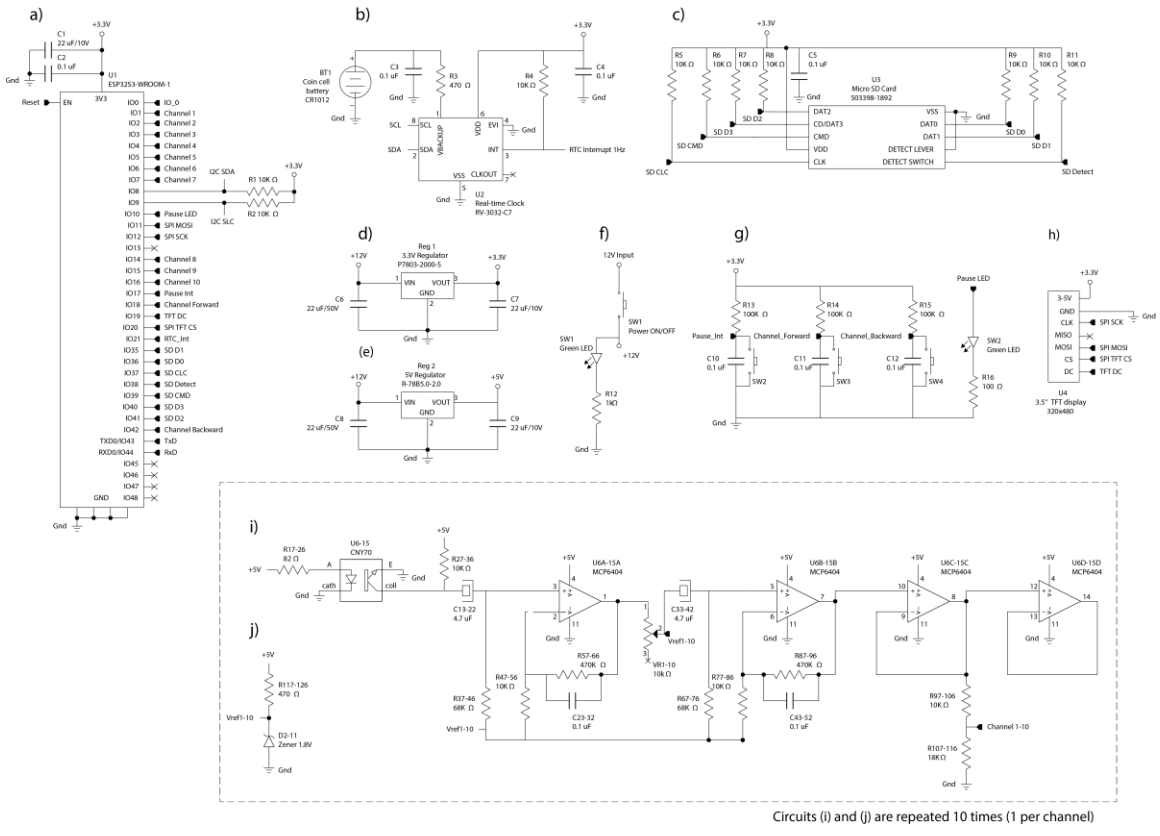


Figure A.1: Functional schematic diagram of the IR cardiac sensing amplification and signal conditioning circuit. See complete bill of materials at the GitHub repository.

To optimise hardware layout, components are distributed across two printed circuit boards (PCBs) connected by a 34-line Flat Flexible Cable. The primary PCB houses most processing and amplification components (a-d, most of i and j), while the secondary PCB contains the LCD screen, switches (f and h), and adjustable resistors (VR1-10, i) for fine-tuning. The electronics are housed in a splash-proof ABS enclosure with custom-made cutouts for the LCD screen, buttons, connectors, and for accessing the microSD (**Fig. A.2**). CNY70 sensors are connected to the end of 3-wire enamelled core cables, which attach to splash-proof connectors at the enclosure.

A.3.2. System deployment

The system is deployed following the procedure described by Burnett et al. (2013). After identifying the approximate location of the animal's heart, a wired CNY70 is attached to the exoskeleton (shell), ensuring alignment as close as possible to the heart. The area should be cleaned and dried before attachment, and while various adhesives can be used, cyanoacrylate generally provides the best results. Proper sensor placement directly over the heart is critical for obtaining a strong signal.



Figure A.2: a) Full system showing the ten amplification knobs at the front, two cabled CNY70 sensors connected on top and a power adaptor; b) glueing a CNY70 sensor to a blue mussel (*Mytilus* sp.); c) several limpet s(Patella sp.) with CNY70 attached to their shell, over their heart; d) the heartbeat of a blue mussel (*Mytilus* sp.) as shown on the LCD screen.

Upon power activation, the device performs a self-check on the real-time clock and microSD card. If malfunctions are detected, an error message is displayed on the LCD screen, and recording is disabled. Otherwise, the system reads and applies the configuration settings from a text file (Pulse_settings.txt) stored in the root directory of the microSD card, which defines key operational parameters such as system name, channel names, sampling rate (5–25 Hz), WiFi settings, time zone and daylight-saving adjustments, display options, and recording mode (continuous or session-based). The configuration file is accessible both physically and via FTP.

Once configured, the system begins recording data from all ten sensors, storing readings as CSV files in the microSD card. Data is saved at one-minute intervals, meaning that if the system is powered off unexpectedly, no more than one minute of data may be lost. To manage file sizes, a new log file is generated every hour. Sensors and the microSD card can be replaced while the system remains operational. A pause button allows users to temporarily halt data logging, preventing disturbances from being recorded, such as during animal handling. Users can scroll through the displayed channel using the channel change push buttons without interrupting the recording of other channels. Holding a channel change button for five seconds switches the device from sampling mode to either settings mode, which displays the current configuration, or server mode, which connects the device to a Wi-Fi network for data transfer via File Transfer Protocol (FTP).

Each saved CSV file includes a metadata header containing device name, sensor names, sampling frequency, and time settings, followed by timestamped readings with millisecond precision for all ten sensors. Firmware updates can be applied via the microSD card, with detailed instructions available in the GitHub repository.

A.3.3. R package *heartbeatr*

The data produced by the system described above consist of a continuous stream of timestamps and fluctuating electrical signals stored in hourly CSV files. The functions within the *heartbeatr* enable the conversion of this data into discrete estimates of heartbeat frequencies at spaced intervals (**Table A.1**). Briefly, `pulse_read()` initiates the metadata processing workflow with a data consistency analysis across all CSV files. This is followed by the condition stage, where the user customize data segmentation and smoothing to fit both quick previews or detailed analyses. This is followed by the process stage, where `pulse_heart()` estimates heartbeat frequency for each interval and recorded channel. This automatic peak detection algorithm in *heartbeatr* is an R adaptation of the Python-based Automatic Multiscale Peak Detection (AMPD) algorithm by Gotlibovych (2018), a refined

version of the method developed by Scholkmann et al. (2012). Here, signals with double-peaked waves, a known characteristic of photoplethysmography, are corrected by `pulse_doublecheck()`,while `pulse_choose_keep()` classifies all heart beats as "keep" or "reject" based on user-defined thresholds for peak count and inter-peak interval variance.

This entire workflow can be executed step-by-step or streamlined using `PULSE()`, a wrapper function that sequentially runs all processing steps. By the end of the workflow, the user receives an estimate of heartbeat frequency for each interval and recorded channel, along with timestamps, quality metrics, and a binary classification of each data point as "keep" or "reject." While the data is now ready for analysis, two additional post-processing steps are often necessary. First, `pulse_normalise()` normalizes heartbeat frequency estimates for the targeted individual, focusing our results on its relative changes rather than absolute values, which could be misleading. Second, `pulse_summarise()` reduces data volume by aggregating heartbeat estimates into larger intervals.

Finally, *heartbeatr* includes two visualization functions to aid quality control, `pulse_plot_raw()` that enables inspection of raw data underlying specific heartbeat estimates, and `pulse_plot()` that provides an overview of heartbeat estimate quality for each recorded channel.

Table A.1: Main functions and descriptions of the *heartbeat* R package.

Category	Function	Description
Ingest	`pulse_read()`	Read target CSV files, check for metadata consistency and bind data.
Condition	`pulse_split()`	Cut data into intervals.
	`pulse_interpolate()`	Applies linear interpolation to ensure optimal sampling rate.
	`pulse_smooth()`	Applies Kernel Smoothing to reduce high-frequency noise.
	`pulse_optimize()`	Calls `pulse_interpolate()` and `pulse_smooth()` sequentially.
Process	`pulse_heart()`	Identifies signal wave peaks and estimates heartbeat frequency.
	`pulse_doublecheck()`	Searches for intervals with two peaks per wave and corrects the heartbeat frequency estimates
	`pulse_choose_keep()`	Classifies heartbeat frequency estimates as "keep" or "reject".
Wrapper	`PULSE()`	Runs all ingest, condition and process functions sequentially from a single call.
Post-processing	`pulse_normalise()`	Normalises heartbeat frequency estimates based on a user-specified control period.
	`pulse_summarise()`	Combines heartbeat frequency estimates by applying a function across user-specified intervals.
Inspection	`pulse_plot_raw()`	Plot raw signals (and highlight identified peaks) to allow inspection of the data underlying a particular heartbeat frequency estimate.
	`pulse_plot()`	Plot all heartbeat frequency estimates to allow inspection of the overall dataset.

A.3.4. System validation and statistical analysis

The performance of the AMPD algorithm implemented in the *heartbeatr* package, along with its noise-handling and artifact-detection functions, was evaluated using data from Seabra et al. (2016). This dataset consists of heartbeat recordings from the intertidal limpet *Patella vulgata*, collected from a rocky shore in northern Portugal (Moledo, 41.841 °N, 8.874 °W) following a 37-day acclimation and thermal stress treatment. The dataset includes 78,769 raw heartbeat readings, corresponding manually assessed heartbeat rates, and a classification of each data point as “keep” or “reject” based on visual inspection of the underlying signal. Heartbeat activity was recorded at 40 Hz for one-minute intervals every 15 minutes.

To ensure compatibility with *heartbeatr*, the dataset was reformatted to match the output structure of the system described in sections 4.1 and 4.2. The reformatted data were then processed using `PULSE()`, which generated automated heartbeat frequency estimates and classified each data point as “keep” or “reject” based on user-defined thresholds. The final validation dataset included both human-assessed (“real”) and *heartbeatr*-processed (“estimated”) heartbeat frequency values and quality ratings, allowing for direct comparison. Rejected data points were retained to evaluate *heartbeatr*'s ability to identify low-quality signals, a key aspect of its workflow.

The validation focused on two key parameters: smoothing intensity, controlled by `bandwidth`, and the standard deviation cutoff for quality ratings, controlled by `lim_sd`. The impact of smoothing was assessed by processing the dataset with `bandwidth` values ranging from 0.0 to 1.0 in 0.1 increments, evaluating the proportion of correctly classified data points (“keep” or “reject”), as well as false positives (data retained by *heartbeatr* but rejected by human assessment) and false negatives. To assess whether using multiple smoothing levels improved performance, `raw_v_smoothed` was set to TRUE (estimating heartbeat frequencies from both smoothed and unsmoothed data, retaining only the value with the lowest inter-peak standard deviation) and FALSE (using only the specified smoothing level). An additional test run was performed where all `bandwidth` values were tested, and the retained estimate was the one with the lowest inter-peak standard deviation across all smoothing levels.

To evaluate the sensitivity of *heartbeatr* to different standard deviation cutoff values, a second set of analyses was conducted with `lim_sd` values ranging from 0.0 to 2.0 in 0.05 increments, using a `bandwidth` of 0.4 and `raw_v_smoothed` set to FALSE. Finally, the accuracy of automated frequency estimates was assessed by computing the 2D Kernel density of human-assessed versus *heartbeatr*-generated heartbeat frequencies, using bandwidth =

0.4, raw_v_smoothed = FALSE, and lim_sd = 0.70, yielding cumulative probability distributions in 0.1 × 0.1 bins.

A.4. Results

The access to a very large dataset of curated, manually-assessed heartbeat frequency estimates, along with the underlying raw data, facilitated a very direct and detailed assessment of the performance of the *heartbeatr* package. While all function parameters can be used to modify the *heartbeatr* workflow, two are particularly critical: the smoothing bandwidth and the cutoff SD value `lim_sd`. Regarding the level of smoothing, our test runs show that the proportion of data points automatically assigned to the correct quality category (as defined by the human-assessed category class) (**Fig. A.3a, d**) is highest when using moderate smoothing (bandwidth between 0.3 and 0.5), after which increasing smoothing levels leads to a decrease in performance. Interestingly, it is also shown that while strategies involving processing data with various levels of smoothing and choosing the best estimate yield generally better performances, the gains are modest and, in some instances, may not justify the computational penalty associated. This is particularly true for the strategy using all tested bandwidths, which takes much longer to run and leads to marginal performance gains.

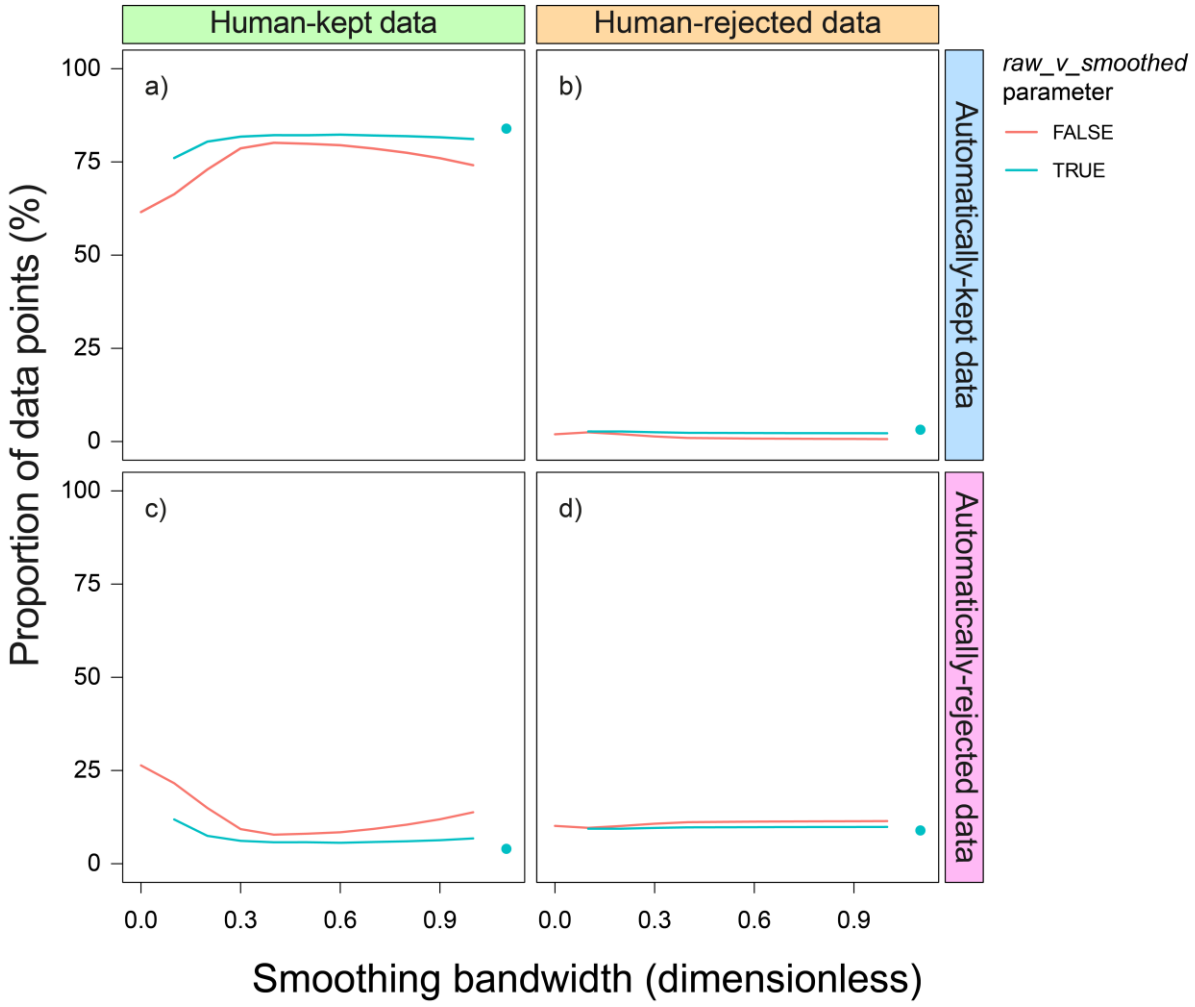


Figure A.3: Impact of signal smoothing intensity (the bandwidth parameter) on the proportion of data points correctly classified as "keep" or "reject" by the *heartbeatr* package. Panels a) and d) correspond to correct classifications (human and *heartbeatr* agree in retaining or rejecting data points), while panels b) and c) correspond, respectively, to false positives (type-1 error, retaining data points that should have been rejected) and false negatives (type-2 error, rejecting data points that should have been retained). In the context of the *heartbeatr* workflow, minimizing the number of data points that fall on panel b) is the priority. Red and blue lines depict the performance curves relative to two distinct workflow strategies. In the simplest and quicker option (red lines), quality was assessed using data smoothed using only the respective bandwidth value. In the other case (blue lines), quality was assessed using not only the same smoothed data but also the raw, unsmoothed data and choosing the best estimate for each data point. Finally, the blue dot depicts a third, more computing-intensive strategy in which the best estimate was chosen from among unsmoothed data and data smoothed at all bandwidth levels tested.

Subsequently, using a bandwidth of 0.4, the sensitivity to different cutoff SD levels was also evaluated (**Fig. A.4**). In this case, our analysis shows that values below 0.4 are too stringent and result in a high number of false negatives (**Fig. A.4c**). Conversely, values above 1.0 are

too lax and result in too many false positives (**Fig. A.4, b**). It's worth noting that, in the context of the high volumes of data that can be produced by the system described in this work, minimizing false positives (type-1 error) should be the priority, and therefore cutoff SD values should be kept lower rather than higher.

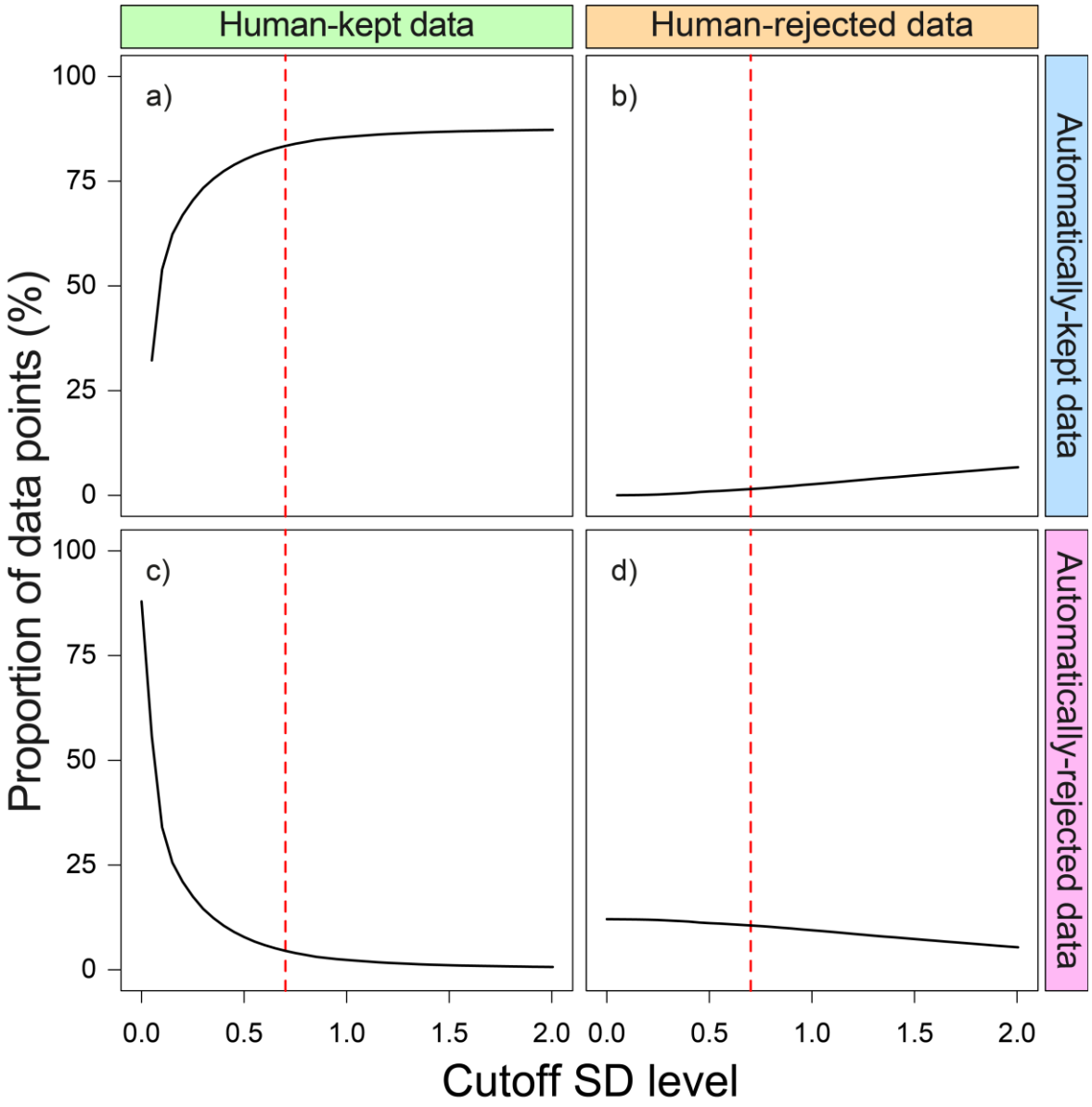


Figure A.4: Impact of cutoff SD level (the lim_sd parameter) on the proportion of data points correctly classified as "keep" or "reject" by the heartbeatr package. Similarly to **Fig. A.3**, panels a) and d) correspond to correct classifications, while panels b) and c) correspond to false positives (type-1 error) and false negatives (type-2 error), respectively. The red dashed line indicates a cutoff SD level of 0.7.

Lastly, we assessed the ability of the *heartbeatr* package to produce accurate heartbeat frequency estimates. This was evaluated by comparing the estimates produced automatically with the corresponding values determined manually (Fig A.5). The analysis shows that not only the vast majority of data points were classified correctly (n = ~74.0 K, corresponding to 94.0 % of all data points [83.4 %

"keep" + 10.6 % "reject"]), most automatic heartbeat estimates match very closely the values determined manually, as can be determined by the concentration of data points along the 1:1 line (95.4 % of the data points in **Fig. A.5a**). In addition, the low number of data points falling on the 2:1 line in **Fig. A.5a**) also indicates that the strategy employed in the *heartbeatr* package to handle instances where each heartbeat is represented in the raw data by two wave peaks is working sufficiently well (2.1 % of the data points in **Fig. A.5a**).

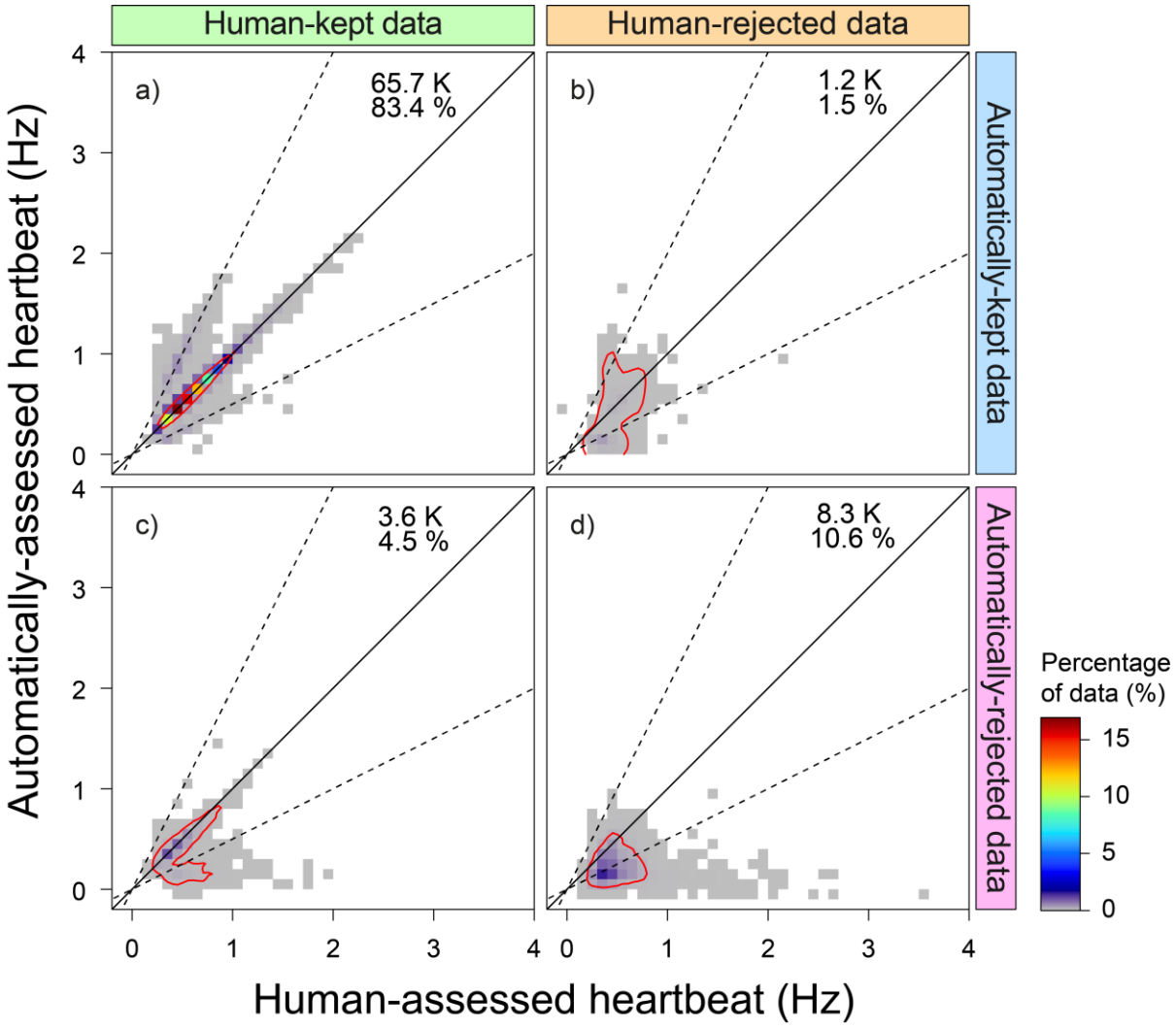


Figure A.5: 2D kernel density plot showing the distribution of automatically-assessed heartbeat frequency estimates against human-assessed values. Data is aggregated in 0.1 x 0.1 bins. The colour scale depicts cumulative probabilities (grey bins are indicative of bin combinations with marginal representation in the overall dataset). The black diagonal line marks a 1:1 relationship between values determined manually and values automatically, while the dashed lines indicate 2:1 (automatically-assessed values are twice the real value) and 1:2 (automatically-assessed values are half the real value) relationships. The red contour encompasses 90% of the data in each panel. Labels in the top-right corner show the number of data points included in each panel and the proportion of data points relative to the entire dataset.

A.5. Discussion

The heart frequency recording system described here represents a significant advancement in long-term cardiac performance assessments of hard-shell organisms, particularly molluscs and crustaceans. The simplified circuit design, compared to that of Burnett et al. (2013), not only provides additional functionalities such as more channels and an LCD screen but, as indicated by our results, is also less sensitive to noise and no longer prone to self-sustaining oscillations. Also, it is more responsive, operating immediately upon power activation. Although this device features wireless data transfer, our experience indicates that it is inefficient for transferring large volumes of data. In such cases, physically accessing the microSD card is preferable. However, the WiFi connection remains the most convenient option for modifying experiment settings or updating the device firmware.

The ability to adjust amplification, combined with the LCD screen providing real-time feedback during sensor placement, enables its use across a wide range of species with different morphologies and sizes. The system has been shown to perform well in small organisms such as periwinkles (*Littorina saxatilis*, B. Han, Nord University, pers. comm.), medium-sized species including blue mussels (*Mytilus edulis*, Alter et al., 2025), abalones (*Haliotis tuberculata*, Habbas et al., 2025), and limpets (*Patella vulgata*, this study), as well as in large bivalves such as *Anodonta abatina* (our team, unp. data) and oysters (*Magallana gigas*, Cozzolino et al., 2024). Although smaller sensors, such as the QRE1113 (Onsemi, USA) were found to produce valid results with a smaller impact on species mobility, we found that CNY70 sensors generally produce superior results, even in organisms smaller than the sensor itself. Hence, alternative sensors should only be considered in cases where the physical size of the CNY70 prevents its application.

The cost of the system, considering parts and labour, can easily exceed 1000€. Still, it does not require any other external equipment, such as an oscilloscope or a dedicated laptop, as was necessary in previous iterations of this methodology (Burnett et al., 2013). This, allied to the fact that it can collect data from ten individuals simultaneously, helps offset the overall cost. Additionally, the open-source nature of this project allows for future development by the community. For example, adapting it as a field instrument is possible with relatively small changes in the power supply and enclosure.

The capacity for long-term cardiac performance assessments is largely enabled by the automated data processing provided by the R package *heartbeatr*. which goes beyond a mere increment over traditional manual data processing. Previous experience has shown that even highly trained individuals can take several months to manually process data from a multi-week experiment despite working exclusively on the task (Seabra et al., 2016; Abbas et al., 2024).

By automating this process, we can significantly reduce workload and increase efficiency. Although automated data processing may still take several hours in some cases, it operates unsupervised, freeing researchers and making long-term experiments feasible. Automation also enables data collection at higher frequencies or even continuously, as large portions of the data can be discarded later without compromising overall quality. Additionally, it allows for more experimental replicates, helping to capture intra-individual variability, commonly high in heart rate data (Braby & Somero, 2006). Using an initially high number of replicates safeguards long-term experiments by compensating for potential replicate loss, which becomes more likely as experiment duration increases. Indeed, the core philosophy of the system is to collect a substantially larger volume of data than needed and selectively retain only high-quality data for analysis. Therefore, a crucial feature of *heartbeatr* is its ability to automatically assign a quality qualifier to each heartbeat assessment, allowing researchers to apply filtering criteria and automatically discard low-quality data. This is not only advisable but necessary. Due to the nature of the AMPD method, peaks are detected even in low-quality data that would be easily rejected by a human observer. Therefore, researchers using *heartbeatr* should leverage the package functionalities to automatically filter out data flagged with a low-quality qualifier, ensuring that only reliable data are retained for analysis.

When setting data filtering thresholds, it is important to balance Type I error (accepting poor-quality data that should be rejected) and Type II error (rejecting good-quality data that could have been used; Akobeng, 2016). Loosening the variability threshold too much increases Type I error by retaining unreliable data. While this reduces Type II error, ensuring that almost no good data are mistakenly rejected, it risks contaminating the dataset, compromising the reliability of the analyses. A more conservative approach with stricter variability thresholds is preferable. Although this may discard some usable data, the system's capacity to collect large datasets, often exceeding user needs, makes over-discarding a negligible concern.

Still, some data evaluated as high quality may present errors, as the algorithm occasionally misinterprets heartbeats with two peaks and registers double the actual frequency. To correct this, users should visualise the processed data by plotting frequency against time, where such errors appear as sudden duplications that return to baseline.

A.6. Acknowledgements

This work was supported by Fundação para a Ciência e Tecnologia (FCT) through the projects ThermalBuffer (POCI-01-0145-FEDER-31088) and OceanLog (PTDC/BIA-BMA/4848/2021), and by Luso-American Development Foundation (FLAD) through the project CCTBON (Science Award Atlantic 2020). LFP received support from FCT through a PhD grant (SFRH/BD/136924/2018), and FPL and RS through CEECInd contracts (10.54499/CEECIND/03185/2018/CP1546/CP1648/CT0004, 10.54499/CEECIND/01424/2017/CP1423/CP1645/CT0006, respectively).

A.7. References

Burnett, N. P., Seabra, R., De Pirro, M., Wethey, D. S., Woodin, S. A., Helmuth, B., Zippay, M. L., Sarà, G., Monaco, C., & Lima, F. P. (2013). An improved noninvasive method for measuring heartbeat of intertidal animals. *Limnology and Oceanography: Methods*, 11(FEB). https://doi.org/10.4319/lom.2013.11.91

Depledge, M. H., & Andersen, B. B. (1990). A computer-aided physiological monitoring system for continuous, long-term recording of cardiac activity in selected invertebrates. Comparative *Biochemistry and Physiology Part A: Physiology*, 96(4), 473–477. https://doi.org/10.1016/0300-9629(90)90664-E

Díaz, S., Settele, J., Brondízio, E. S., Ngo, H. T., Agard, J., Arneth, A., Balvanera, P., Brauman, K. A., Butchart, S. H. M., Chan, K. M. A., Garibaldi, L. A., Ichii, K., Liu, J., Subramanian, S. M., Midgley, G. F., Miloslavich, P., Molnár, Z., Obura, D., Pfaff, A., Polasky, S., Purvis, A., Razzaque, J., Reyers, B., Chowdhury, R. R., Shin, Y. J., Visseren-Hamakers, I., Willis, K. J., & Zayas, C. N. (2019). Pervasive human-driven decline of life on Earth points to the need for transformative change. *Science*, 366(6471), eaax3100. https://doi.org/10.1126/science.aax3100

Ghamari, M. (2018). A review on wearable photoplethysmography sensors and their potential future applications in health care. *International Journal of Biosensors & Bioelectronics*, 4(4). https://doi.org/10.15406/ijbsbe.2018.04.00125

Gotlibovych, I. (2018). pyampd: Automatic multiscale-based peak detection in Python. GitHub. https://github.com/ig248/pyampd

Innes, A. J., & Houlihan, D. F. (1981). A review of the effects of temperature on the oxygen consumption of intertidal gastropods. *Journal of Thermal Biology*, 6(4), 249–256. https://doi.org/10.1016/0306-4565(81)90013-9

Kearney, M., & Porter, W. (2009). Mechanistic niche modelling: Combining physiological and spatial data to predict species' ranges. *Ecology Letters*, 12(4), 334–350. https://doi.org/10.1111/j.1461-0248.2008.01277.x

Levinton, J. S., Volkenborn, N., Gurr, S., Correal, K., Villacres, S., Seabra, R., & Lima, F. P. (2020). Temperature-related heart rate in water and air and a comparison to other temperature-related measures of performance in the fiddler crab Leptuca pugilator (Bosc 1802). *Journal of Thermal Biology*, 88, 102502. https://doi.org/10.1016/j.jtherbio.2019.102502

Masson-Delmotte, V., Zhai, P., Pirani, A., Connors, S. L., Péan, C., Berger, S., Caud, N., Chen, Y., Goldfarb, L., Gomis, M. I., Huang, M., Leitzell, K., Lonnoy, E., Matthews, J. B. R., Maycock, T. K., Waterfield, T., Yelekçi, O., Yu, R., & Zhou, B. (Eds.). (2021). Climate change 2021: The physical science basis. Contribution of Working Group I to the Sixth Assessment Report of the Intergovernmental Panel on Climate Change. *Cambridge University Press*. https://doi.org/10.1017/9781009157896

Pasparakis, C., Davis, B. E., & Todgham, A. E. (2016). Role of sequential low-tide-period conditions on the thermal physiology of summer and winter laboratory-acclimated fingered limpets, Lottia digitalis. *Marine Biology*, 163(2). https://doi.org/10.1007/s00227-015-2779-5

Pereira, L., Seabra, R., Loureiro, B., Arenas, F., & Lima, F. P. (2025). Intertidal environmental chamber: An automatic system to accurately simulate the thermal complexity of intertidal environments. *Methods in Ecology and Evolution*: *Practical tools*.

Seabra, R., Wethey, D. S., Santos, A. M., Gomes, F., & Lima, F. P. (2016). Equatorial range limits of an intertidal ectotherm are more linked to water than air temperature. *Global Change Biology*, 22(10), 3320–3331. https://doi.org/10.1111/gcb.13321

Scholkmann, F., Boss, J., & Wolf, M. (2012). An efficient algorithm for automatic peak detection in noisy periodic and quasi-periodic signals. *Algorithms*, 5(4), 588–603. https://doi.org/10.3390/a5040588

Tomasetti, S. J., Hallinan, B. D., Tettelbach, S. T., Volkenborn, N., Doherty, O. W., Allam, B., & Gobler, C. J. (2023). Warming and hypoxia reduce the performance and survival of northern bay scallops (Argopecten irradians irradians) amid a fishery collapse. *Global Change Biology*, 29, 2092–2107. https://doi.org/10.1111/gcb.16575

Appendix B

A wireless temperature control system for field and laboratory experiments in aquatic mesocosms

Luís F. Pereira, Bruno Loureiro, Rui Seabra and Fernando P. Lima.

B.1. Abstract

Increasing temperatures driven by climate change are profoundly altering ecological dynamics, particularly in standing waters such as ponds and pools. These systems have long been central to metacommunity ecology, offering valuable insights into how planktonic communities respond to environmental gradients and how changes in their composition influence ecosystem functioning. Through a combination of empirical and experimental research on mesocosm communities, scientists aim to uncover the mechanisms underlying the effects of multiple stressors on planktonic communities in the context of global change. Remote ponds, often embedded in intricate ecosystems, present unique opportunities for such studies. However, monitoring and controlling temperature in remote locations can pose significant technical and logistical challenges. To address these challenges, we introduce a wireless temperature control and monitoring system specifically designed for mesocosm experiments. This system enables real-time, remote management of water temperature, accommodating natural fluctuations and simulated warming scenarios. Designed with affordability and scalability in mind, this innovative approach facilitates a wide range of experimental applications, providing a unique tool for advancing our understanding of global change impacts within diverse aquatic ecosystems.

Keywords

Temperature, aquatic mesocosm, standing waters, planktonic communities, common-garden experiments.

Open source repository

Complete bill of materials, hardware and firmware of the Mesocosm system can be found in the following GitHub repository: https://github.com/coastalwarming/Wireless_mesocosm

B.2. Introduction

Aquatic ecosystems are being increasingly influenced by climate change, with rising temperatures affecting species physiology, phenology, and distributions (IPCC, 2022). These changes can directly impact species by differentially affecting fitness across life stages—adults are often more resilient than larvae—and indirectly through synergetic interactions between (Barbosa et al., 2017; Macaulay et al., 2020). However, experiments still rely on constant temperature regimes that fail to reflect the natural fluctuations observed in the environment (Willming & Maul, 2016; Willming et al., 2013).

Current methods for controlling water temperature in micro- and mesocosm studies often rely on simple heating systems that maintain constant temperatures and require manual adjustments to simulate variability. Although some systems have been designed to monitor and replicate thermal variability in both indoor and outdoor setups (Hermann et al., 2022; Wang et al., 2020), they often face technical challenges that limit their effectiveness for long-term or remote experiments. Temperature measurement and control in mesocosms also pose logistical challenges. Wired communication systems frequently fail over longer distances (>10 m; Hermann et al. (2022)), leading to data gaps from sensor miscommunication. Positioning mesocosm tanks closer together to improve sensor communication can compromise the ability to capture essential thermal variability across landscapes, such as differences in sun and wind exposure. Additionally, mesocosms are often situated in remote areas to study minimally disturbed aquatic ecosystems, creating logistical challenges for data collection and experimental adjustments, such as modifying temperature offsets in heated tanks.

To overcome these limitations, we developed a temperature monitoring and control system that enables long-distance communication between tanks, allowing researchers to remotely collect data, modify experimental conditions, and assess system integrity via an internet connection.

B.3. Design and features

The Mesocosm unit consists of a controller that monitors the system, communicates wirelessly, and regulates the temperature of a water reservoir. It can be used in laboratory settings for coordinated experiments across multiple aquaria or outdoors with water tanks. Mesocosm units can interconnect to form a synchronized system, supporting networks of up to 125 units. Each unit is equipped with identical hardware and firmware, with its role determined by a configuration text file stored on a microSD card. Users can edit this file to customize the network structure to meet specific experimental conditions and objectives. The

only requirement is that each network must include a single Master unit, which manages communication among the units and provides connectivity to the internet.

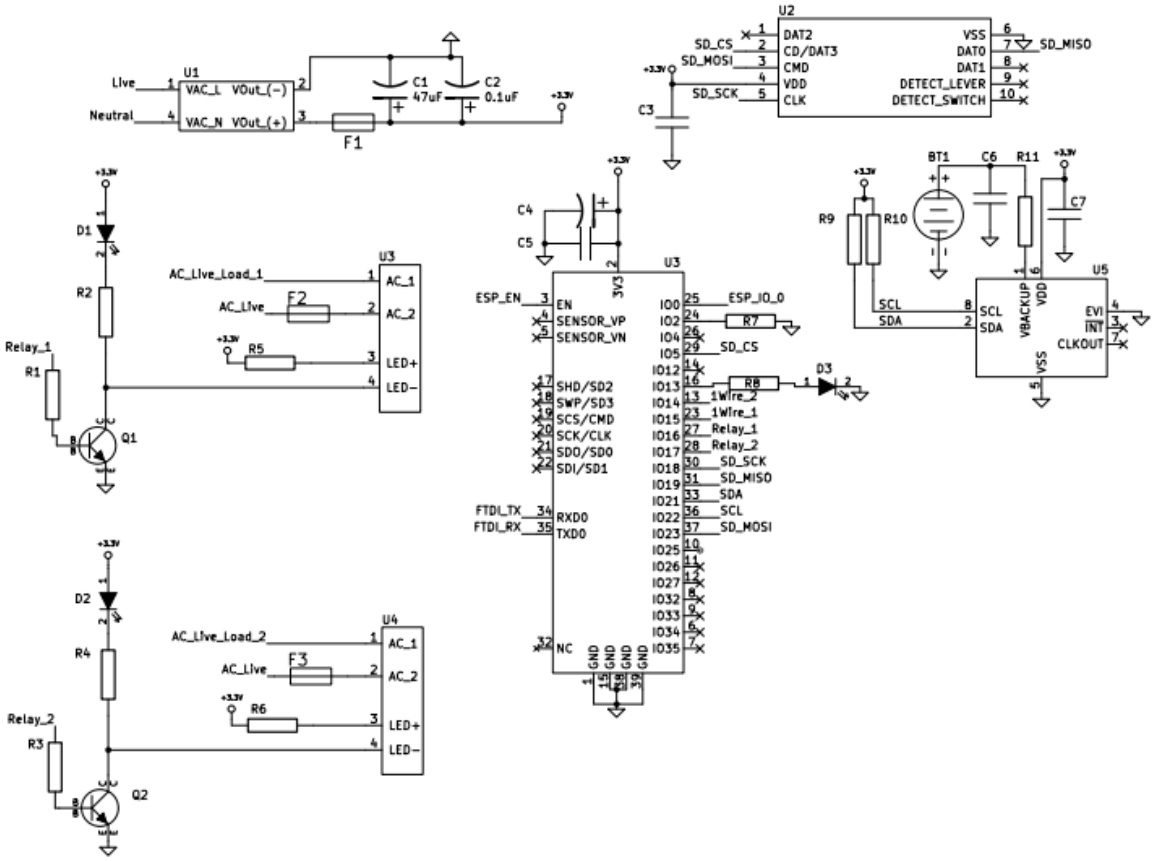


Figure B.1: Functional schematic diagram of Mesocosm system circuit. See complete bill of materials at the GitHub repository.

The hardware for all units is built around a microcontroller (Espressif ESP32; **Fig. B.1** and **Table B.1**), which manages two 3-ampere relays capable of controlling two water heaters, each with a maximum power rating of 690 W. Additionally, the system incorporates two high-precision temperature sensors (12-bit Waterproof DS18B20, Maxim Integrated, USA), a real-time clock module (RV3032) for accurate timekeeping, and a 32 GB micro-SD card for local data storage. Each mesocosm unit continuously records data logs, including timestamps, temperature sensor readings, and the operational state of the water heaters (On or Off), at one-minute intervals, saved as daily CSV files. Wireless communication between mesocosm units is via the ESPNOW protocol, a low-power, long-range data transfer method. This functionality is further enhanced by a compact, wide-range antenna (2.3 to 6.0 GHz) mounted externally on the waterproof enclosure, ensuring robust connectivity even in challenging environments.

The mesocosm hardware consists of a single printed circuit board (PCB) design (128.6 x 98.6 mm; **Fig. B.2a, b**) housed within a polycarbonate IP67-rated enclosure (120 x 160 x 91 mm), which is resistant to ultraviolet light and thermal fatigue (**Fig. B.2c**). The units operate using alternating current (230V or 110V), which powers both the water heaters and the microcontroller responsible for overseeing all system operations. Each unit is equipped with two 300-watt water heaters, providing efficient and redundant heating capabilities, while temperature data is captured by two high-precision sensors. Electrical protection is ensured by glass fuses, which safeguard against external power surges at the power supply and individual heater malfunctions. Connections for both the water heaters and temperature sensors are routed through sealed cable glands to maintain waterproofing. Inside the enclosure, these components connect to the PCB via screw connectors, facilitating quick and easy replacement if needed. This robust design ensures durability and reliability in various experimental conditions.

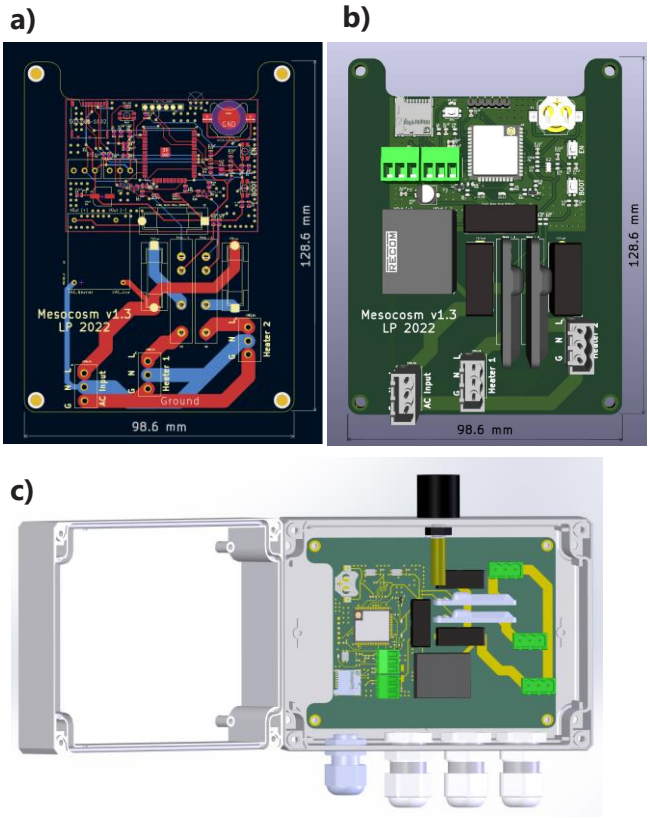


Figure B.2: a) Electronic board layout; b) Electronic 3D board layout (128.6 x 98.6 mm); c) Mesocosm unit composed by a Polycarbonate IP67 box (160x120x91 mm).

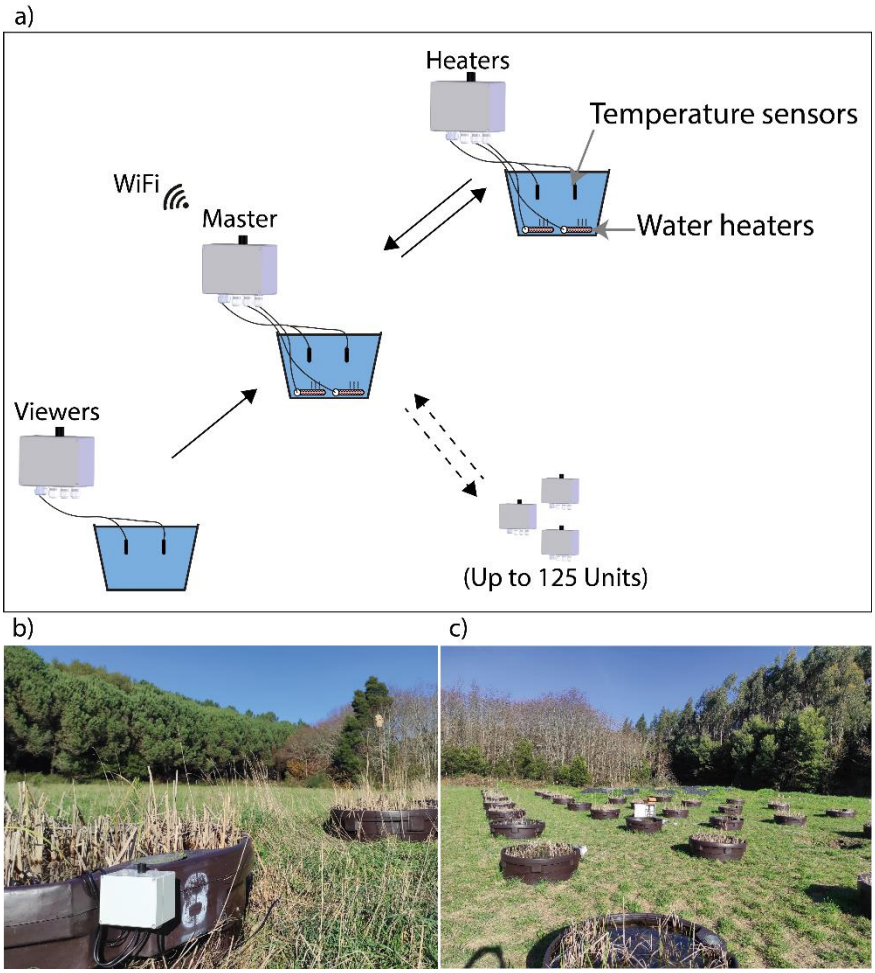


Figure B.3: a) Mesocosm system network architecture; b) Close-up view of a Mesocosm unit fixed to its pond; c) Overall Mesocosm system perspective encompassing 36 ponds, distributed along a 100 x 100 meter area in Vairão (Longitude: 41.325890, Latitude: -8.677546; Portugal).

B.4. Operation

The Mesocosm units are designed for deployment in individual ponds or aquariums, with each unit assigned one of three roles: Viewer (temperature monitor), Heater (temperature control), or Master (system coordinator).

- Viewer: The Viewer's primary function is to read its temperature sensors, store the readings on its microSD card, and transmit the data to the Master.
- Heater: The Heater performs the same functions as the Viewer but also controls two water heaters to maintain the tank temperature within a specified offset.

- Master: In addition to the Heater's responsibilities, the Master assumes three key tasks:

    1. Receiving all communications from Heaters and Viewers.

    2. Calculating and sending the current environmental temperature (average of Viewer readings) to all Heaters.

    3. Uploading all temperature data (from Heaters and Viewers) to an online platform via Wi-Fi.

A system can include any combination of Viewers and Heaters, but only one unit can function as the Master. The role and configuration of each unit are defined in a simple text file (.TXT) stored on its SD card. By default, the mesocosm units communicate with each other every two minutes. Data exchange is as follows:

1. Viewers and Heaters send their current temperature to the Master.
2. Master uses the data from the Viewers to calculate the average environmental temperature.
3. Master sends the new average environmental temperature, current temperature offset and timestamp to all units via ESPNOW and to the online platform via Wi-Fi.
4. Viewers and Heaters receive data from Master and update their settings.
    4.1. Viewers will only care for the timestamp of the received message to readjust its internal clock accordingly if necessary.
    4.2. Heaters will also incorporate the new average environmental temperature and temperature offset.
5. Heaters control their water heaters (On/Off) according to their current temperature and the most recent target, defined as the average environmental temperature plus the offset, both of these values received from the master.

The Master ability to establish a Wi-Fi connection (if interned is present), is not necessary for the system to work but it can enable it to send and receive online data. It can send the temperature data from all devices (received by the Master unit), the operational status of temperature sensors and SD card access status to a third-party website (**Fig. B.4**; Blynk IoT platform, USA). Additionally, it can receive data, including a new temperature offset (via Blynk platform); two decimals resolution, e.g., 2.10 ºC) or a time clock adjustment using the Network Time Protocol (NTP; "www.pool.ntp.org").

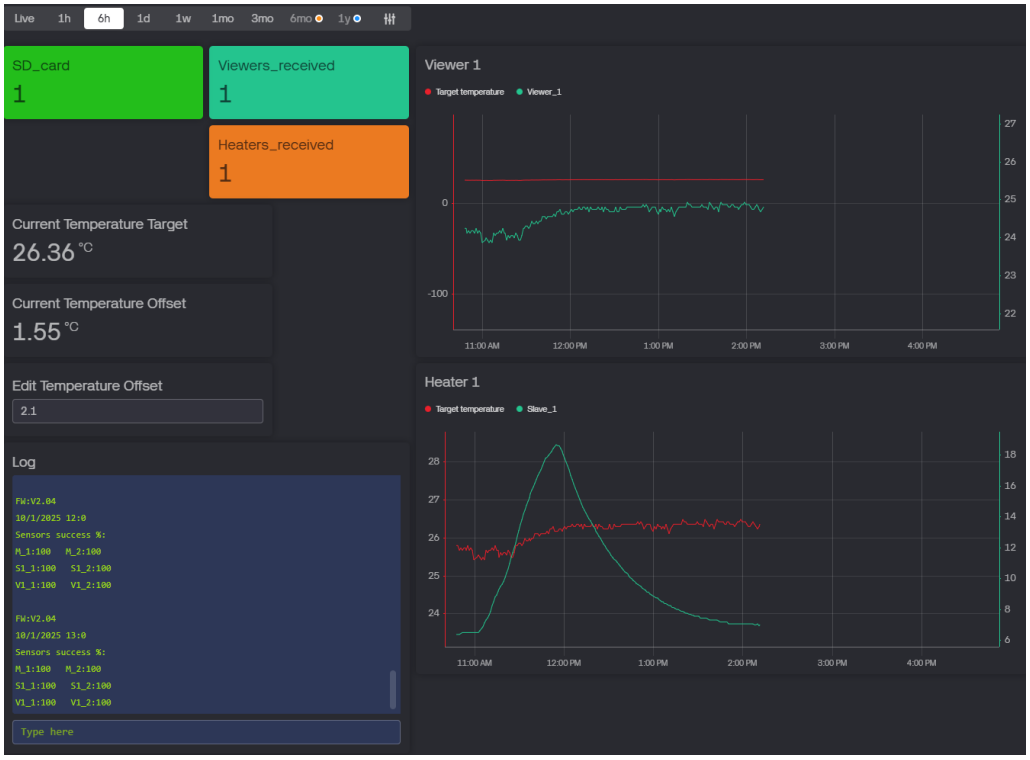


Figure B.4: Online dashboard appearance on Blynk IoT platform (Blynk, Inc., USA).

B.5. Performance and future improvements

To evaluate the capabilities of the mesocosm system, we conducted two trials. The first trial aimed to assess the wireless communication performance of the system. For this, we deployed three units (a Master and two Heaters) in an open field in Vairão (Longitude: 41.325890, Latitude: -8.677546, Portugal). The Heater units were positioned at equal distances from the Master, with separations of 10 m, 75 m, and 150 m. This trial did not involve water ponds or Viewers, as the objective was solely to measure communication performance. The units were mounted on vertical bars at a height of 1.5 m and logged data for 24 hours at each distance, using 2-minute communication intervals. The second trial aimed to simulate a realistic field setup. This experiment took place at the same site and involved five mesocosm units (a Master, two Heaters, and two Viewers). The units were deployed in a 500-liter freshwater pond, with typical field distribution (10 m between devices; **Fig. B.3b, c**). Each unit was equipped with two submersible temperature sensors (DS18B20) place inside the pond, while the Master and Heater units also operated two 300 W water heaters. These trials allowed us to test both the communication capabilities and the practical functionality of the system under field conditions, providing valuable insights into its performance and reliability.

The wireless communication performance was predominantly successful (**Fig. B.5**), particularly at distances of up to 75 m, where the success rate exceeded 99.5%. At these distances, communication messages were rarely missed, and when they were, consecutive message losses were never observed, meaning that communication interruptions never lasted longer than 2 minutes. At the 150 m distance, however, the success rate dropped significantly to 68%, with occasional "silent" periods lasting up to 38 minutes (representing 19 consecutive missed messages at the 2-minute communication rate). Despite these extended interruptions, the Heaters were able to eventually re-establish communication with the Master. Importantly, such "silent" periods at 150 m are unlikely to significantly affect real-world experiments, as Heaters rely on the last received message to maintain operations. Additionally, large water reservoirs (500 L) have substantial thermal inertia, resulting in slow temperature changes and making them tolerant to brief and temporary communication losses. Thus, even at extended distances, the system remains reliable and well-suited for most field applications.

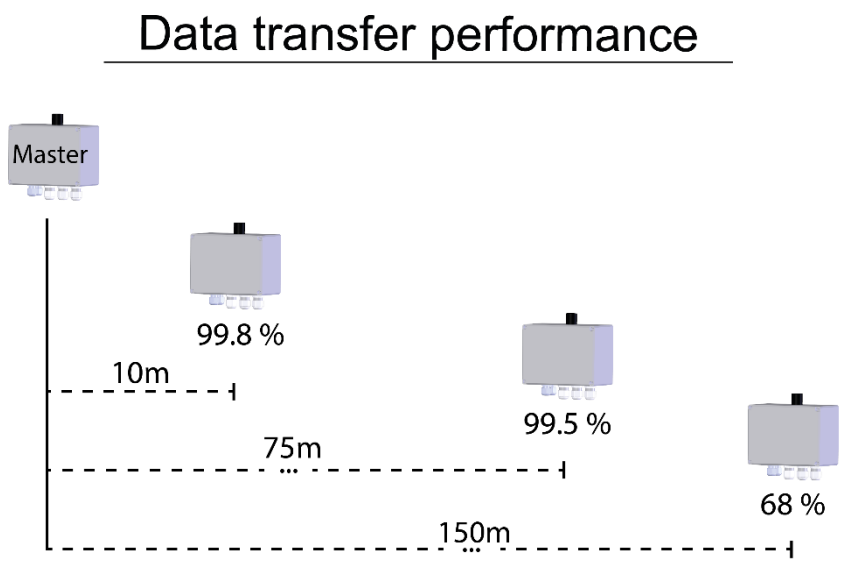


Figure B.5: Data transfer success between Mesocosm units at 10 m, 75 m and 150 m from the Master in Trial 1. Percentual values refer to minimum delivery success found within the three communicating devices (Master and two Heaters). Success rates refer to data found on the Master Logs (stored in the microSD card) after periods of 24 h periods, communicating every two minutes.

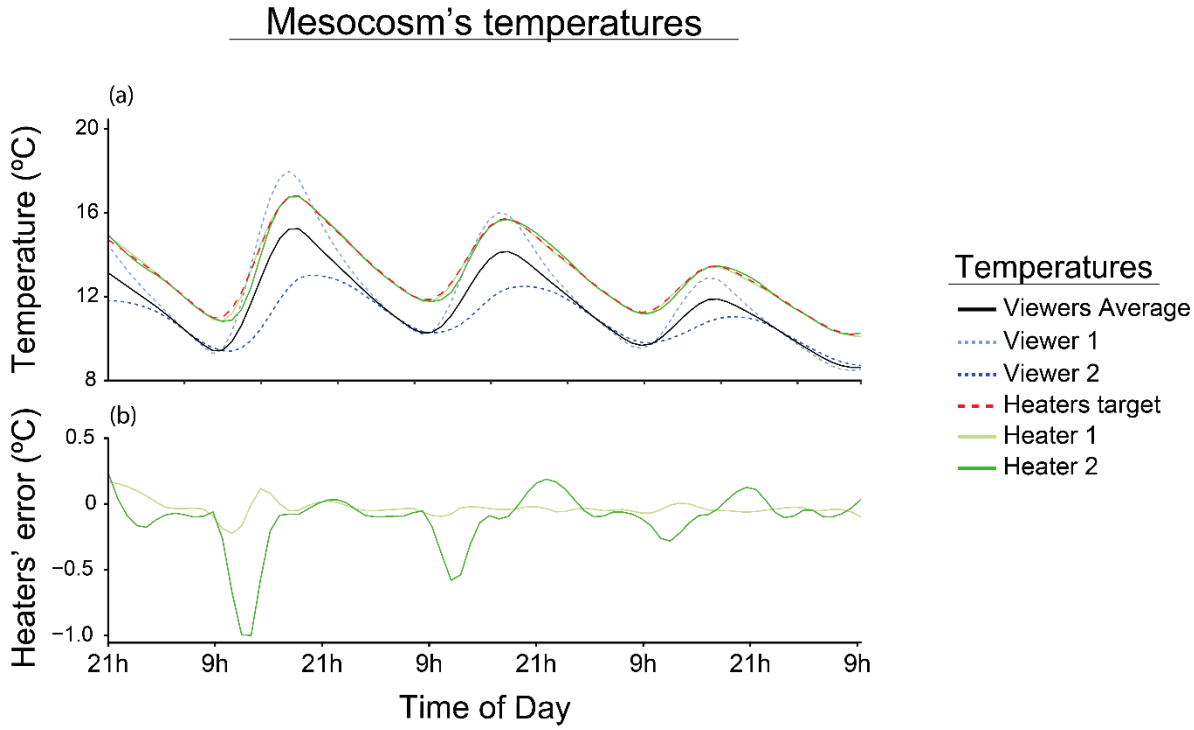


Figure B.6: a) Temperature data from all five units (a Master, two Heaters and two Viewers), together with the Viewers average and Heater's target; b) Heaters' error between the observed and target temperature for the two units.

The second trial also demonstrated a high communication performance (>99%) and revealed effective temperature monitoring and control. However, notable differences were observed between the Viewers and Heaters. The Viewers recorded average temperatures ranging from 8.81 ºC to 15.71 ºC (**Fig. B.6a**), with significant variations between units, often up to 5 ºC. Similarly, the Heaters generally performed well in maintaining their target temperatures but exhibited noticeable discrepancies between tanks. These differences were primarily attributed to the replicate ponds being situated in areas with varying sun exposure, leading to contrasting warming rates throughout the day. This setup was intentional as it allows to better capture the site's thermal profile (both sun-exposed and shaded sites), it also provided valuable insights into the Heaters' temperature control performance. Heater 2, in particular, showed a greater error (Fig. A6b) than Heater 1, with a maximum deviation of -1.11 ºC compared to 0.24 ºC. This discrepancy appeared to be correlated with rapid warming periods at noon. However, these differences diminished to less than 0.2 ºC within two hours, and the overall average errors for the whole trial were minimal at 0.03 ºC and 0.06 ºC for Heater 1 and Heater 2, respectively. Although these errors are noteworthy, they are unlikely to have a significant impact on the outcome of field experiments, as these often span over six months. Moreover,

these issues could be mitigated by increasing the power of the water heaters (currently set at 300 W).

The elimination of extensive cabling in this system is being effectively leveraged in both field and laboratory setups, enabling the deployment of large networks with minimal technical constraints. In the field, the system's remote data capabilities are being utilized by the Institute of Aquatic Ecology (HUN-REN Centre for Ecological Research, Hungary) in four networks of 24 units each, deployed across remote regions of northern Hungary. Similarly, a research team from the National Museum of Natural Sciences (CSIC, Madrid, Spain) has deployed a network for field experiments. In laboratory settings, the Hungarian research team is also operating a network of 48 units, with plans to expand it to 96 units, demonstrating the scalability and versatility of the system.

On future perspectives, there are two aspects of this system could be improved: the network's dependence on the Master unit and the power requirement for the Viewers. The reliance on the Master represents a critical limitation, as a malfunction could incapacitate the entire system. To address this, we plan to leverage the shared hardware and firmware among all units to implement a system where Viewers and Heaters can detect the Master's absence via wireless communication (using the ESPNOW protocol) and autonomously assign a replacement. This redundancy is feasible in a wireless system that is not connected to a central unit by electrical cables. The second aspect, the mains power requirement for Viewers (230 V or 110 V) is not strictly necessary, as these units do not have to operate water heaters. Hence, completely remote Viewer units could enable to capture temperatures from even broader areas. This could be partially resolved through battery power and optimized firmware. By further exploring the low-power capabilities of the ESP32 microcontroller, Viewers could operate for months on battery power while reading and transmitting temperature data. This could however require a new distance communication performance test, as greater distances (>75 m) may result in occasional missed messages and force the Viewer to spend additional energy locating the Master's frequency, thus reducing battery life.

In conclusion, the Mesocosm system presented here is a promising tool for conducting large-scale, distributed field experiments. Its open-source nature allows the scientific community to develop and share future upgrades and modifications, fostering collaborative improvements and expanding its applications.

B.6. Acknowledgements

During this work, Luis F. Pereira received support from Fundação para a Ciência e Tecnologia (FCT) through a PhD grant (SFRH/BD/136924/2018.) Fernando P. Lima and Rui Seabra received support from FCT through CEECInd contracts (10.54499/CEECIND/03185/2018/CP1546/CT0004, 10.54499/2021.03268.CEECIND/CP1668/CT0001).

B.7. References

Barbosa, M., Inocentes, N., Soares, A. M. V. M., & Oliveira, M. (2017). Synergy effects of fluoxetine and variability in temperature lead to proportionally greater fitness costs in Daphnia: A multigenerational test. *Aquatic Toxicology*, *193*, 268-275. https://doi.org/10.1016/j.aquatox.2017.10.017

Hermann, M., Jansen, R., van de Glind, J., Peeters, E. T. H. M., & Van den Brink, P. J. (2022). A transportable temperature and heatwave control device (TENTACLE) for laboratory and field simulations of different climate change scenarios in aquatic micro- and mesocosms. *HardwareX*, *11*, e00307. https://doi.org/10.1016/j.ohx.2022.e00307

IPCC. (2022). *Climate Change 2022 – Impacts, Adaptation and Vulnerability: Working Group II Contribution to the Sixth Assessment Report of the Intergovernmental Panel on Climate Change* [Interview]. Cambridge University Press.

Macaulay, S. J., Buchwalter, D. B., & Matthaei, C. D. (2020). Water temperature interacts with the insecticide imidacloprid to alter acute lethal and sublethal toxicity to mayfly larvae. *New Zealand Journal of Marine and Freshwater Research*, *54*(1), 115-130. https://doi.org/10.1080/00288330.2019.1614961

Wang, T., Xu, J., Molinos, J. G., Li, C., Hu, B., Pan, M., & Zhang, M. (2020). A dynamic temperature difference control recording system in shallow lake mesocosm. *MethodsX*, *7*, 100930. https://doi.org/10.1016/j.mex.2020.100930

Willming, M. M., & Maul, J. D. (2016). Direct and indirect toxicity of the fungicide pyraclostrobin to Hyalella azteca and effects on leaf processing under realistic daily temperature regimes. *Environmental Pollution*, *211*, 435-442. https://doi.org/10.1016/j.envpol.2015.11.029

Willming, M. M., Qin, G., & Maul, J. D. (2013). Effects of environmentally realistic daily temperature variation on pesticide toxicity to aquatic invertebrates. *Environmental Toxicology and Chemistry*, *32*(12), 2738-2745. https://doi.org/10.1002/etc.2354

Appendix C

Multispectral: an open-source platform for continuous and adjustable photobiology experiments

Luís F. Pereira, Bruno Loureiro, Rui Seabra and Fernando P. Lima.

C.1. Abstract

Photobiology examines the interaction between light and biological systems, shedding light on fundamental processes such as photosynthesis, circadian rhythms, and photoreception. In benthic communities dominated by raphid diatoms, synchronized cell motility during low tides plays a critical role in shaping primary productivity and sediment bio-stabilization. However, the precise light stimuli driving this process remain poorly understood. Current methodologies offer limited spectrum options and lack control over light intensity. To address these limitations, we have developed a versatile device for dynamic light experiments, featuring adjustable intensity over time to create complex light profiles. The system is highly adaptable, supporting different LED models to enable custom spectra. Designed to be affordable and user-friendly, this innovative tool lowers barriers to experimentation, empowering researchers to conduct precise photobiological studies and advance our understanding of light's effects on microorganisms.

Keywords

Photobiology, phototaxis, diatoms, benthic sediment, in vitro photochemistry, circadian rhythm, optogenetics.

Open source repository

Complete bill of materials, hardware and firmware of the Mesocosm system can be found in the following GitHub repository: https://github.com/coastalwarming/Multispectral

C.2. Introduction

Diatoms area diverse group of microalgae, renowned for their ecological and physiological adaptability, particularly their ability to move (Nakov et al., 2018). In benthic ecosystems, vertical mobility is a prominent behaviour exhibited by motile pennate diatoms within microphytobenthic communities (Consalvey et al., 2004; Serôdio et al., 2001). This migration is most evident in intertidal and shallow subtidal habitats, where diatoms rhythmically shift between sediment layers in sync with tidal and circadian cycles (Coelho et al., 2011; Palmer & Round, 1967). The phenomenon can be visually striking, promoting changes in sediment coloration as diatom cells ascend to the surface during low tide and retreat to deeper layers during high tide or nighttime (Serôdio & Campbell, 2021).

Vertical migration serves essential biological and ecological functions, including optimizing photosynthesis, enhancing nutrient uptake, and facilitating processes such as sexual reproduction (Admiraal, 1984; MacIntyre et al., 1996). It also plays a key role in sediment bio-stabilization and carbon assimilation, contributing to the overall productivity of these environments (Taylor & Paterson, 1998). While there is evidence of an endogenous biological clock driving this behaviour, the specific environmental factors—such as light spectrum and intensity — remain poorly understood (Serôdio, 2021; Serôdio & Paterson, 2022). A significant limitation in studying these drivers has been the lack of laboratory tools. Although previously developed devices have made important progresses (Gerhardt et al., 2016; Morales et al., 2021), no commercially available or open-source system currently offers the flexibility to accommodate different light spectra or simulate realistic circadian cycles. To address these challenges, we have developed a versatile device for dynamic light experiments, featuring adjustable light intensity over time to create complex and realistic light profiles. Its compact and adaptable design enables multiple independent and autonomous experiments to be conducted simultaneously on standard 24-well microplates, significantly accelerating experimental workflow.

C.3. Design and features

The Multispectral is a compact, modular device comprising a stack of functional elements, including 3D-printed structural components, printed circuit boards (PCBs), LEDs, an LCD display, and a 40x40 mm cooling fan (0.15 m^3/min), all securely integrated into a single cohesive unit (**Fig.C.1a**). The device footprint is 128.5 x 82.25 x 39 mm (length x depth x height) and is mainly delimited by the two main 3D print parts (Top lid and Lens support, **Fig.C.1b**). The Multispectral is designed to act as a lid on typical 24-well microplates (12.5 x 85.5 mm) with 16.2 mm diameter wells, which are commercially available (preferably opaque)

or can be 3D printed as well. It is powered by an external power-wall transformer (12V), hence requires proximity to mains power to operate. On the Top lid there's a cooling fan (blowing inwards), an 0.96-inch display LCD and three pushbuttons that allow the selection of the intended experiment.

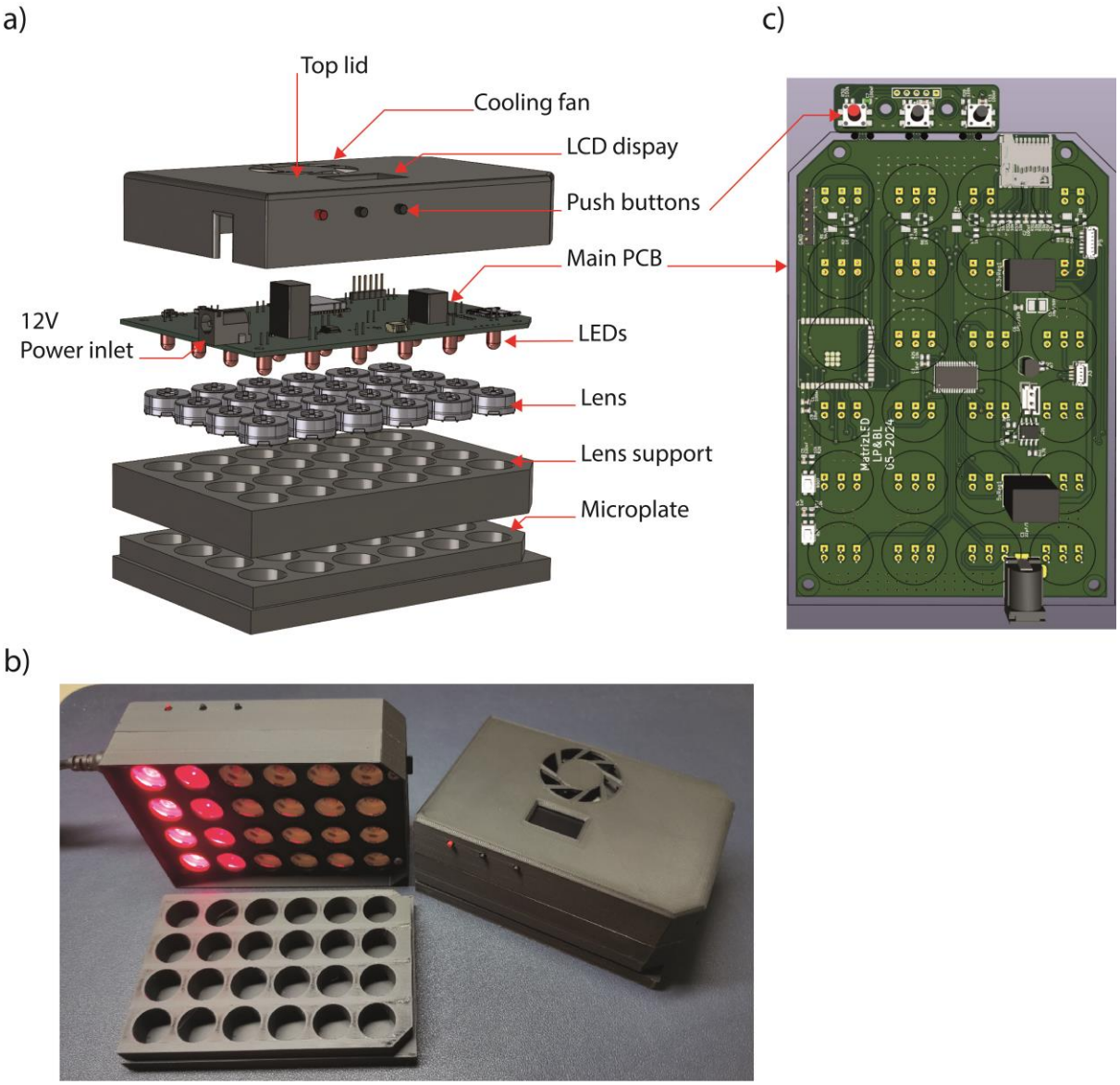


Figure C.1: a) Multispectral 3D explosion view; b) Main and push-buttons PCBs 3D view; c) Perspective of two Multispectral units, left unit is open to show lens and LED light and the right unit is placed on top of the microplate, ready to be used.

There are two PCBs (**Fig.C.1c**), a main PCB that fits inside the Top lid and contains most the electronics, including a 12V power-jack inlet for power supply, a microSD card socket and all the LEDs, and second small PCB that holds the pushbuttons and is fixed on the Top lid front from the inside by two M2.5 x 3 mm screws. The temperature sensor (12-bit DS18b20, Analog Devices, USA) is fixed on the main PCB and it monitors the temperature on the LED driver (TLC5947DAP, Texas Instruments, USA), as this will be the most heat emitting component. The two PCBs are designed as a single joined unit and attached by easily broken panel joints), which lowers its costs and simplifies production. Individual illumination to each well is provided by a single LED with a dedicated 70º dispersion lens, to ensure the homogeneous lighting of the well. LED models are not predetermined, and the main PCB is prepared for various LED pads. In fact, each microplate well can have a single LED or two in parallel. The limitations to the LED disposition or models' choice are the current consumption, with a maximum of 350 mA per well or a total of 1.5 A across all 24-wells. The intensity adjustment of LEDs is inherently constrained by their model specifications. Each LED intensity is controlled independently through electric current regulation, capped at the model's nominal values.

C.4. Operation

To initiate an experiment, the user has to ensure that the microSD card is inserted in the respective socket, power the device (via the 12V external transformer) and select the intended experimental profile. A profile consists of a simple text file, stored in the root directory of the microSD card with a sequence of instructions that determines the time intervals and intensities (0% to 100%) that will be applied to the 24 LEDs (**Fig. C.2a**; see below for further information on the design of the profile). If several profiles are available on the microSD card, the user can scroll through these by pressing the scroll buttons on the Top lid front view (black pushbuttons; **Fig, C.1c**). To start an experiment, the user must scroll to the intended profile and press the selection button (red pushbutton; **Fig. C.2b**). While an experiment is ongoing, the LCD will display critical information about the current profile duration (**Fig. C.2c**). To cancel the experiment before its programmed end, the user can simply press the selection button for three seconds.

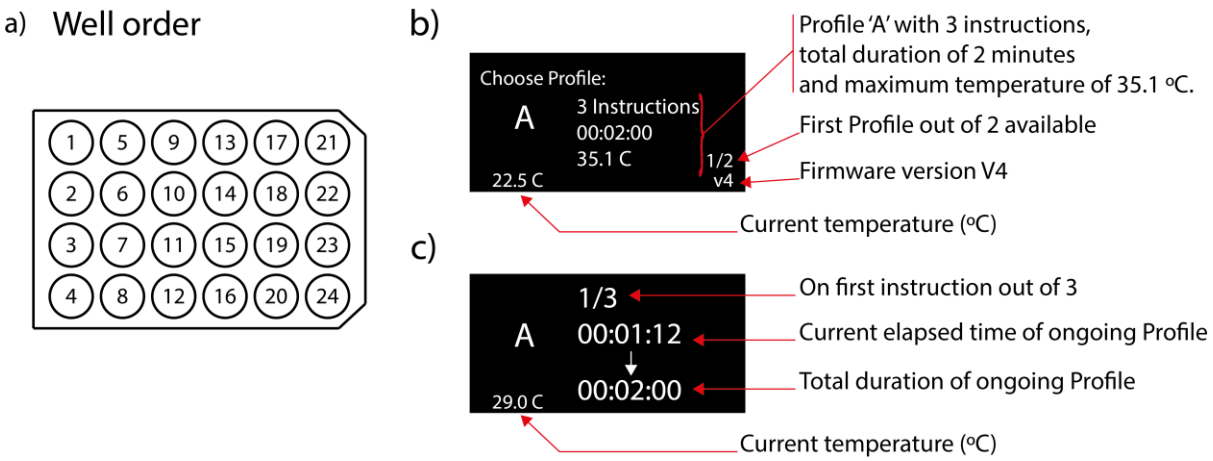


Figure C.2: a) Wells numbering for profile experiment design; b) LCD display during initial Profile choosing; c) LCD display during ongoing Profile.

A Multispectral profile consists of a series of text instructions on a text file (.txt;), present on the root directory of a microSD card inserted on the Multispectral. Each instruction corresponds to one line, with a maximum of 100 instructions per file. The first instruction indicates the temperature that triggers the cooling fan action, to inhibit further heating of the device. Subsequent instructions describe the durations and intensities that configure the experiment (hereafter setting instructions). Each of these instructions describe an independent behaviour for the whole device and will be followed sequentially, meaning that a new instruction/line is only executed after the previous one has finished. The setting instructions are by two set of digits separated by a dash. The digits on the left side of the slash correspond to the duration of that instruction in seconds (0 to 86400 seconds) and the ones on the right side of the slash correspond to the light intensities for each of the 24 LEDs (**Fig. C2a**). The latter is composed of a sequence of 24 light intensity values (one per LED/well), in a 3-digit percentage format (000 to 100), adding up to a 72-digit long sequence. For example, a profile of an experiment lasting 240 seconds with varying light intensities on the first three wells, would be as follows:

35.2

60-100050025100100100100100100100100100100100100100100100100100100100100100100100100

60-050100000100100100100100100100100100100100100100100100100100100100100100100100100

120-025025100100100100100100100100100100100100100100100100100100100100100100100100100

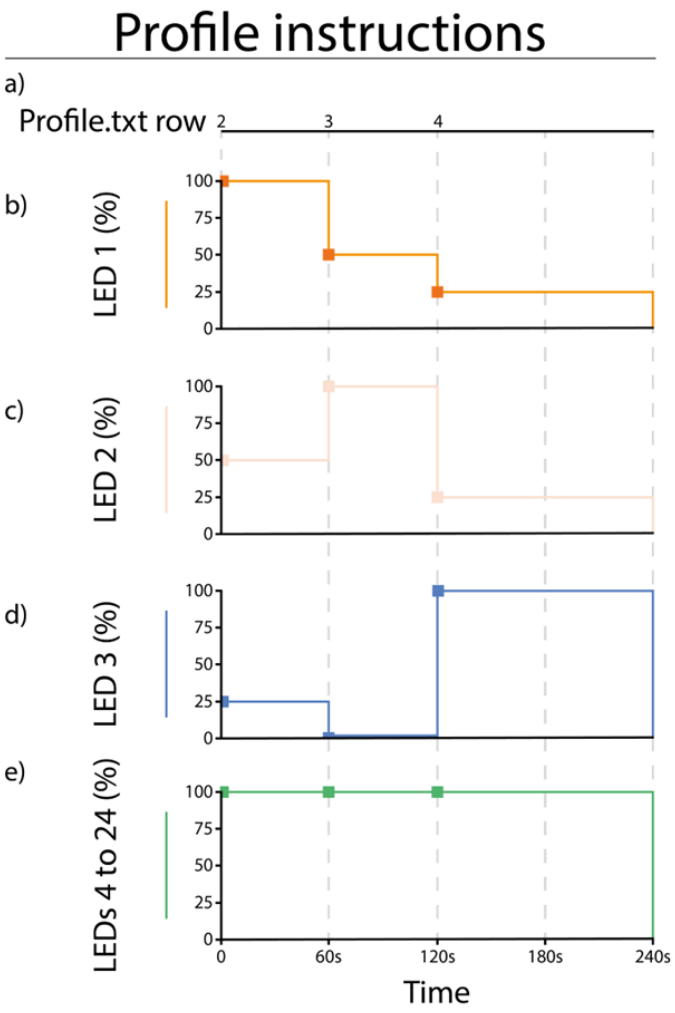


Figure C.3: a) Wells numbering for profile experiment design; b) Example profile rows; c) Light intensities of LED 1; d) Light intensities of LED 2; e) Light intensities of LED 3; f) Light intensities of all other LEDs (4th to 24th).

Deconstructing these set of instructions/rows we have:

- On the first row, we set the maximum temperature of 35.2 ºC (**Fig.C.3a**), meaning that any temperature higher than that will prompt the cooling fan operation.
- On the second row we first have the duration for the first experimental event of this profile (‘60’ for 60 seconds). Then, separated by a dash (‘-‘), we define the light intensity for each of the 24 LEDs using a 3-digit percentage value per LED. Therefore, on the second row we set the first LED at 100 % (‘100’, **Fig.C.3b**), the second at 50 % (‘050’,

Fig.C.3c), the third at 25 % ('025', **Fig.C.3d**), while all the remaining 21 LEDs (4th to 24th, **Fig.C.3e**) at 100 % during the whole experiment.

- After the initial 60 seconds of experiment, the third row will be executed, representing another 60 second period with immediate changes on the LEDs intensities. The first three LEDs would then be at 50 %, 100 % and 0 % ('000'). Note that being 0 % means that the LED will stay turned off for the duration of this step.
- Finally on the last row, LEDs would be set to 25 %, 25 % and 100 % for the first three LEDS respectively, for a 120 second period, after which the experiment will finish, and all LEDs would turn off.

C.5. Current application

The Multispectral device is currently in use by the Photobiology Department at the Centre for Environmental and Marine Studies (CESAM), University of Aveiro (Portugal). While its results are not yet available and fall outside the scope of this thesis, its current application demonstrates its potential to advance future research in photobiology. The units developed are being employed to investigate the light stimuli driving the vertical migration of diatoms in benthic sandy sediments.

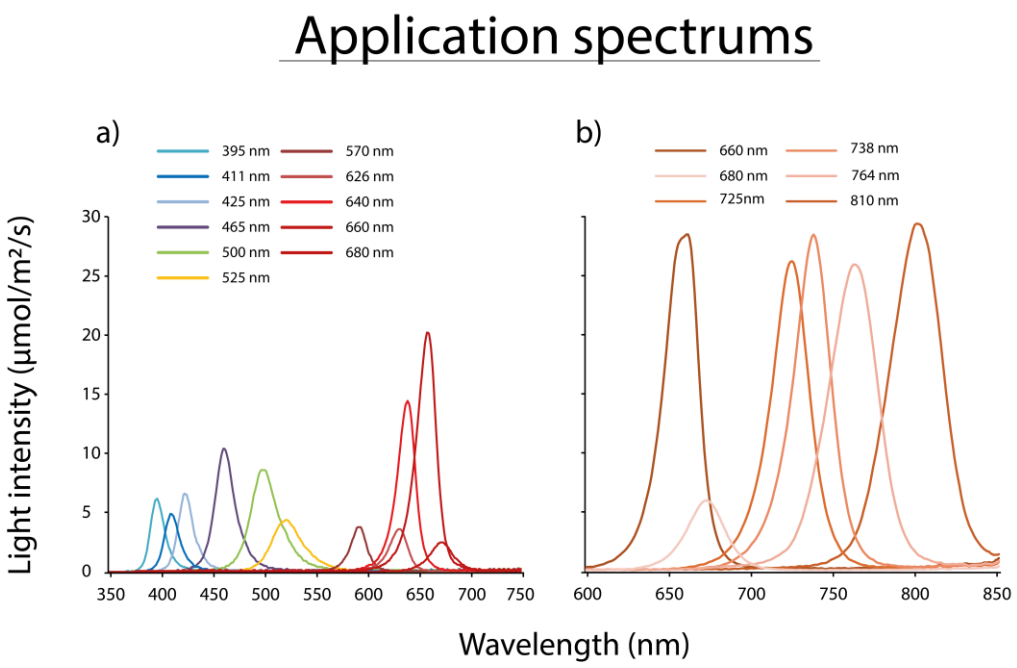


Figure C.4: a) Nominal intensity readings along the wavelengths emitted by Multispectral units aimed at evaluating effects of visible light; b) Nominal intensity readings along the wavelengths emitted from one Multispectral unit aimed at evaluating effects of near infrared light; Readings obtained via SpectraPen min (Photoystems Instruments, Poland) at 1 nm resolution (n = 4 LEDs). Note: Missing readings from 591 nm peak emission LED were not obtained at the time of this document.

This Multispectral has been configured for two distinct approaches: two units designed to evaluate the impact of visible light and a third unit focused on near-infrared wavelengths. The first two units utilize LEDs covering a close-range sweep of the visible spectrum (**Fig. C.4**), with wavelengths ranging from 395 nm to 680 nm and the same LED model. The third unit targets the near-infrared range, with peak wavelengths from 660 nm to 810 nm (**Fig. C.4b**). To enhace data production at each wavelength, this units were designed to have repeated LED models on every microplate column. As a proxy for diatom vertical migration, researchers are performing chlorophyll fluorometry (PAM) measurements, as the chlorophyll a content in diatoms provides clear evidence of their upward movement. Additionally, through minor mechanical adaptations, the Multispectral device has been adapted for use with suspension cultures in 4 ml Wheaton tubes, suggesting promising applications for investigating the photophysiological responses of other microorganisms.

Finally, like the other devices described in this thesis, the open-source design of the Multispectral aims to ensure easy accessibility and to inspire further development within the scientific community, fostering collaboration and enhancing its capabilities for future research.

C.6. Acknowledgements

During this work, Luis F. Pereira received support from Fundação para a Ciência e Tecnologia (FCT) through a PhD grant (SFRH/BD/136924/2018.) Fernando P. Lima and Rui Seabra received support from FCT through CEECInd contracts (10.54499/CEECIND/03185/2018/CP1546/CT0004, 10.54499/2021.03268.CEECIND/CP1668/CT0001).

C.7. References

Admiraal, W. (1984). The ecology of estuarine sediment-inhabiting diatoms. *Progress in phycological research*, *3*, 269-322.

Coelho, H., Vieira, S., & Serôdio, J. (2011). Endogenous versus environmental control of vertical migration by intertidal benthic microalgae. *European Journal of Phycology*, *46*(3), 271-281. https://doi.org/10.1080/09670262.2011.598242

Consalvey, M., Paterson, D. M., & Underwood, G. J. (2004). The ups and downs of life in a benthic biofilm: migration of benthic diatoms. *Diatom Research*, *19*(2), 181-202. https://doi.org/10.1080/0269249X.2004.9705870

Gerhardt, K. P., Olson, E. J., Castillo-Hair, S. M., Hartsough, L. A., Landry, B. P., Ekness, F., Yokoo, R., Gomez, E. J., Ramakrishnan, P., & Suh, J. (2016). An open-hardware platform for optogenetics and photobiology. *Scientific reports*, *6*(1), 35363. https://doi.org/doi.org/10.1038/srep35363

MacIntyre, H. L., Geider, R. J., & Miller, D. C. (1996). Microphytobenthos: the ecological role of the “secret garden” of unvegetated, shallow-water marine habitats. I. Distribution, abundance and primary production. *Estuaries*, *19*, 186-201. https://doi.org/10.2307/1352224

Morales, N. M., Patel, M. T., Stewart, C. J., Sweeney, K., & McClean, M. N. (2021). Optogenetic tools for control of public goods in Saccharomyces cerevisiae. *Msphere*, *6*(4). https://doi.org/10.1128/mSphere.00581-21

Nakov, T., Beaulieu, J. M., & Alverson, A. J. (2018). Accelerated diversification is related to life history and locomotion in a hyperdiverse lineage of microbial eukaryotes (Diatoms, Bacillariophyta). *New Phytologist*, *219*(1), 462-473. https://doi.org/doi.org/10.1111/nph.15137

Palmer, J. D., & Round, F. E. (1967). Persistent, vertical-migration rhythms in benthic microflora. VI. The tidal and diurnal nature of the rhythm in the diatom Hantzschia virgata. *The Biological Bulletin*, *132*(1), 44-55. https://doi.org/10.2307/1539877

Serôdio, J. (2021). Diatom motility: mechanisms, control and adaptive value. *Diatom gliding motility*, 159-183. https://doi.org/10.1002/9781119526483.ch7

Serôdio, J., & Campbell, D. A. (2021). Photoinhibition in optically thick samples: Effects of light attenuation on chlorophyll fluorescence-based parameters. *Journal of Theoretical Biology*, *513*, 110580. https://doi.org/10.1016/j.jtbi.2021.110580

Serôdio, J., da Silva, J. M., & Catarino, F. (2001). Use of in vivo chlorophyll a fluorescence to quantify short-term variations in the productive biomass of intertidal microphytobenthos. *Marine Ecology Progress Series*, *218*, 45-61. https://doi.org/10.3354/meps218045

Serôdio, J., & Paterson, D. M. (2022). Role of microphytobenthos in the functioning of estuarine and coastal ecosystems. In *Life below water* (pp. 894-906). Springer. https://doi.org/10.1007/978-3-319-98536-7_11

Taylor, I., & Paterson, D. (1998). Microspatial variation in carbohydrate concentrations with depth in the upper millimetres of intertidal cohesive sediments. *Estuarine, Coastal and Shelf Science*, *46*(3), 359-370. https://doi.org/10.1006/ecss.1997.0288